

UNCLASSIFIED

AD NUMBER
AD846145
NEW LIMITATION CHANGE
TO Approved for public release, distribution unlimited
FROM Distribution authorized to U.S. Gov't. agencies and their contractors; Critical Technology; JAN 1969. Other requests shall be referred to Space and Missile Systems Organization, AFSC, Los Angeles, CA 90043.
AUTHORITY
SAMSO USAF ltr, 28 Feb 1972

THIS PAGE IS UNCLASSIFIED

SAMSO-TR-69-7 VOL II PART I

RADIATION EFFECTS ON SPACE POWER SUBSYSTEMS (HANDBOOK)
VOLUME II PART 1

R. H. Kingsland
V. R. Honnold
R. D. Loveland
R. L. Russell
R. L. Skavland

Hughes Aircraft Company
Fullerton, California

January 1969
FR 69-10-69
Contract F04701-68-C-0145

JAN 21 1969

Space and Missile Systems Organization,
Air Force Systems Command,
Los Angeles, California 90045

SAMSO-TR-69-7 VOL II PART 1

RADIATION EFFECTS ON SPACE POWER SUBSYSTEMS (HANDBOOK)

VOLUME II PART 1

R. H. Kingsland
V. R. Honnold
R. D. Loveland
R. L. Russell
R. L. Skavland

Hughes Aircraft Company
Fullerton, California

January 1969
FR 69-10-69
Contract E04701-68-C-0145
~~STAT-11 #2 UNCLASSIFIED~~

... controls and each
... nationals may be
... (S.M.T.S.)
Space and Missile Systems Organization,
Air Force Systems Command,
Los Angeles, California 90045

FOREWORD

This report was prepared by Hughes Aircraft Company, Fullerton, California, under Contract F04701-68-C-0145. The work was performed under the direction of the Space and Missile Systems Organization, Air Force Systems Command. Technical monitoring of the contract was performed by Capt W. Morris and Lt W. Stine. Technical direction was provided by W. Hodson of Aerospace Corporation, El Segundo, California.


This study commenced in December 1967 and was completed in November 1968. The work was performed primarily by personnel of the Radiation Effects Research Department of Hughes-Fullerton, under the general supervision of T. D. Hanscome, Manager of the Radiation Effects Research Department, and K. R. Walker, Head of the Electronics Section. R. E. Kingsland was the Project Engineer.

The study was a group effort and the chief contributors were:

V. R. Honnold
R. D. Loveland
R. L. Russell
R. L. Skavland

This technical report has been reviewed and is approved.

Approved:


WILLIAM L. STINE, 2d Lt, USAF
Project Engineer
Survivability Office

ABSTRACT

This report provides data and guide lines which will enable circuit designers to assess and design for the effects of radiation on space power subsystems. Radiation effects on resistors, capacitors, bipolar transistors, diodes, integrated circuits, MOSFET's, SCR's and other electronic components are included. In addition, a section on catastrophic failure in semiconductors dealing with latch-up and burn-out is presented. Radiation effects on plastic and elastomeric materials commonly used in space systems are given. Various system and circuit hardening concepts for the electronic circuit designer are presented. Part II, a classified supplement not included in this volume, contains information on the radiation environment, shielding techniques, radiation effects on metals and alloys and solar cells, and thermo-mechanical effects.

BLANK PAGE

TABLE OF CONTENTS

	<u>Page</u>
FOREWORD	ii
ABSTRACT	iii
TABLE OF CONTENTS	v
LIST OF FIGURES	viii
LIST OF TABLES	xiv
 1.0 INTRODUCTION	 1-1
 2.0 DESCRIPTION OF COMPONENT EFFECTS	 2-1
2.1 Resistors	2-4
2.2 Capacitors	2-6
2.3 Bipolar Transistors	2-8
2.3.1 Calculating Transient Effects	2-8
2.3.2 Calculating Permanent Effects	2-22
2.3.3 Estimating Transient Effects	2-23
2.3.4 Estimating Permanent Effects	2-25
2.3.5 Surface Effects	2-39
2.3.5.1 Passivated and Unpassivated Devices	2-40
2.3.5.2 Radiation Effects in the Unpassivated Device	2-42
2.3.5.3 Radiation Effects in the Passivated Device	2-49
2.3.5.4 Device Selection Recommendations	2-50
2.3.6 Beta Annealing	2-54
2.4 Diodes	2-56
2.5 Integrated Circuits	2-61
2.5.1 General Discussion	2-61
2.5.2 Permanent Damage Effects	2-62
2.5.2.1 Gates	2-63
2.5.2.2 Flip-Flops	2-63
2.5.3 Transient Effects	2-72

TABLE OF CONTENTS (Continued)

	<u>Page</u>
2.6 Catastrophic Failure	2-87
2.6.1 PNP Latch-Up	2-87
2.6.2 Second Breakdown Latch-Up	2-92
2.6.3 Thin Film Interconnect Burn-Out	2-94
2.6.4 Bonding Wire Burn-Out	2-97
2.6.5 Junction Damage	2-99
2.6.5.1 Effects of Circuit Resistance	2-99
2.6.5.2 Typical Circuit and Component Resistances	2-103
2.6.5.3 Experimental Studies	2-106
2.6.5.4 Theoretical Studies	2-121
2.6.5.5 Radiation Studies	2-127
2.7 MOSFET's	2-136
2.8 Silicon Controlled Rectifiers	2-138
2.9 Solar Cells (See Classified Supplement)	
2.10 Other Components	2-145
 3.0 MATERIAL EFFECTS (See Classified Supplement for Additional Information)	 3-1
3.1 Mechanisms	3-1
3.1.1 Atomic Displacements	3-1
3.1.2 Atomic Ionization	3-1
3.1.3 Thermomechanical Effects	3-2
3.2 Organics	3-2
3.2.1 Elastomers	3-3
3.2.2 Plastics	3-4
3.2.2.1 Fluorethylene Polymers	3-6
3.2.2.2 Cellulosics	3-11
3.2.2.3 Polyamide (Nylon)	3-11
3.2.2.4 Polyesters (Unfilled)	3-11
3.2.2.5 Amino Resins	3-11
3.2.2.6 Polymide	3-12
3.2.3 Organic Fluids	3-12

TABLE OF CONTENTS (Continued)

	<u>Page</u>
4.0 GENERAL SYSTEM AND CIRCUIT HARDENING CONCEPTS	4-1
4.1 Description	4-1
4.2 Linear Circuits	4-6
4.3 Nonlinear Circuits	4-11
4.4 Photocurrent Compensation	4-16
4.5 Filtering	4-20
4.6 Charge Control	4-24
4.7 Reduction of Time Constants	4-28
4.8 Magnetic Devices	4-31
4.9 Summary	4-31
 APPENDIX 1 TABULATED TRANSISTOR RADIATION EFFECTS DATA	 A-1
REFERENCES	R-1
BIBLIOGRAPHY	B-1

LIST OF FIGURES

<u>Number</u>	<u>Title</u>	<u>Page</u>
1-1	Significant Nuclear Weapon Radiation Components	1-3
1-2	Types of Radiation Effects on Electronics	1-3
2-1	Relative Susceptability of Components to Circuit Failure In Ionizing Environment (10^8 rad(Si)/s)	2-2
2-2	Susceptability of Components to Circuit Failure in a Neutron Environment	2-2
2-3	System Transistor Failure as a Function of Neutron Dose	2-3
2-4	Equivalent Model of a Resistor Under Irradiation	2-5
2-5	Equivalent Model of a Capacitor Under Irradiation	2-5
2-6	Bipolar Transistor in Radiation Induced Saturation	2-9
2-7	Simplified Equivalent Circuit of an NPN Transistor Under Irradiation	2-9
2-8	Depletion Width as a Function of V_B at Avalanche and b	2-13
2-9	ΔW as a Function of V_B at Avalanche and b	2-15
2-10	τ vs Stored Charge at Various ΔW 's	2-16
2-11	Diode Storage Time Measurement Circuit	2-17
2-12	Transistor Radiation Storage Time Model	2-21
2-13	Radiation Storage Time Nomograph	2-21
2-14	Beta Degradation vs Neutron Dose for Typical Transistors	2-24
2-15	Primary Photocurrent (i_{pp}) vs f_T	2-26
2-16	Primary Photocurrent (i_{pp}) vs P_C (Silicon Transistors)	2-27
2-17	Primary Photocurrent (i_{pp}) vs P_C (Germanium Transistors)	2-28
2-18	Radiation Storage Time (t_{SR}) vs f_T	2-29
2-19	Radiation Storage Time (t_{SR}) vs P_C (Silicon Transistors)	2-30
2-20	Radiation Storage Time (t_{SR}) vs P_C (Germanium Transistors)	2-31
2-21	Normalized h_{FE} Degradation as a Function of f_T and Neutron Dose	2-38
2-22	Gain versus Gamma Exposed for a PNP Ge Alloy 2N396A Transistor	2-45
2-23	Gain Degradation of a PNP Si Mesa 2N1132 Transistor	2-46

LIST OF FIGURES (Continued)

<u>Number</u>	<u>Title</u>	<u>Page</u>
2-24	Radiation Damage of a PNP Si Alloy 2N1676 Transistor	2-47
2-25	Radiation Damage of a NPN Si Diffused Junction 2N1248 Transistor	2-48
2-26	Effect of Radiation on Leakage Current of a 2N2222 Transistor	2-53
2-27	Effect of Radiation on Leakage Current of a 2N2801 Transistor	2-53
2-28	Annealing Factor of Transistors as a Function of Time After a Neutron Pulse	2-55
2-29	Primary Photocurrent vs $\dot{\gamma}$ for Various Diodes	2-58
2-30	Primary Photocurrent vs I_0	2-60
2-31	Basic Gate Circuits	2-64
2-32	Degradation of Trigger Threshold Level for ac Coupled DTL Flip-Flops	2-70
2-33	Degradation of Trigger Threshold Level for dc Coupled DTL Flip-Flops	2-71
2-34	Degradation of Trigger Threshold Level for RCTL Flip-Flops	2-73
2-35	Degradation of Trigger Threshold Level for RTL Flip-Flops	2-74
2-36	Degradation of Trigger Threshold Level for One-Shot Multivibrators	2-75
2-37	Output Response vs Dose Rate for the DTL932 (0 State)	2-76
2-38	Output vs Dose Rate for the DTL932 (1 State)	2-77
2-39	Current Surges vs Dose Rate for the DTL932 (1 State)	2-78
2-40	Current Surges vs Dose Rate for the DTL932 (0 State)	2-79
2-41	Transistor Secondary Photocurrent vs Dose Rate for the DTL932	2-80
2-42	PN Junction Isolated Integrated Circuit	2-89
2-43	Equivalent Circuit for Latch-Up	2-91
2-44	Transistor Second Breakdown Characteristic	2-93
2-45	Current vs Pulse Width Burn-Out Thresholds for 0.55 mil Metallization (A Geometry)	2-98

LIST OF FIGURES (Continued)

<u>Number</u>	<u>Title</u>	<u>Page</u>
2-46	Current vs Pulse Width Burn-Out Thresholds for 0.55 mil Metallization (B Geometry)	2-98
2-47	Equivalent Semiconductor Circuits at High Dose Rates	2-101
2-48	Theoretical Failure Curves for Silicon Junctions for Reverse Polarity Voltages	2-109
2-49	Experimental Data Points for Failure of the Anode-Cathode Junction of a MC-357 Diode for Reverse Polarity Voltage Pulses	2-109
2-50	Experimental Data Points for Failure of the Anode-Cathode Junction of 1N459 Diode for Reverse Polarity Voltage Pulses	2-110
2-51	Experimental Data Points for Failure of the Anode-Cathode Junction of a 1N482A Diode for Reverse Polarity Voltage Pulses	2-110
2-52	Experimental Data Points for Failure of the Anode-Cathode Junction of a 1N1095 Diode for Reverse Polarity Voltage Pulses	2-111
2-53	Experimental Data Points for Failure of the Base-Emitter Junction of a 2N2222 Transistor for Forward and Reverse Polarity Voltage Pulses	2-111
2-54	Experimental Data Points for Failure of the Base Emitter and Collector-Emitter Junctions of a 2N1132 Transistor for Forward and Reverse Polarity Voltage Pulses	2-112
2-55	Experimental Data Points for Failure of the Base-Emitter Junction of a 2N699 Transistor for Reverse Polarity Voltage Pulses	2-112
2-56	Experimental Data Points for Failure of the Base-Emitter Junction of a 2N498 Transistor for Reverse Polarity Voltage Pulses	2-114
2-57	A Composite of Experimental Data Points for the Failure of the Anode-Cathode Junction for Six Diodes. Intercomparison is Made By Plotting Power Per Unit Area vs Pulse Duration. Also shown are the theoretical failure curves	2-114

LIST OF FIGURES

(Continued)

<u>Number</u>	<u>Title</u>	<u>Page</u>
2-58	A Composite of Experimental Data Points for the Failure of the Base-Emitter Junction for Eight Transistors. Intercomparison is Made by Plotting Power Per Unit Area vs Pulse Duration. Also shown are the theoretical failure curves.	2-115
2-59	Transistor Power Rating vs Collector-Base Junction Area	2-116
2-60	Diode Forward Current Rating vs Junction Area	2-118
2-61	A Composite of Experimental Data Points for which No Failure was Achieved for the Anode-Cathode Junction for Ten Large Area Diodes. Intercomparison is made by Plotting Power Per Unit Area vs Pulse Duration. Also shown are the theoretical failure curves.	2-119
2-62	Plots of the Semi-Empirical Failure Equations Obtained from Theory and the Experimental Data Points	2-119
2-63	A Comparison of Experimental Data Points for a 2N2222 Transistor and Points from a Paper by Davis and Gentry. Also shown are the theoretical failure curves from this paper and the curve by Davis and Gentry.	2-120
2-64	Thermal Equivalent Circuit	
2-65	Simplified Equivalent Circuit	2-122
2-66	Peak Power Dissipation for Silicon Transistors	2-126
2-67	Circuit Used for Measuring Secondary Photocurrent (i_{pp2})	2-128
2-68	Power Dissipation vs Pulse Width for Radiation Induced Burn-Out for Various Transistors	2-129
2-69	Comparison of Wursch and Bell's and Hughes Radiation Induced Burn-Out Data	2-133
2-70	Pulse Power vs Pulse Width for Electrical Burn-Out of IC Kit Parts	2-134
2-71	Comparison of Wursch and Bell's and Hughes Electrical Burn-Out Data for IC Kit Parts	2-135
2-72	SCR Radiation-Induced Switching Threshold	2-140
2-73	SCR Circuit Configuration	2-140

LIST OF FIGURES

(Continued)

<u>Number</u>	<u>Title</u>	<u>Page</u>
2-74	t_s' Measurement Circuit and Waveforms	2-142
2-75	Photocurrent-Switching Time Correlation	2-143
2-76	Neutron Dose Effects on Various SCR Parameters	2-144
2-77	SCR Current Limiting Circuitry	2-146
3-1	Relative Radiation Stability of Elastomers	3-5
3-2	Relative Radiation Resistance of Thermoplastic Resins	3-7
3-3	Relative Radiation Stability of Thermosetting Resins	3-8
3-4	Approximate Tolerance of Lubricants to Gamma Radiation	3-14
4-1	Telemetry Encoder Circuitry	4-3
4-2	Motor Control Circuitry	4-3
4-3	dc-dc Converter Circuitry	4-5
4-4	Diode-Capacitor Circuitry	4-5
4-5	Prolongement of Circuit Recovery Time	4-10
4-6	Circuit for Compensation of Primary Photocurrent	4-17
4-7	Circuit for Compensation of Secondary Photocurrent	4-17
4-8	Circuit for Compensation of Photocurrents and Noise	4-19
4-9	Circuit for Shunting Primary Photocurrent Around the Collector Impedance	4-19
4-10	Circuit for Shunting Primary Photocurrent Around the Base-Emitter Impedance	4-21
4-11	Circuit for Shunting Primary Photocurrent Around the Emitter Load	4-21
4-12	Sample/Hold Circuitry	4-23

LIST OF FIGURES (Continued)

<u>Number</u>	<u>Title</u>	<u>Page</u>
4-13	Equivalent Circuit of a Capacitor During Irradiation	4-27
4-14	Capacitor Radiation Response vs Capacitor Value	4-27
4-15	Transient Response vs Capacitor Initial Conditions	4-29
4-16	ac Coupled Amplifier for Testing Transient Recovery	4-29

LIST OF TABLES

<u>Number</u>	<u>Title</u>	<u>Page</u>
2-1	Typical i_{pp} at 10^8 rad(Si)/s	2-10
2-2	Measured Transistor Equilibrium Photocurrent	2-32
2-3	Measured Transistor Photocurrent and Radiation Storage Time	2-36
2-4	Radiation Test of Unpassivated Devices	2-44
2-5	2N2222 NPN Silicon Planar Transistor	2-51
2-6	2N2801 PNP Epitaxial Planar Transistor	2-52
2-7	Measured Diode Equilibrium Photocurrent at Three Reverse-Bias Voltages	2-59
2-8	Critical Radiation Thresholds for Damage Failure in DTL Gates for Fan-Out of 10	2-65
2-9	Critical Radiation Thresholds for Damage Failure in RTL, RCTL Gates for Fan-Out of 15	2-66
2-10	Summary of Microcircuit Failure Levels	2-67
2-11	Normalized Degradation of Loading Capability for DTL Circuits After 2.7×10^{14} n/cm ² (E > 10 keV)	2-69
2-12	Critical Radiation Thresholds for Transient Radiation Effects for RTL, RCTL OFF Gates. Averages of Four Circuits of Each Type	2-83
2-13	Failure Threshold Levels for RTL and RCTL Flip-Flops	2-84

LIST OF TABLES (Continued)

<u>Number</u>	<u>Title</u>	<u>Page</u>
2-14	Critical Radiation Thresholds for Transient Radiation Effects for DTL Gates. Averages for Four Circuits of Each Type	2-85
2-15	Failure Threshold Levels for DTL Flip-Flops	2-86
2-16	Interconnect Burn-Out Current	2-96
2-17	Integrated Circuit Radiation Induced Currents	2-99
2-18	Typical Diode Semiconductor Resistances under Irradiation	2-105
2-19	Wire Resistance	2-106
2-20	Transistor Thermal Characteristics	2-125
2-21	Device Failure Modes Due to Dose Rate Effects	2-130
3-1	Comparison of Air and Vacuum Effects on FEP Teflon	3-10
4-1	Transistor Burn-Out Current and Time	4-4

1.0 INTRODUCTION

One of the objectives of this program is to provide data and guide lines (a handbook) which will enable circuit designers to assess and design for the effects of radiation on space power subsystems. It is assumed that the designers are not particularly knowledgeable in radiation effects technology. Therefore, the proposed handbook will contain, in addition to design data, a sufficient amount of background and tutorial material to insure that the circuit designers are made aware of the problems associated with designing circuits to operate in a nuclear radiation environment.

The survivability of a space power subsystem exposed to a nuclear detonation depends on the interaction of the nuclear radiations with the components, circuitry, and subsystems. The significant components of the nuclear radiations and their effects are illustrated in Figure 1-1. Usually, the radiation effects of concern caused by these components are:

- . Transients due to ionizing radiation.
- . Permanent degradation due to neutron and ionizing radiation fluence.
- . Catastrophic failure caused by rate of energy deposition.

The ionizing radiation is an intense radiation pulse of high dose rate and short time duration. This radiation interacts with matter through the Compton, photoelectric, and pair production processes. The interaction with the components and materials that constitute an

electronic system result in charge redistribution throughout the system. Currents will flow during this pulse and, in many cases, continue to flow after the pulse terminates. Degradation due to the radiation fluence (integrated dose) to materials and components is due to displacement of atoms within the material. The neutron component is the predominant producer of displacements and affects semiconductor materials in particular. The ionizing radiation can also cause damage through high energy deposition resulting in catastrophic failure.

Typical radiation-induced system effects are shown in Figure 1-2 and are classified below:

- . Transient rate effect: In this case the electronic response exhibits a time history which is characteristic of the radiation pulse.
- . Transient relaxation effects: This effect exhibits a maximum change immediately after the radiation pulse. The relaxation effect then recovers from the disturbed state with inherent system time constants. Circuit and system recovery in this case may take milliseconds even though the initial disturbance was created by a radiation pulse of less than a microsecond.
- . Direct and indirect permanent effects: Direct permanent effects are due to material and component damage within the system and are not correctable or repairable in times of interest to the system mission. Indirect permanent effects include component burnout due to high current transients (catastrophic failure). Other indirect effects, such as those which might be observed

81132-93

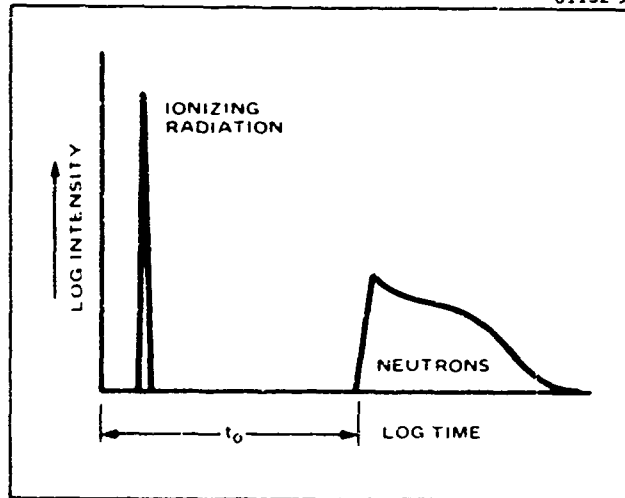


FIGURE 1-1 Significant Nuclear Weapon Radiation Components

81132-94

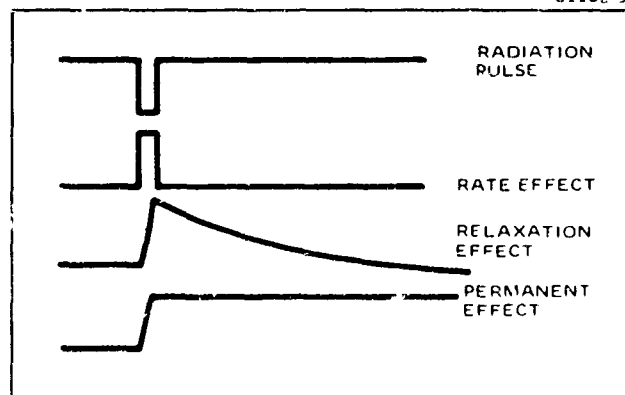


FIGURE 1-2 Types of Radiation Effects on Electronics

in digital systems are those which cause an electronic change which cannot be corrected (because of inaccessibility) during times of interest for the system. For instance, the change of state of a memory element or digital control system is an indirect permanent effect. This type of effect could be reversed or erased if the system were accessible through manual or remote control.

The particular type of effect generated by the nuclear environment will depend upon the specific operational mode of the system at the time of exposure. The significant transient interactions occur in circuitry which is powered and operating at the time of exposure. However, even without power, currents are generated (in any material) due to secondary electron emission and absorption. The direction of these currents is uncertain because they depend on the equilibrium established between electrons absorbed from the incident radiation and electrons emitted from the exposed material. Equilibrium condition is a function of the incident spectrum and the geometry of the situation. Typically, for a fission gamma ray spectrum, the emitted charge (q) can be calculated from the following equation:

$$Q = \dot{\gamma} A 5 \times 10^{-13} \text{ (coulombs)} \quad (1-1)$$

where $\dot{\gamma}$ = dose rate rad(Si)/s
 A = exposed area in cm²

This emitted charge can be replaced to a greater or lesser degree by absorbing charge emitted from surrounding material. Circuit equilibrium will be established by a current flow. If the electronics

are powered, these replacement currents can cause significant effects; however, these effects may not be prime survivability factors in a nuclear weapon environment; i.e., active semiconductor devices produce photocurrents which are usually of much larger magnitude than the replacement currents, even though the latter are important for interpreting analytical or experimental results.

2.0 DESCRIPTION OF COMPONENT EFFECTS

Figure 2-1 shows the relative threat to normal circuit operation of a wide variety of electronic components operated in an ionizing radiation environment. Both active and passive components exhibit transient responses as a function of high dose rate radiation pulses due to internal and external ionization leakage and scattering as a result of Compton and photoelectric effects.

Figure 2-2 shows the threat to circuit operation of similar electronic components exposed to fast neutrons. Lattice displacements, due to accumulated neutron dose, cause permanent parameter degradation.

Both Figures 2-1 and 2-2 show passive components to be less sensitive to the radiation environment. Within a given type of component, a choice should be made to select the technology or construction technique least affected by the environment. For instance from Figure 2-1, solid core carbon composition resistors are superior to carbon film air core resistors. Active components are by far the most sensitive to transient and total dose radiation effects. Semiconductors are the most sensitive of the active components, but utility, space, and power requirements dictate that semiconductors be used in most system designs. Radiation effects in semiconductors must be minimized by careful component selection and circuit designs that consider the magnitude of component responses and effects.

One of the most important component electrical parameters effected by radiation is the transistor current gain parameter β . Figure 2-3 illustrates the effects of neutron damage to a representative unhardened system. The system damage commences at a neutron fluence less than 10^{11} n/cm². Approximately 18% of the transistors

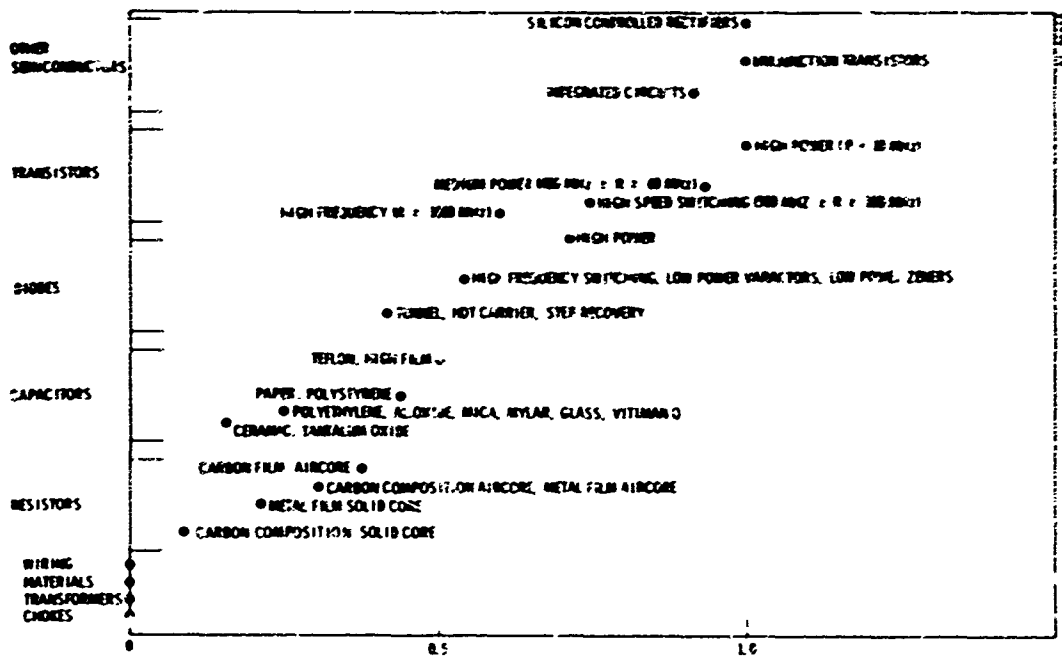


FIGURE 2-1 Relative Susceptibility of Components to Circuit Failure In Ionizing Environment (10^8 rad(Si)/s)

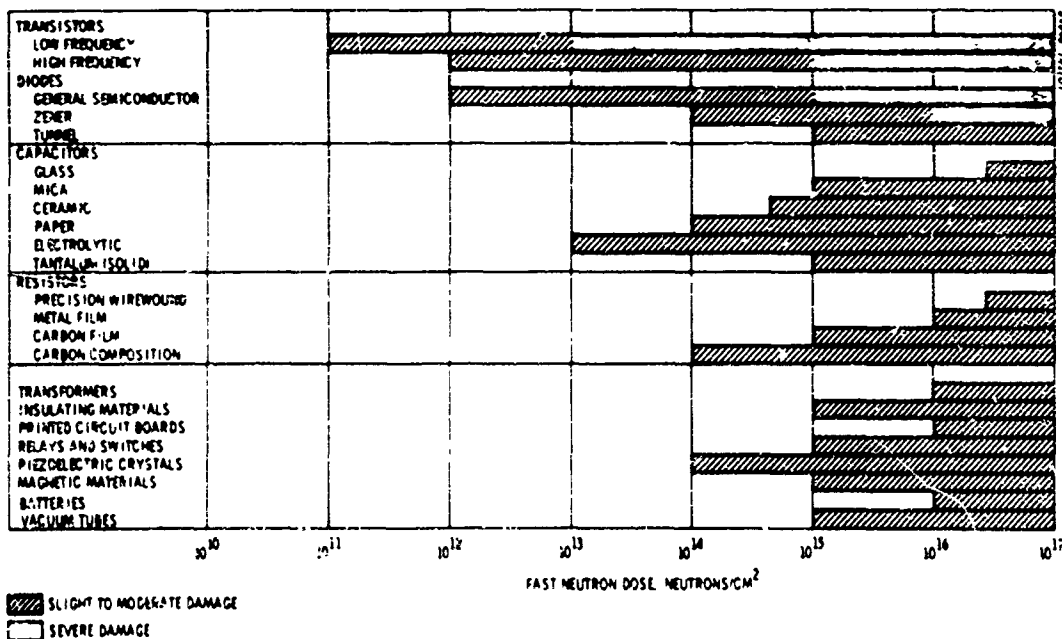


FIGURE 2-2 Susceptibility of Components to Circuit Failure in A Neutron Environment

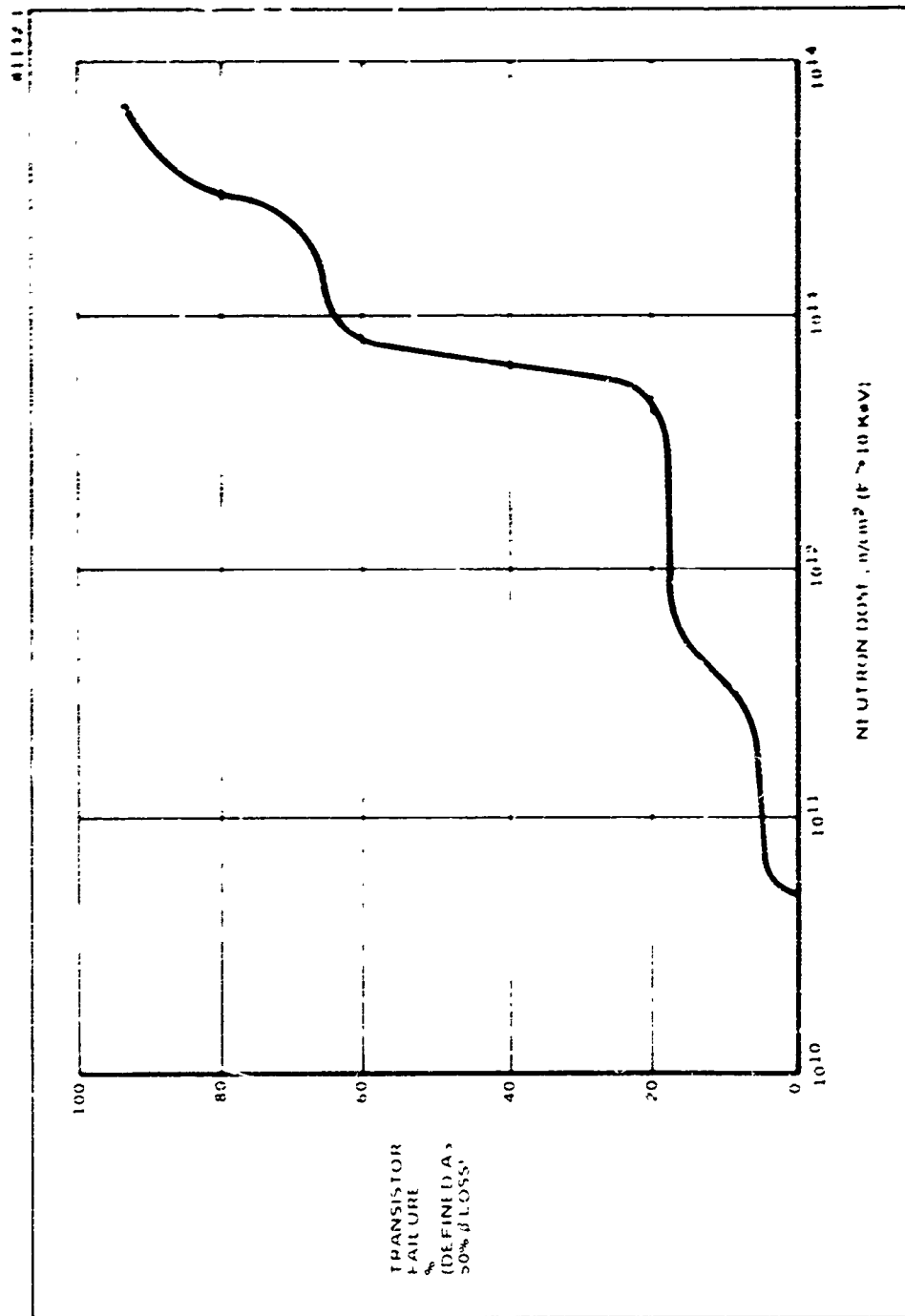


FIGURE 2-3 System Transistor Failure as a Function of Neutron Dose

fail (50% loss of β) at 10^{12} n/cm² (these types of devices are power transistors with a gain bandwidth product (f_T) of less than approximately 10 MHz.) Devices of this frequency and power range are generally used in power subsystems.

2.1 Resistors

Resistors exhibit transient responses due to external ionization leakage in the material surrounding (or inside) the resistor, and the charge scattering into or from the resistor material results in net replacement currents. These effects are illustrated by the model in Figure 2-4. The replacement current is represented by the current generator (I) injected into the center of the resistor and the ionization is represented by a radiation induced shunt leakage resistance (R_g). Representative expressions for calculating worst case I and R_g for two types of resistors are shown.⁽¹⁾ These resistor types represent the worst (metal film) and best types for use in a radiation environment.

Resistor effects and some general guidelines are summarized below:

- . Resistor effects persist only during the radiation pulse.
- . Resistor effects will generally be negligible in any circuitry under consideration since semiconductor effects will normally predominate.
- . No permanent damage to resistors will be sustained due to ionizing radiation or neutron fluence in most environments.

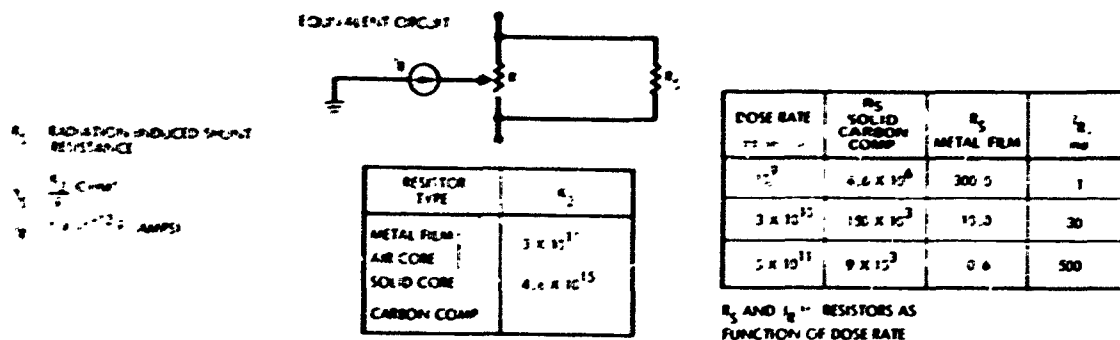


FIGURE 2-4 Equivalent Model of a Resistor Under Irradiation

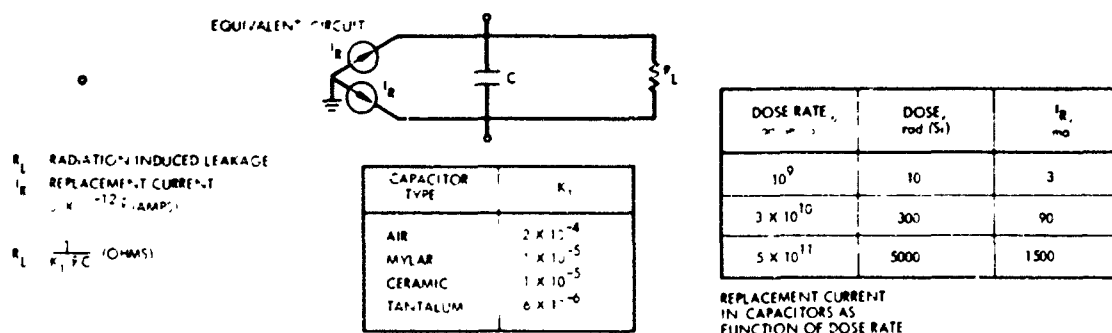


FIGURE 2-5 Equivalent Model of a Capacitor Under Irradiation

- . Potting material will reduce the leakage effects. The values of R_g and the expressions for calculating R_g listed in Figure 2-4 are for the worst case condition (air environment).
- . Use solid core carbon composition resistors wherever possible.
- . Use the lowest values of resistance possible consistent with power considerations.
- . When metal film or wire wound resistors are necessary, use solid rather than air core spool types.
- . The current (I) may flow into or out of the resistor.

2.2 Capacitors

Capacitors exhibit ionization leakage and replacement current effects due to ionizing radiation similar to the effects in resistors. A capacitor model and representative worst case parameters are shown in Figure 2-5.⁽¹⁾ The replacement current is represented by the current generator (I) on each side of the capacitor and the ionization is represented by the radiation induced leakage resistance (R_L).

Capacitor effects and general guidelines for capacitor selection and application are summarized below:

- . The major ionization leakage and replacement current effects persist only during the radiation pulse. Some long term leakage effects persist for time periods after the irradiation and may be significant in some cases.

- . Potting material will reduce capacitor effects by decreasing injected currents.
- . Mica, ceramic, glass, tantalum oxide, mylar, aluminum oxide, and vitamin Q capacitors are best choices. Ceramic is the best choice for small capacitors and tantalum oxide is the best choice for large capacitors.
- . Keep capacitor values as low as possible and capacitor voltages as low as possible consistent with design goals.
- . The voltage change on a capacitor due only to internal leakage will be relatively small. Voltage change can be calculated from the following expression:

$$V = V_0 \exp(-x/x_c) \quad (2-1)$$

where

- V = voltage remaining after the radiation pulse
- V_0 = initial voltage
- x = absorbed dose in rad(Si)
- $x_c = 10^5$ for mylar and 10^6 for ceramic and mica capacitors

For example, at a dose rate of 5×10^9 rad(Si)/s and a pulse width of 30 ns the voltage change is negligible since $V = V_0 e^{-.00015} \approx V_0$. Even at a dose rate of 5×10^{11} rad(Si)/s the change in voltage for ceramic capacitors is only 2%.

2.3 Bipolar Transistors

2.3.1 Calculating Transient Effects (1,2,3,4)

During exposure to a high dose rate radiation pulse, the predominate effect in semiconductors is due to internal ionization effects. This internal ionization results in the creation of hole-electron pairs and effectively produces an internal current generator whose magnitude is dependent on the incident radiation level. The radiation-induced current is referred to as primary photocurrent (i_{pp}) and is observed as the change in the leakage current (ΔI_{CBO}) which flows across a reverse biased collector-base or diode junction. For bipolar transistors, a secondary photocurrent also occurs. This is the collector-emitter current that flows as a result of i_{pp} being multiplied by the transistor current gain.

An additional effect in bipolar transistors, defined as radiation storage time (t_{sR}), occurs when the transistor is driven hard into saturation. Saturation will continue in this case after the radiation pulse terminates. The prolonged saturation time is t_{sR} .

These concepts are illustrated in Figure 2-6. A simplified equivalent circuit for an NPN transistor in radiation-induced saturation is illustrated in Figure 2-7. The primary photocurrent (i_{pp}) splits into I_X and ΔI_B at the point of injection. The current division will depend on the impedances in the two paths. The collector current will be limited at saturation by external circuitry, and any overdrive available in i_{pp} will extend the saturation time by t_{sR} . Note that I_X may serve as a forcing function to excite external reactive circuitry and prolong the disturbance for times longer than those due to radiation pulsewidth and t_{sR} . In circuits containing

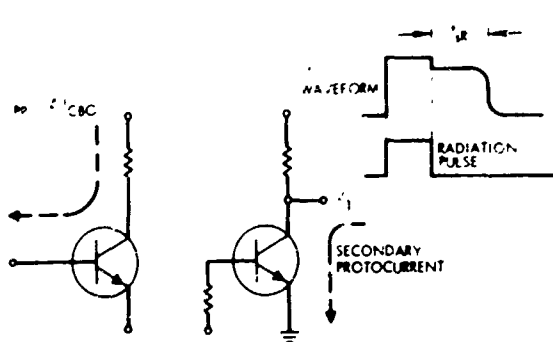


FIGURE 2-6 Bipolar Transistor in Radiation Induced Saturation

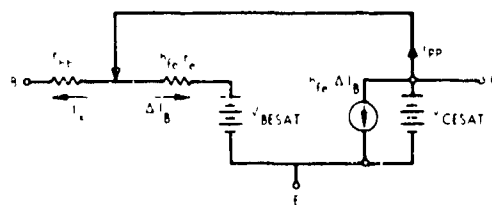


FIGURE 2-7 Simplified Equivalent Circuit of an NPN Transistor Under Irradiation

high impedances in the base circuit, most of i_{pp} will flow into the transistor. Note that the transistor saturation is usually independent of base circuitry. An effective way of reducing the saturation effect is to use a radiation controlled current sink on the transistor base which effectively makes $i_{pp} \approx I_X > \Delta I_B$.

From a design standpoint, photocurrent generation is significant between 10^3 and 10^{12} rad(Si)/s. At high radiation dose rates (10^{12} rad(Si)/s), photocurrents generated will cause saturation of nearly all circuits. At 10^8 rad(Si)/s photocurrents in low-level, high-speed devices will be 10 microamperes or more as illustrated in Table 2-1.

TABLE 2-1 Typical i_{pp} at 10^8 rad(Si)/s

Device	i_{pp}
Fairchild Developmental TTL Device	10 microamperes
2N2369	14 microamperes
2N2784	30 microamperes
2N709	40 microamperes
2N918	65 microamperes
2N914	150 microamperes
2N2222	1.4 milliamperes

Techniques are available for predicting t_{sR} (2) and i_{pp} (3,4) for low power transistors. i_{pp} is a linear function of dose rate and t_{sR} is an exponential function of dose rate. The radiation parameters i_{pp} and t_{sR} are predicted using device electrical parameter (stored

charge or storage time, avalanche voltage, and capacitance vs voltage parameters) values.

For example, transistor equilibrium photocurrent (i_{ppC}) is related to transistor high-current storage time (t_s) by the following equation ($P_c < 0.8 \text{ W}$)⁽³⁾:

$$i_{ppC} \approx \Delta I_{CBO} \approx \frac{K \dot{\gamma}}{0.83 \times 10^8} (t_s + .03) \quad (2-2)$$

where: ΔI_{CBO} is the radiation-induced change in collector-base leakage current in mA

$\dot{\gamma}$ is the radiation dose rate in rad(Si)/s

t_s is in μs and measured with $I_B = 100 \text{ mA}$, 5 μs pulse;

$I_{CS} = 80 \text{ mA}$

$K = 1.0 \text{ mA/rad}$ for Si NPN planar and mesa transistors,
 2.0 mA/rad for Si PNP planar and mesa transistors, and
 4.0 mA/rad for Ge PNP mesa transistors ($P_T < 0.8 \text{ W}$)

Statistical confidence levels have been established for the Si NPN prediction constant, K . For PNP devices, the constants have been developed from theory and limited experimental data. For Si NPN transistors, Equation 2-2 will predict equilibrium photocurrents within ± 30 to ± 60 percent of the true value. This accuracy can be compared with the ± 10 to ± 25 percent accuracy for an actual photocurrent measurement, referenced to a given radiation rate. For a given rate, actual photocurrents produced by a given type transistor may range over more than a 4 to 1 spread.

Transistor and diode equilibrium and nonequilibrium photo-currents can also be predicted from device electrical parameters using the following techniques⁽⁴⁾

Measure capacitance versus voltage characteristics. Plot capacitance versus junction* voltage data using log-log scale (junction voltage = reverse bias voltage at terminals plus junction energy gap voltage of 0.72 volt). Determine logarithmic slope (b) as follows:

$$b = \frac{\log_{10} C_{100} - \log_{10} C_1}{2} \quad (2-3)$$

Measure dc avalanche voltage (V_A) at 100 μ A reverse leakage current. Calculate junction voltage at avalanche (V_B)

$$V_B = V_A + 0.72 \quad (2-4)$$

Using Figure 2-8 enter at the V_B value and slope (b) from step 1. Read depletion width at $V_B = 1.0$ volt (w_1).

Calculate junction area, A,

$$A = \frac{C_1 w_1}{K K_0} \quad (2-5)$$

*The term junction refers either to the diode junction or to the transistor collector-base junction.

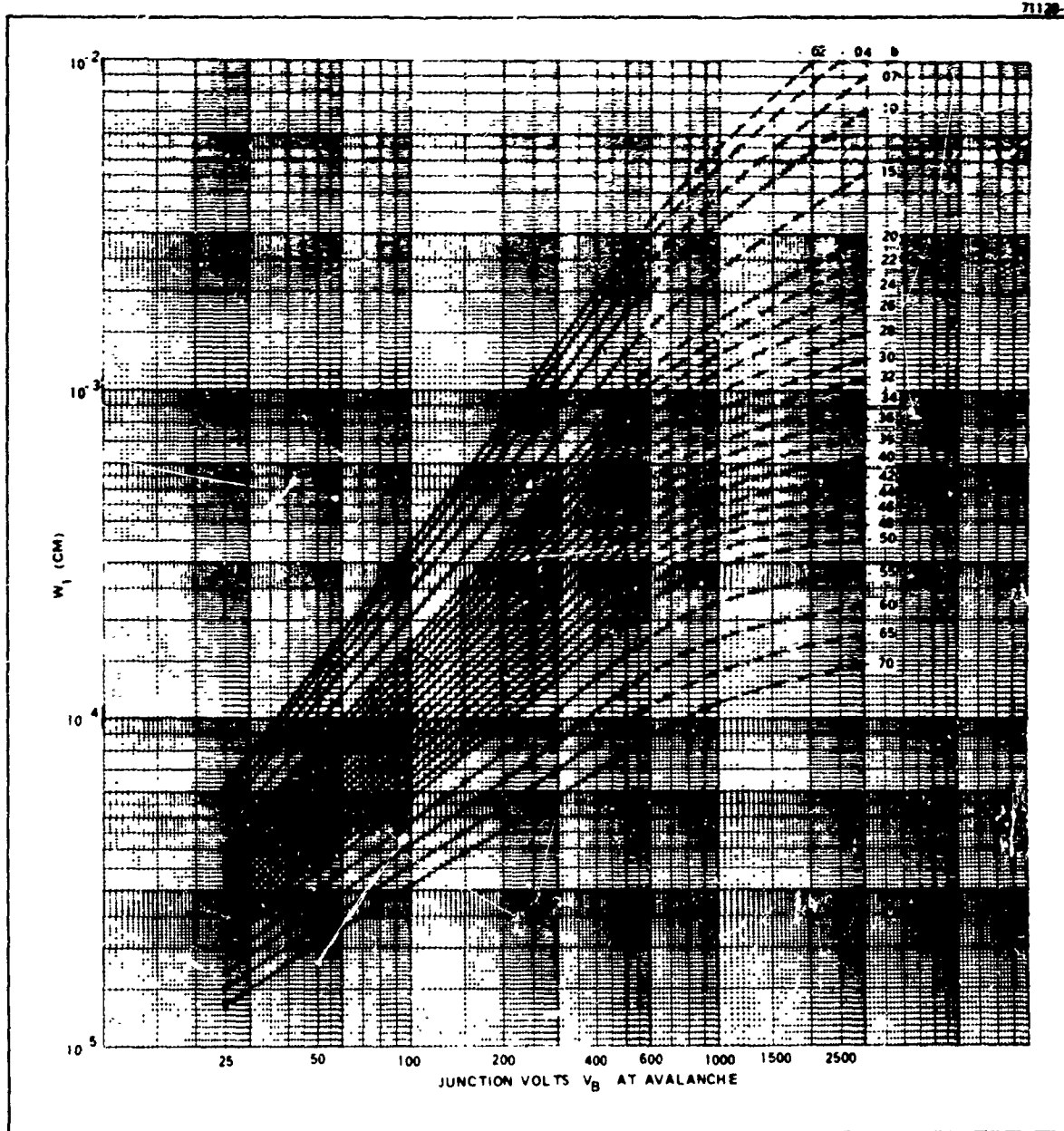


FIGURE 2-8 Depletion Width as a Function of V_j at Avalanche and b

where $K K_0 \text{ (Si)} = 1.044 \text{ pF/cm}$

Determine minority carrier lifetime. Measure junction stored charge (Q) for a forward current of 0.1 mA (use method 4061 of MIL-STD-750) as noted by Reference 4. Read lifetime ($\tau_{0.1}$) using charts of Figures 2-9 and 2-10.

For diodes, if $\tau_{0.1} < 20$ microseconds, measure junction storage time, t_s using the test setup in Figure 2-11. The storage time measurement technique differs from the usual diode reverse recovery measurement arrangement in that the diode is quiescently in the reverse biased condition and is turned on by the input pulse. This method allows use of higher forward currents without damage to diodes since the average current is much smaller than in the usual arrangement. Using the measured t_s calculate lifetime (τ_s) from the relation

$$\tau_s = \frac{t_s}{\left[\operatorname{erf}^{-1} \left(\frac{I_f}{I_f + I_r} \right) \right]^2} \quad (2-6)$$

For transistors, if $\tau_{0.1} < 160 \text{ ns}$, measure collector-base storage time (t_{sd}), and calculate τ_{sd} using Equation 2-6. This combined τ_s (or τ_{sd}) and $\tau_{0.1}$ method maximizes the accuracy of prediction and the simplicity of measurement.

Calculate diffusion length, L

$$L = \sqrt{D\tau} \quad (2-7)$$

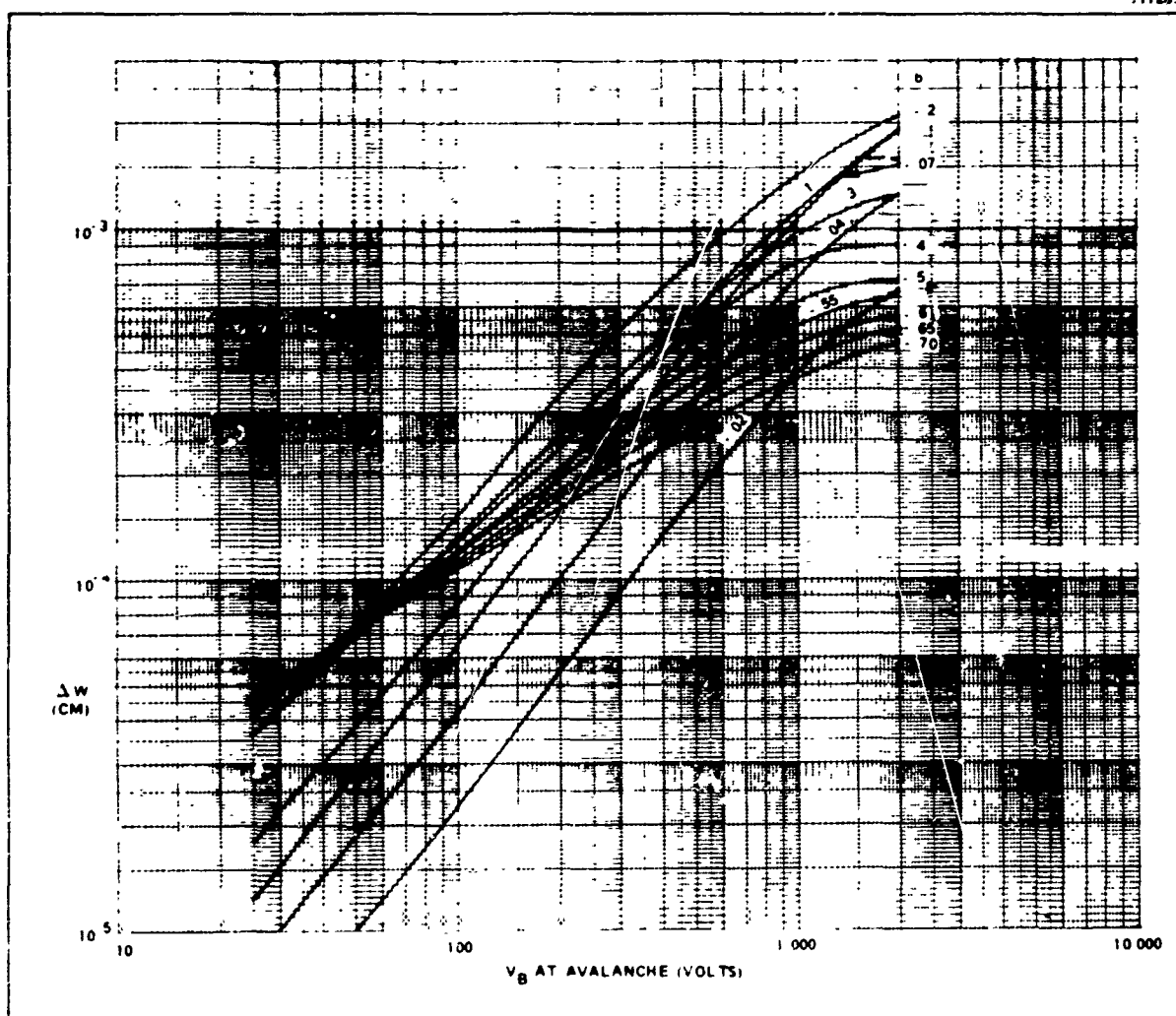


FIGURE 2-9 ΔW As A Function of V_B At Avalanche and b

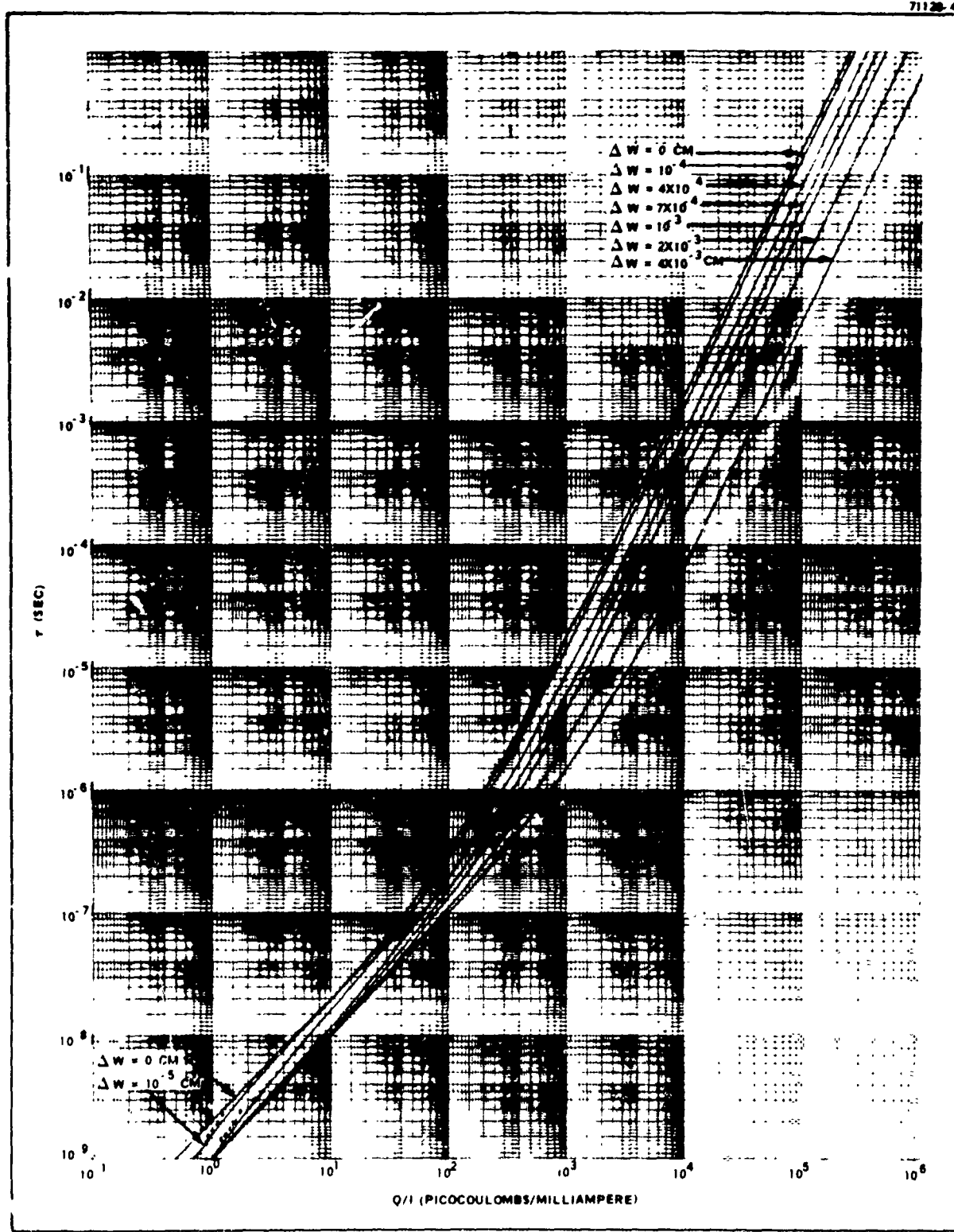


FIGURE 2-10 τ vs Stored Charge at Various ΔW 's

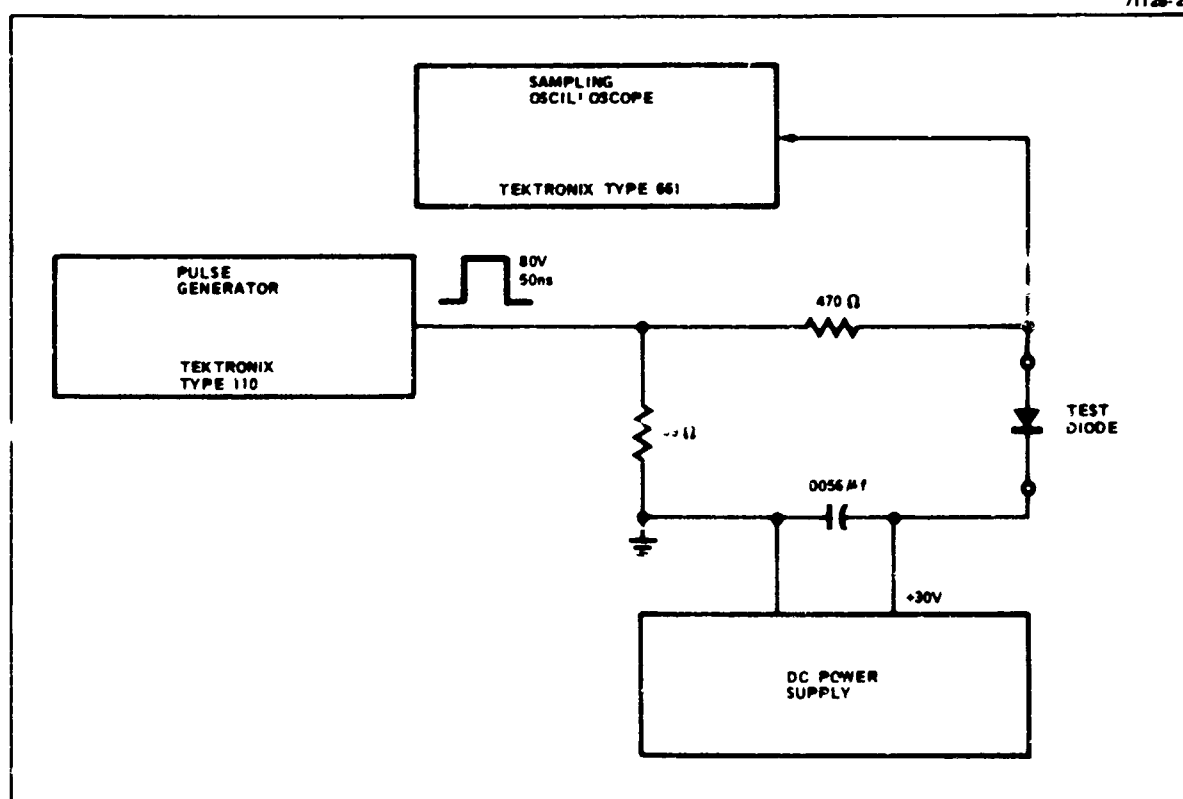


FIGURE 2-11 Diode Storage Time Measurement Circuit

where D is the diffusion constant ($D = 12.9 \text{ cm}^2/\text{s}$ for intrinsic silicon). Use $\tau_{0.1}$ or τ_s . For highly doped devices, the diffusion constant must be corrected for the effect of the impurity concentration, i.e., determine the effective D . The correction will probably be negligible for diodes with $V_A > 500$ volts. Reference 4 gives an iterative procedure to determine the effective D , and hence the effective L .

Calculate depletion width (w) at the voltage of interest

$$w = w_1 V_B^{-b} \quad (2-8)$$

where V_B = reverse bias terminal voltage plus 0.72 volt

Calculate i_{pp}

$$i_{pp} = qgA \left\{ \left[w + L \operatorname{erf} \sqrt{\frac{t}{\tau}} u(t) - w + L \operatorname{erf} \sqrt{\frac{t - t_p}{\tau}} u(t - t_p) \right] \right\} \quad (2-9)$$

where $qg = 6.36 \times 10^{-6} \dot{\gamma}$

For silicon material, t_p = radiation pulsewidth, and $\dot{\gamma}$ = absorbed dose rate in rad(Si)/s, when

$$\begin{aligned} t \gg \tau, i_{pp} &= \text{equilibrium photocurrent} = \Delta I_{CBO} \text{ (for transistors)} \\ &= qgA(w + L). \end{aligned}$$

For corrections for transistor i_{pp} predictions, at times less than the effective minority carrier lifetime in the collector ($t < \tau$), the collector-base diffusion component ($i_{pp} \text{ (base)}$) becomes important. Nonequilibrium photocurrent calculated from Equation 2-9 for $t < \tau$ should be corrected by the addition of $i_{pp} \text{ (base)}$. The $i_{pp} \text{ (base)}$ is given by

$$i_{pp} \text{ (base)} = (9.458)(10)^{-5} \dot{\gamma} A \sqrt{T_e} \text{ amperes} \quad (2-10)$$

or

$$i_{pp} \text{ (base)} = \frac{(2.02)(10)^{-5} \dot{\gamma} A}{\sqrt{f_T}} \text{ amperes} \quad (2-11)$$

T_e is the corrected base transit time in seconds measured with the transit time bridge described by Ashar.⁽⁵⁾ f_T is the measured gain bandwidth product of the transistor in Hertz. $\dot{\gamma}$ is the dose rate in rad(Si)/s and A is the junction area in cm^2 .

Radiation-induced photocurrent in transistors tends to turn the transistor ON. At a critical dose rate level, the transistors used in most circuit applications will saturate due to secondary photocurrent. The extension of saturation time (beyond the radiation pulsewidth) has been defined as radiation storage time (t_{SR}) and can be predicted using the following techniques⁽²⁾.

The transistor model in Figure 2-12 describes transistor operation in the saturation condition. The effect of radiation is to charge the storage element (S). This charge at the end of the radiation

pulsewidth (t_p) is :

$$Q_m = \tau \left[\Delta I_{CBO} \left(1 - e^{-t_p/\tau} \right) - \frac{I_{CS} + I_{B2}}{h_{FE} + 1} + I_{B2} \right] \quad (2-12)$$

where

- τ = collector minority carrier lifetime
- ΔI_{CBO} = equilibrium photocurrent
- I_{CS} = collector saturation current
- I_{B2} = base current at end of radiation pulse.

Storage time will persist until Q_m discharges to zero.
Storage time is calculated from the following expression:

$$t_{sR} = \tau \ln \left[\frac{\frac{Q_m}{\tau} + \frac{I_{CS} + I_{B2}}{h_{FE} + 1} - I_{B2}}{\frac{I_{CS} + I_{B2}}{h_{FE} + 1} - I_{B2}} \right] \quad (2-13)$$

A nomograph developed to solve Equations 2-12 and 2-13 is shown in Figure 2-13. Also included in this figure is a chart relating open-base storage time (t_{sR}^*) to the transistor electrical storage time, t_s (at $I_B = 100$ mA, 5 μ s pulse, and $I_C = 80$ mA).

The procedure for determining t_{sR} is: 1) measure electrical storage time t_s ; 2) measure pulsed h_{FE} at $I_C = 20$ mA; 3) calculate I_{CS} and I_{B2} for the particular circuit of interest; 4) enter nomograph

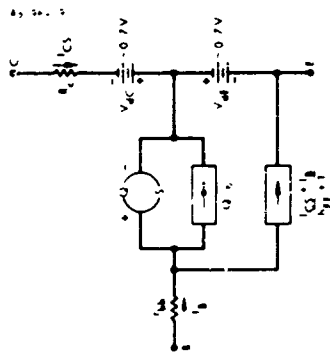


FIGURE 2-12 Transistor Radiation Storage Time Model

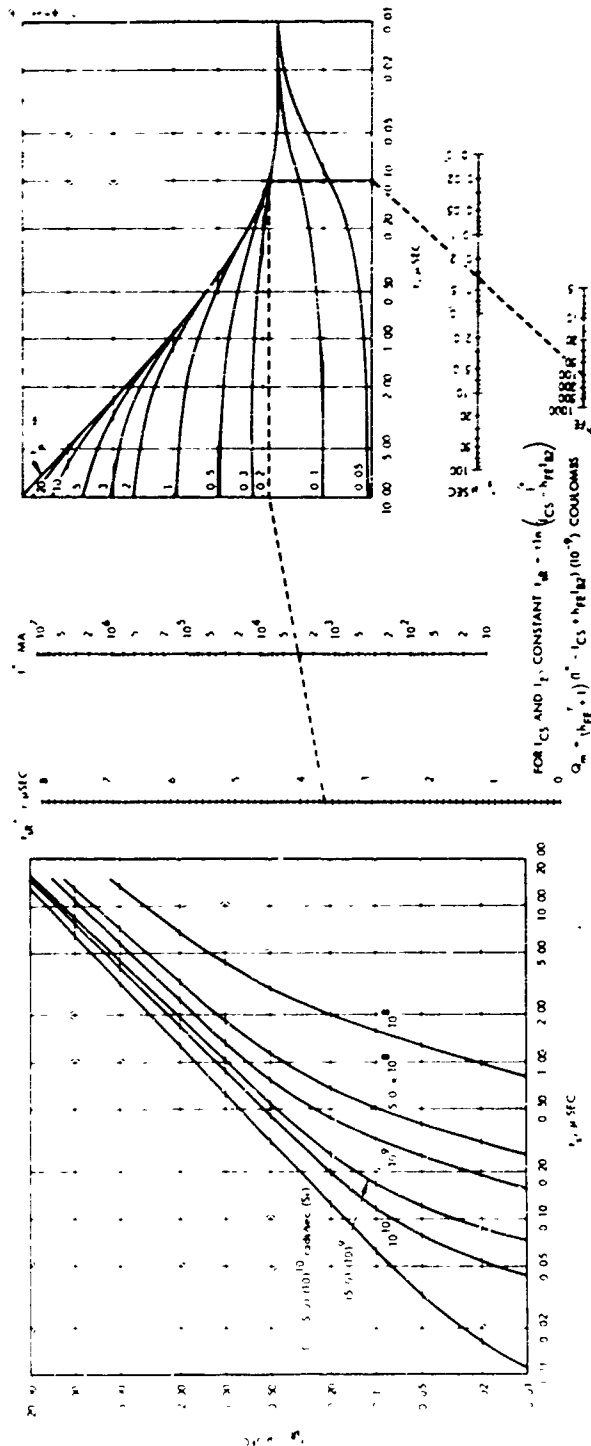


FIGURE 2-13 Radiation Storage Time Nomograph

and calculate t_{sR} at the dose rate and pulsewidth of interest; and
 5) if I_{CS} and I_{B2} are not constant, circuit equations must be integrated and solved for time to discharge Q_n .

2.3.2 Calculating Permanent Effects

Bipolar transistors are particularly susceptible to neutron-induced permanent damage. The damage threshold for most low-frequency high-power transistors will occur between 1×10^{11} and 1×10^{12} n/cm². Transistor parameters will be affected in the following manner:

- . f_T - will not change significantly for most transistors
- . V_{BE} - will increase
- . V_{SAT} - will increase
- . I_{CO} - will increase
- . h_{FE} - will decrease

The most significant change is the decrease in h_{FE} produced by the decrease in base minority-carrier lifetime. Recombination in the base region increases resulting in a decrease of the number of carriers injected from the emitter that reach the collector. After exposure to 1×10^{12} n/cm² some power transistors may have less than 10% of their initial h_{FE} remaining. High frequency, low-power transistors experience the smallest h_{FE} degradation. The increases in V_{BE} , V_{SAT} and I_{CO} will not be significant at 1×10^{12} n/cm².

Beta, or current gain capability, is by far the most

seriously degraded parameter for power circuits. This is illustrated in Figure 2-14, which shows measured beta degradation curves as a function of accumulated neutron dose for the 2N1016, 2N1613 and 2N2784 transistors. These transistors have power ratings of 150 watts, 0.8 watts and 0.3 watts respectively. Note the characteristic shape as the high power devices suffer beta degradation at lower neutron doses than do the low power devices.

An approximate expression for the transistor current-gain degradation is given by:^(1,6)

$$\frac{\beta_f}{\beta_i} \approx \frac{1}{1 + \left(\frac{7.0 \times 10^{-6}}{f_T} \right) \phi} \quad (2-14)$$

where β_f is the device current gain after irradiation,
 β_i is the device current gain before irradiation,
 ϕ is the neutron fluence in n/cm^2 ; energies ≥ 10 keV
 f_T is the device current gain-bandwidth product.

Note the dependence of β degradation on the gain-bandwidth product (f_T).

2.3.3 Estimating Transient Effects

Since transient radiation responses can be correlated to certain transistor electrical and/or geometrical parameters, a series of graphs have been developed⁽⁷⁾ which make it possible to estimate radiation responses. These graphs are derived from experimental data. The curves have an accuracy of better than one order of magnitude and should provide valuable information to the design engineer.

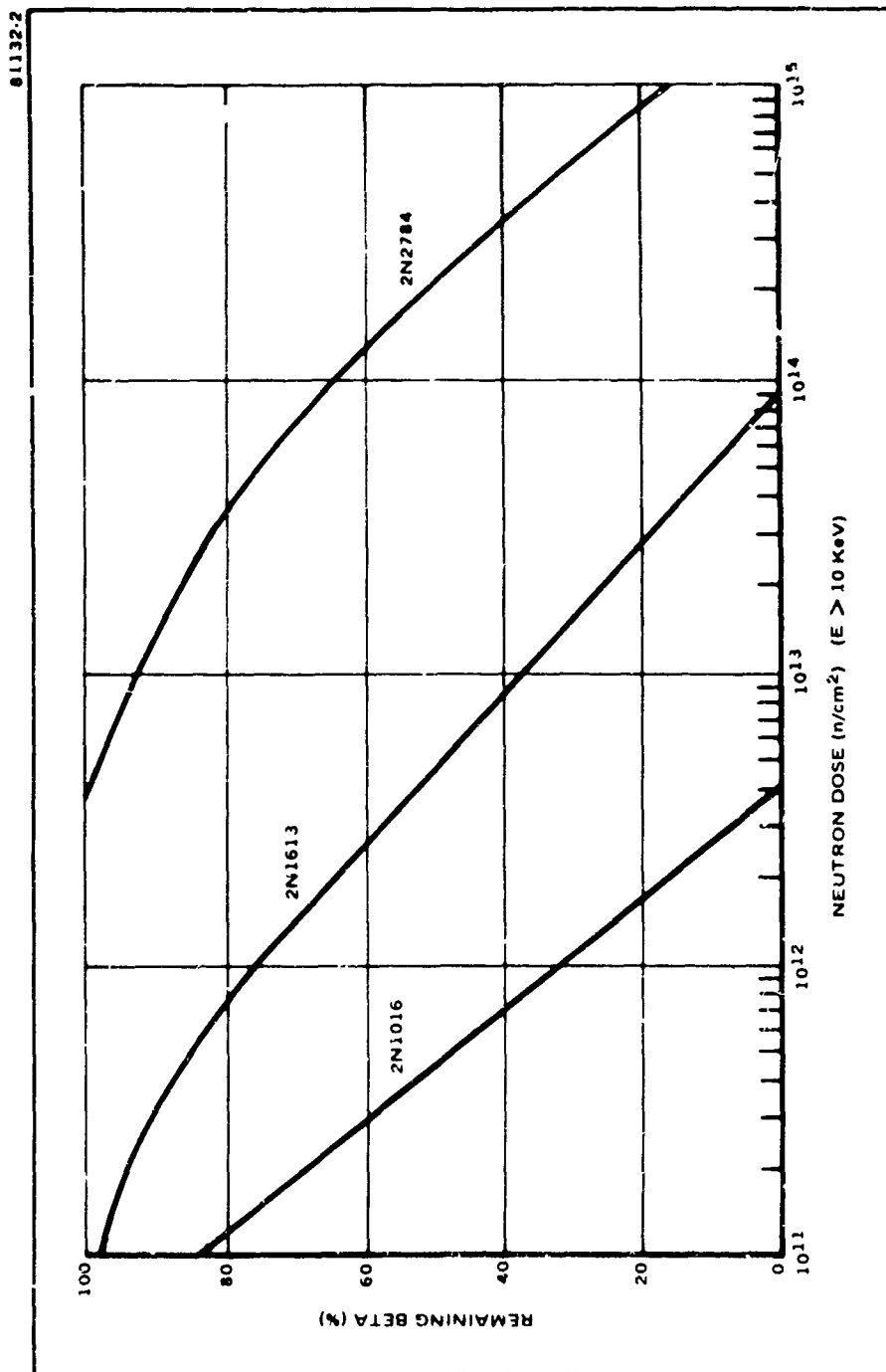


FIGURE 2-14 Beta Degradation vs Neutron Dose for Typical Transistors

Figures 2-15, 2-16 and 2-17 provide estimates of primary photocurrents i_{pp} as a function of f_T and transistor power ratings (P_C). The P_C is the rating at 25°C case temperature. Figure 2-15 should be used for silicon transistors rated at or below 2.5 watts. Also remember that i_{pp} is directly proportional to dose rate (to $\sim 10^{10}$ rad(Si)/s) and estimates of i_{pp} may be scaled accordingly. At rates higher than 10^{10} rad(Si)/s predictions are subject to increased error. Figure 2-16 should be used for silicon transistors rated at 3 watts or greater and Figure 2-17 should be used for estimates of i_{pp} for germanium transistors.

Figures 2-18, 2-19, and 2-20 provide estimates of radiation storage time (t_{sR}) for silicon and germanium transistors at a dose rate of approximately 6×10^9 rad(Si)/s. Figure 2-18 should be used for low power silicon transistors with P_C less than 3 watts and Figure 2-19 for silicon transistors with P_C greater than 3 watts (24°C case). Note the dependence of radiation storage time on f_T . Figure 2-20 provides an estimate of t_{sR} for germanium transistors as a function of P_C .

Table 2-2 lists the measured i_{pp} of various transistors at three bias voltages. Table 2-3 lists the measured i_{pp} and t_{sR} for 45 transistors (average of six samples). Appendix 1.0 is a tabulation of transistor radiation effects data.

2.3.4 Estimating Permanent Effects

Neutron-induced permanent degradation of transistors can be estimated using Figure 2-21 which shows normalized h_{FE} as a function of neutron dose for f_T 's of 1, 10, 100, 1K MHz. This graph was constructed by solving Equation 2-14 for the respective f_T 's at various neutron doses and will provide data for the design engineer of all transistors of better than $\pm 50\%$ accuracy. This, by knowing f_T and the expected neutron dose the decrease in h_{FE} can be predicted.

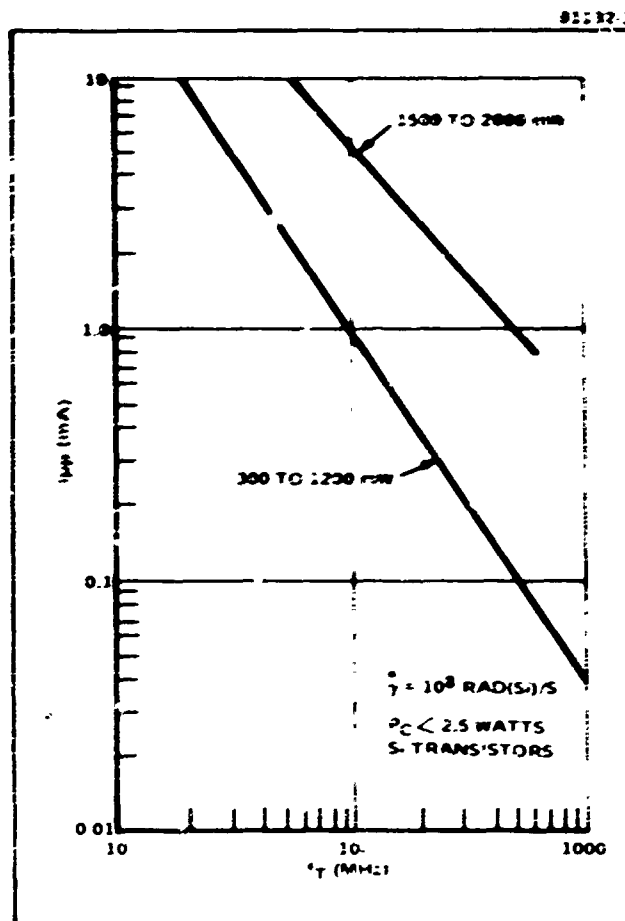


FIGURE 2-15 Primary Photocurrent (i_{pp}) vs f_T

81132-4

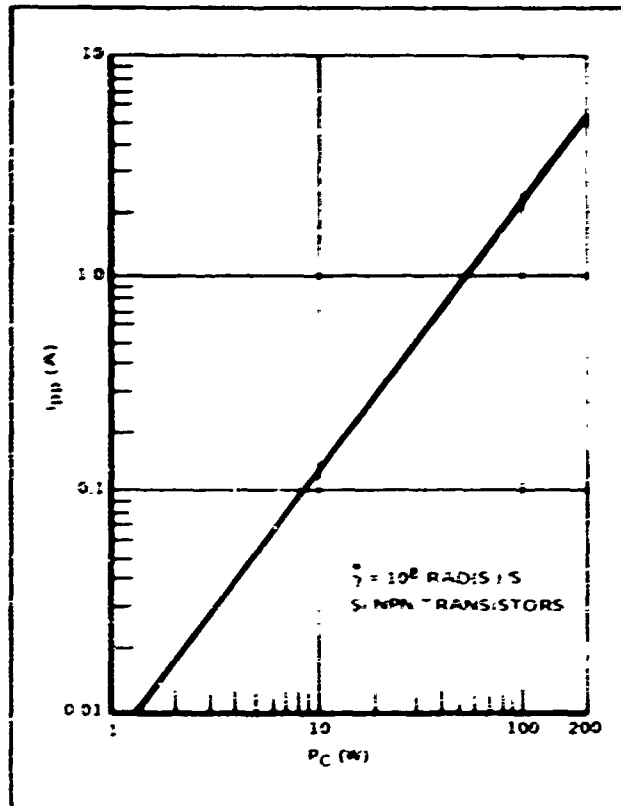


FIGURE 2-16 Primary Photocurrent (i_{pp}) vs P_C
(Silicon Transistors)

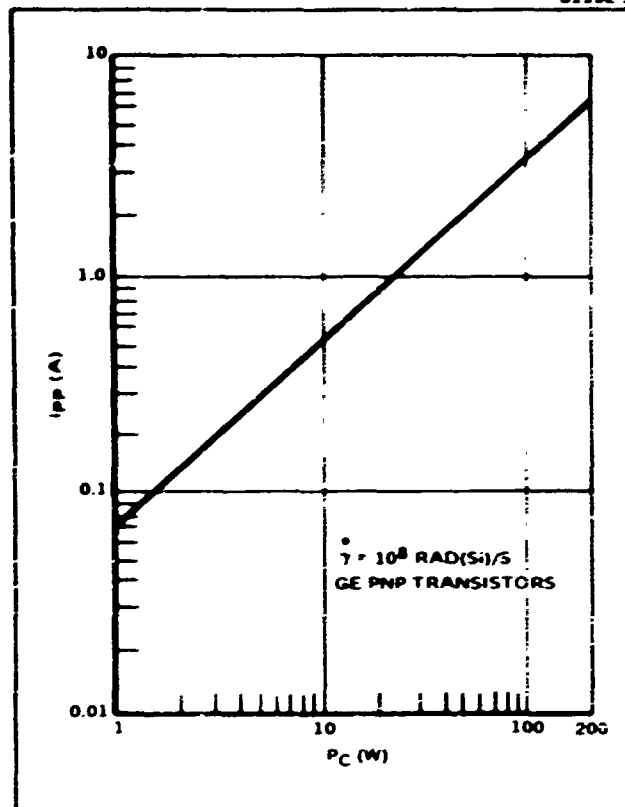


FIGURE 2-17 Primary Photocurrent (I_{PP}) vs P_C
 (Germanium Transistors)

81132-6

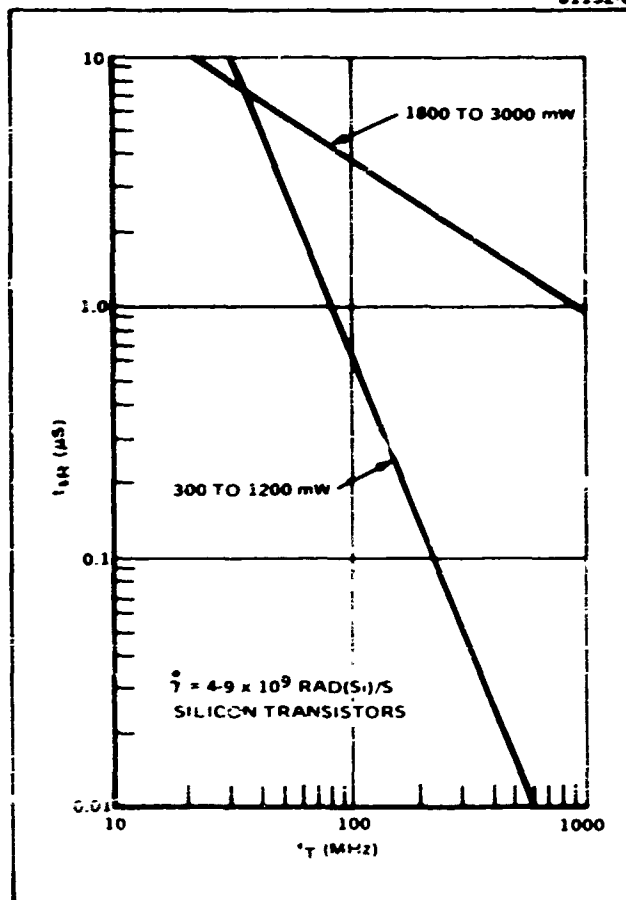


FIGURE 2-18 Radiation Storage Time (t_{SR}) vs f_T

01132-7

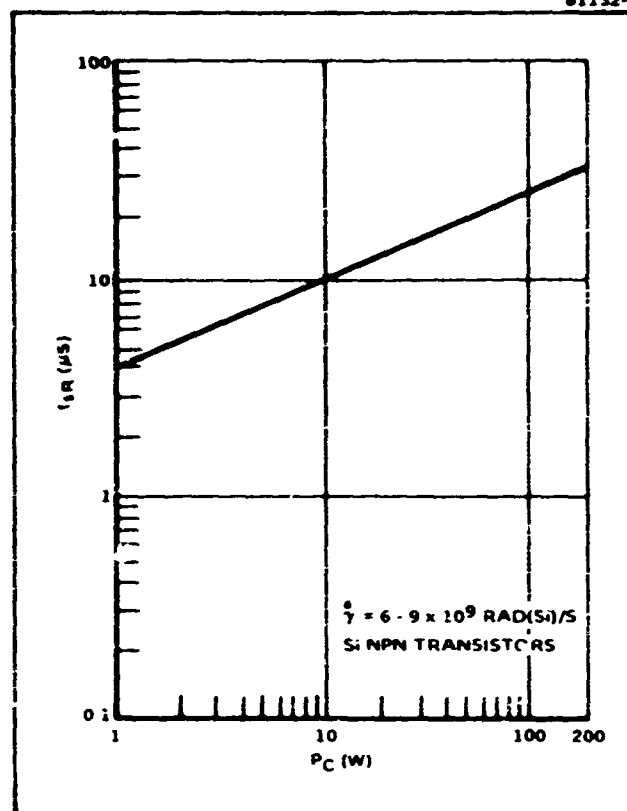


FIGURE 2-19 Radiation Storage Time (t_{SR}) vs P_C (Silicon Transistors)

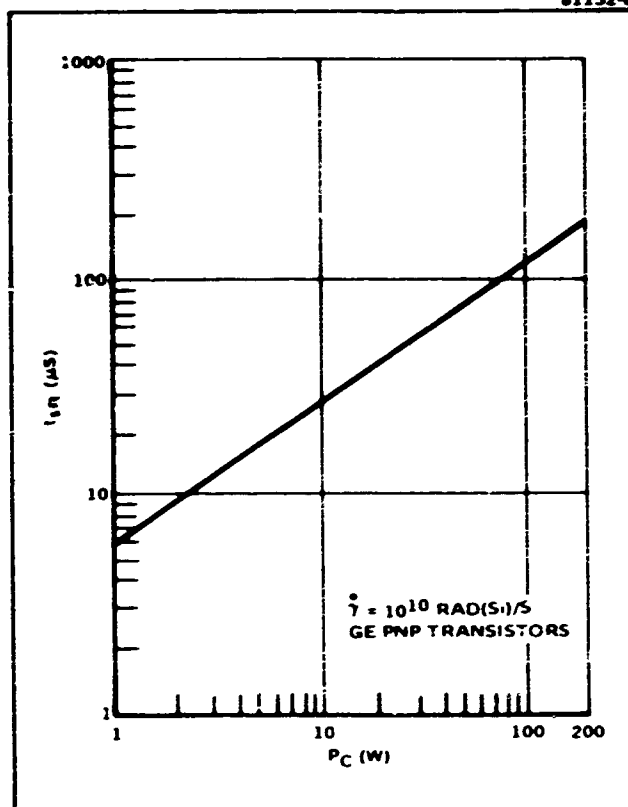


FIGURE 2-20 Radiation Storage Time (t_{SR}) vs P_C
(Germanium Transistor)

TABLE 2-2 Measured Transistor Equilibrium Photocurrent (37)

(Measured Equilibrium i_{pp} at 3.0, 6.0 and 15.0 Volts)

Transistor		$\dot{\gamma}$ $\times 10^8$ rad (SI)/sec	Equilibrium i_{pp} (mA) @ V_{BB} (volts) =		
No	Type		3.0	6.0	15.0
1	2N3242A	0.545	2.44	2.47	2.60
2		0.538	2.48	2.51	2.55
3		0.550	3.61	3.70	3.81
4		0.542	3.09	3.16	3.36
5		0.480	2.96	2.99	3.20
6		0.500	2.80	2.87	3.07
7		0.485	2.27	2.31	2.33
8	2N835	19.9	1.34	1.41	1.64
9		20.0	1.84	1.97	2.20
10		20.0	1.91	2.04	2.41
11		19.7	1.43	1.56	1.77
12		19.2	1.77	1.84	2.21
13		20.0	1.77	1.90	2.07
14		21.0	1.760	1.83	2.16
15	2N956	0.500	1.21	1.23	1.28
16		0.500	1.23	1.24	1.28
17		0.500	1.11	1.13	1.21
18		0.500	0.880	0.920	0.960
19		0.500	1.07	1.09	1.13
20		0.508	0.947	0.967	0.993
21		0.485	0.835	0.900	0.967
22	2N2222	0.555	1.08	1.13	1.15
23		0.490	0.967	1.02	1.10
24		0.550	1.29	1.31	1.51
25		0.500	1.25	1.28	1.47
26		0.538	1.13	1.15	1.27
27		0.588	0.953	1.01	1.09
28		0.512	0.947	0.960	1.01
29	2N916	0.500	0.393	0.396	0.433
30		0.488	0.375	0.388	0.408
31		0.500	0.437	0.450	0.464
32		0.512	0.461	0.501	0.541
33		0.512	0.459	0.477	0.517
34		0.473	0.395	0.408	0.453

TABLE 2-2 (Continued)

(Measured Equilibrium i_{pp} at 3.0, 6.0 and 15.0 Volts)

Transistor		$\dot{\gamma}$ $\times 10^8$ rad (Si)/sec	Equilibrium i_{pp} (mA) @ V_{BB} (volts) =		
No.	Type		3.0	6.0	15.0
35	2N2938	19.5	3.79	4.45	4.99
36		19.5	2.80	2.93	3.28
37		20.0	3.87	5.20	6.27
38		20.8	4.00	4.13	4.40
39		20.5	4.35	4.48	4.93
40		20.5	4.53	4.93	5.15
41		20.5	4.57	4.77	5.15
42	2N708	19.9	8.60	9.13	9.93
43		20.1	8.80	9.33	10.1
44		20.2	10.3	10.7	11.6
45		20.5	11.3	12.0	13.0
46		21.0	9.67	10.3	11.0
47		19.5	15.3	16.4	16.9
48	2N930	0.500	1.88	1.91	1.99
49		0.495	1.88	1.90	1.95
50		0.500	2.07	2.08	2.15
51		0.500	2.24	2.32	2.35
52		0.500	1.96	2.00	2.12
53		0.500	1.50	1.52	1.57
54		0.468	3.53	3.64	3.80
55	2N1711	0.545	3.87	4.00	4.13
56		0.525	3.57	3.71	3.84
57		0.525	4.75	4.83	5.15
58		0.550	3.89	4.03	4.21
59		0.550	4.27	4.45	4.80
60		0.525	5.47	5.55	5.63
61		0.462	4.48	4.56	4.61
62	2N3648	19.9	4.83	5.09	5.63
63		20.0	5.15	5.55	5.81
64		20.9	3.60	4.11	4.72
65		20.1	4.96	5.23	5.49
66		20.0	4.27	4.72	5.07
67		19.9	4.59	4.85	5.25
68		19.5	7.32	7.73	8.19

Table 2-2 (Continued)

(Measured Equilibrium i_{pp} at 3.0, 6.0 and 15.0 Volts)

Transistor		$\dot{\gamma}$ $\times 10^8$ rad (SI)/sec	Equilibrium i_{pp} (mA) @ V_{BB} (volts) =		
No	Type		3.0	6.0	15.0
69	2N918	20.3	2.92	3.99	4.99
70		20.0	1.69	1.79	1.95
71		20.0	2.65	3.45	4.45
72		20.3	1.76	1.89	1.96
73		20.8	2.20	2.37	2.44
74		19.5	3.52	3.71	3.92
75	2N697	0.512	0.520	0.555	0.627
76		0.505	0.413	0.427	0.480
77		0.500	0.336	0.355	0.389
78		0.550	0.371	0.411	0.424
79		0.525	0.333	0.381	0.408
80		0.550	0.405	0.459	0.520
81		0.500	0.443	0.456	0.499
82	2N1613	0.500	2.27	2.33	2.40
83		0.550	2.15	2.28	2.35
84		0.545	1.99	2.03	2.05
85		0.512	2.03	2.07	2.09
86		0.550	2.31	2.35	2.44
87		0.550	1.85	1.89	1.95
88		0.508	1.99	2.02	2.05
89	2N3498	0.525	6.00	6.27	6.67
90		0.525	4.24	4.51	4.64
91		9.525	4.40	4.59	4.95
92		0.500	4.00	4.48	4.67
93		0.545	3.87	4.35	4.40
94		0.500	3.87	4.13	4.40
95		0.488	3.31	3.35	3.37
96	2N1893	0.550	3.45	3.52	3.72
97		0.512	3.47	3.60	3.73
98		0.500	3.95	4.03	4.08
99		0.510	3.44	3.71	3.91
100		0.525	2.90	3.04	3.07
101		0.500	4.17	4.37	4.41
102		0.512	3.53	3.67	3.77

Table 2-2 (Continued)

(Measured Equilibrium i_{pp} at 3.0, 6.0 and 15.0 Volts)

Transistor		$\dot{\gamma}$ $\times 10^8$	Equilibrium i_{pp} (mA) @ V_{BB} (volts) =		
No	Type	rad (SI)/sec	3.0	6.0	15.0
103	2N3511	20.0	5.57	5.84	6.16
104		19.7	5.84	5.97	6.16
105		20.0	4.77	4.90	5.25
106		19.7	4.59	4.77	5.12
107		19.7	4.27	4.53	4.93
108		18.9	4.48	4.67	5.01
109		20.0	4.85	4.93	5.17
110	2N744	20.5	0.967	1.07	1.13
111		20.0	1.13	1.18	1.29
112		20.2	1.23	1.30	1.43
113		20.8	1.17	1.27	1.40
114		20.0	1.65	1.72	1.85
115		19.5	1.50	1.83	2.10
116		20.3	1.37	1.45	1.65
117	2N706	19.5	5.20	5.73	6.27
118		19.6	14.13	15.3	16.13
119		20.5	10.67	11.7	12.00
120		20.5	14.00	15.0	16.20
121		19.7	11.20	11.9	12.73
122		20.8	13.3	1.20	14.7
123	2N2481	20.0	1.73	1.93	2.09
124		20.0	1.45	1.55	1.65
125		20.0	2.41	2.95	3.21
126		20.7	1.41	1.45	1.51
127		19.5	1.59	1.62	1.67
128		20.5	1.23	1.29	1.37
129		20.3	1.63	1.70	1.79
130	2N718A	0.500	2.09	2.19	2.23
131		0.500	1.71	1.75	1.77
132		0.500	2.92	2.96	2.98
133		0.500	2.43	2.47	2.49
134		0.500	3.00	3.04	3.07
135		0.500	2.43	2.47	2.49
136		0.485	1.87	1.91	1.947

TABLE 2-3 Measured Transistor Photocurrent And
Radiation Storage Time(3,4)

Type	Mfr	Description	f_T (MHz)	$t_{SR}^{**@}$ $5 \times 10^9 \text{ rad(Si)}/s$ (μs)	$i_{pp}^{**@}$ $10^8 \text{ rad(Si)}/s$ (mA)	P_C (mW)
2N174	RCA	Ge PNP AJ 3	*.01	150	5430	150,000
2N329A	Ray	Si PNP AJ	*.5	5.76	43.2	380
2N329A	Ray	Si PNP "Mexa"	2.0	1.07	1.07	380
2N338	ETC	Si NPN GJ	2.0	3.97	6.00	125
2N338	GE	Si NPN GJ	*20	7.09	0.764	125
2N404	ETC	Ge PNP AJ		3.80	18.9	150
2N404	RCA	Ge PNP AJ	*.13	2.48	13.5	150
2N559	WE	Ge PNP MS	300	1.18	2.58	--
2N697	GE	Si NPN PL	50	5.15	6.16	2,000
2N700A	Mot	Ge PNP MS	500	0.95	3.14	--
2N705	Syl	Ge PNP ME	300	0.25	0.564	150
2N706	RCA	Si NPN K	350	0.024	0.085	1,000
2N708	Mot	Si NPN PE	300	0.024	0.167	1,200
2N708	RCA	Si NPN PE	300	0.017	0.096	1,200
2N709	Syl	Si NPN PE	600	-	0.045	500
2N718A	TRW	Si NPN PL	60	6.72	10.9	1,800
2N720A	TRW	Si NPN PL	50	5.75	11.3	1,800
2N732	Mot	Si PNP PE	120	1.31	4.45	1,500
2N760A	Tns	Si NPN PL	*.65	6.38	3.39	500
2N834	Mot	Si NPN ME	350	0.037	0.136	500
2N834	NSC	Si NPN EP	350	0.099	0.340	500
2N852	TI	Si NPN ME	300	0.0293	0.125	300
2N914	Ray	Si NPN PE	300	0.0783	0.173	1,200
2N916	TRW	Si NPN PE	300	0.042	9.494	1,200
2N918	Aml	Si NPN PL	600	-	0.066	300
2N918	Mot	Si NPN PE	600	0.390	0.289	300
2N930	Aml	Si NPN PL	30	4.55	1.92	300
2N930	NSC	Si NPN PL	30	7.63	3.87	300
2N964	Syl	Ge PNP ME	460	0.123	0.405	300
2N1132	Syl	Si PNP PE	60	1.51	2.98	2,000
2N1184B	RCA	Ge PNP AJ 3	.12	24.0	413	7,500
2N195	WE	Ge PNP MS	550	1.51	5.73	250
2N1490	Bax	Si NPN MS 3	*.04	21.5	2160	75,000
2N1499A	Spg	Ge PNP "MADT"	100	0.23	0.786	60
2N1500	Spg	Ge PNP "MADT"	120	0.13	0.679	60
2N1613	Aml	Si NPN PL	60	4.44	7.54	3,000

TABLE 2-3 (Continued)

Type	Mfr	Description	f_T (MHZ)	t_{sR}^{**Q} $5 \times 10^9 \text{ rad(Si)/s}$ (μs)	i_{pp}^{**Q} 10^8 rad(Si)/s (mA)	P_G (mW)
2N613	GI	Si NPN PL	60	3.38	5.82	3,000
2N1893	GE	Si NPN PL	50	9.02	15.7	3,000
2N2222	Mot	Si NPN PE	250	2.59	2.30	1,800
2N2222	NSC	Si NPN PE	250	2.76	2.51	1,800
2N2222	Spg	Si NPN PE	250	2.43	1.62	1,800
2N2369	Tns	Si NPN PE	500	-	0.043	1,200
2N2481	GI	Si NPN PE	300	0.065	0.165	1,200
2N2784	Syl	Si NPN PE	1000	-	0.035	300
2N2855	SSP	Si NPN PE	60	9.36	40.5	5,000

* f_B

** Average Value of Six Samples

AJ = Alloy Junction

GJ = Grown Junction

EP = Epitaxial

ME = Mesa Epitaxial

MS = Mesa

PE = Planar Epitaxial

PL = Planar

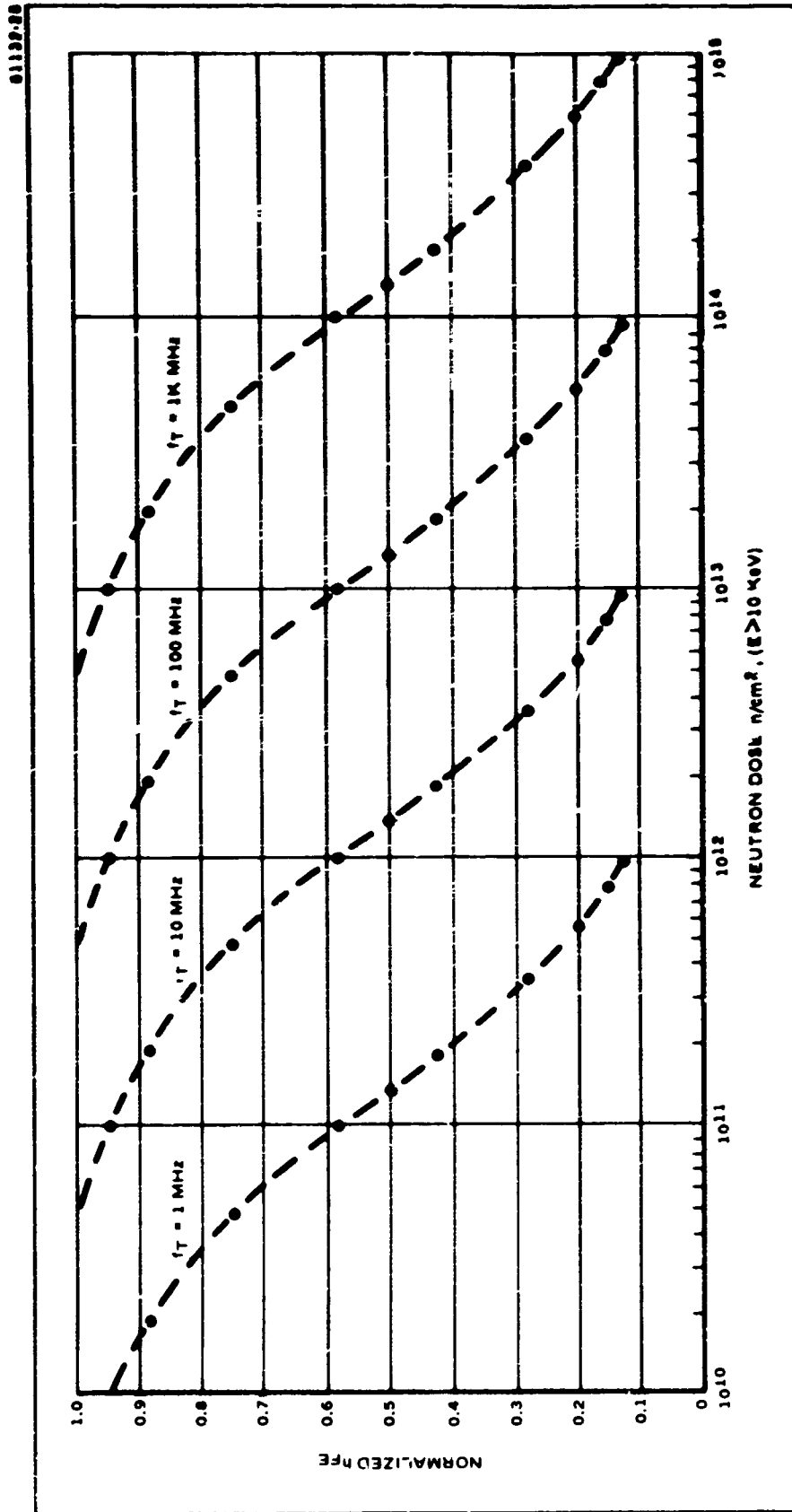


FIGURE 2-21 Normalized h_{FE} Degradation as a Function of f_T and Neutron Dose

2.3.5 Surface Effects

Exposure of a semiconductor device to high energy radiation results in two fundamental effects that can affect both surface and bulk. The first is associated with the electronic structure of the atoms of the material and the transfer of the incident radiation to the structure. This energy transfer in turn results in excitation and ionization of the atomic electrons that can be followed by a range of physical and chemical effects in the material of the device. The second effect produced by incident high energy radiation is the actual displacement of atoms from their normal position in the material lattice structure. This can occur, for example, in the collision of a fast neutron with a lattice atom in which the kinetic energy transferred to the lattice is sufficient to overcome the energy with which it is bound in the lattice. While the two effects are thus fairly distinct they are not unrelated. The displaced atom, for example, produced by the fast neutron, will ionize the material as it loses its kinetic energy. Again, there is evidence that in ionic crystals, an initial ionizing event, produced, for example, by the interaction of a high energy photon with an atomic electron, leads to the production of a displaced atom from a repulsion effect.

Early investigations of the effect of high energy radiation in semiconductor devices, dealt almost exclusively with the effect of bulk displacements on transistor gain. With the failure of the Telstar satellite in 1962,⁽⁸⁾ however, and the explanation of the effect as a result of surface radiation damage in transistors in the command circuits, resulting from the ionizing effects of space radiation, attention was directed to the problem of radiation induced surface effects.

Charge present in states at a semiconductor surface, will, depending upon the polarity of the charge, attract or repel mobile charge carriers from the bulk. This rearrangement of charge leads to one of three conditions. In the first, a depletion region is formed just under the surface, in which the mobile charge carrier density is reduced from that in the bulk, in effect forming a high resistivity region adjacent to the surface. In the second condition, which is a further progression of the first, the depleted region develops a sub-region next to the surface that consists of a conducting layer of charge opposite to that of the bulk. As an example of this consider an N-type semiconductor. The presence of a negative surface charge repels electrons from the surface regions leaving a space charge (the depletion region) of positive donors "depleted" of electrons. For a sufficiently large negative surface charge, holes will be attracted to the surface and will form the inverted conducting layer. The third condition results from a surface charge polarity that attracts rather than repels majority carriers. The resulting enhanced conducting layer at the surface is termed an accumulation layer. For example in an N-type semiconductor, the accumulation layer, consists of electrons forming a low resistivity conducting region next to the surface, that acts to shunt normal bulk carrier motion, degrading device performance.

2.3.5.1 Passivated and Unpassivated Devices

The grown junction, the alloy junction transistor and subsequently the mesa are examples of the unpassivated semiconductor device. In these devices the state of the surface generally was uncontrolled and junction interfaces were exposed to the ambient. It is characteristic of the unpassivated surface, that in anything but a very clean vacuum, it will tend to pick up a number of atomic layers of the ambient, usually oxygen. As a result of this process, surface states,

representing potential electron or hole trapping sites are produced at the semiconductor surface. These have been termed "fast" states, since they can interchange charge rapidly with the bulk, fast representing relaxation times of the order of 10^{-7} seconds. In addition to these states, other states, termed "slow" states will also form that are associated with foreign ions that are found in the semiconductor surface. The importance of these states is that they can directly control the electrical character of the device surface and consequently transistor gain and junction leakage currents.

In the passivated device⁽⁹⁾ as typified by the contemporary planar and planar-epitaxial transistor, these deleterious effects were preformedly modified. For the device the silicon surface is covered by a deliberately grown layer of oxide about 10^3 to 10^4 \AA in thickness. This has the effect of isolating the semiconductor surface from the ambient, thus passivating it. In a study made by Atalla,⁽¹⁰⁾ oxides grown at a temperature of 1000°C in dry or wet oxygen were stable over long periods of time. Measurements indicated that there were no effects from slow surface states and in the presence of either wet or dry nitrogen no shifts in surface conductivity resulted from the introduction of slow states. On the other hand, as in the case of the unpassivated surface, fast states are present with surface densities of the order of $10^{10} - 10^{11} \text{ cm}^{-2}$. Thus, the addition of the passivated layer generally improved unirradiated device performance by simply isolating the silicon surface under the oxide, from the ambient produced slow states. The result is a very low I_{CBO} and a more stable gain. The growth of the silicon oxide also improves emitter efficiency at low currents.

2.3.5.2 Radiation Effects in the Unpassivated Device

In general, unpassivated device response to radiation is complicated, with the results depending in varying degrees upon manufacturing processes. This accounts for the fact that particular device types from different manufacturers will lack uniformity in their response to radiation. The evidence appears to indicate, however, that the predominant effect of ionizing radiation in the unpassivated device is the formation of a conducting channel that is associated with a particular type of conducting layer as previously described. As discovered by Brown,⁽¹¹⁾ an anomalous leakage current can flow in an NPN structure as a result of conducting channel, in the form of an N-type inversion layer, across the P-region. This leads to a current paralleling that of the main junction current but due to a flow of the same conductivity type as the emitter and collector end regions. In the presence of radiation the channel will form as a result of the ionization of the ambient, the resulting ions diffusing or drifting to the semiconductor surface as a result of the fringing electric fields present at an exposed reversed bias junction.⁽¹²⁾ This effect, occurring at the collector base junction in a mesa device, was invoked by Blair⁽¹³⁾ in accounting for device malfunction in the Telstar satellite.

In general, the surface effect in the unpassivated device will be evident for radiation doses of the order of 10^3 rad(Si) as compared to 10^7 rad(Si) for the bulk effect. Saturation will occur at doses of the order of 10^7 rad(Si) for the surface effect.⁽¹²⁾ Experiments show that reverse bias leakage current for diodes and I_{CBO} and h_{FE} for transistors are the parameters most susceptible to the radiation surface effect.

In the diode, leakage currents can increase several orders of magnitude, and may or may not saturate. In the transistor, I_{CBO} exhibits a similar behavior. Common emitter current gain (h_{FE}) decreases with radiation exposure. Recovery can occur, however, and is enhanced by baking, the application of forward biasing, or exposure to radiation without bias.

Since the collector junction bias plays a role in the formation of the radiation induced channel, a strong dependence of I_{CBO} on applied bias should be observed. This was observed by Peck⁽⁸⁾ who demonstrated that a combination of both bias and radiation is necessary to produce I_{CBO} degradation. Generally, it was found that for a given radiation dose, I_{CBO} increased with increasing collector-base bias, and correspondingly, at a given bias I_{CBO} increased with increasing radiation dose. Peck also obtained evidence that a difference of potential between the transistor case and the semiconductor also affected I_{CBO} . The results, however, were not reproducible. A fairly extensive series of tests was carried out by Cocca and Koeppelaker⁽¹⁴⁾ on the effects of ionizing radiation on selected semiconductor devices from the approved parts list for the Nimbus satellite. Table 2-4 lists the unpassivated components tested.

A Co^{60} gamma source was utilized to perform the tests at a dose rate of 10^5 rad(Si)/h. The transistors had a 10 V collector-base junction voltage. The signal diodes were reverse-biased at the same potential. Bias supply voltages were monitored throughout the test and remained within two percent of their rated values. Typical results are shown in Figures 2-22, 2-23, 2-24 and 2-25.

TABLE 2-4 Radiation Test of Unpassivated Devices (14)

Type	Class	No. Tested	Material	Structure	Case Connection	f_t , in, Mc
2N396A	PNP	6	Ge	Alloy	Base	Low level switch 5
2N1132	PNP	6	Si	Mesa	Collector	Power switch 60
2N1248	NPN	5	Si	Diffused Junc.	Isolated	Low noise 5
2N1358A	PNP	5	Ge	Alloy	Collector	Power switch 5
2N1676	PNP	5	Si	Alloy	Collector	Low level 40
1N758A	Zener	5	Si	Voltage regulator ...
1N914	...	5	Si	Computer switch ...

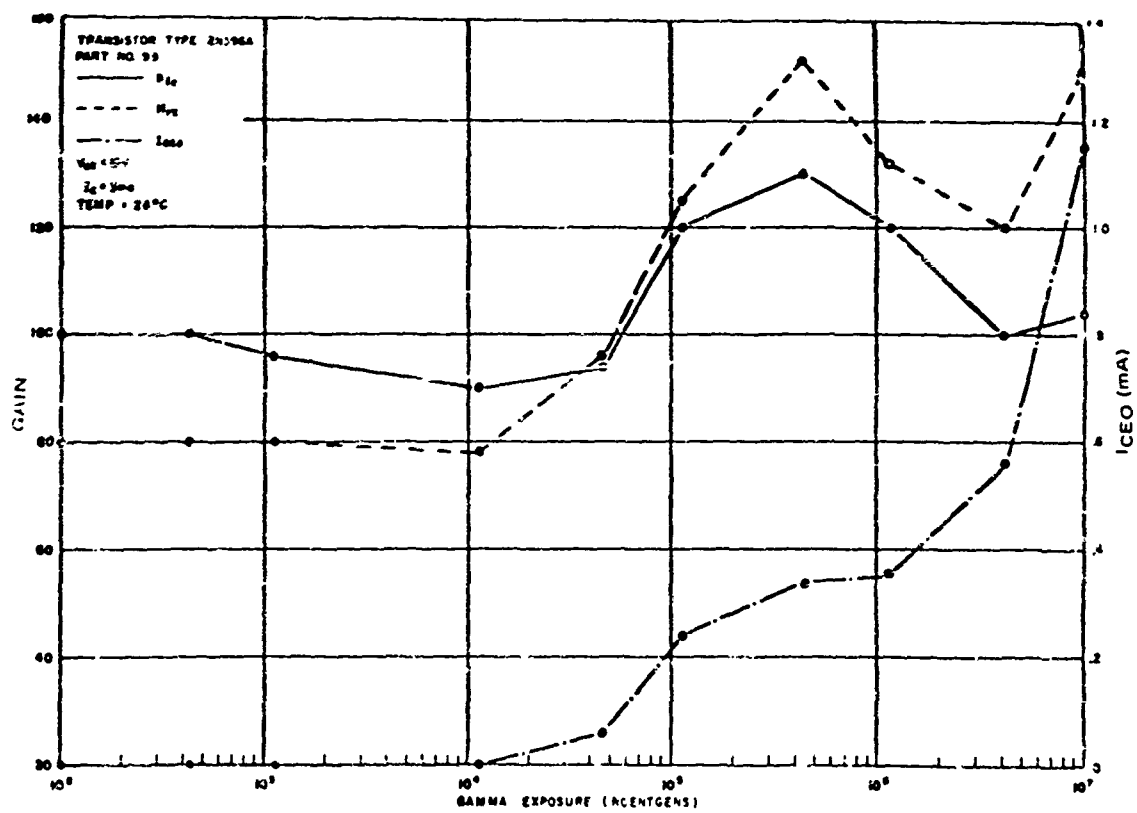


FIGURE 2-22 Gain versus Gamma Exposed for a PNP Ge Alloy 2N396A Transistor

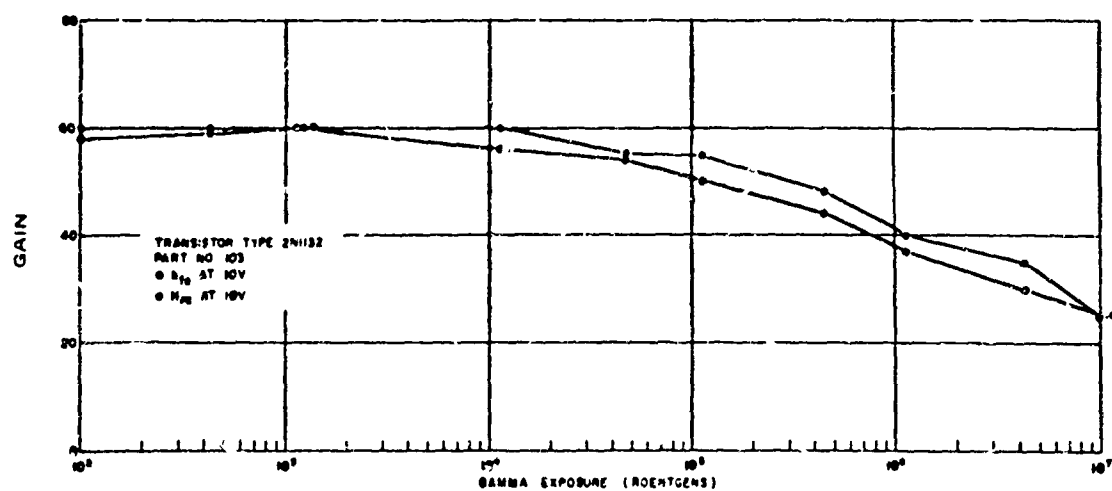


FIGURE 2-23 Gain Degradation of a PNP Si Mesa 2N1132 Transistor

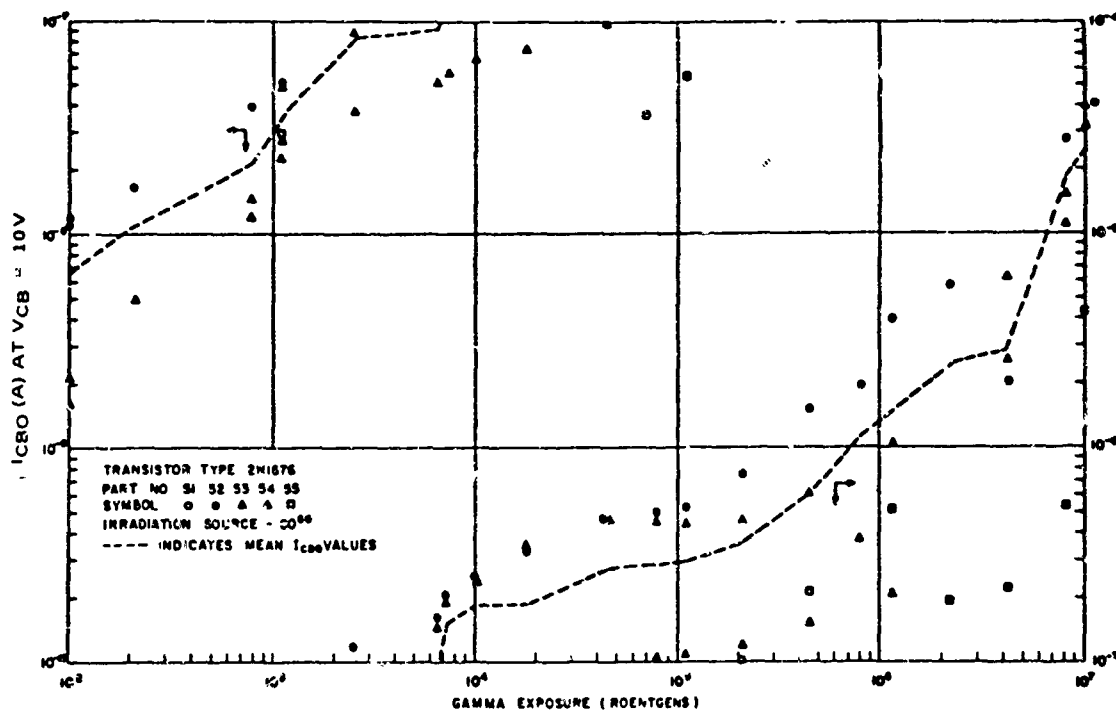


FIGURE 2-24 Radiation Damage of a PNP Si Alloy 2N1676 Transistor

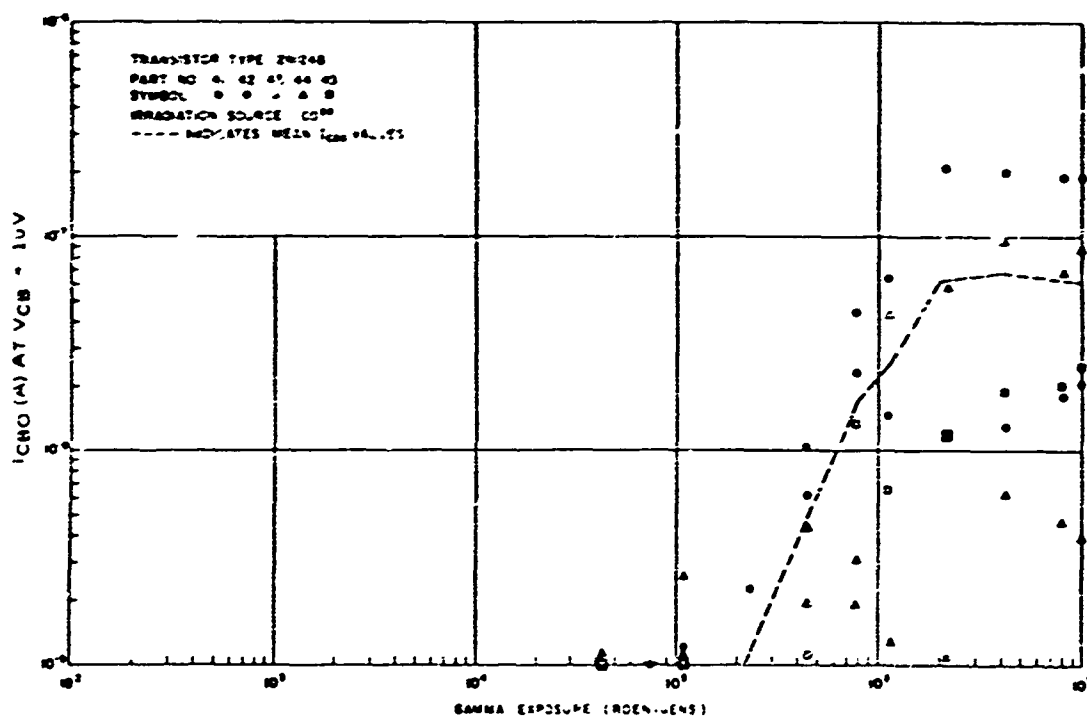


FIGURE 2-25 Radiation Damage of a NPT Si Diffused Junction
 2N1248 Transistor

2.3.5.3 Radiation Effects in the Passivated Device

The silicon planar transistor passivated with a layer of thermally grown silicon dioxide represents a distinct advance over its predecessor, in effectively isolating the surface, particularly the junction regions, from the ambient. This isolation, however, in sandwiching an insulating material between the silicon and the ambient, necessarily places in contact with it a material that can interact itself in a complex way with the ambient. Accordingly, experiments have demonstrated that, while the planar is an improvement over the mesa transistor, for example, ionizing radiation will affect planar operation as well.

In experiments carried out by Hughes⁽¹⁵⁾ a total of 150 silicon planar devices were studied before, during, and after exposure to 1×10^6 rad(Si) of cobalt 60 gamma irradiation at a rate of 2.75×10^4 rad(Si)/min and at an ambient temperature of 25°C . Both NPN and PNP devices were tested and significant differences were observed in two types in their response to radiation. For a 2N2222, the common emitter current gain, in a selection of 10 units, showed a decrease ranging from 11 to 41 percent as a result of exposure to 1×10^6 rads(Si). Five of the units were held at a collector-base bias of 15 volts and the other five were unbiased. There was no significant difference noted in the response of the two groups. For PNP transistors, only a "relatively" small amount of h_{FE} decrease was observed when the devices were unbiased during irradiation. When the PNP devices were biased during irradiation, however, h_{FE} decreased by "tens of percent." In addition, PNP devices exhibited an increase in I_{CBO} of two to four orders of magnitude during irradiation. In order to test the possible effect of the encapsulating gas surrounding the device, an irradiation under high vacuum was carried out. In this test 2N2801 PNP transistors

were tested and the results indicated that the I_{CBO} and gain degradation persisted under radiation exposure both with and without bias. It was concluded, therefore, that the surface degradation of the silicon planar device does not depend on conditions external to the device. It is not evident that this conclusion also holds for the NPN device, however, since vacuum-irradiation tests were not reported. The transistor gain test data are presented in more complete form in Tables 2-5 and 2-6, taken from Hughes paper.⁽¹⁵⁾ The behavior of the leakage current (I_{CBO}) as a function of dose is shown for a 2N2222 in Figure 2-26 and for a 2N2801 in Figure 2-27.

2.3.5.4 Device Selection Recommendations

The radiation test results given above make it clear that there will be degraded device performance in an ionizing environment. This will be true for the passivated as well as the unpassivated device. Generally, the effect depends on bias and radiation and it is recommended that provision be made for bias removal if circuit considerations permit. The data of Hughes⁽¹⁵⁾ appears to warrant the recommendation that NPN planar devices be used rather than PNP type insofar as gain degradation is concerned. In the dose ranges up to 10^5 rad(Si), the radiation induced increase in I_{CBO} appears to be about the same for each type. To the extent that circuit selection and design permit, operation with forward bias on emitter-base and collector-base junctions seems preferable. Under normal bias conditions with collector-base reverse-bias, the smallest bias level consistent with circuit requirements should be used.

For unpassivated devices, germanium is recommended in applications where only small fractional changes in I_{CBO} can be tolerated. Silicon unpassivated devices exhibit order of magnitude changes in I_{CBO} . A silicon mesa 2N1132 exhibits a I_{CBO} decrease of

TABLE 2-5 2N2222 NPN Silicon Planar Transistor (15)

h_{FE} at $V_{CE} = 2.5$ V and $I_C = 2.5$ mA

Unit	Before Irradiation	After (10^6 rad)	% Difference	Reverse Bias During Irradiation V_{CBO} Volts
1	100	80	20	+15
2	150	110	27	+15
3	175	115	34	+15
4	175	120	31	+15
5	175	120	31	+15
6	155	110	29	0
7	160	120	25	0
8	110	65	41	0
9	62	55	11	0
10	95	64	33	0

Table 2-6 2N2801 PNP Epitaxial Planar Transistor (15)

Beta (h_{fe})

Unit	Before Irradiation	After Irradiation (10^6 rad)	% Difference	Collector- Base Bias During Irradiation
1	106	23	78.2	-15 V dc
2	100	33	67.0	-15 V dc
3	90	40	55.5	-15 V dc
4	160	105	34.4	-15 V dc
5	150	38	74.8	-15 V dc
6	175	100	42.8	-5 V dc (60 cps)
7	80	28	65.0	-15 V dc
8	130	80	38.4	-15 V dc
9	95	53	44.2	-15 V dc
10	105	95	9.5	0
11	130	24	81.6	-15 V dc
12	105	26	75.2	-15 V dc
13	115	100	13.0	0
14	110	95	13.6	0
15	105	90	14.3	0

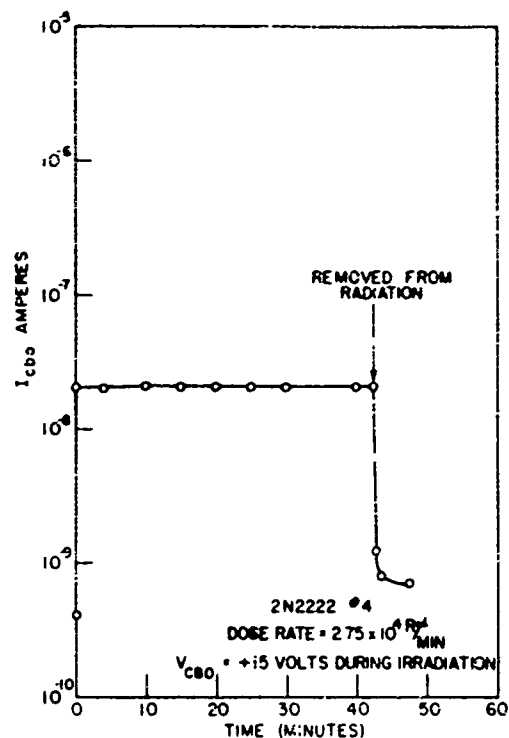


FIGURE 2-26 Effect of Radiation on Leakage Current of a 2N2222 Transistor

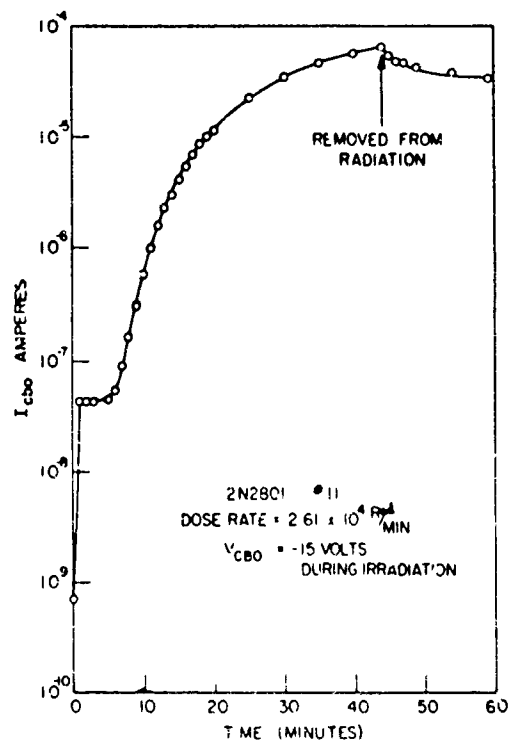


FIGURE 2-27 Effect of Radiation on Leakage Current of a 2N2801 Transistor

about an order of magnitude in the range $10^4 - 10^5$ rad(Si) with h_{FE} decreasing in the same range by about 12%.

2.3.6 Beta Annealing

Immediately after a neutron pulse, transistor beta is degraded to lower values than at later times. This phenomenon has been called rapid or beta annealing. In order to relate this time-dependent beta degradation to permanent beta degradation, an annealing factor is used. The annealing factor (f) at time (t) after a neutron pulse, is defined as:

$$f = \frac{\frac{1}{\beta(t)} - \frac{1}{\beta_i}}{\frac{1}{\beta_f} - \frac{1}{\beta_i}} \quad (2-16)$$

where β_i , β_f and $\beta(t)$ are the initial, final, and time-dependent betas. It follows that the annealing factor is the factor by which the neutron fluence must be increased to evaluate time-dependent beta degradation from the permanent beta degradation. For example, suppose the annealing factor is two at 1 ms, and one wishes to determine the beta degradation at 1 ms after a neutron pulse of 1×10^{14} n/cm². The beta decrease at 1 ms is then equal to the permanent decrease at 2×10^{14} n/cm².

Many annealing factors have been measured at Hughes,⁽¹⁶⁾ and an active program is now extending these measurements as well as developing a theoretical model for the effect. A few examples of this data are shown in Figure 2-28, where annealing factors for the 2N2222, 2N1613, 2N5016, and 2N709 transistors are shown for times between 200 μ s and 100 s. The fact that the annealing factors have significant

values over so many decades of time demonstrates that the rapid annealing factor must be considered in the selection of components.

The analysis⁽¹⁷⁾ shows that diffusion predominates in the time regime between a few ms and several s. The data agree with a relatively simple \sqrt{t} law, and the parameters derived from the data are consistent with a simple model that depends on the diffusion of atomic defects. An analysis that predicts the time dependence at earlier times than a few ms is now being developed.

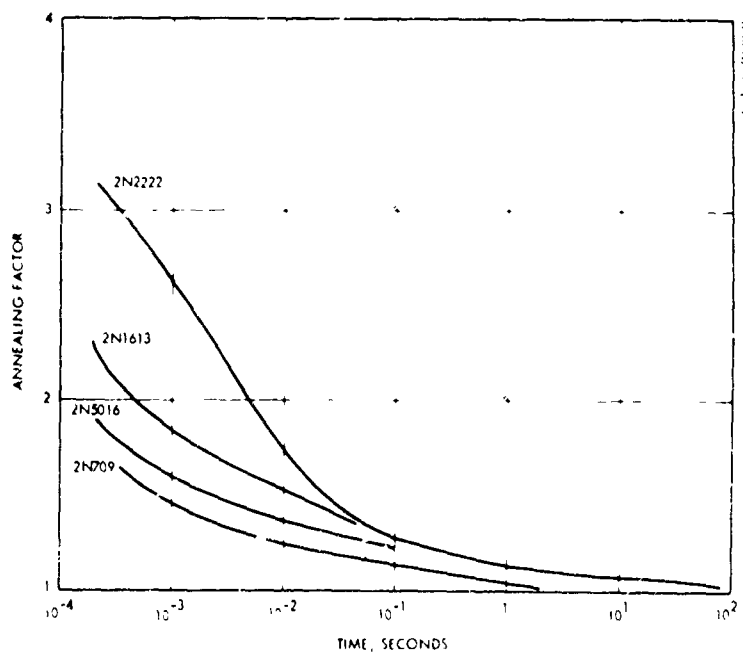


FIGURE 2-28 Annealing Factor of Transistors as a Function of Time After a Neutron Pulse

2.4 Diodes

The effects of nuclear radiation on semiconductor diodes are transient in nature. The permanent damage caused by neutrons can usually be considered negligible. Reverse-biased diodes will conduct during the radiation pulse and forward-biased diodes will conduct slightly more.

The total equilibrium photocurrent response of a reverse-biased diode is composed of a depletion component and an equilibrium diffusion component. In equation form: ^(1,4)

$$\begin{aligned} i_{pp} &= i_{ppw}(\text{depletion}) + i_{ppl}(\text{diffusion}) \\ &= qgA(w + L) \end{aligned} \tag{2-17}$$

where: q = charge on the electron
 g = generation rate
 A = junction area
 w = width of depletion region
 L = diffusion length

The generation rate of electron-hole-pairs is directly proportional to the radiation dose rate (\dot{V}). Consequently, equilibrium photocurrent is directly proportional to dose rate (assuming the density of induced electron-hole-pairs does not exceed the doping level of the semiconductor diode).

Photocurrent values will range from tens of milliamperes to several tens of amperes. The amount of photocurrent depends on the power

rating and reverse voltage rating of the diodes. Diode types can be arranged in an order of increasing i_{pp} generation as follows:

- . Hot carrier
- . Step recovery
- . High frequency switching
- . Varactors (low power)
- . Medium current diodes (50 mA to 1A)
- . Power diodes > 1 A

The differences in the first four types may be negligible. Tunnel diodes are the most radiation-hard active devices. Shockley diodes and SCR's will turn on during the radiation pulse and remain on until power is removed and should be avoided or used with caution. Zener diodes operating well in the zener region will conduct more heavily during the radiation pulse; however, this effect should be negligible.

Figure 2-29 shows the measured photocurrent as a function of gamma radiation for a number of diodes. Note that at a dose rate of 5×10^8 rad(Si)/s photocurrents range from 0.2 mA to 30 mA.

Table 2-7 is a tabulation of measured diode photocurrents at various dose rates and three different reverse-bias voltages.

Figure 2-30 shows measured photocurrent as a function of the diode maximum forward rectified current (I_0) for several diodes at two dose rates. This curve can be used to estimate diode photocurrent when no measured data is available.

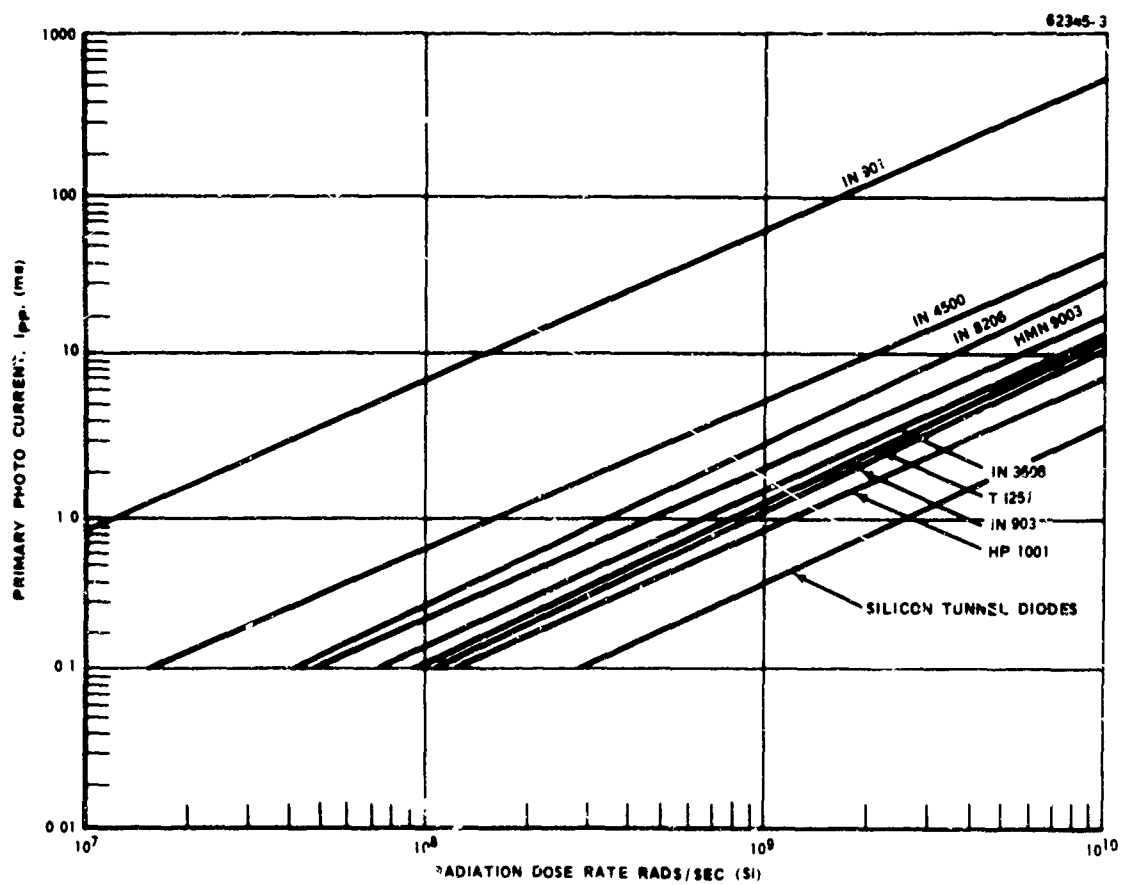


FIGURE 2-29 Primary Photocurrent vs $\dot{\gamma}$ for Various Diodes

TABLE 2-7
MEASURED DIODE EQUILIBRIUM PHOTOCURRENT
AT THREE REVERSE BIAS VOLTAGES (4)

Diode No.	Type	Dose Rate * 10^8 rad (Si)/s	Equilibrium i_{pp} (mA)/reverse bias (volts)		
			at V_{BB1}	at V_{BB2}	at V_{BB3}
1	1N643	5.0	9.53/1.6	10.43/12.7	11.03/24
8	1N3730	5.0	11.93/1.6	13.26/12.7	13.93/24
14	1N3064	5.0	1.00/1.6	1.13/12.7	1.21/24
21	1N3070	5.0	3.28/1.6	3.88/12.7	4.38/24
35	1N691	5.0	15.00/3.1	15.86/12.7	16.53/24
42	1N697	5.0	16.00/3.1	16.66/12.7	17.53/24
49	1N4087	5.0	1.53/1.6	1.77/12.7	1.96/24
61	1N3600	5.0	0.57/1.6	0.78/12.7	0.88/24
68	1N914	5.0	0.41/1.6	0.55/12.7	0.76/24
109	1N659	5.0	0.68/1.6	0.82/12.7	0.94/24
116	1N4533	5.0	0.29/1.6	0.41/12.7	0.50/24
143	1N662	5.0	0.60/1.6	0.84/12.7	1.10/24
55	1N4376	20.0	0.57/1.6	1.12/12.7	2.48/26
28	1N3595	0.50	2.13/3.1	2.33/12.7	4.00/46
75	1N645	0.50	21.20/3.1	21.20/12.7	23.73/46
82	1N649	0.50	22.13/4.5	22.80/12.7	23.47/46
88	1N483B	0.50	7.65/3.1	7.87/12.7	8.45/46
95	1N485B	0.50	4.35/3.1	4.35/12.7	4.88/46
102	1N3577	0.50	13.67/3.1	13.67/12.7	14.13/46
123	1N3189	0.50	63.73/4.5	69.07/12.7	71.73/46
129	1N3191	0.50	106.7 /28.5	120.0 /40.0	130.0 /46
136	1N560	0.50	Saturated	Saturated	90.0 /46

* Normalized dose rate.

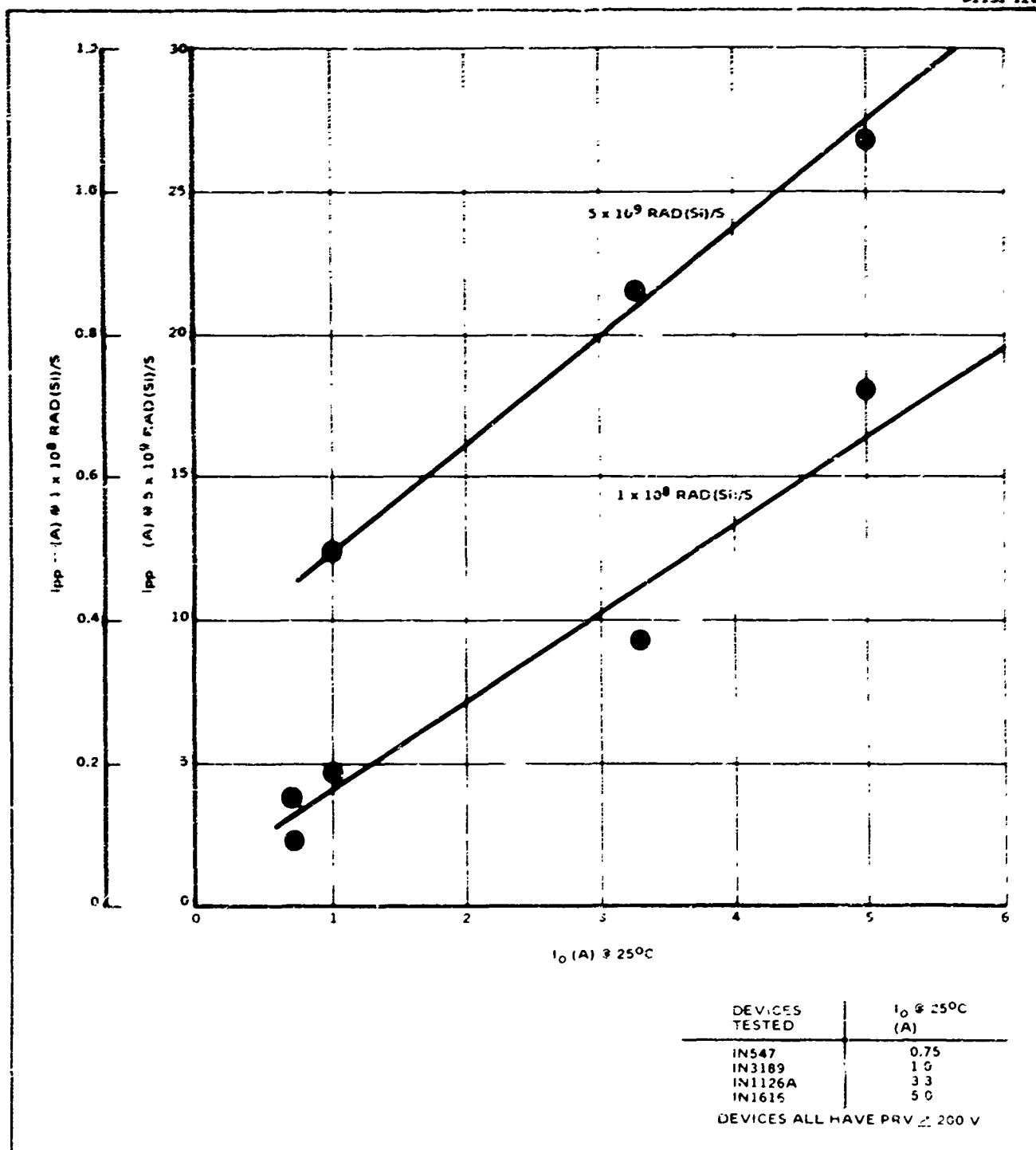


FIGURE 2-30 Measured Diode Photocurrent
(Data taken at 0.2 μs Pulse Width)

2.5 Integrated Circuits

2.5.1 General Discussion

Although integrated circuits currently are not widely used in power supply subsystems, they nevertheless have several important influences on power subsystem operation in a nuclear environment. The first consideration is that integrated circuits are finding increasing application in power supplies particularly in the control functions for pulse width modulated switching regulators. Another recent development that will influence power supply design is the integrated circuit low current regulator designed for on-card regulation. On-card regulation appears attractive both from electrical considerations and radiation considerations when compared with the alternate technique of building a high wattage supply and distributing the power to circuit cards. The above considerations will influence future power subsystem design.

An important problem connected with integrated circuits, which is associated with currently existing systems and their interaction with radiation, is that many of the loads for space power subsystems consist entirely of integrated circuits. Integrated circuits can prevent a severe transient load on the power supplies under irradiation. Therefore, discussions of the effects of radiation on integrated circuits are included.

Integrated circuits behave as assemblages of components on exposure to a high dose rate transient radiation pulse. Primary photocurrent (i_{pp}), external ionization, and secondary emission effects occur. The radiation environment may cause all integrated circuits to either turn ON or OFF or saturate depending on the type of circuit (digital or linear) and

the circuit application. Storage time analogous to t_{SR} for transistors also occurs. However, in monolithic integrated circuits, the most important transient effect is due to the substrate response to ionizing radiation, and the substrate interaction with the active devices. For high radiation levels, the substrate photocurrents are on the order of amperes and may exist for several microseconds.

Many integrated circuits in an electronic system will be ON and saturated when the transient radiation dose rate reaches 1×10^5 rad(Si)/s. Therefore, the prime consideration in hardening integrated circuits above this level should be the prevention of catastrophic failures. See Section 2.6.

In regard to neutron damage, presently available monolithic integrated circuits have critical radiation thresholds well in excess of 10^{13} n/cm² for normal fan-outs.

Neutron damage effects and transient radiation effects are summarized below.

2.5.2 Permanent Damage Effects

Neutron radiation produces the following effects in integrated circuits:

- . h_{FE} decreases
- . Leakage currents increase
- . Minority carrier lifetime decreases
- . Breakdown voltages increase

The predominant effect will be to decrease h_{FE} . As h_{FE} decreases, the available circuit output current decreases, output voltages in the ON state increase and eventually circuits cease to function properly, particularly if fully loaded.

2.5.2.1 Gates

Typical integrated gate circuits are shown in Figure 2-31. The principal damage in monolithic circuits is the degradation of the output transistor dc forward current gain, h_{FE} . This is not apparent in the OFF state of a gate circuit, since no current flows during this condition. For this reason, neutron damage tests are performed with the gate circuit in the ON state. In this state the transistor is saturated. As the current gain degrades, the collector current decreases and the device may come out of saturation. If this occurs the output voltage (V_{ON}) will begin to increase. Circuit failure occurs when V_{ON} reaches a value such that adequate noise margin can no longer be maintained. The critical value of V_{ON} is assumed to be 0.3 volts for RTL and RCTL gates and 0.5 volts for the DTL gates. The neutron fluence at which these values are reached is defined as the critical radiation threshold for permanent damage.

In order to observe measurable damage at a neutron dose of 2.7×10^{14} n/cm², very large fan-outs are required. Tests were performed with fan-outs of 10 and 15.⁽¹⁸⁾ Tables 2-8, 2-9 and 2-10 list these threshold damage levels.

2.5.2.2 Flip-Flops

The effect of neutron degradation of flip-flop circuits are evaluated in two ways.⁽¹⁸⁾ The first method consists of observing the

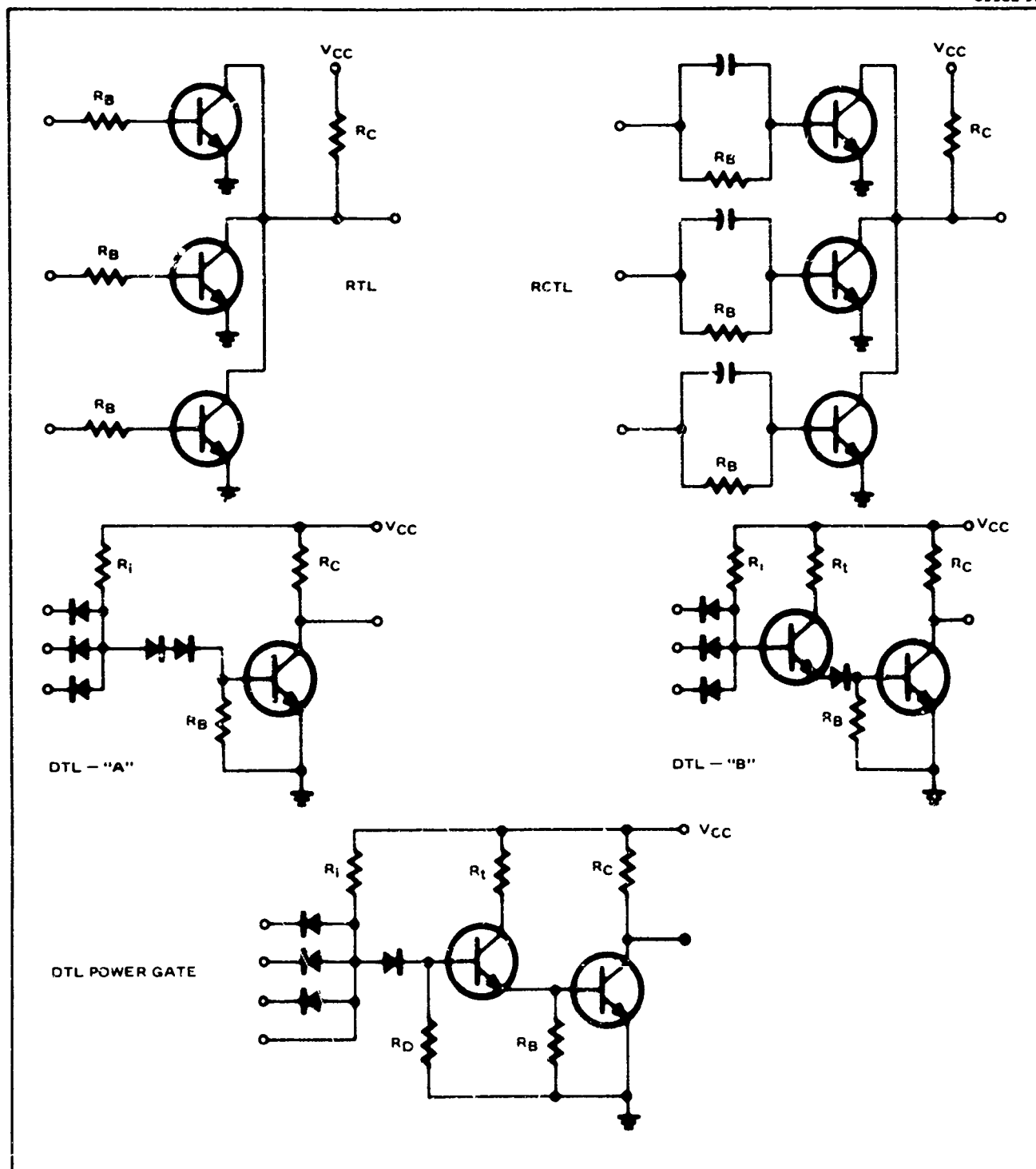


FIGURE 2-31 Basic Gate Circuits

TABLE 2-8 Critical Radiation Thresholds For
Damage Failure In DTL Gates For
Fan-Out of 10 (18)

CIRCUIT TYPE	CRITICAL RADIATION THRESHOLD n/cm ² (E > 10 keV)
DTL GATES: Fairchild DT ₁ L 930 GME 254 G 3 Motorola MC 206 Signetics D9004H Siliconix A06A Tex. Inst. SN341A Westinghouse WM201T Hughes DTL20	6×10^{13} 1.8×10^{14} 8×10^{13} 9×10^{13} $\sim 1 \times 10^{14}$ $< 1 \times 10^{12}$ $< 1 \times 10^{12}$ $\sim 2 \times 10^{13}$
DTL POWER GATES: Fairchild DT ₁ L 932 GME 264 P Motorola MC204G Signetics D9007H Siliconix A02A	$\sim 8 \times 10^{14}$ $> 5 \times 10^{14}$ $\sim 5 \times 10^{14}$ $> 5 \times 10^{14}$ $> 5 \times 10^{14}$

TABLE 2-9 Critical Radiation Thresholds For
Damage Failure in RTL, RCTL Gates
For Fan-Out Of 15 (18)

CIRCUIT TYPE	CRITICAL RADIATION THRESHOLD n/cm^2 ($E > 10$ keV)
LOW POWER RTL GATES:	
Fairchild MM4L 910	$1.2 - 1.4 \times 10^{14}$
GME 134D2	$0.6 - 1.4 \times 10^{14}$
STANDARD RTL GATES:	
Amelco "G"	$1.2 - 1.7 \times 10^{14}$
Fairchild MM4L 903	$0.3 - 1.6 \times 10^{14}$
RTL POWER GATES:	
Amelco "B"	
GME 153E3	$1.7 - 1.8 \times 10^{14}$
RCTL GATES:	
Sprague USO 104 A	$\sim 8 \times 10^{12}$
Tex. Inst. SN 512	$\sim 8 \times 10^{12}$

TABLE 2-10
Summary Of Microcircuit Failure Levels (18)

Device	Circuit Type	Neutron Radiation Failure Level (n/cm ² E > 10 keV)
SN5420	Dual, 4-input NAND gate	> 3.32 x 10 ¹⁴ *
TNG3111	Dual, 4-input NAND gate	> 3.32 x 10 ¹⁴ *
5604	Dual, 4-input NAND gate	> 3.32 x 10 ¹⁴ *
SG40	Dual, 4-input NAND gate	> 3.32 x 10 ¹⁴ *
7901000 (MS282)	Dual, 4-input NAND gate	3.32 x 10 ¹⁴ *
RD210	Dual, 4-input NAND gate	> 3.32 x 10 ¹⁴ *
USX1050M	Single, 4-input NAND gate	> 3.32 x 10 ¹⁴ *
μA709	Operational Amplifier	3.32 x 10 ¹⁴
μA711	Dual Comparator	> 3.32 x 10 ¹⁴

* Fan-out = 10

output voltage V_{ON} of the ON half of the flip-flop and treating it as another ON gate. The other method is to measure the trigger level sensitivity by applying a clock-pulse of varying amplitude after each interval of irradiation.

In the first method, V_{ON} will increase as the current gain degrades and the collector-current comes out of saturation. Circuit failures can be defined when V_{ON} exceeds the noise-margin of the OFF half of the circuit and tries to turn it ON. It will also exceed the noise-margin of the loading circuits and tend to turn them ON. Thus, the critical radiation threshold for this condition is the same as that for the equivalent gate circuit. Table 2-11 shows the degradation of the load driving capability of the DTL flip-flops in comparison with that for DTL gates of identical output circuit construction after $2.7 \times 10^{14} \text{ n/cm}^2$. The load driving capability is directly related to the transistor current gain.

The trigger level sensitivity is measured as a function of neutron fluence for all of the flip-flops.⁽¹⁸⁾ The DTL flip-flops consisted of ac coupled and dc coupled type. The results were:

- . The trigger threshold level for ac coupled DTL flip-flops begins to degrade at about $4 \times 10^{13} \text{ n/cm}^2$ and falls off about 10 to 20 percent at $2.7 \times 10^{14} \text{ n/cm}^2$.
(See Figure 2-32)
- . No change in trigger threshold level is observed in dc coupled DTL flip-flops at $2.7 \times 10^{14} \text{ n/cm}^2$.
(See Figure 2-33)

TABLE 2-11 Normalized Degradation Of Loading
Capability For DTL Circuits After
 2.7×10^{14} n/cm² (E > 10 keV) (18)

CIRCUIT	MANUFACTURER	TYPE	I_{LF}/I_L	
			Min.	Max.
DTL 930	Fairchild	Standard Gate	0.45	0.52
DTL 931	Fairchild	Flip-Flop	0.46	0.55
MC 206	Motorola	Standard Gate	0.36	0.42
MC 209	Motorola	Flip-Flop	0.36	0.49
264 P	GME	Power Gate	0.59	0.66
264 B	GME	Flip-Flop	0.62	0.68
D 9004 H	Signerics	Standard Gate	0.34	0.40
D 9006 H	Signetics	Flip-Flop	0.25	0.30

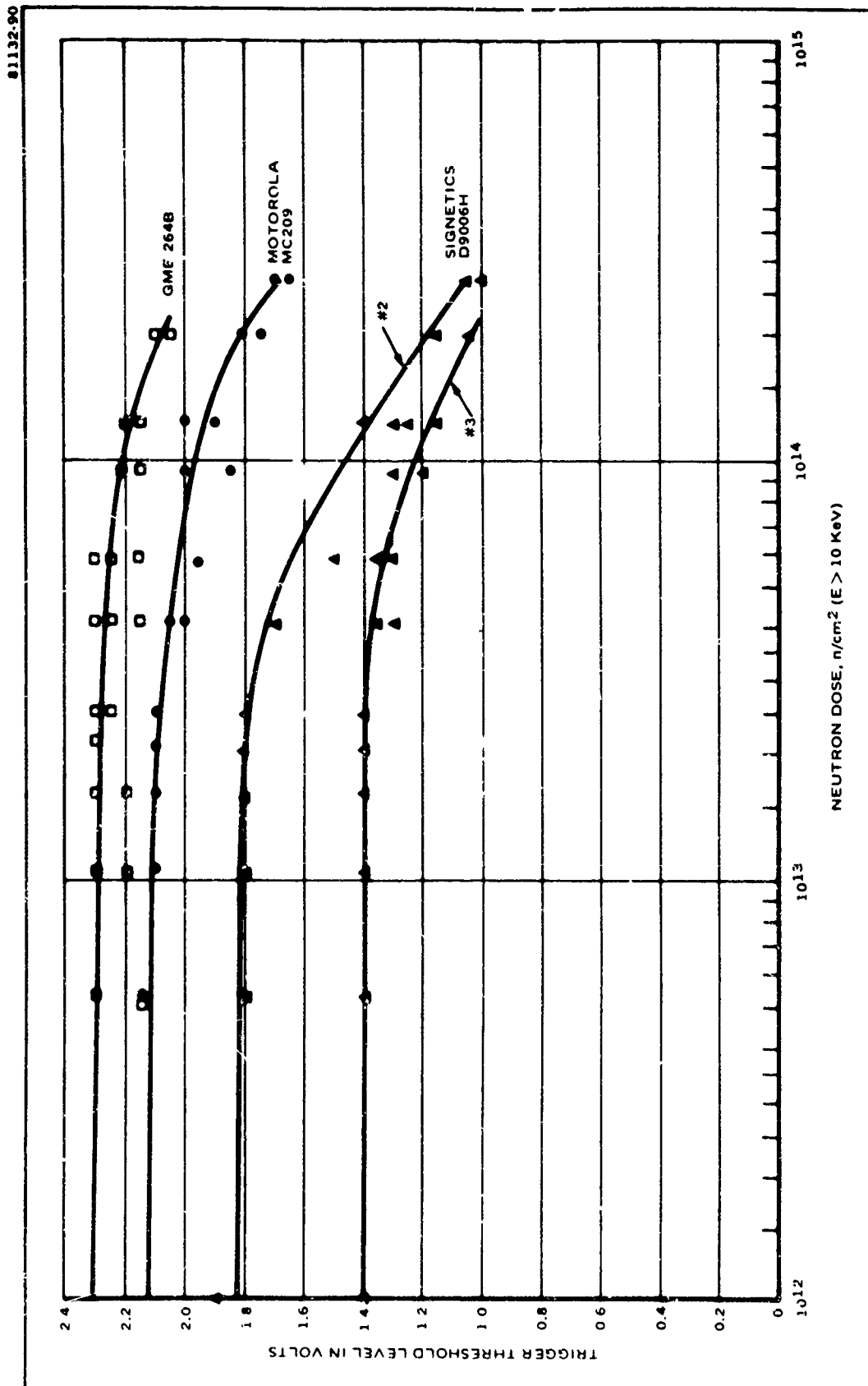


FIGURE 2-30 Degradation of Trigger Threshold Level for ac Coupled DTL Flip-Flops

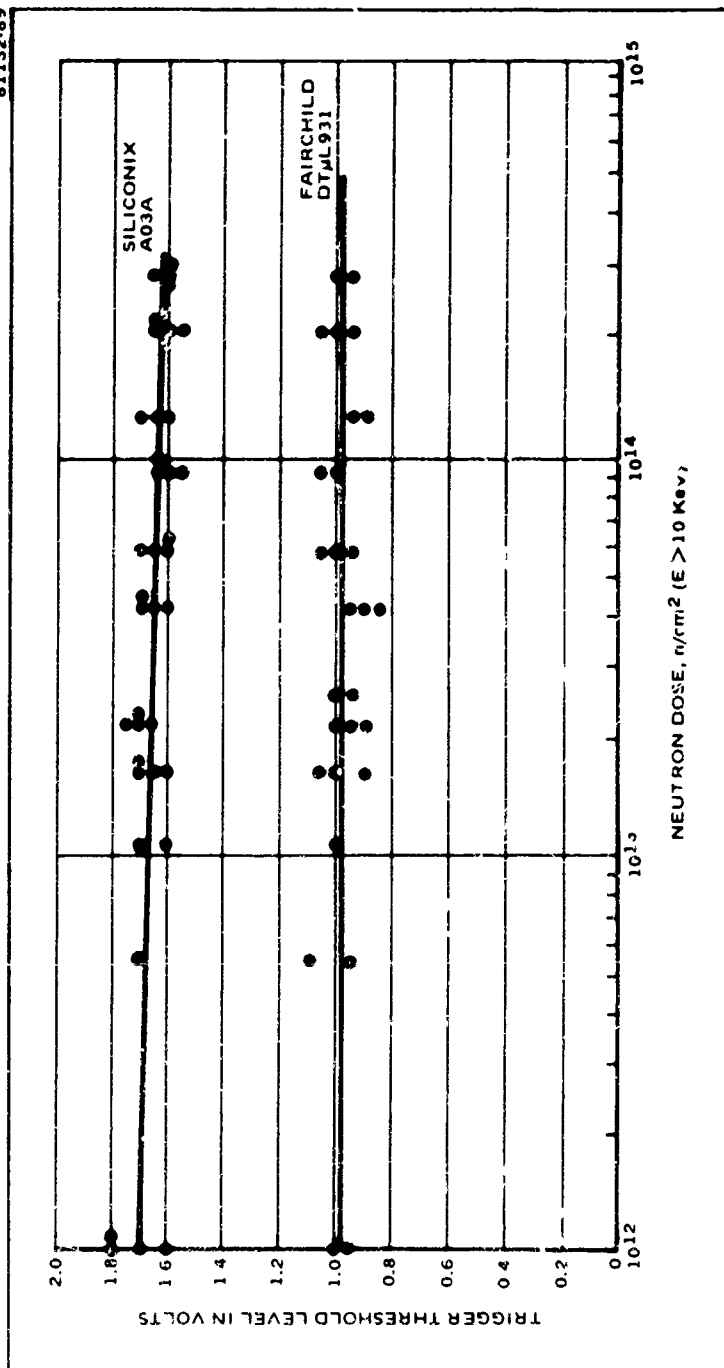


FIGURE 2-33 Degradation of Trigger Threshold Level for dc Coupled DTL Flip-Flops

- The trigger threshold level of RTL and RCTL flip-flops either remains unchanged or increases slightly at $2.7 \times 10^{14} \text{ n/cm}^2$. (See Figures 2-34 and 2-35)
- One-shot multivibrators are similar to flip-flops. The trigger threshold levels for ac coupled DTL types decrease in the same way. (See Figure 2-36)

In no case is the change in trigger level sensitivity great enough to produce failure for neutron fluences up to $2.7 \times 10^{14} \text{ n/cm}^2$. Thus, the critical radiation threshold for failure is largely determined by the loss of noise-margin for the equivalent gate circuit.

2.5.3 Transient Effects

The transient radiation effects generally result in a pulse at the output of the circuit. These pulses are passed from one circuit to the next which may trigger flip-flops, be amplified by each succeeding amplifier or produce effects in the output that may or may not be significant, depending on the system. These transient pulses can be considered as a form of noise pulse. These noise pulses can turn the devices ON or OFF for short periods of time. If the loading circuits (fan-out) are not affected by these noise pulses, then no false information is injected into the system. However, circuit failure during radiation occurs when the radiation induced circuit output voltage exceeds the noise margin of these devices which act as a load for the circuit under test. The duration or width of the noise pulse is also of significance. Detailed radiation effects data⁽¹⁹⁾ are presented in Figures 2-37 through 2-41 for one type of integrated circuit.

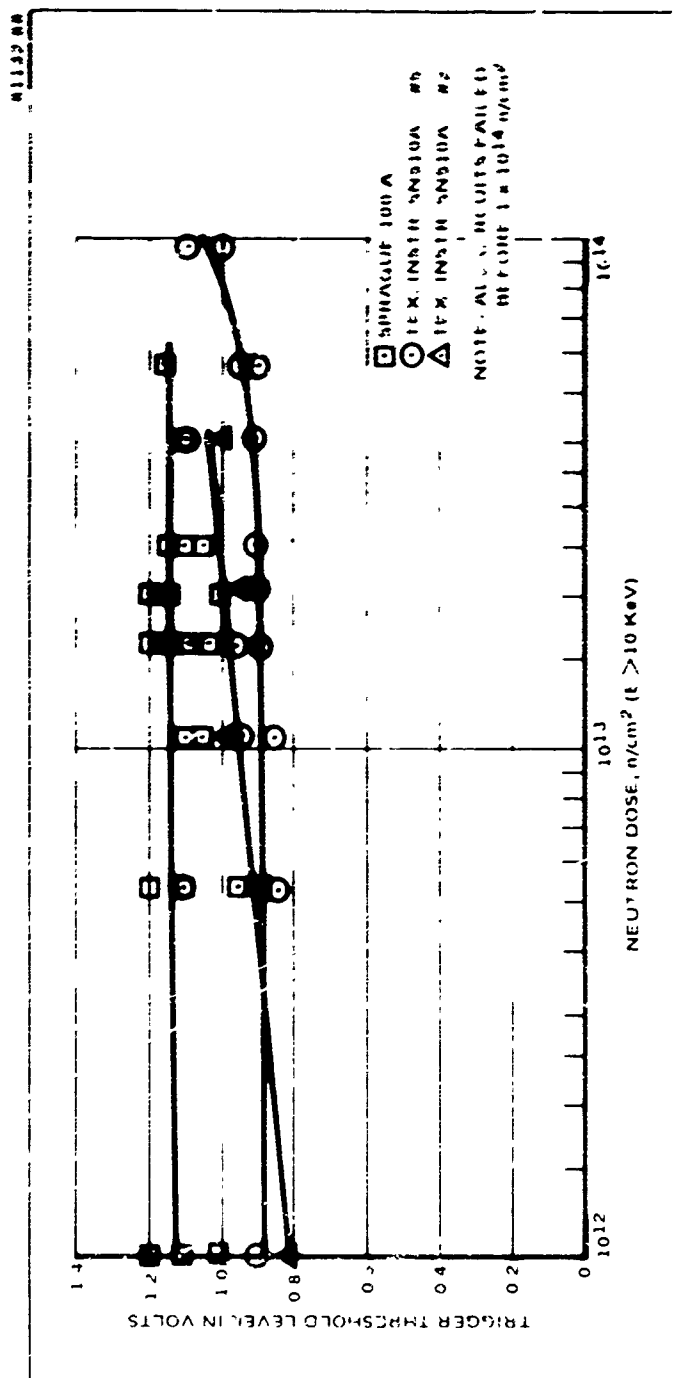


FIGURE 2-34 Degradation of Trigger Threshold Level for RTTL Flip-Flops

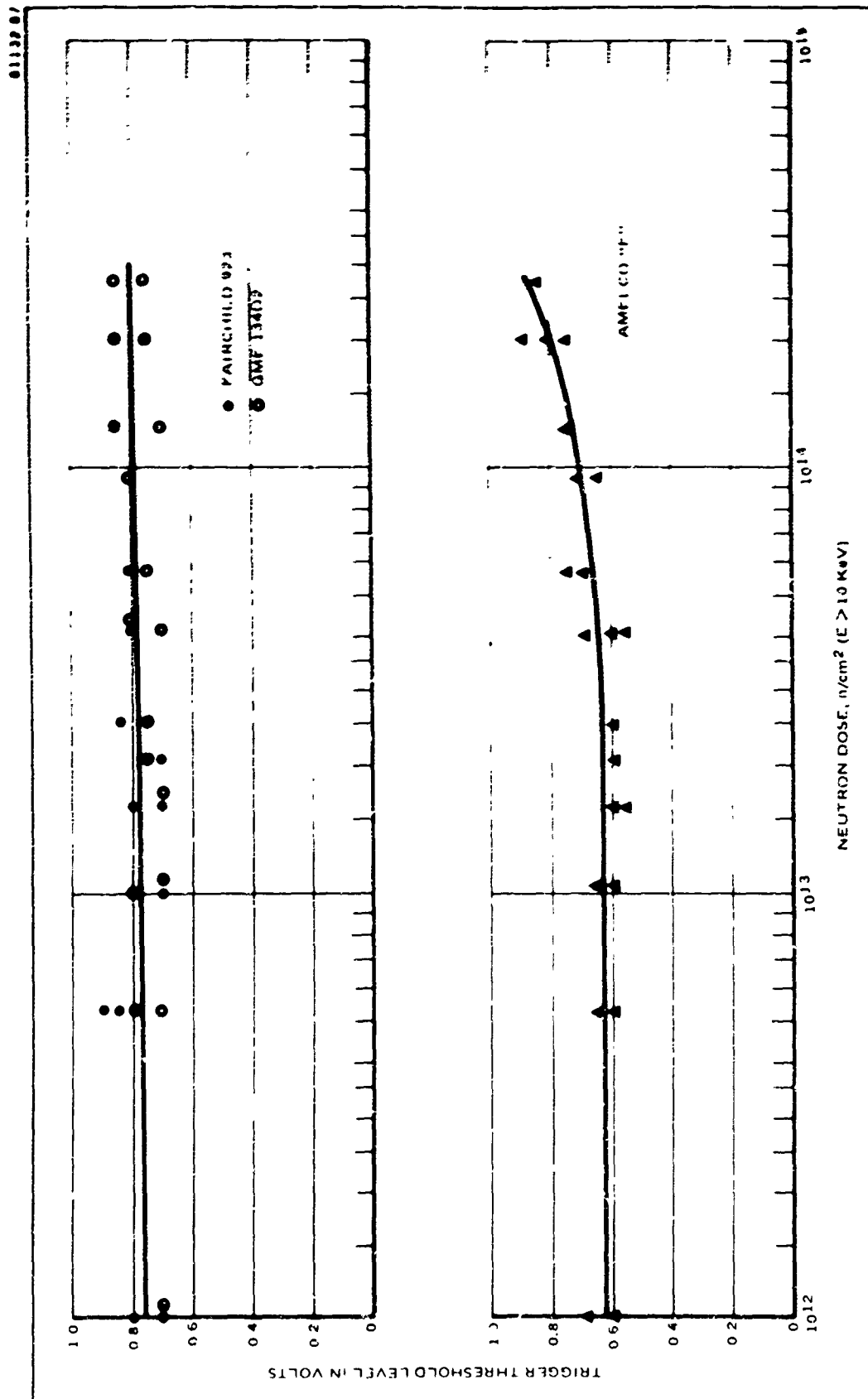


FIGURE 2-35 Degradation of Trigger Threshold Level for RTL Flip-Flops

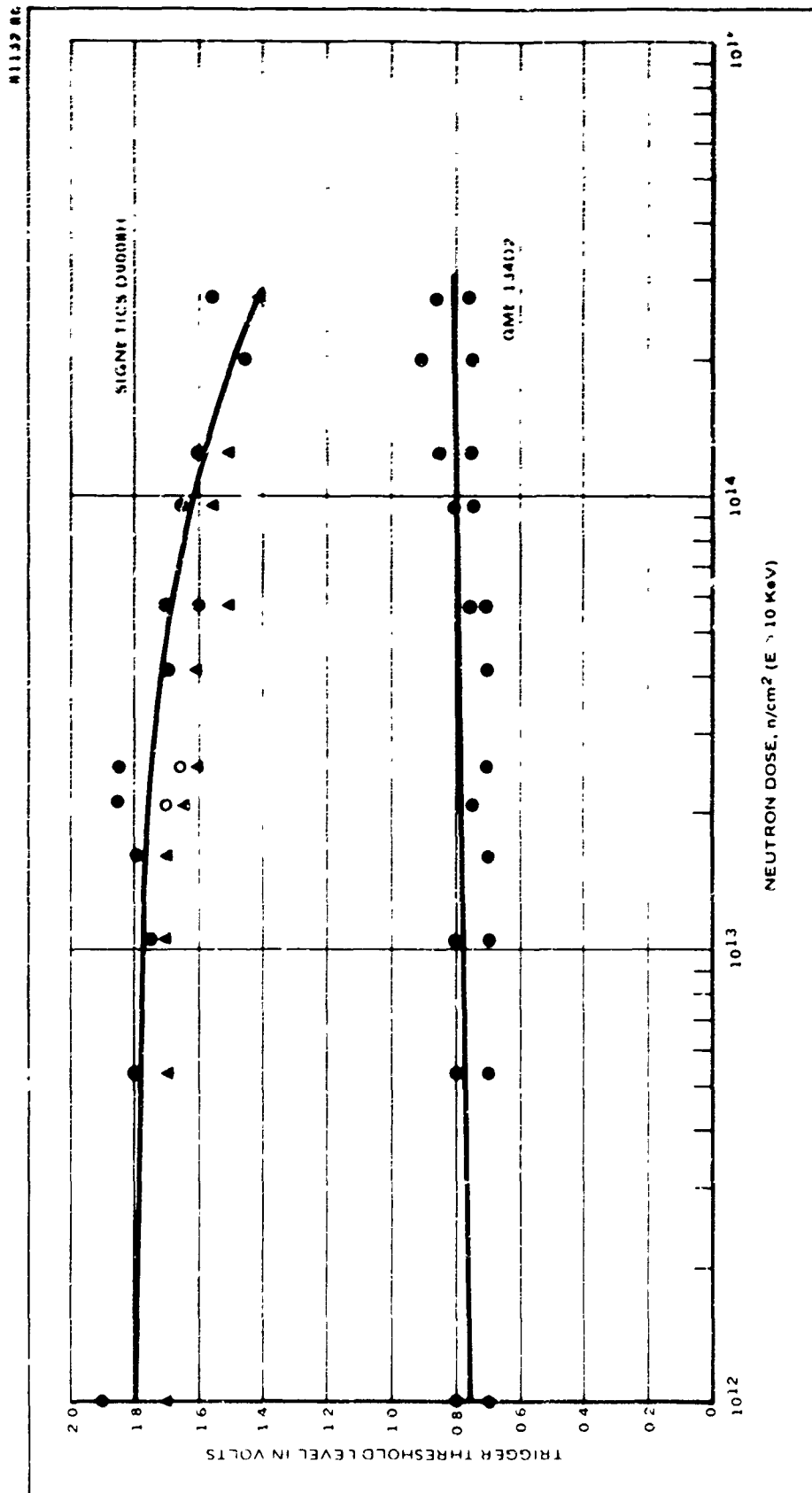


FIGURE 2-36 Degradation of Trigger Threshold Level for One-Shot Multivibrators

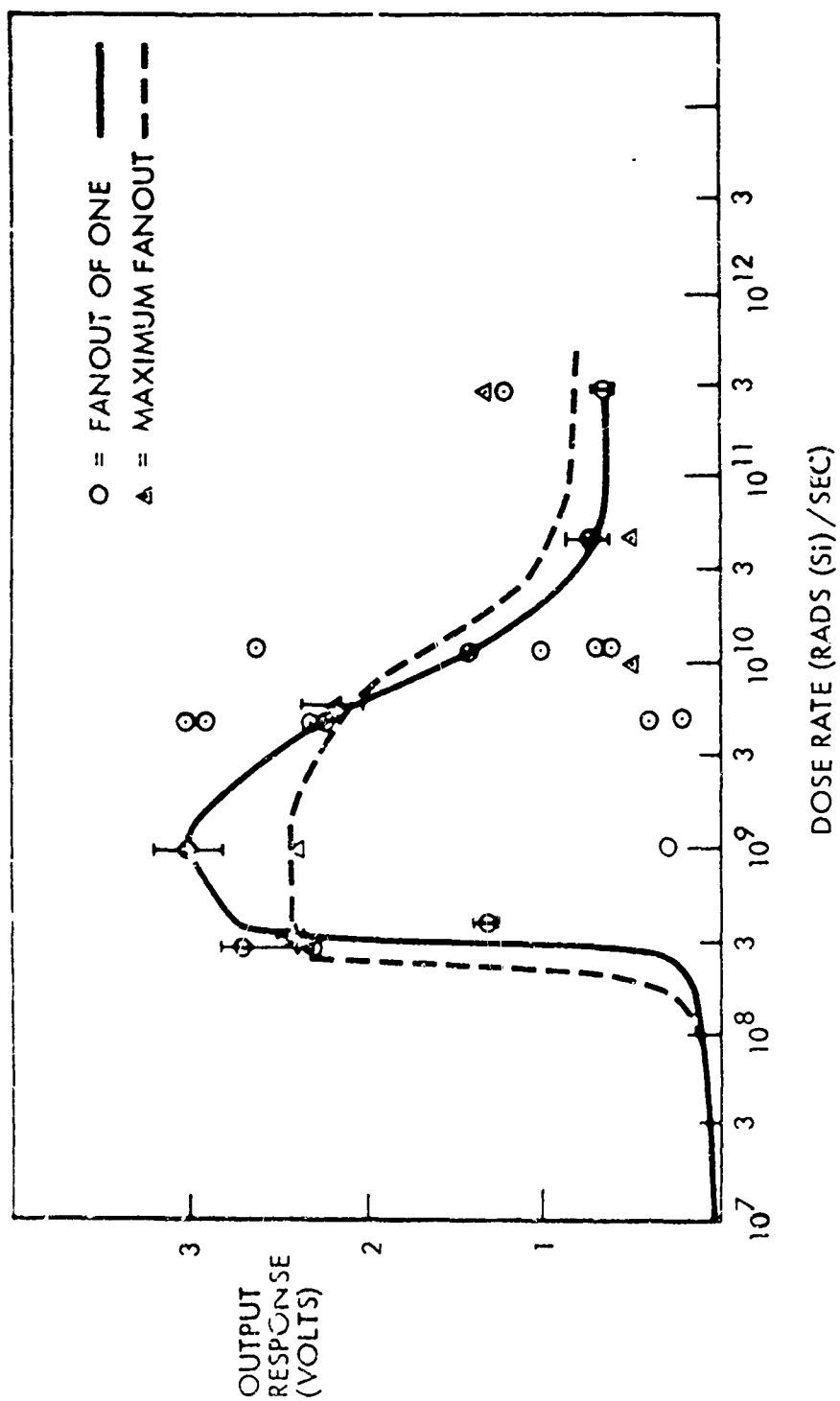


FIGURE 2-37 Output Response vs Dose Rate for the DTAL932 (0 State) (19)

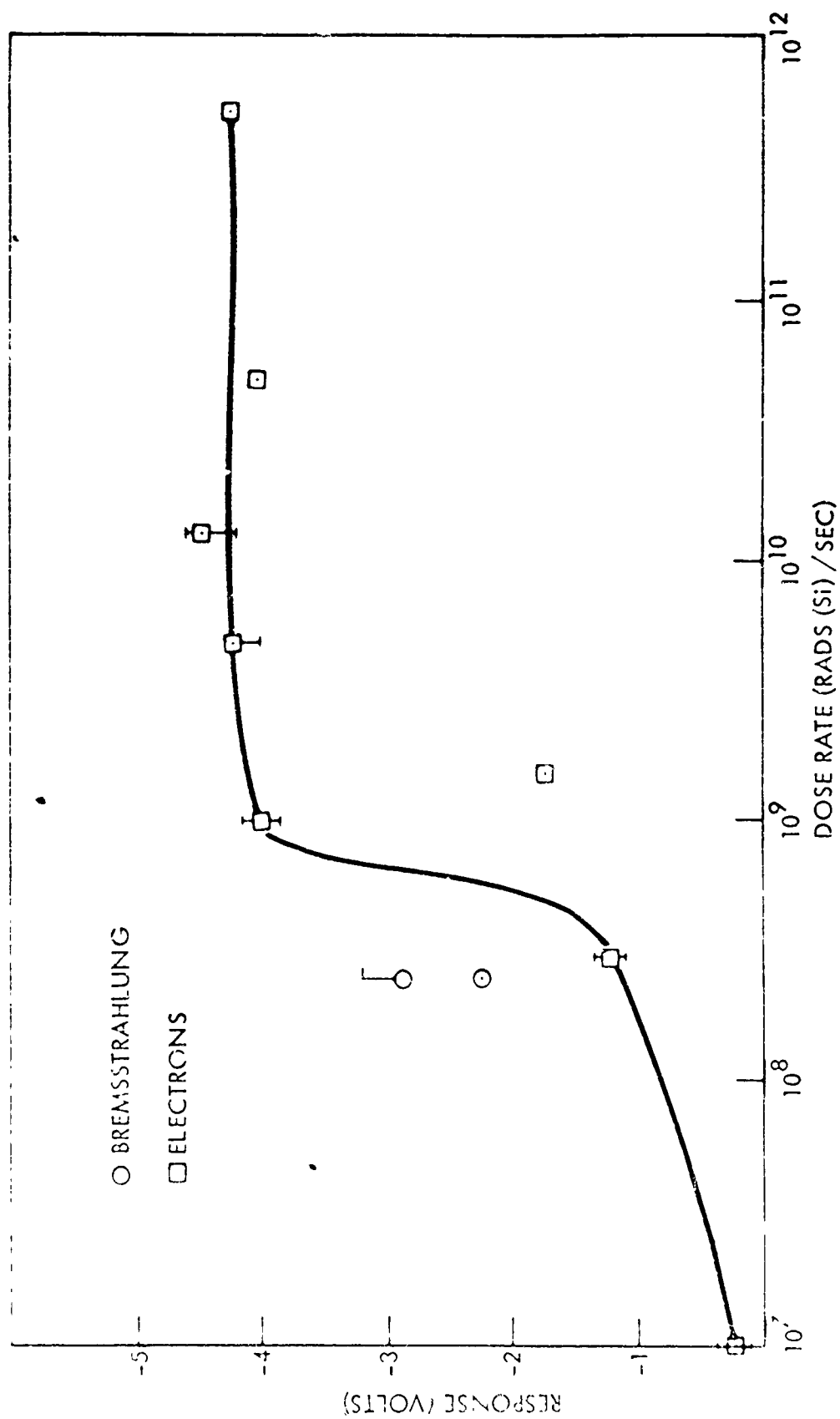
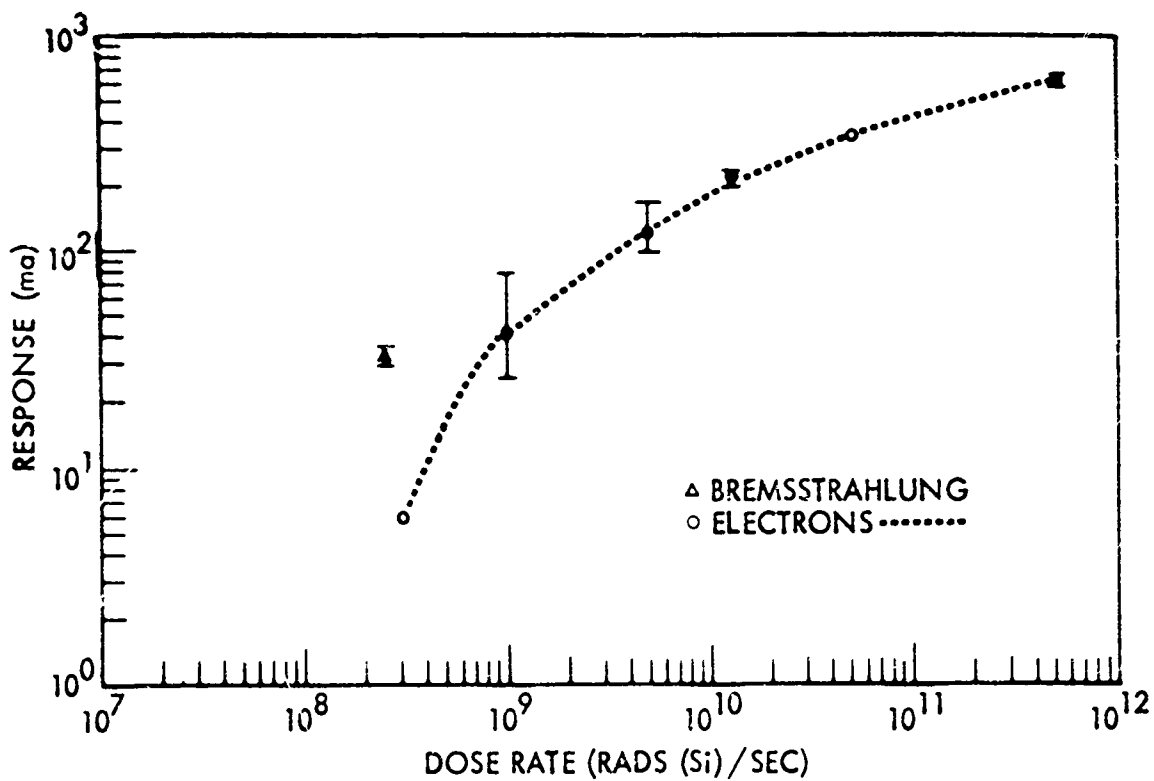
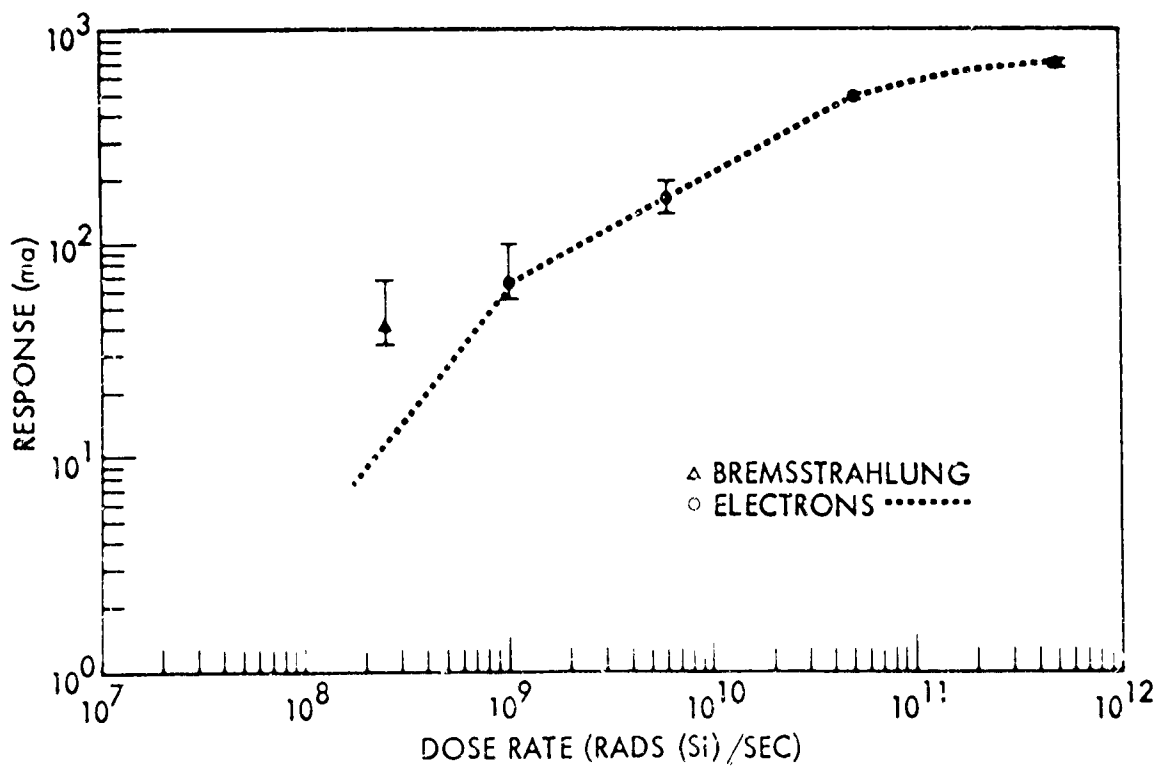


FIGURE 2-38 Output vs Dose Rate for the DTU L932 (1 State) (19)

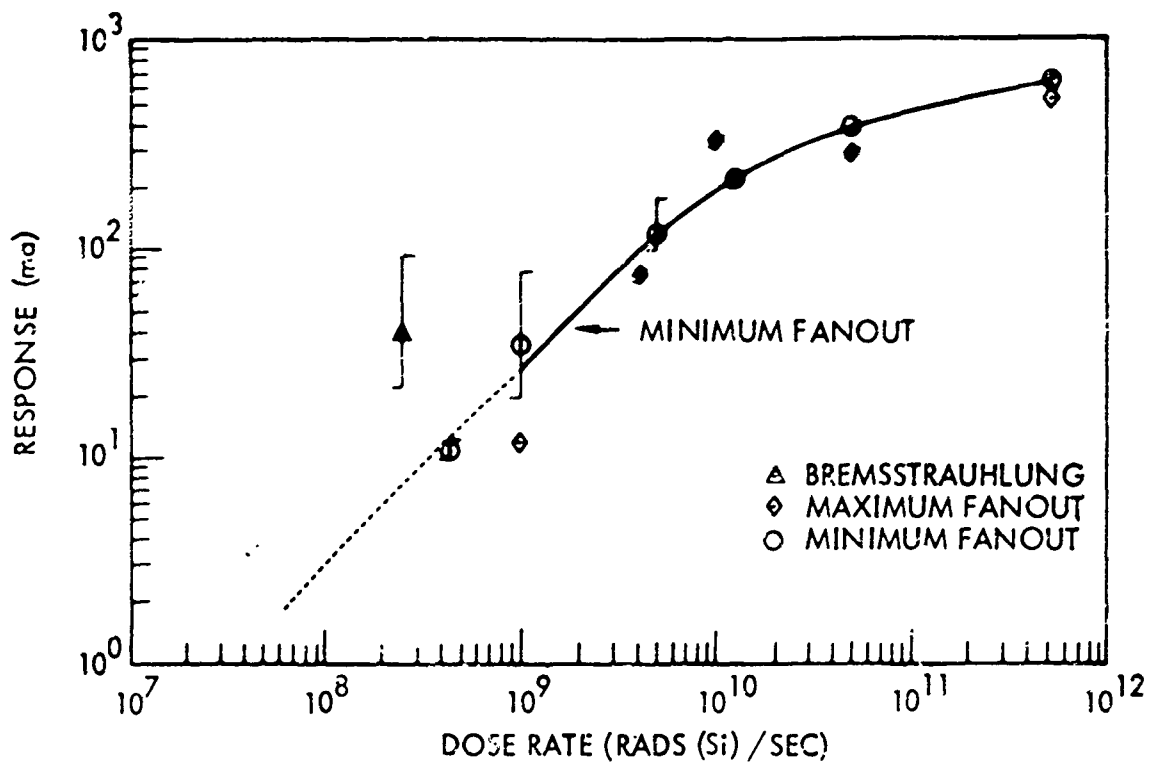


A CURRENT IN GROUND LEAD

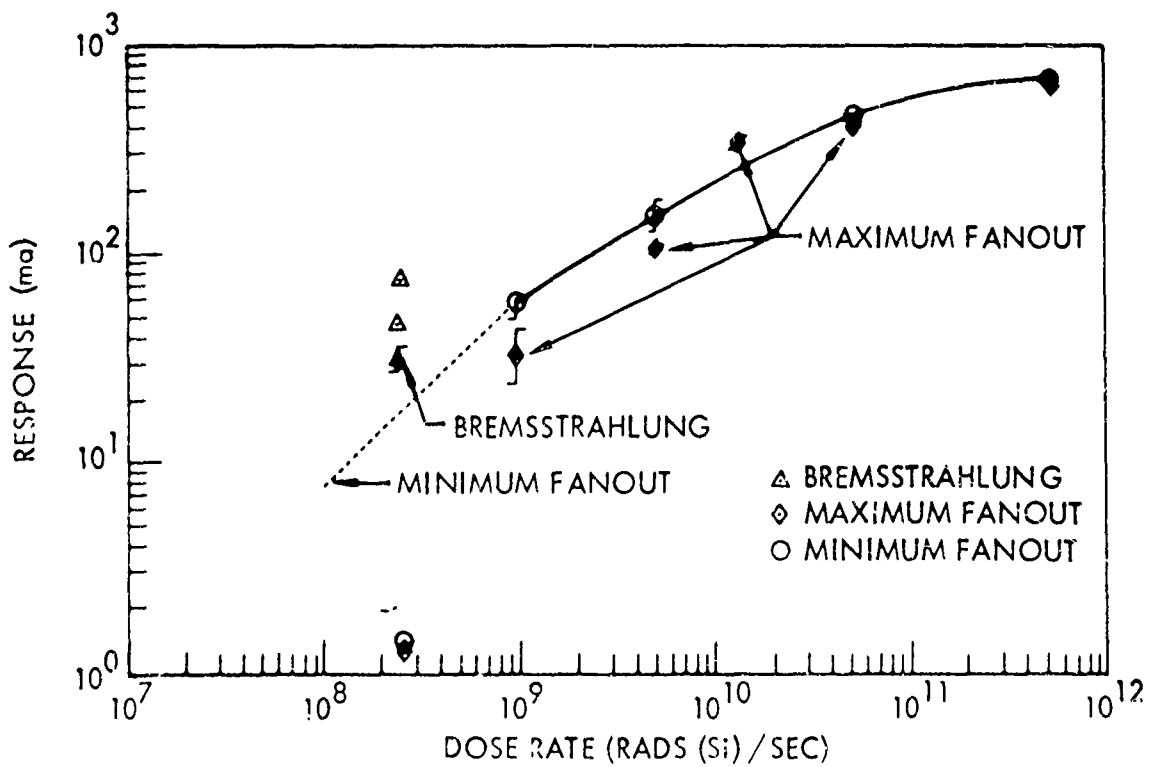


B CURRENT IN POWER SUPPLY LEAD

FIGURE 2-39 Current Surges vs Dose Rate for the DTM932 (1 State)⁽¹⁹⁾



A GROUND LEAD



B POWER SUPPLY LEAD

FIGURE 2-40 Current Surges vs Dose Rate for the DTL932 (0 State) (19)

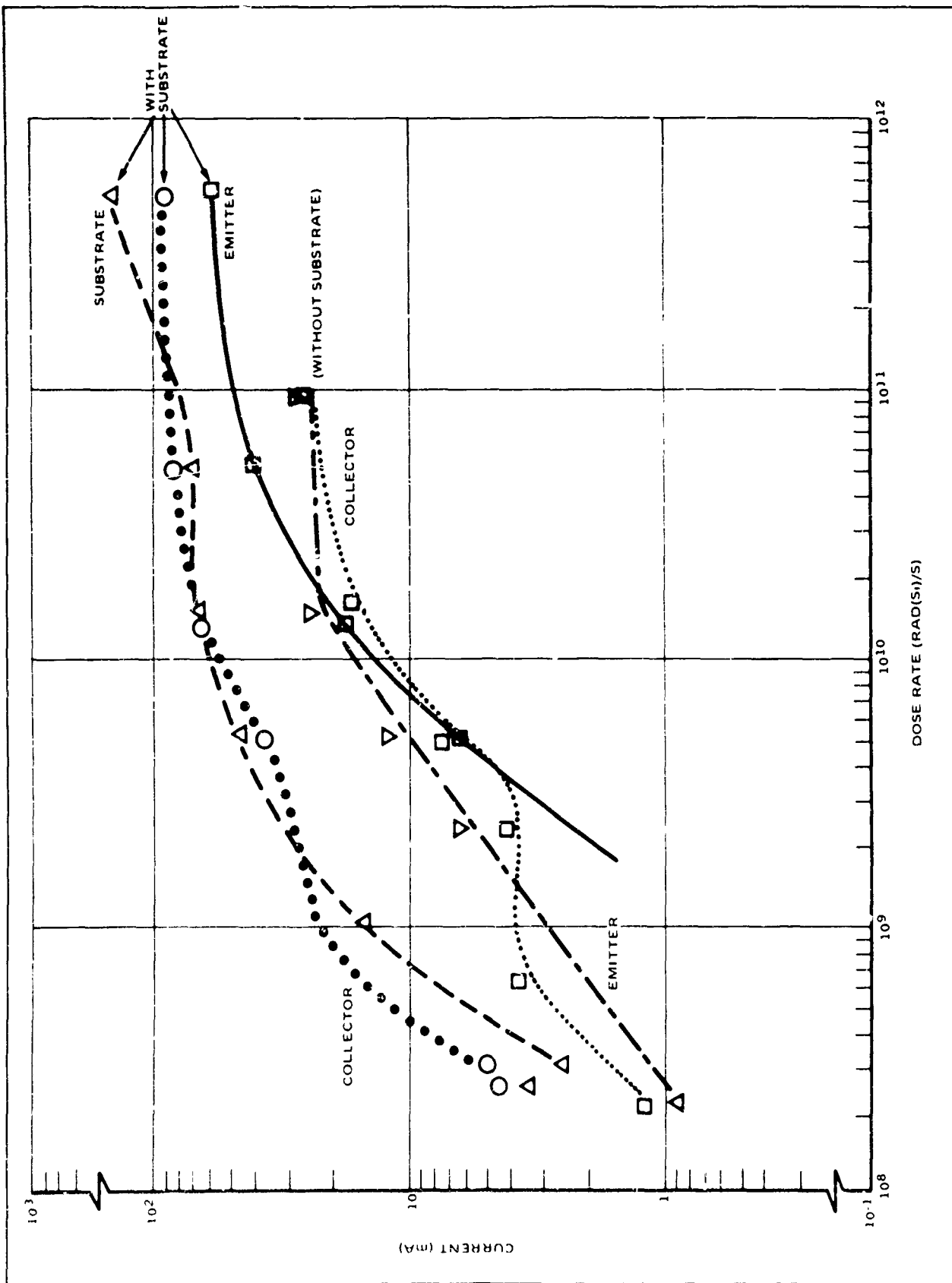


FIGURE 2-41 Transistor Secondary Photocurrent vs Dose Rate for the D9L932 (19)

The results of experimental evaluations are summarized below and in Tables 2-12 through 2-15.⁽¹⁸⁾ The qualitative features to be observed in these results are as follows (not that "more sensitive" means "lower threshold"):

- . RCTL circuits are more sensitive to transient radiation disturbances than either RTL or DTL circuits. (See Tables 2-12 and 2-13)
- . The best RTL and DTL circuits are about equally sensitive i.e. no superiority of logic type. (See Tables 2-12 through 2-15)
- . Low power RTL gates and flip-flops are more sensitive than the higher power types. (See Tables 2-12 and 2-13)
- . DTL gates without internal load resistors are more sensitive than those with the internal load resistors. (See Table 2-14)
- . RTL ON gates are insensitive. (See Table 2-12)
- . In the majority of cases, DTL gates are more sensitive in the ON state than in the OFF state. (See Table 2-14)
- . Fan-in has no effect on circuit responses as far as loading effects are concerned.

- . Fan-out has no effect on the sensitivity of DTL gates, but sensitivity increases slightly for RTL and RCTL gates. (See Table 2-12)
- . Flip-flops are more sensitive (to self-triggering) than gates of the same logic type except for DTL gates without internal load resistors. (See Tables 2-13 and 2-15, and Tables 2-12 and 2-13.)

**TABLE 2-12 Critical Radiation Thresholds For Transient
Radiation Effects For RTL, RCTL OFF Gates.
Averages Of Four Circuits Of Each Type. (18)**

RTL, RCTL CIRCUIT TYPE	OFF FAILURE THRESHOLD RADS(Si)/SEC	
	FANOUT = 0	FANOUT = 5
LOW POWER RTL GATES:		
Fairchild MW μ L910	7×10^7	4×10^7
GME 134D2	2×10^8	1×10^8
STANDARD RTL GATES:		
Amelco "G"	5×10^8	4×10^8
Fairchild MW μ L903	6.5×10^8	2×10^8
RTL POWER GATES:		
Amelco "B"	3×10^8	5×10^8
GME 153D3	6×10^8	2×10^8
RCTL GATES:		
Sprague US0104A	1×10^6	$< 1 \times 10^6$
Tex. Inst. SN512	2×10^6	2×10^6

Note: No response observed in ON-state for RTL gates.
See text re: RCTL gates.

TABLE 2-13 Failure Threshold Levels For RTL and RCTL Flip-Flops (18)

CIRCUIT DESCRIPTION	SELF-TRIGGER THRESHOLD RADS(SI)/SEC	THRESHOLD TO TRIGGER ON-GATE ($e_o = -3V$) RADS(SI)/SEC
RTL FLIP-FLOPS:		
Amelco Type F	1×10^9	1×10^9
Fairchild DTL 923	3×10^8	4×10^8
GME 134 D2 (Low Power)	6×10^7	2.5×10^7
RCTL FLIP-FLOPS:		
Sprague US 0100	1×10^7	4×10^6
Tex. Inst. SN510	1×10^7	2.5×10^6
RTL MONOSTABLE:		
GME 134 D2	5×10^7	5×10^7
RCTL MONOSTABLE:		
Tex. Inst. SN518A	2×10^5	$< 10^6$

Note: These data represent the average of the failure threshold levels for four circuits of each type.

TABLE 2-14 Critical Radiation Thresholds For Transient Radiation Effects For DTL Gates. Averages For Four Circuits Of Each Type. (18)

DTL CIRCUIT TYPE		FAILURE THRESHOLD RADS(SI)/SEC	
		OFF-STATE	ON-STATE
CIRCUITS WITH INTERNAL LOAD RESISTORS:			
Fairchild	DTL 930	5×10^8	$\sim 1 \times 10^9$
GME	254-G3	2×10^8	1×10^9
Hughes	DTL-20	1×10^9	7.5×10^8
Motorola	MC-206	5×10^8	5×10^7
Signetics	9004H	3.5×10^8	1×10^8
POWER GATES WITH COMPLEMENTARY OUTPUTS:			
Fairchild	DTL 932	1×10^9	3×10^8
Signetics	9007H	3×10^7	$> 1 \times 10^9$
CIRCUITS WITH NO INTERNAL LOAD RESISTORS:			
GME	264P	5×10^7	1×10^9
Motorola	MC-204G	1×10^7	1×10^9
Siliconix	A02A	6×10^7	4×10^7
Siliconix	A06A	6×10^7	4×10^7
Tex. Inst.	SN341A	1×10^6	5×10^6
Westinghouse	WM201T	7×10^7	6×10^6

TABLE 2-15 Failure Threshold Levels For DTL Flip-Flops (18)

CIRCUIT DESCRIPTION	SELF-TRIGGER THRESHOLD RADS(SI)/SEC	THRESHOLD TO TRIGGER ON-GATE ($e_o = -3V$) RADS(SI)/SEC
A. C. COUPLED CLOCK:		
GME 264 B	2×10^7	5×10^8
Motorola MC-209	2×10^7	2×10^8
Signetics D9006H	9×10^7	3.5×10^7
D. C. COUPLED CLOCK:		
Fairchild DTL 931	5×10^8	1×10^9
Siliconix A03A	9×10^6	2×10^8 *
MONOSTABLE:		
Signetics D9008H	$> 10^9$	3.7×10^7

* Measured at -2 Volts since the normal output voltage of this circuit is only 2.5 volts.

2.6 Catastrophic Failure

The main concern in assessing power and system vulnerabilities in the study environment is catastrophic failures in semiconductors due to burn-out caused by high level radiation induced currents. These radiation induced currents can cause catastrophic failures in semiconductors due to the following mechanisms:

- . Thin film interconnect burn-out in integrated circuits.
- . Bonding wire burn-out in integrated circuits and discrete devices.
- . Junction damage (burn-out) in integrated circuits and discrete devices.

The sources of these currents are a result of the interaction of the transient radiation with the semiconductors themselves. These transient sources will be due to primary and/or secondary photocurrent generation in diodes, transistors, and integrated circuits.

The general discussion in this section is concerned with short time transient effects having time history only slightly longer than the radiation pulse (tens of microseconds) as opposed to the long-time effects associated with latch up and second breakdown. However, these latter effects are discussed below for completeness and dismissed as not being a particular problem in modern well-designed circuits.

2.6.1 PNPN Latch-Up

The isolating substrate of an integrated circuit in combination with transistors and resistors forms complex PNPN structures as shown in

Figure 2-42. The substrate isolation junction is normally reverse-biased but when large photocurrents flow in a high resistivity substrate, unexpected bias voltages can be generated. A few cases have been reported^(20, 21, 22, 23) in which these radiation generated bias voltages have resulted in a PNPN switch action called latch-up. PNPN latch-up can also occur in complementary transistor pairs formed by a quadruple diffusion process.^(21, 22) This failure mechanism is catastrophic from a systems viewpoint because the power-supply current must be interrupted to restore normal circuit operation. The currents, which flow during latch-up, can also burn-out thin-film metal interconnections and small bonding wires causing complete circuit failure.

Latch-up was first observed at low dose-rates in 1964 during radiation tests on some triple-diffused integrated circuits.⁽²⁰⁾ Most of these circuits are triple or quadruple diffused in 70 x 100 mil silicon chips and do not use gold doping. The large chip areas (3 to 4 times greater than modern circuits) and the long storage times associated with active devices result in the generation of large photocurrents in these circuits at low dose-rates. Modern integrated circuits using epitaxial construction, small chip areas, and gold doping have not been observed to exhibit PNPN latch-up.

Hughes has performed many tests on many types of integrated circuits^(24, 25) at dose-rates up to 5×10^9 rad(Si)/s and total doses of 5000 rad/pulse and has never observed latch-up in any except some of the triple-diffused circuits. These tests included the Fairchild DT_L930, 932, 962 and μ A709 circuits.

Hughes Radiation Effects Research Department has also made measurements on the SN352A general purpose amplifier, one of the first

81132 73

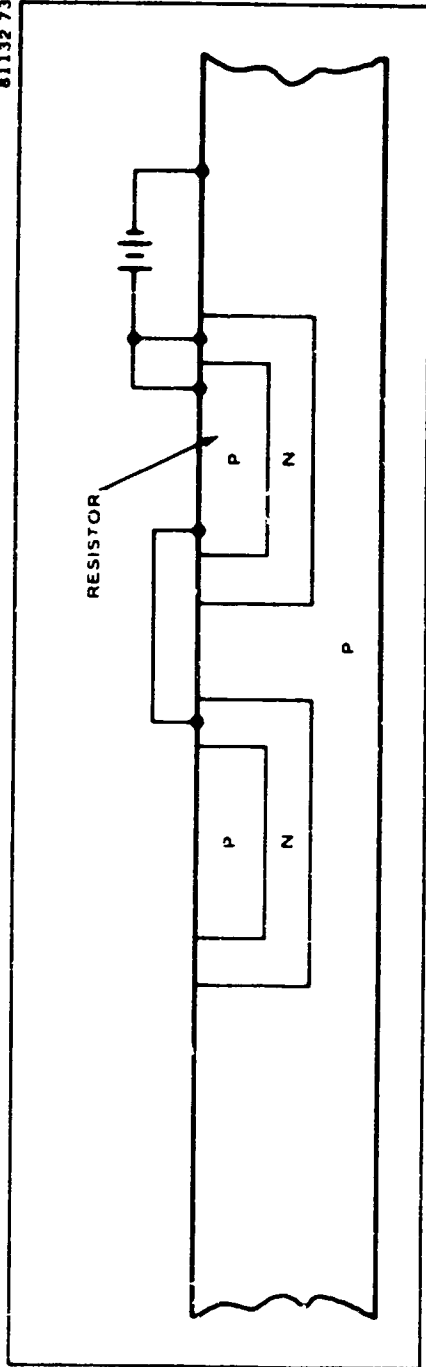


FIGURE 2-42 PN Junction Isolated Integrated Circuit

circuits which was observed to exhibit latch-up. Common emitter current gains greater than one have been measured for the NPN transistor formed by the N collector of a transistor, the P substrate and the N region under a diffused P type resistor as illustrated in Figure 2-42. The equivalent circuit for PNP action is shown in Figure 2-43. Modern integrated circuits are usually designed to keep the h_{FE} of parasitic transistors much less than 1. The high value of h_{FE} for the parasitic transistor could explain the ease with which some SN352A circuits can be made to latch-up. (20)

The latch-up mechanism cannot occur in dielectrically-isolated circuits and utilizing these circuits where feasible will eliminate this problem.

Latch-up tendencies can be reduced in junction isolated circuits if the following manufacturing techniques are employed.

- . Gold dope the integrated circuits to reduce lifetime and lower the h_{FE} of parasitic transistors so that $h_{FE} \ll 1$.
- . Increase physical separation of resistors and transistors.
- . Increase breakdown voltage between resistor N island and the P substrate by utilizing epitaxial construction.
- . Increase the P doping of the substrate and reduce N doping of collector region adjacent to the substrate by epitaxial construction.

81132-74

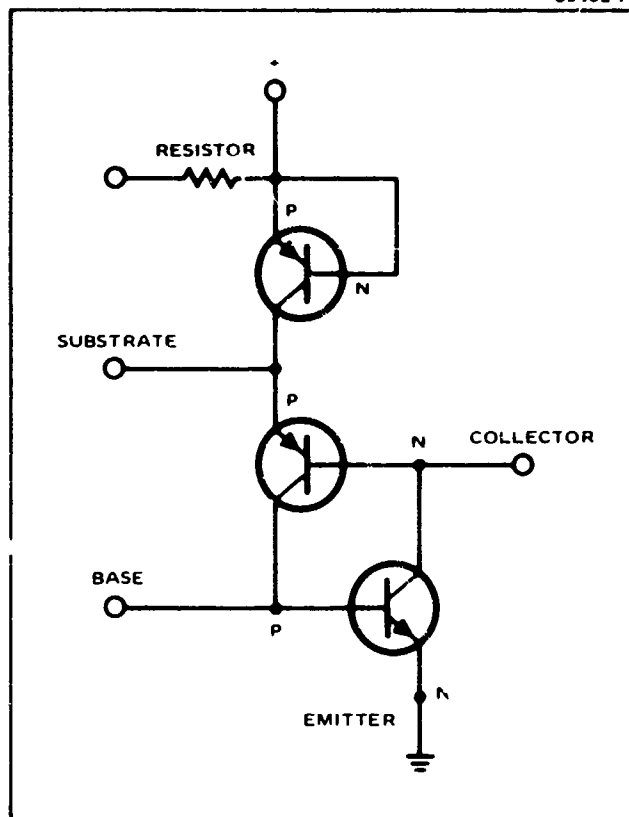


FIGURE 2-43 Equivalent Circuit for Latch-Up

- . Provide several well distributed connections between the substrate and the negative voltage supply terminal. A P+ guard ring structure in the substrate would be ideal if it is feasible. This change would help prevent the collector-substrate junction from becoming forward-biased.
- . Provide several well distributed connections between the resistor N island and the positive voltage supply. This procedure would guarantee that the junction between the P and N regions of the resistor was shorted so that one mode of PNP action would be eliminated.

Even if all integrated circuits utilize dielectric isolation, a malfunction can still occur due to a possible short circuit current path, through series transistor junctions to ground. This condition exists for example, in the Fairchild DM1932 buffer gate and the 709 op amp. It is also recommended that an electrical pulse-current screening test be devised for all circuits. Such a test will eliminate circuits with improper current-limiting or faulty interconnections.

2.6.2 Second Breakdown Latch-Up

Second breakdown latch-up is a voltage breakdown mechanism which can occur in discrete transistors and integrated circuit transistors under certain conditions. Second breakdown latch-up has occurred in only one type of integrated circuit tested to date. The cause of this one failure has been identified as poor design.⁽²⁶⁾ It is believed that second breakdown will not occur in well designed integrated circuits.

Figure 2-44 illustrates the second breakdown characteristics. Second breakdown will not occur if a load line such as RL_2 avoids the

81132-75

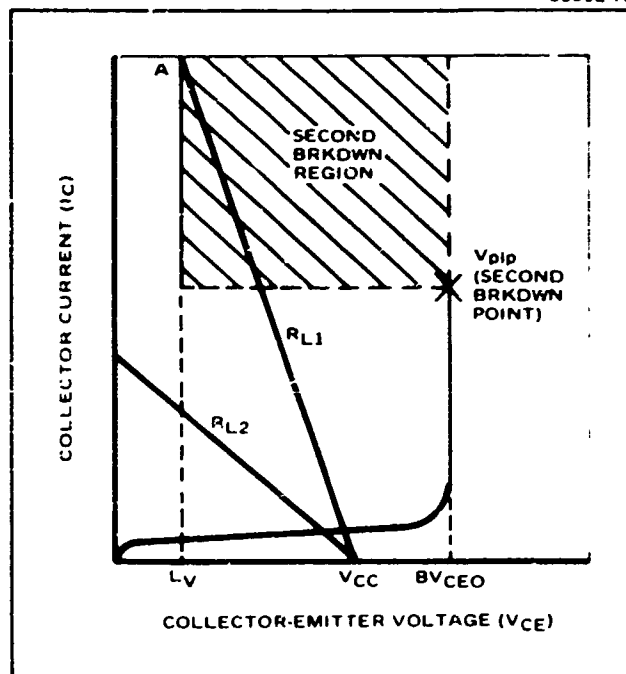


FIGURE 2-44 Transistor Second Breakdown Characteristic

the second breakdown region. However, if the transistor operates along RL_1 , it will experience second breakdown as it enters the second breakdown region, will latch-up at point A where RL_1 intersects the latch-up voltage line L_V , and may burn out unless the current is limited. This situation is of particular interest in the transient radiation environment since a transistor may be normally working along RL_2 but the transient radiation changes the load line to RL_1 , and also turns the transistor ON. Thus, the transistor can be triggered into second breakdown by radiation provided certain conditions are met. The first condition is that the supply voltage (V_{cc}) must be greater than the latch-up voltage L_V . L_V is equal to the sustaining voltage ratings sometimes given on transistor specification sheets. A second condition is that the supply must be capable of furnishing the sustaining current. This failure mode should not be a particular problem in space power subsystems since the first condition above specifies that the supply voltage be relatively close to the maximum collector to emitter voltage, BV_{CEO} for the transistors generally used in circuits where this failure would be catastrophic range from 60 to 100 volts.

2.6.3 Thin-Film Interconnect Burn-Out

At high radiation dose rates, circuits using PN junction isolation are particularly vulnerable to ionizing radiation because power-supply currents can be shunted directly to ground through the isolation junction associated with diffused resistors. The resistor is formed by a base-type P diffusion in an isolated N-type island. The N region is normally returned to V_{cc} so that the junction between the P resistor and the N island will always be reverse-biased. The P-type substrate is always connected to ground or the most negative voltage supply in the circuit. A short-circuit photocurrent path, therefore, exists from the power supply to the N region, through the isolation junction, and then to ground.

Since resistors normally occupy at least 50% of the integrated circuit chip area and are normally located within the same isolation region, their isolating PN junction is by far the largest photocurrent generator in the circuit. This failure mechanism is also possible in dielectrically isolated circuits which employ diffused resistors.

A shunt photocurrent path also exists where the circuit design results in a series combination of PN junctions between the power supply and ground that is not limited by a resistor. Examples of this type of circuit are complementary and totem pole output circuits. Ordinarily, the power supply can be designed to supply these currents. However, at high dose rates, these currents may increase to the ampere level, or even greater. Then, the small gold or aluminum bonding wires or aluminum interconnections may burn out causing permanent circuit failure. Compatible thin-film resistors will eliminate the shunt current path associated with diffused resistors, but shunt circuit paths through a series of circuit PN junctions can only be eliminated or current limited by circuit design.

The thin-film interconnects are the most vulnerable to over-currents due to their small cross-sectional area (typically 1 micron x 0.5 mil). The 1 mil diameter wires normally used for bonding are about a factor of 20 to 50 greater in cross sectional area and should require about a factor of 20 to 50 more power to cause burn-out.

Burn-out of thin-film interconnects occurs near the place where the metallization crosses a dielectric isolation fence or at the "windows" cut out of the oxide layers. The metallization is effectively stressed at these points due to a change in deposition depths, or there may be slight steps, or ridges at the material interfaces. These

stress points cause different effects in the various transistor geometries and close correlation with calculations based on a fuse type consideration is not possible due to the effect of the step or ridge.

For moderately high dose rates (10^{10} to 10^{11} rad(Si)/s), the worst case time duration, produced by a radiation disturbance in currently used monolithic integrated circuits, is approximately 5 μ s (due to a 30 ns radiation pulse plus radiation-induced storage time effects). The measured currents required to burn-out four metallization widths in 5 μ s are tabulated in Table 2-16.

TABLE 2-16 Interconnect Burn-Out Current ⁽²⁷⁾

<u>Interconnect Width (Mil)</u>	<u>Burn-Out Current (A)</u>
0.44 to 0.55	1.0 to 2.0
0.66	2.1
0.81	2.8
1.42	4.0

The substrate currents in existing monolithic integrated circuits at the above dose rate levels can range from 1 to 4 A or larger. Therefore, it appears that currently used integrated circuits may be vulnerable to catastrophic failure. The reduction of current carrying capacity due to multiple fence crossings and other stresses caused by manufacturing techniques may raise the vulnerability in some circuitry.

Figures 2-45 and 2-46 are representative current-time plots of the measured failure thresholds.⁽²⁷⁾ These data are for the same metallization width, but the stresses due to fence crossings were different. The difference in the curves is attributed to these different stresses. By knowing the metallization pattern dimensions, one may predict where the burn-out will occur. Circuitry laws state that parallel currents add; therefore, the base metallization with two parallel strips can take twice as much current as the emitter metallization which has only one strip. If the same current exists in both the emitter and the base, the emitter metallization will suffer burn-out first.

Radiation Incorporated developed an expression for the burn-out current for microsecond time scales which predicts a value 2.5 times the observed experimental value.⁽²⁷⁾

These studies consider an unstressed interconnect and the differences between theoretical calculations and measured data can well be explained if the interconnect is stressed by a fence crossing or a scratch or defect in the material. Failures plotted in Figures 2-45 and 2-46 occurred at a stress point. Lockheed has shown that hot spots form at the point where an interconnect crosses an oxide step.⁽²⁸⁾

Table 2-17 lists some measured power supply currents for some integrated circuits at specific dose rates.

2.6.4 Bonding Wire Burn-Out

Bonding wire burn-out has been observed in some cases but has generally been accompanied with chip damage. At this writing, it has not

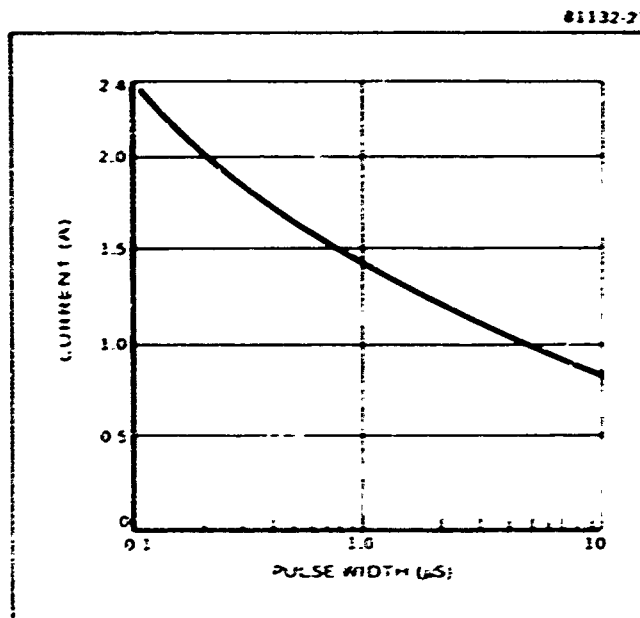


FIGURE 2-45 Current vs Pulse Width Burn-Out Thresholds for 0.55 mil Metallization (A Geometry)

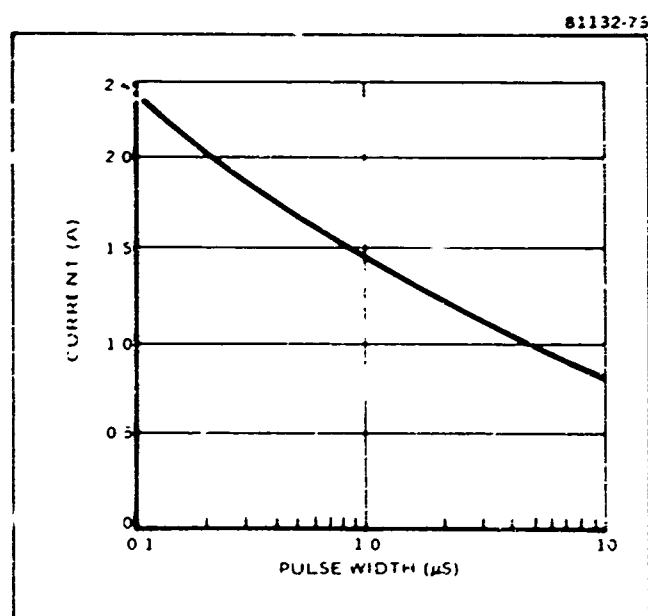


FIGURE 2-46 Current vs Pulse Width Burn-Out Thresholds for 0.55 mil Metallization (B Geometry)

TABLE 2-17 Integrated Circuit Radiation Induced Currents

Type	Transient Power Supply Current (A)	Dose Rate (Rad(Si)/s)	
μ A 709	2 to 3	2×10^9	(Ref 26)
DTL 932	0.800	1×10^{12}	(Ref 29)
DTL 9040	0.800	3×10^{10}	(Ref 30)
*TI 911 Read Pre-amplifier	2.5	6×10^9	(Ref 31)

*Failed catastrophically due to interconnect burn-out in power supply line.

been established which occurs first. Intuitively, it would appear that the junction will short and cause the bonding wire to burn out. If this is true, the bonding wire burn-out level is higher than the junction damage level.

2.6.5 Junction Damage

2.6.5.1 Effects Of Circuit Resistance

The threat to semiconductor junctions is due to the high photocurrent generated by the transient radiation. This current multiplied by the voltage across the devices increases the power being dissipated in the device. If the power dissipation is sufficient, the device will be destroyed. At very high dose rates the photocurrents become extremely high and may be limited by device resistances normally too small to be considered.

Use of the standard photocurrent prediction expressions at high dose rate levels can predict hundreds, thousands, or higher amperes of photocurrent. While the validity of using the prediction technique at high levels may be questionable, there is no question that large currents will flow. For currents of this magnitude, circuit resistance usually considered negligible becomes significant. These resistances include such things as the resistance per unit length of wire, the resistance of contacts in a connector, and the resistance of the ohmic contact, and leads in semiconductor components.

Consider the circuit of Figure 2-47A. The resistance is composed of all resistance in the circuit including the lead resistance and interconnect resistance of the diode. During irradiation the current $i(\dot{\gamma})$ will flow. Two situations can exist. For the case where

$$V - i(\dot{\gamma})r > \approx 0 \quad (2-17)$$

reverse bias will still appear across the junction in the diode. In this case

$$i(\dot{\gamma}) = i_{pp} \quad (2-18)$$

where

i_{pp} = primary photocurrent.

81132-77

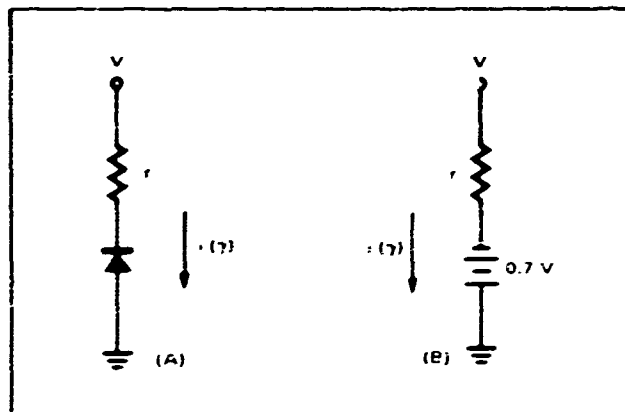


FIGURE 2-47 Equivalent Semiconductor Circuits at High Dose Rates

When

$$V - i(\dot{\gamma}) r \approx 0 \quad (2-19)$$

reverse bias will no longer appear across the junction. In this case the current is limited by the circuit resistance (r) and

$$i(\dot{\gamma}) = \frac{V}{r} \quad (2-20)$$

and

$$i(\dot{\gamma}) < i_{pp} \text{ (predicted)} \quad (2-21)$$

in the worst current limited case the diode will forward bias. In this case the equivalent circuit during radiation is shown in Figure 2-47B. The diode is now effectively operating as a voltage limited current source much the same way as solar cells operate under solar illumination. The expression for $i(\dot{\gamma})$ becomes:

$$i(\dot{\gamma}) = \frac{V + 0.7}{r} \quad (2-22)$$

Equation 2-22 will differ insignificantly from Equation 2-20 for source voltage (V) greater than approximately 10 volts.

2.6.5.2 Typical Circuit and Component Resistances

The typical resistance of an irradiated transistor from emitter to collector assuming silicon is a perfect conductor can be estimated. The assumption of perfect conduction for the silicon appears reasonable.

The carrier generation rate (g) per unit of radiation dose rate in silicon is 4.2×10^{13} electron-hole pairs/cm³ - rad.⁽¹⁾ The mean lifetime (τ) can be as long as 10^{-4} seconds, assuming equal amounts of N and P-type material per device, the average mobility (μ) is about $\frac{10^3 \text{ cm}^2}{\text{volt} \cdot \text{sec}}$. The number of excess carriers (n) generated at 10^{10} rad(Si)/s is:

$$\begin{aligned} g \dot{\gamma} &= 4.2 \times 10^{13} (10^{10}) \\ &= 4.2 \times 10^{23} \frac{\text{electron-hole pairs}}{\text{cm}^3 \cdot \text{sec}} \end{aligned} \quad (2-23)$$

The conductivity will be:

$$\begin{aligned} \sigma &= n e u \tau \\ &= (4.2 \times 10^{23})(1.6 \times 10^{-19})(10^3)(10^{-4}) \\ &= 5.7 \times 10^3 \text{ mhos/cm} \end{aligned} \quad (2-24)$$

where

$$e = \text{charge on the electron.}$$

The conductivity of hard drawn copper at room temperature is about 6×10^5 mhos/cm. Therefore, the assumption that the silicon approximates a good conductor on exposure to $\geq 10^{10}$ rad(Si)/s is justified. The above calculation is worst case, however, since both mean lifetimes and mobility will decrease under this level of radiation. There are not enough data available to consider this influence on the radiation induced conductivity at this time.

The sources for resistances which add to give the equivalent resistance of a transistor under irradiation are: (32)

- . ~ 40 mils of 0.7 to 1 mil diameter wire
- . Bonding pad (4 x 4 mil) which usually contribute negligible resistance
- . Interconnect 0.01 to 0.1 ohm/square
(This is a length dependent problem. Typical length is ≈ 10 square therefore 0.1 \rightarrow 1 ohm)
- . Bond to junction.

For typical low power, high frequency devices, the minimum resistance will be in the range of 0.1 to 1 ohm for the collector-to-emitter resistance. For typical power device the resistance is approximately one order of magnitude lower because power devices do not require the interconnect. Therefore, for power devices, the worst case resistance will be in the range of 0.01 to 0.1 ohm.

A typical value of anode-to-cathode resistance for an irradiated diode, assuming silicon is a perfect conductor, can be estimated in a similar manner. Diode resistances will vary according to construction technique where the sources of resistance are the lead resistance and the ohmic contacts made to the silicon. Typical diode resistances are shown in Table 2-18.

TABLE 2-18 Typical Diode Semiconductor Resistances Under Irradiation

<u>Types</u>	<u>Ohms</u>
Computer Diode	0.050
Zener	0.050
Rectifier	0.010

These resistances can be assumed constant and independent of dose rate.

The resistance of wiring and connectors inside an electronic package can furnish some current limiting. A typical electronic package will contain several printed circuit cards and the necessary wiring to a connector on the surface of the package. The connector joins the package to the main spacecraft harness. Where possible, the wiring from the connector is hand-wired to the printed circuit boards although card connectors are not uncommon. The resistance through a typical connector has been measured and falls between 0.6 m Ω and 1.3 m Ω . Wiring from the connector to a card will average approximately 1 foot in length. Unless other requirements dictate (such as voltage drop), wiring will generally be selected according to Table 2-19.

TABLE 2-19 Wire Resistance

<u>Current (A)</u>	<u>Gauge</u>	<u>Ω/ft at 50°C</u>
5	22	0.018
7.5	20	0.011
10	10	0.0071
13	16	0.0045
17	14	0.0028
23	12	0.0018

A path through a typical electronic package including circuit and converter wiring but excluding components will be on the order of 20 m Ω .

The above discussion indicates that there will be no significant current limiting due to inherent device resistances of 0.01 to 0.05 Ω for currents up to a few thousand A for a 20 to 30 V system. Wiring and connector resistance cannot be counted on for current limiting since the energy source may be connected to the threatened device by only a few inches of wire.

2.6.5.3 Experimental Studies

Experimental studies have provided some guidelines for use in estimating the power level required to cause junction failures Wunsch and Bell's⁽³³⁾ paper provides the most useful data for estimating potential junction failures as a result of currents generated by a nuclear weapon environment. They derive an expression for the power

per unit area required to destroy a junction as a function of time. This expression (Equation 2-25) is derived using a thermal model which assumes the junction is pulsed in the reverse direction and all of the voltage is dropped across the junction.

$$P/A = \sqrt{\pi K \rho c_p} [T_m - T_i] t^{-\frac{1}{2}} \quad (2-25)$$

where

- P = power in watts
- A = junction area
- K = thermal conductivity
- ρ = density
- c_p = specific heat
- T_m = failure temperature
- T_i = initial temperature
- t = pulse duration in microseconds

Three cases are considered:

1. Heating from 25° to 675°C which is the failure temperatures suggested by Davis and Gentry⁽³⁴⁾ and other workers.
2. Heating from 25° to the melting temperature of silicon of 1415°C.
3. Same as case 2 except the currents are assumed to be concentrated in 1/10 of the junction area.

Equation 2-25 can be written as $P/A = Kt^{-\frac{1}{2}}$ and plots as a straight line on log-log paper with a slope of $-\frac{1}{2}$. These plots allow a convenient comparison of devices with different junction areas.

Figure 2-48 is a plot of the three cases listed above. Wunsch and Bell measured the failure thresholds for over 1200 devices of approximately 80 different types. Transistors, diodes, rectifiers, and zener diodes were included. The times utilized were in the range of 0.1 to 20 μ s and the power level ranged up to 8 kW per pulse. Most of the junctions were pulsed in the reverse direction at the avalanche voltage thus insuring that all of the voltage was dropped across the junction.

Figures 2-49 through 2-52 are data on diodes. Some junctions were pulsed in the forward direction and were found to require more power for destruction. Some of the transistors were pulsed from collector-to-emitter and found to burn-out at about the same level as if the emitter-base were pulsed. Intuitively, this would be expected since the collector-base junction is much larger than the emitter-base junction. Therefore, it makes no difference whether the emitter-base or collector-emitter base terminals are pulsed. Wunsch and Bell's data does not substantiate this, however, since they found that either one or both junctions burned-out in devices pulsed collector-to-emitter.

Figures 2-53 and 2-54 show data on forward pulsing of devices and collector-emitter pulsing. The emitter-base junction was used for most of the measurements. Wunsch and Bell concluded that the predominant failure mode, for these μ s and sub μ s pulses, is localized melting across the junction. The melted regions form resistive paths across the

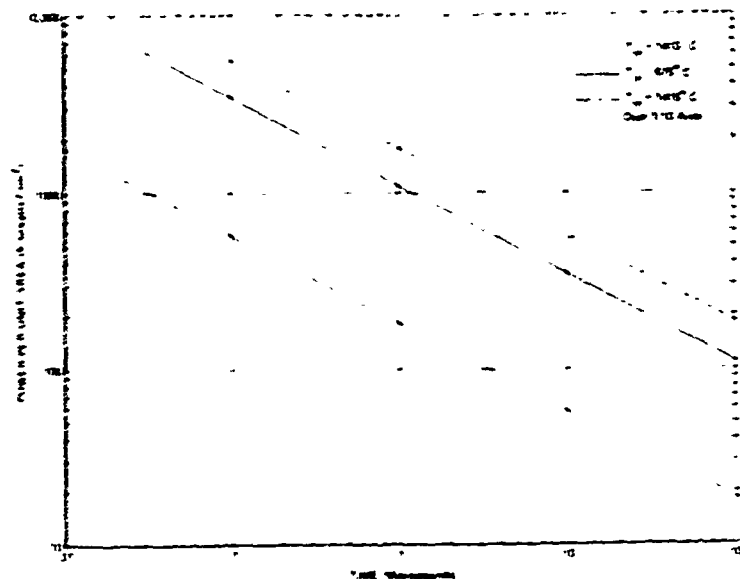


FIGURE 2-48 Theoretical Failure Curves for Silicon Junctions for Reverse Polarity Voltages (33)

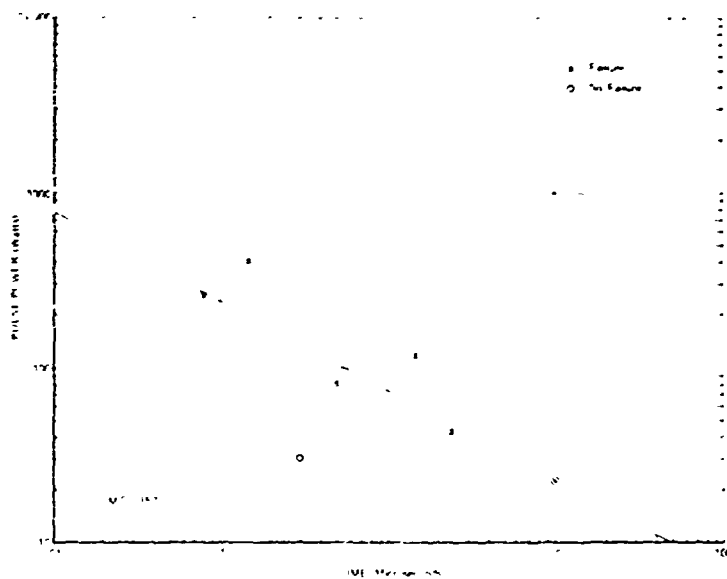


FIGURE 2-49 Experimental Data Points for Failure of the Anode-Cathode Junction of a MC-357 Diode for Reverse Polarity Voltage Pulses. (33)

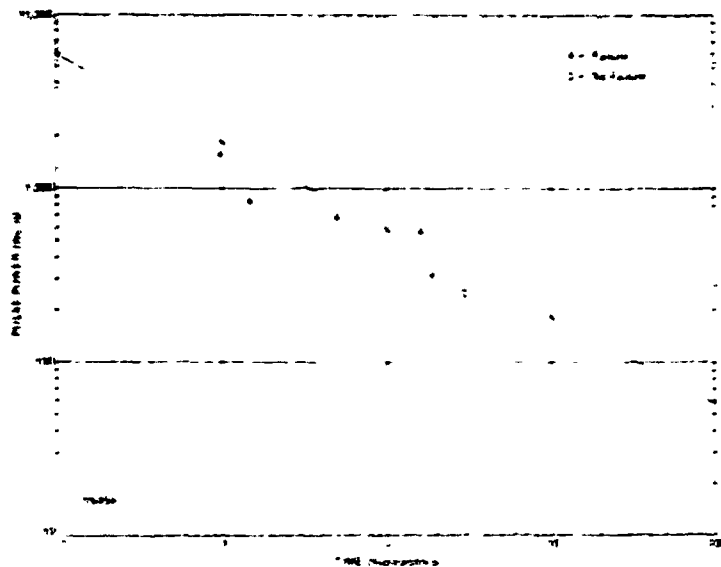


FIGURE 2-50 Experimental Data Points for Failure of the Anode-Cathode Junction of 1N459 Diode for Reverse Polarity Voltage Pulses (33)

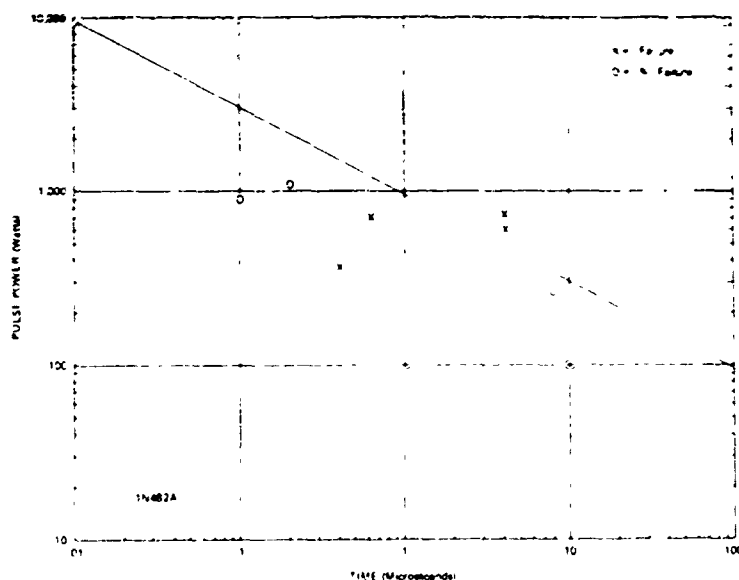


FIGURE 2-51 Experimental Data Points for Failure of the Anode-Cathode Junction of a 1N482A Diode for Reverse Polarity Voltage Pulses. (33)

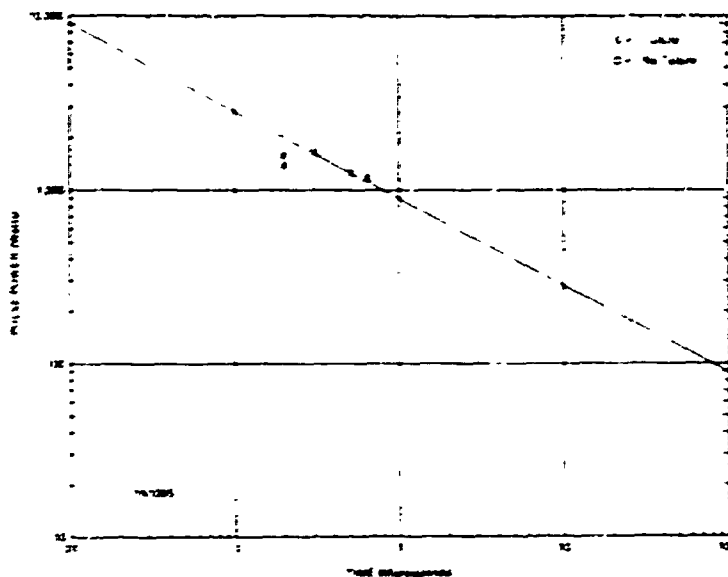


FIGURE 2-52 Experimental Data Points for Failure of the Anode-Cathode Junction of a 1N1095 Diode for Reverse Polarity Voltage Pulses. (33)

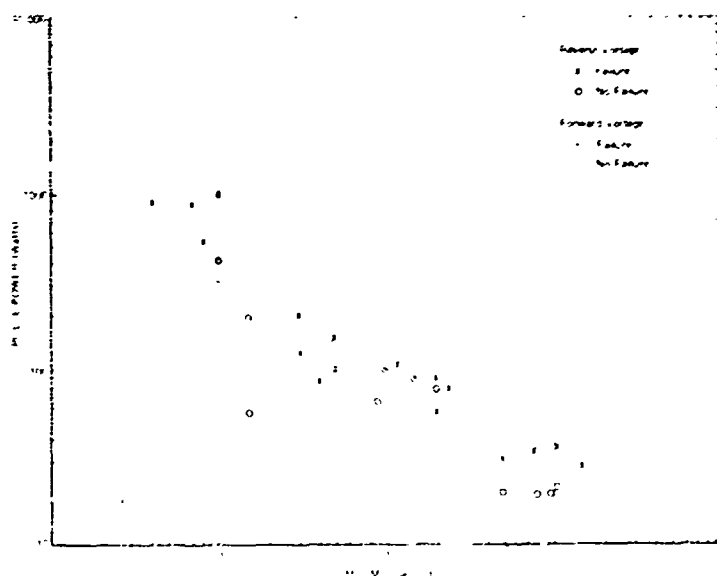


FIGURE 2-53 Experimental Data Points for Failure of the Base-Emitter Junction of a 2N2222 Transistor for Forward and Reverse Polarity Voltage Pulses. (33)

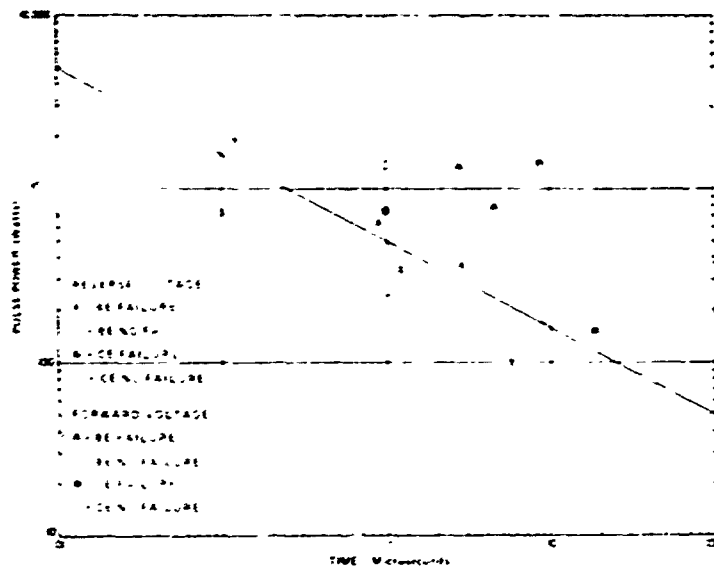


FIGURE 2-54 Experimental Data Points for Failure of the Base-Emitter and Collector-Emitter Junctions of a 2N1132 Transistor for Forward and Reverse Polarity Voltage Pulses. (33)

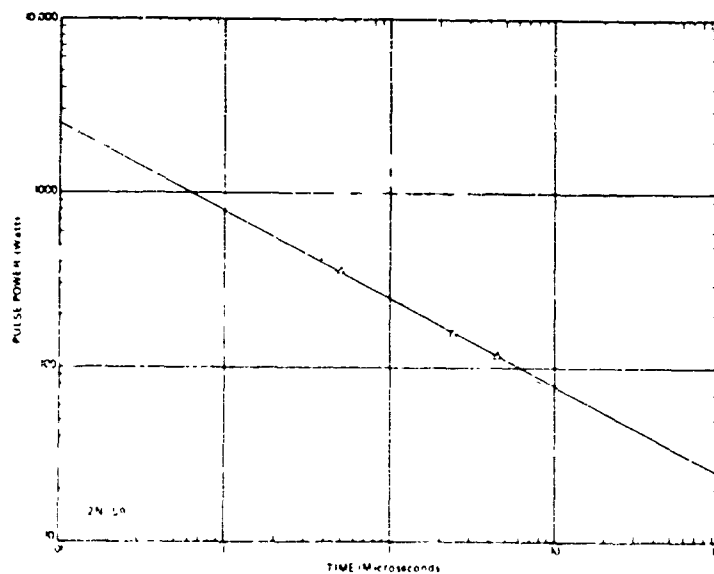


FIGURE 2-55 Experimental Data Points for Failure of the Base-Emitter Junction of a 2N699 Transistor for Reverse Polarity Voltage Pulses. (33)

junction which shorts out or masks any other junction action. This conclusion was based on examination of some of the samples which failed where the damage was evident. It appeared that localized melting had occurred. In some devices sufficient melting had taken place that a flow of melted silicon could be observed. In an actual system the junctions will normally not be subjected to avalanche voltages but the junctions will be back biased. Radiation effectively increases the conductivity of the silicon to that of a good conductor and the bias voltage will be dropped entirely across the junction. Figures 2-55 and 2-56 are additional data.

Figures 2-49 through 2-54 provide good guidelines for assessing junction failure potential. Figure 2-49 is illustrative of integrated circuit devices. Figures 2-50, 2-51 and 2-52 are representative of low level rectifiers or switching diodes. Figures 2-53 and 2-54 are representative of NPN and PNP low power transistor respectively. Figures 2-55 and 2-56 are representative of medium power transistors. Note that these curves are plotted with an ordinate expressed in watts so that junction area is not specified. Figures 2-57 and 2-58 are plots of power failure thresholds per unit area for diodes and transistors. The important point to note is that most of the failure points lie within the worst case limits defined in Figure 2-48.

Figures 2-49 through 2-56 can be used to estimate the power level failure threshold for other device types by scaling the data to the power ratings of the devices without knowing the junction area. Figures 2-57 and 2-58 indicate relatively consistent results by considering the power per unit area to cause burn-out. The power rating of a transistor is proportional to the junction area as indicated in Figure 2-59. Therefore, order of magnitude estimates can be made on other device types by linear extrapolation of the data in Figures 2-49

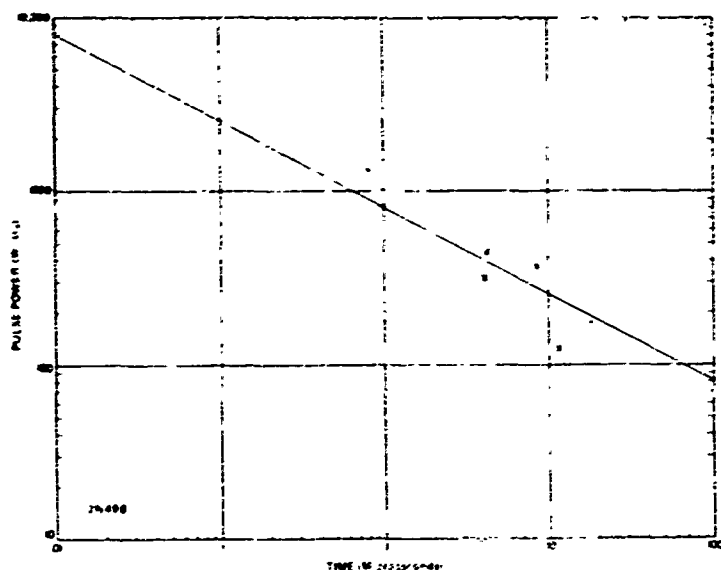


FIGURE 2-56 Experimental Data Points for Failure of the Base-Emitter Junction of a 2N498 Transistor for Reverse Polarity Voltage Pulses. (33)

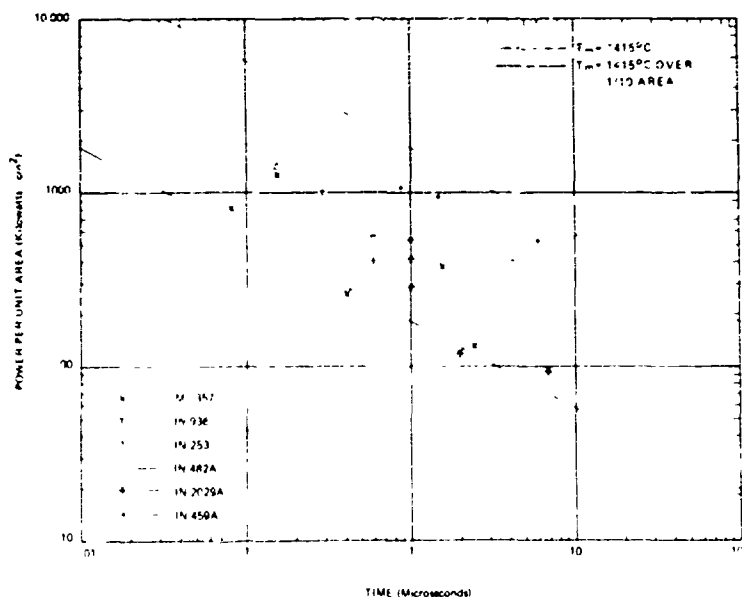


FIGURE 2-57 A Composite of Experimental Data Points for the Failure of the Anode-Cathode Junction for Six Diodes. Inter-comparison is Made By Plotting Power Per Unit Area vs Pulse Duration. Also shown are the theoretical failure curves. (33)

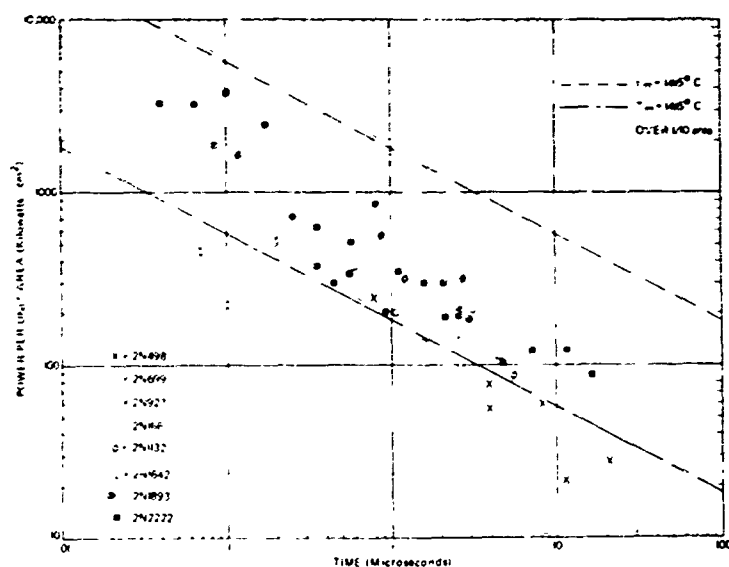


FIGURE 2-58

A Composite of Experimental Data Points for the Failure of the Base-Emitter Junction for Eight Transistors. Intercomparison is Made by Plotting Power Per Unit Area vs Pulse Duration. Also shown are the theoretical failure curves. (33)

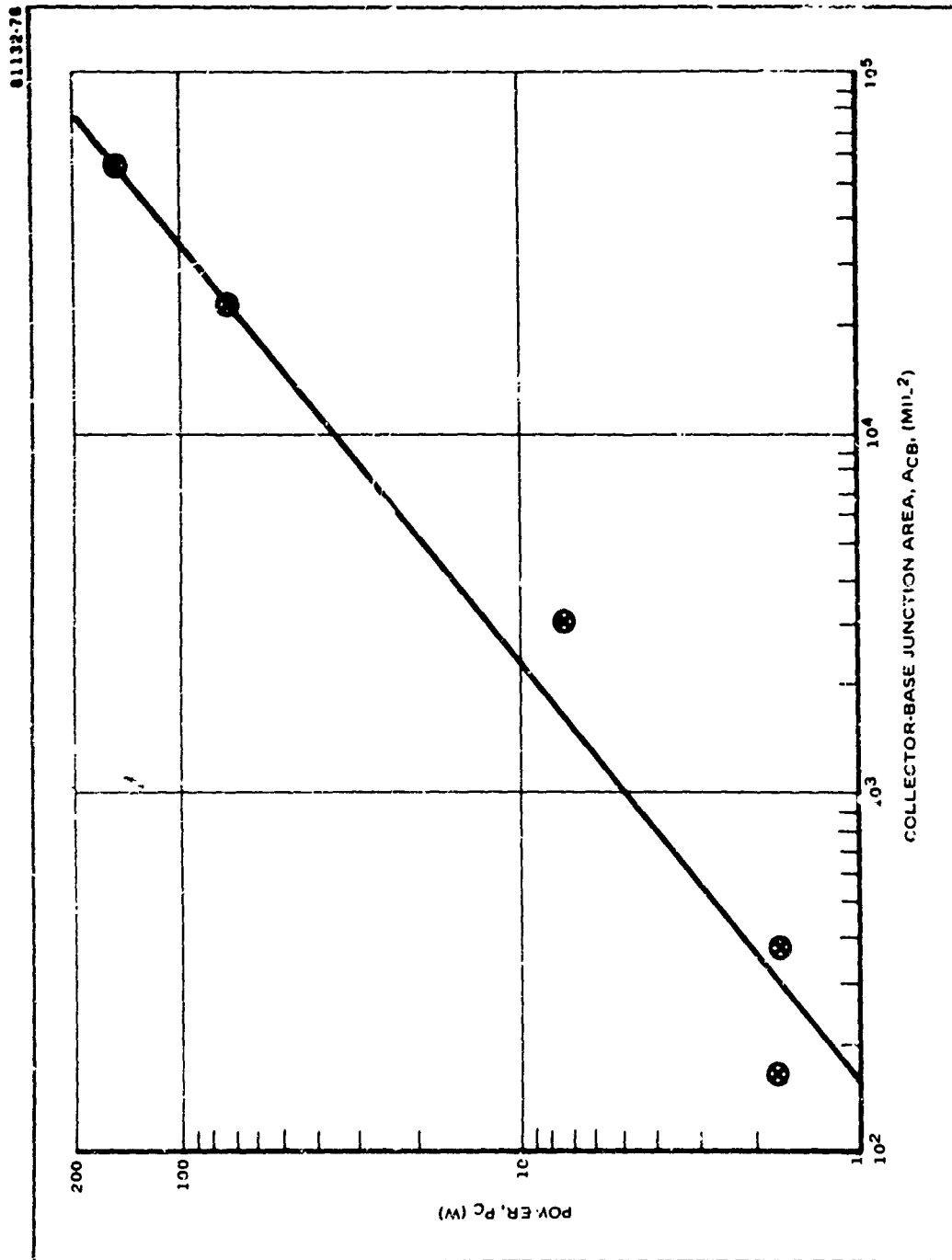


FIGURE 2-59 Transistor Power Rating vs Collector-Base Junction Area

through 2-56 to other power ratings. For example, the data on the 4 watt 2N498 transistor in Figure 2-56 indicates a failure threshold of about 850 watts at 1 μ s. If a 20 watt device is considered, the power required for burn-out would be approximately 5 times the watt value (i.e., 4250 watts at 1 μ s).

A similar rationale can be established for diodes. Figure 2-60 illustrates the average forward rectified current rating (I_0) as a function of junction area. Therefore, the diode data can be extrapolated on the basis of the diode I_0 rating.

Figure 2-61 illustrates diode data where the diodes did not fail due to insufficient pulse power to burn out the devices. The striking point is that when power per unit area is considered, most of the points fall on the safe side of the theoretical failure.

Figure 2-63 is a comparison of Wunsch and Bell's data with Davis and Gentry's curves for the 2N2222 transistor. Davis and Gentry (34) considered longer duration pulses than Wunsch and Bell in their work. There is general agreement for over five orders of magnitude in pulse duration. Figure 2-63 is a plot of the average of the constants of the lines for Figure 2-49 through 2-56 when converted to a power per unit area basis. The equations for these lines are:

$$\text{All devices} \quad P/A = 480 \, t^{-\frac{1}{2}} \quad (2-26)$$

$$\text{Transistors} \quad P/A = 310 \, t^{-\frac{1}{2}} \quad (2-27)$$

$$\text{Diodes} \quad P/A = 560 \, t^{-\frac{1}{2}} \quad (2-28)$$

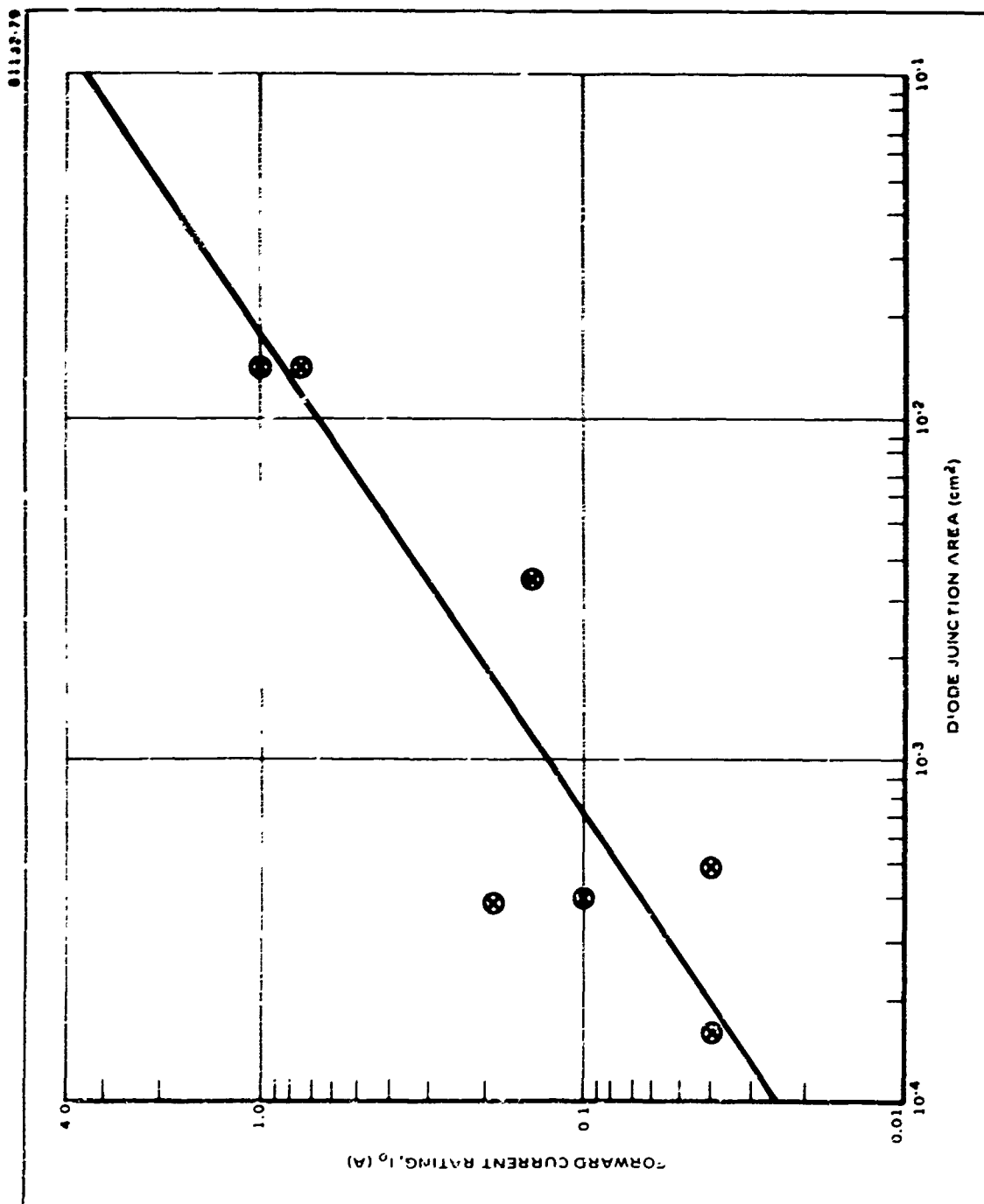


FIGURE 2-60 Diode Forward Current Rating vs Junction Area

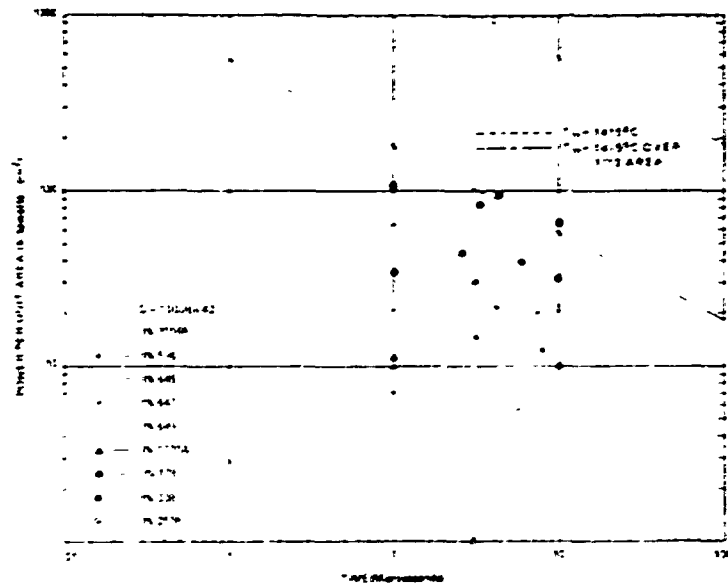


FIGURE 2-61 A Composite of Experimental Data Points for which No Failure was Achieved for the Anode-Cathode Junction for Ten Large Area Diodes. Intercomparison is made by Plotting Power per Unit Area vs Pulse Duration. Also shown are the theoretical failure curves. (33)

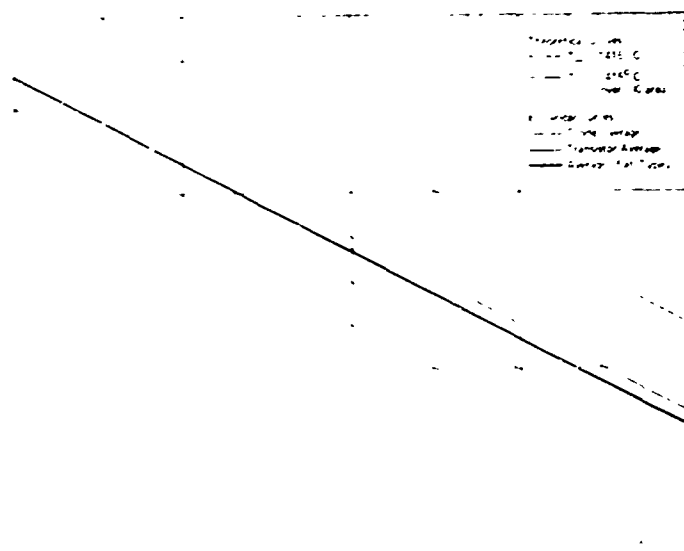


FIGURE 2-62 Plots of the Semi-Empirical Failure Equations Obtained from Theory and the Experimental Data Points. (33)

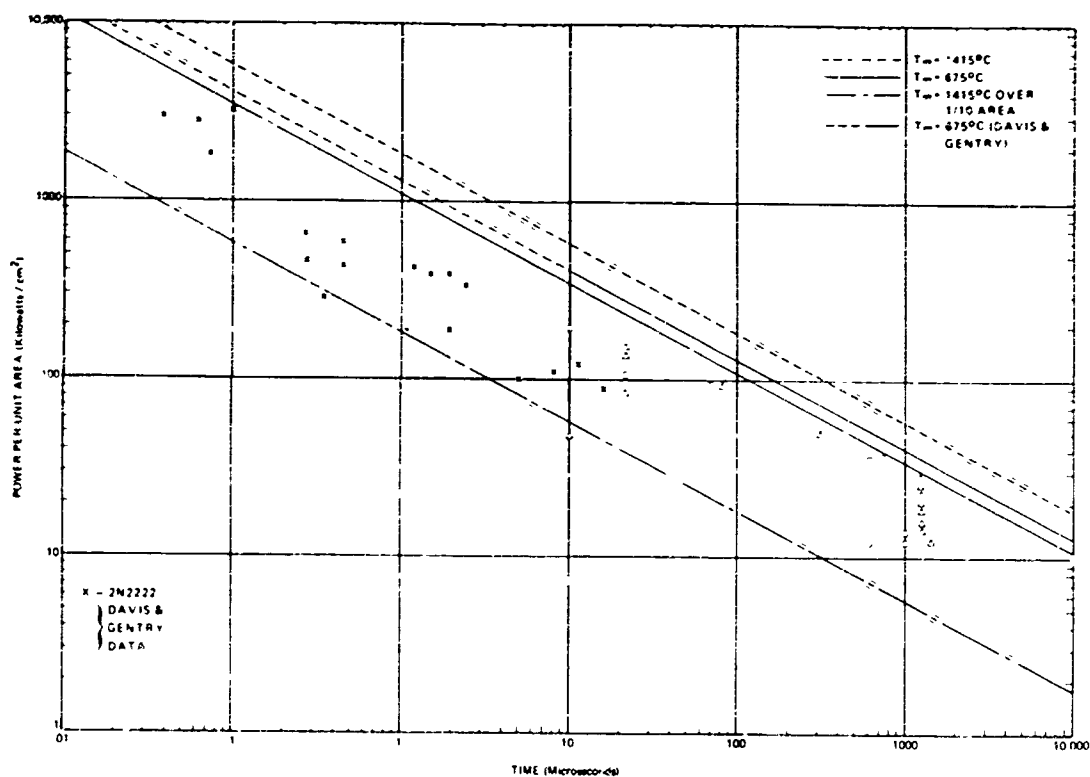


FIGURE 2-63 A Comparison of Experimental Data Points for a 2N2222 Transistor and Points from a Paper by Davis and Gentry.⁽³⁴⁾ Also shown are the theoretical failure curves from this paper and the curve by Davis and Gentry.⁽³³⁾

These averages lie very close together and are about midway between the worst case limits. These expressions can be used to estimate failure loads within at least an order of magnitude for most diodes and transistors. The only piece of information required is the junction area or, as discussed, the power rating.

2.6.5.4 Theoretical Studies

An approach to the problem for transistors was considered by Marshall⁽³⁵⁾ where the thermal parameters of the device were used to predict device burn-out.

The allowable peak power dissipation of a transistor junction can be calculated if the thermal resistances and the thermal time constants of the device are known. The equivalent thermal circuit of any transistor is shown in Figure 2-64. The total thermal junction-to-air resistance is:

$$\theta_{JA} = \theta_{JC} + \theta_{CS} + \theta_{SA} \quad (2-29)$$

The steady-state or dc junction temperature can be calculated as:

$$T_J = P_D \theta_{JA} + T_A \quad (2-30)$$

where P_D is the steady-state power dissipated in the transistor,

$$P_D = I_B V_{BE} + I_C V_{CE} \quad (2-31)$$

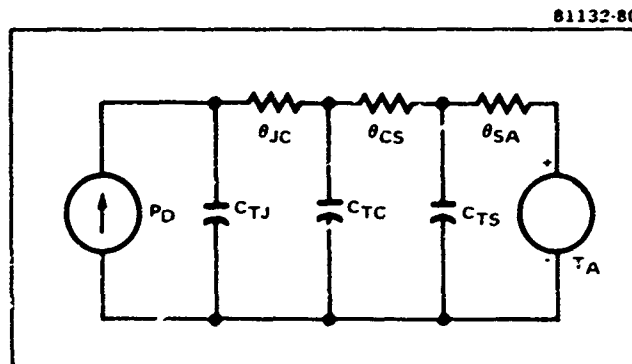


FIGURE 2-64 Thermal Equivalent Circuit

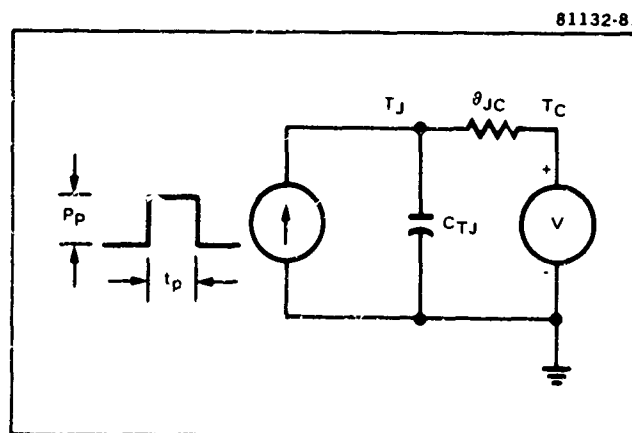


FIGURE 2-65 Simplified Equivalent Circuit

If the maximum allowable junction temperature (T_J) is specified, the maximum allowable dc power is given by:

$$P_D (\text{max}) = (T_J (\text{max}) - T_A) / \theta_{JA} \quad (2-31)$$

The equations are somewhat more complex for the transient case because the pulse power dissipation depends on the thermal capacitance as well as the thermal resistance. The expected repetition rate of transient radiation pulses is extremely low. The following equations will, therefore, assume a single rectangular power pulse of width (t_p). It will also be assumed that the transistor case is attached to an infinite heat sink; i.e., the case temperature is equal to the ambient temperature. The resulting equivalent circuit is shown in Figure 2-65. With these assumptions, the junction temperature at the end of the pulse is:

$$T_J = T_C + P_P \theta_{JC} \left[1 - \exp(-t_p / \tau_{JC}) \right] \quad (2-32)$$

where P_P is the pulse power and τ_{JC} is the junction-to-case thermal time constant, and is equal to $\theta_{JC} \times C_{TJ}$. The term $\left[1 - \exp(-t_p / \tau_{JC}) \right]^{-1}$ is referred to by manufacturers as the transistor coefficient of power, C_{PJC} .

If $\exp(-t_p / \tau_{JC})$ is expanded into a power series, the following result is obtained:

$$\exp(-t_p/\tau_{JC}) = 1 - \frac{t_p}{\tau_{JC}} - \left(\frac{2t_p}{\tau_{JC}}\right)^2 - \left(\frac{3t_p}{\tau_{JC}}\right)^3 \dots - \left(\frac{nt_p}{\tau_{JC}}\right)^n \quad (2-33)$$

If t_p is much smaller than τ_{JC} , the high-order terms in the series are insignificant and $\exp(-t_p/\tau_{JC})$ can be approximated by $1 - t_p/\tau_{JC}$. Therefore:

$$\left(C_{PJC}\right)^{-1} \approx t_p/\tau_{JC} \quad (\text{for } t_p \ll \tau_{JC}) \quad (2-34)$$

When this expression is substituted in Equation 2-32, the following expression for junction temperature is obtained:

$$T_J = T_C + P_P \theta_{JC} t_p/\tau_{JC} \quad (2-35)$$

The peak power which can be dissipated in the junction is therefore

$$P_P = \frac{(T_J(\text{max}) - T_C) \tau_{JC}}{\theta_{JC} t_p} \quad (2-36)$$

The thermal resistance (θ_{JC}) can be measured or calculated from the data given on transistor specification sheets. The maximum allowable junction temperature should be selected to meet the device application requirements. Thermal time constants were measured for integrated circuit transistors in flat pack, TO-5 cans, and dual-in-line packages. It was found that at least three superimposed time constants were involved for each package type. The shortest measured time constant of significance was found to be 1 ms. This value agrees quite well with the values reported in the literature for transistors in TO-5 cans.

The maximum power dissipations and thermal resistances for 2N708 and 2N709 transistors mounted in TO-5 cans are given in Table 2-20. The 2N708 and 2N709 transistors have characteristics which are similar to transistors which are used in modern integrated circuits.

TABLE 2-20 Transistor Thermal Characteristics (35)

	θ_{JA}	P_{DJA}	θ_{JC}	P_{DJC}
2N708	480°C/w	360 mW	150°C/w	1.2 w
2N709	585°C/w	300 mW	200°C/w	0.5 w

The values in Table 2-20 were used to calculate the allowable peak power dissipation for these transistors for various values of t_p and τ_{JC} for which $t_p/\tau_{JC} < 0.1$. These data are plotted in Figure 2-66.

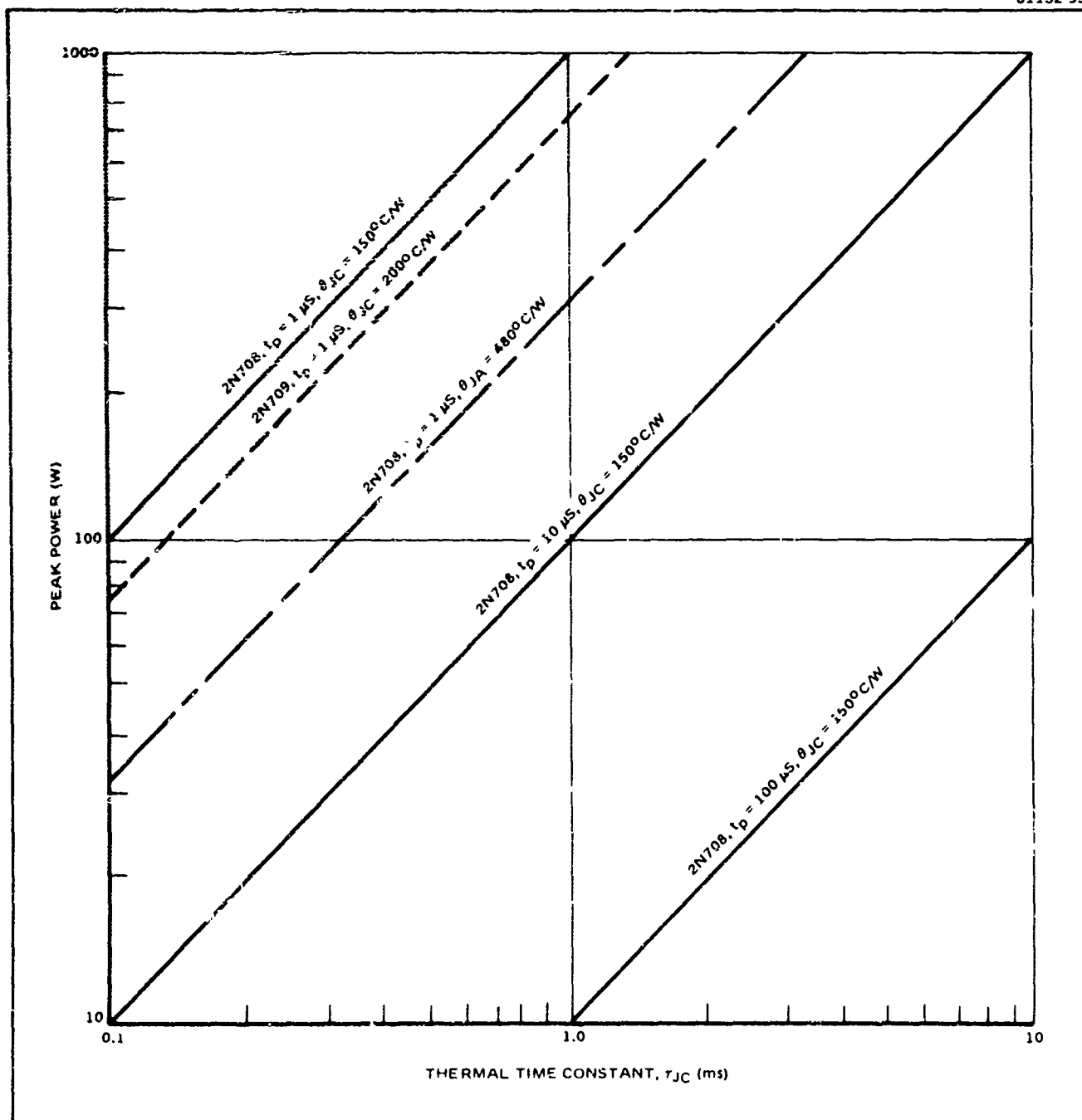


FIGURE 2-66 Peak Power Dissipation for Silicon Transistors

It is immediately apparent that, for radiation pulse widths of 1 μ s or less, the allowable peak power dissipation is greater than 100 watts even for short thermal time constants.

If the results for the 2N708 for a $\tau_{JC} = 1 \mu$ s are plotted on a figure such as 2-53, the resulting line is a reasonably good fit for the forward pulsed data. Intuitively, this might be expected since in the forward pulsed condition and in the condition where the thermal parameters are defined, the device bulk properties have more effect than in the case where the bulk properties can effectively be removed either by radiation or by avalanche pulsing.

2.6.5.5 Radiation Studies

Twenty devices were tested at the Hughes Linear Accelerator for catastrophic failure due to excessive secondary photocurrent (i_{pp2}).⁽³⁶⁾ The circuit used for measuring i_{pp2} is shown in Figure 2-67. The base lead was left open so that all the primary photocurrent (i_{pp}) would generate secondary photocurrent.

A plot of the pulse width (of the radiation pulse) versus the power (watts) generated by the secondary photocurrent is shown in Figure 2-68 for those transistors that suffered catastrophic failure.

The dose rate failure modes of the transistors that suffered catastrophic failure are analyzed in Table 2-21. Comparing these data with that in Figure 2-56 indicates a reasonable correlation between the radiation-induced burn-out and the electrical bench testing at the avalanche voltage.

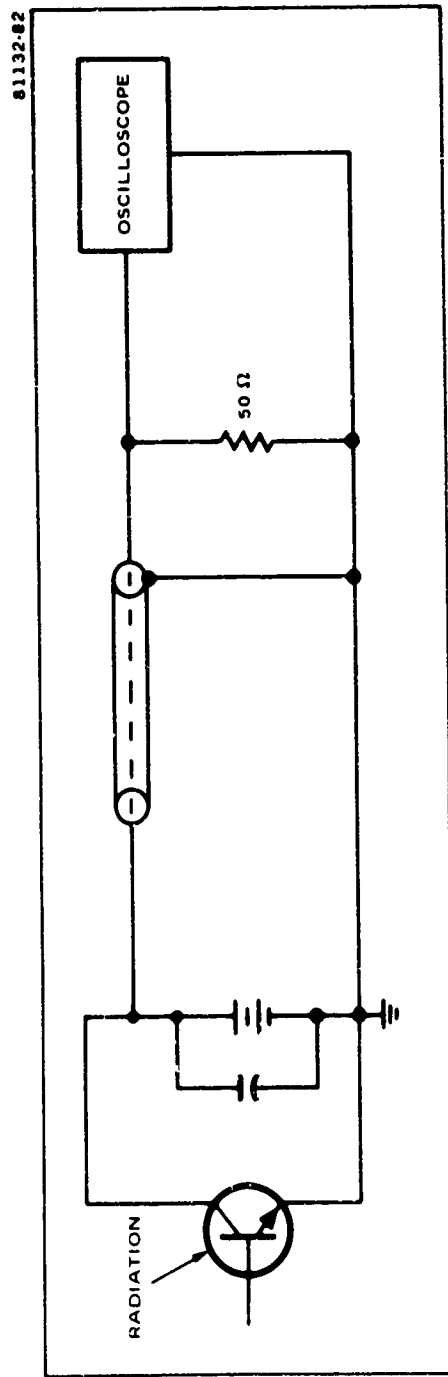


FIGURE 2-67 Circuit Used for Measuring Secondary Photocurrent (i_{pp2})

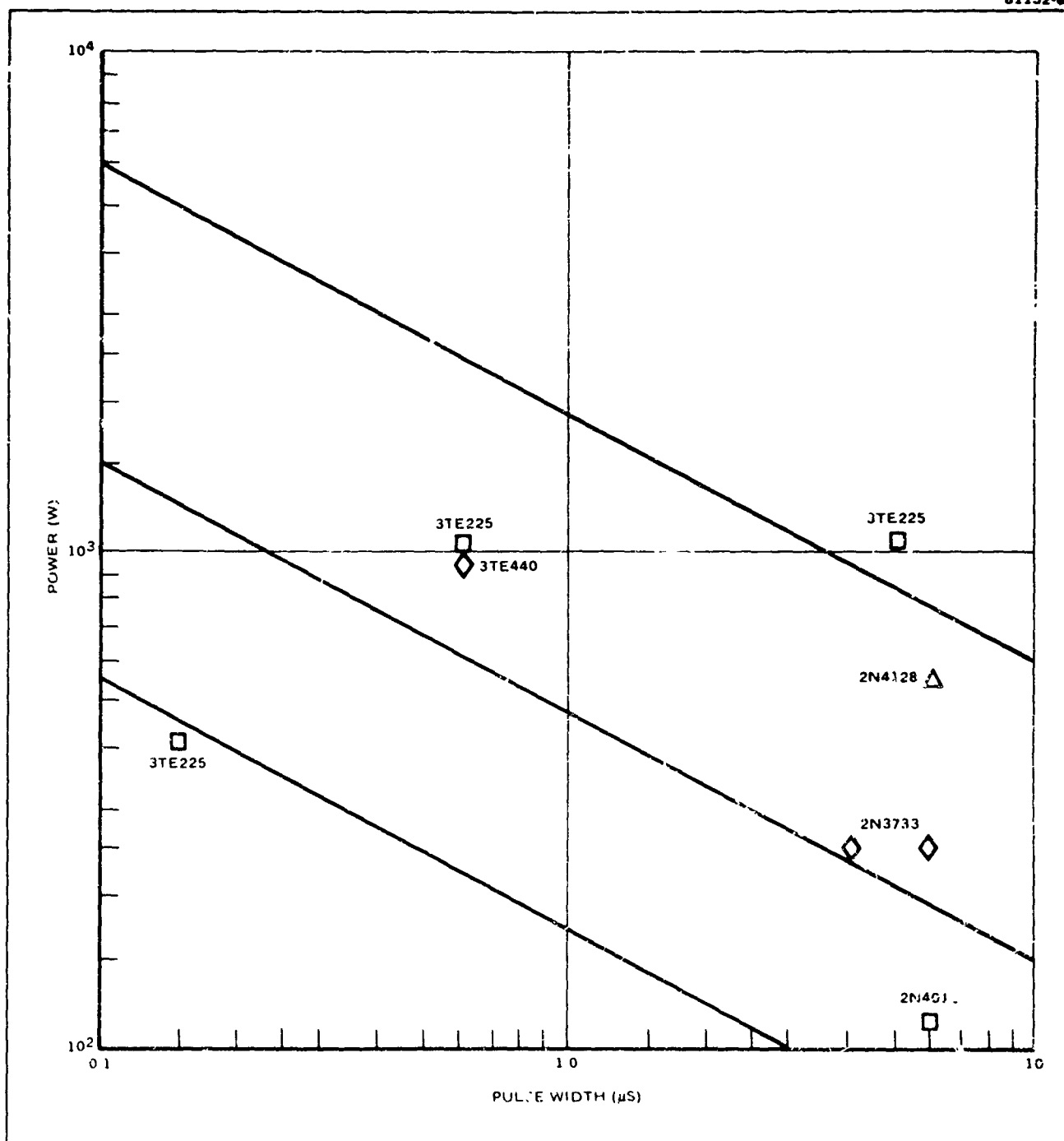


FIGURE 2-68 Power Dissipation vs Pulse Width for Radiation Induced Burn-Out for Various Transistors

TABLE 2-21 Device Failure Modes Due To Dose Rate Effects

Transistor Type	$\dot{\gamma}$ 10 ¹⁰ rad(Si)/s	t (μ s)	I (A)	Power (Watts)	Dose Rate Failure Mode*						
					1	2	3	4	5	6	7
2N2270 ¹	3	6	20	560	X						
2N2270 ²	3	6	20	560	X						
2N2270 ³	3	6	20	560	X						
2N3733 ³	3	6	9	252		X	X	X			
2N3733 ⁴	3	6	14	392	X						
2N3733 ⁵	3	6	14	392	X						
2N3733 ⁷	3	4	9	252			X	X			
2N4012 ³	3	6	9	252	X						
2N4012 ⁴	2	6	4	112			X	X			
2N4012 ⁵	3	6	6	196	X						
2N4128 ¹	3	6	18	504	X						
2N4128 ⁵	3	6	20	560						X	
3TE225 ¹	3	5	38	1064						X	
3TE225 ²	1.2	0.6	37	1036						X	
3TE225 ³	6	0.15	15	420						X	
3TE440 ³	3	0.6	35	980						X	
PT2917 ¹	1.4	6	120	3360	X						
PT2917 ²	2	1	120	3360						X	X
TA7036 ¹	3	6	20	560	X						
TA7036 ²	3	6	19	531	X						

* See next page for dose rate failure mode definition

Definition of Transistor Failure Modes for Table 2-21

- 1 No sustained damage**
- 2 Base lead burned off at chip**
- 3 Emitter lead burned through between post and chip**
- 4 Too much carbon on chip to analyze damage**
- 5 Internal open, potted construction prevents further analysis**
- 6 Ceramic header loose from heat sink**
- 7 Chip shorted emitter to collector**

Figure 2-69 illustrates an important concept. The Hughes electrical test data on the 2N2222 is plotted along with Wunsch and Bell's data extrapolated. The Hughes data was taken by pulsing the transistor base and allowing unlimited collector-emitter current to flow. The collector voltages were kept below the maximum ratings on the Hughes data. The important point is that a much higher (order of magnitude approximately) power level was required to burn-out the transistors for this case as opposed to the avalanche condition. If the assumption that avalanche and radiation are identical with respect to burn-out potential, then these data illustrate the potential vulnerability to radiation induced catastrophic failure of transistors which normally would be working below the failure threshold.

Figures 2-70 and 2-71 illustrate some Hughes generated electrical test data on integrated circuit transistor kit parts consisting of transistors and interconnects mounted on a header. There are five collector-base geometries (A through E). The junctions (emitter base and collector base) were pulsed in the forward direction. An attempt was made to establish which junction (E-B or C-B) will burn-out first. The burn-out dependence on area was also studied. As indicated in Figure 2-70, the data spread did not allow either determination to be made. Figure 2-71 is the data plotted in power per unit area with Wunsch and Bell's limit drawn for reference. Many of the devices lay outside these limits which is understandable since most of these are emitter-base junctions and the power per unit area is determined by dividing a relatively large number by a very small one. The small number has a large error associated with its determination. An additional variable in these data is that interconnect burn-out is also evident. The only information to be gleaned from these

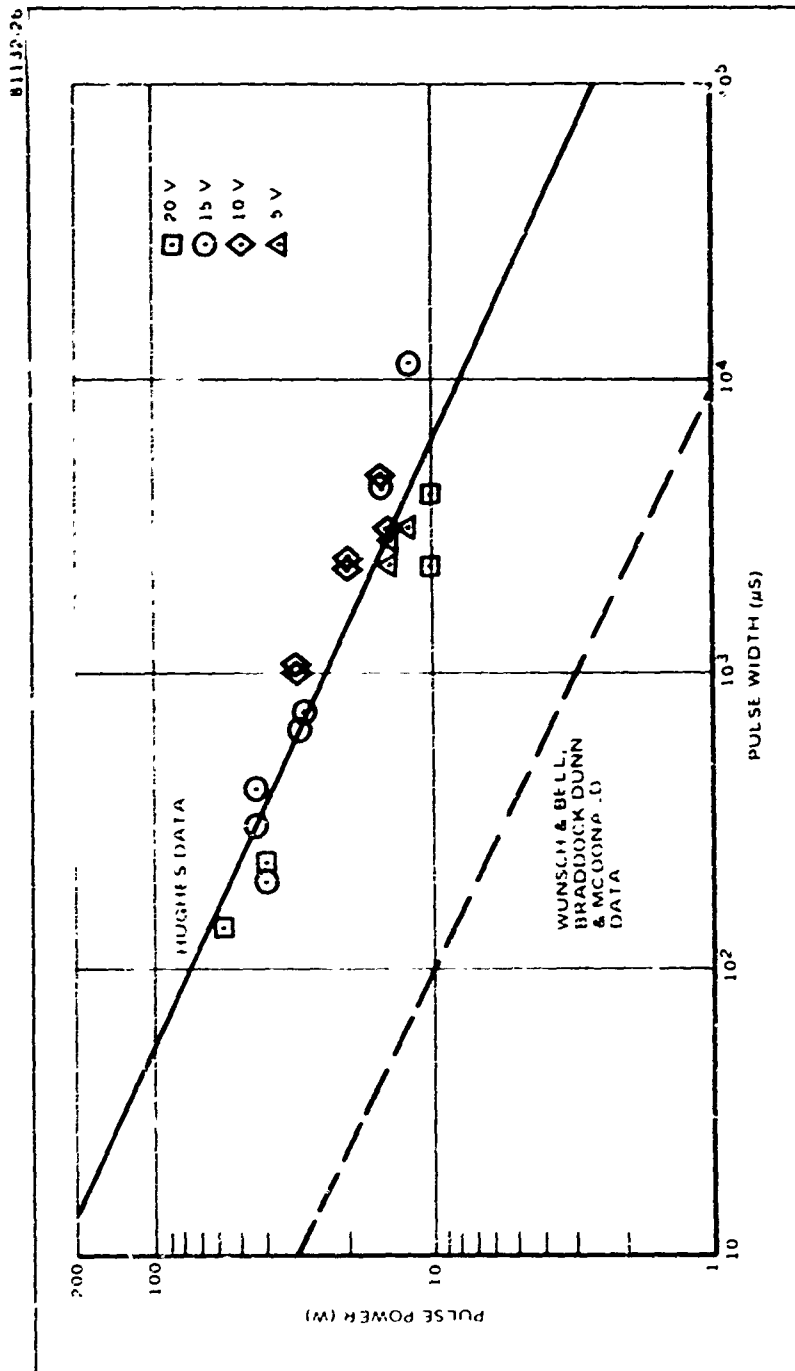


FIGURE 2-69 Comparison of Wunsch and Bell and Hughes Radiation Induced Burn-Out Data

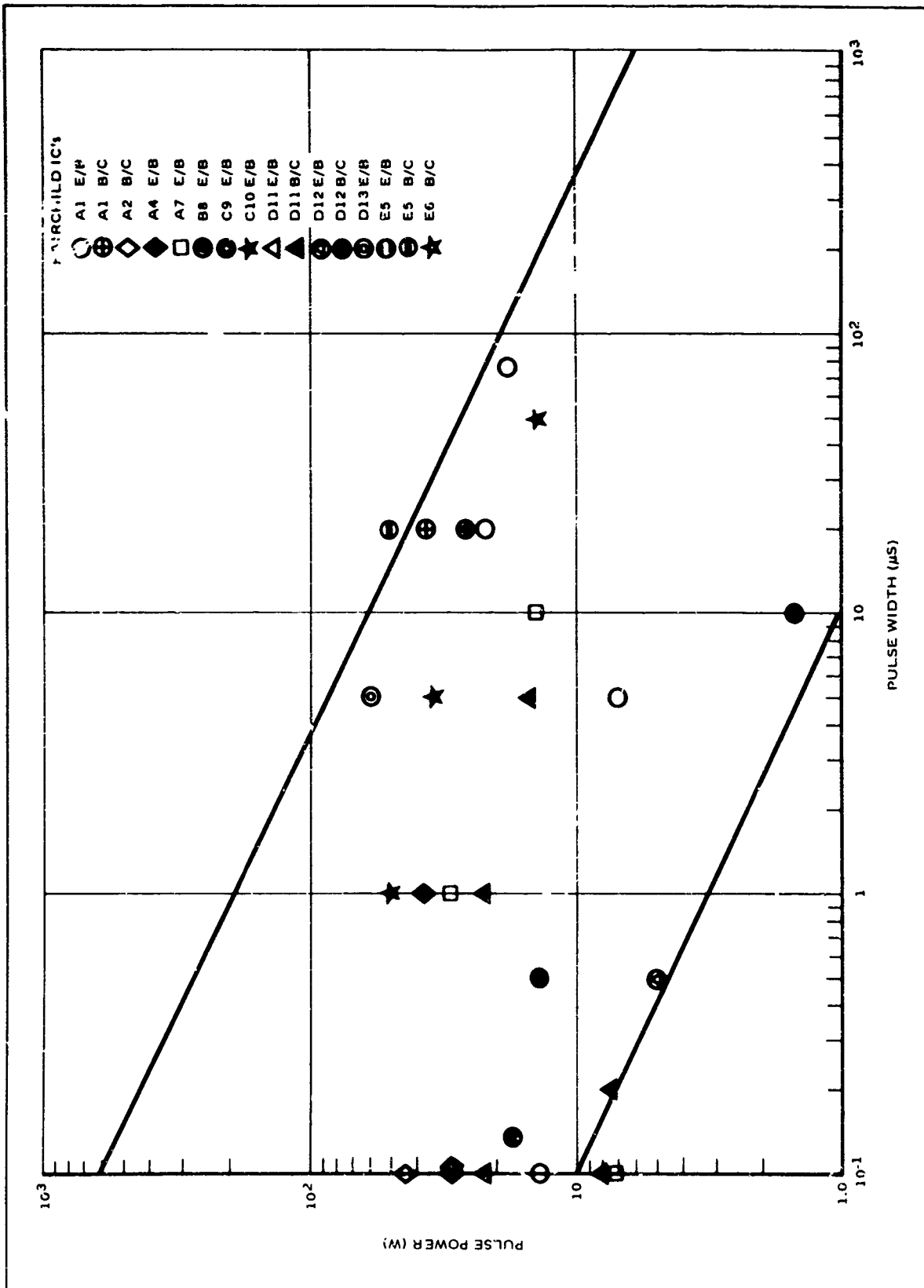


FIGURE 2-70 Pulse Power vs Pulse Width for Electrical Burn-Out of IC Kit Parts

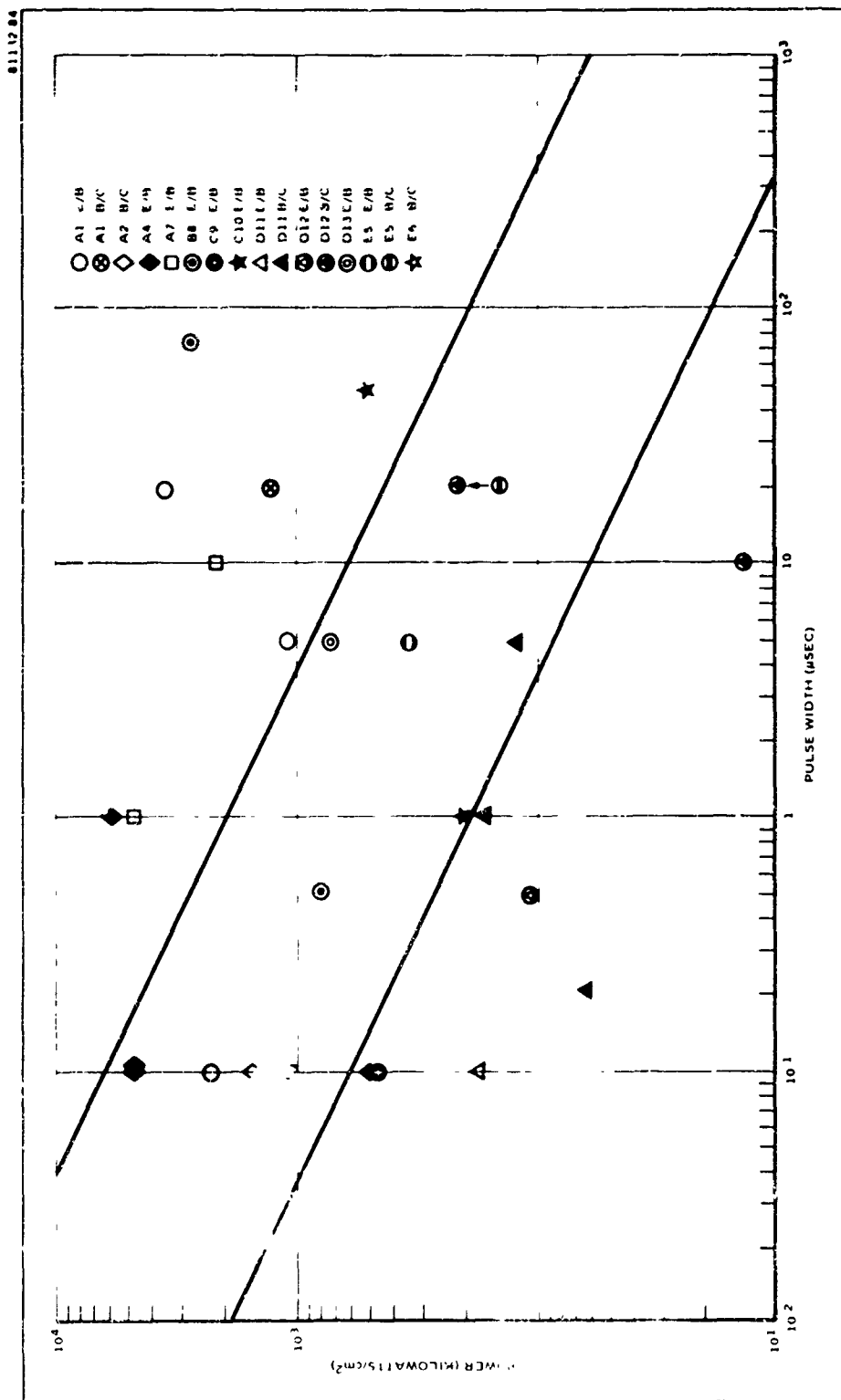


FIGURE 2-71 Comparison of Wursch & Bell's and Hughes Electrical Burn-Out Data for IC Kit Parts

data is that they are representative of what happens in integrated circuit transistors, but the various failure modes are not separable. The data is in the same general power level area as Wunsch and Beil's data shown in Figures 2-54 through 2-63.

2.7 MOSFET's

MOSFET's and integrated MOSFET arrays are particularly attractive for employment in space systems because of their low power requirements and their low weight per function. They are, however, very susceptible to permanent damage at very low integrated radiation doses (gamma and/or space electron radiation). The threshold for permanent damage for most currently available MOSFET's is $\sim 10^4$ rad(Si). Shielding can be employed to reduce the radiation dose to acceptable levels if necessary. Of course there is a weight penalty to consider when using shielding, especially in space systems. Gate-turn-on-voltage (V_T) is the parameter most affected by radiation. V_T usually becomes more negative and can exceed -10 V at 10^5 rad(Si). (38)

MOSFET's are not significantly affected by neutron irradiation. No significant changes in electrical parameters have been observed at neutron doses up to 2×10^{15} n/cm² ($E > 10$ keV). (38)

As in the case of other semiconductors, MOSFET's are affected by transient ionizing radiation causing the generation of junction photocurrents. Radiation-induced electrical transients may cause permanent damage (burn-out). Transient effects on MOSFET's and system considerations are:

- . A drain-to-source substrate photocurrent is exhibited
- . Secondary photocurrents are not present

- . There are no radiation storage time effects analogous to those in bipolar transistors. However, long decay times which are a function of the high gate impedance have been observed after the radiation pulse terminates.
- . Currently available circuits which use MOSFET's as resistors may have radiation-induced short circuit paths.
- . Punch through of the gate insulation under irradiation does not pose a threat if diode limiters are fabricated as part of the circuit.
- . On large integrated arrays, the drain-substrate photocurrents become significant and approach the same order of magnitude as the photocurrents observed for monolithic integrated circuits with comparable geometry. Therefore, for power supply leads and other interconnections, burn-out is a threat.
- . There appears to be no PNP latch-up mechanism in MOSFET arrays.
- . State-of-the-art devices with silicon-on-sapphire construction and short carrier lifetimes may have less photocurrent by two orders of magnitude than equal geometry bipolar devices. Radiation-induced short circuit paths may be eliminated and the damage threshold could be improved. However, these devices are not currently available in quantity.

- . Shielding should be provided against normal space radiation to insure mission completion.
- . Current limiting resistors should be provided to prevent burn-out.

Examination of the above summary indicates that the radiation threat to MOSFET's reduces to catastrophic burn-out of power supply or circuit interconnections as a result of large radiation-induced transient currents. The threat to the power subsystem will be due to the substrate currents as in the case of monolithic integrated circuits.

2.8 Silicon Controlled Rectifiers

Silicon controlled rectifiers (SCR's) are four-layer semiconductor devices which regenerate and switch upon application of an input pulse. After removal of the input, the devices remain in the switched state. Like most semiconductor devices, SCR's are sensitive to ionizing radiation. Radiation generates a photocurrent within the device. If this photocurrent is above a certain threshold level, then the SCR switches and changes its output voltage and current states. Radiation switching thresholds vary over a range of at least four orders of magnitude (10,000:1) for available SCR types and typical circuit design techniques. Of particular interest to the designer are the worst-case radiation thresholds, below which switching will never occur.

It has been found⁽³⁹⁾ that the transient radiation switching thresholds (critical radiation exposure rate) for SCR's are functions of the radiation-pulse width. For pulse widths greater than a critical value, the exposure rate required to trigger an SCR becomes constant.

This critical value is a function of the device minority-carrier lifetime and device "turn on" delay time. For pulse widths less than the critical value, the exposure rate required to trigger an SCR increases rapidly as the pulse width approaches zero. The dependence of the switching threshold of a 2N3027 SCR on pulse widths and radiation exposure dose rate can be seen in Figure 2-72. The critical pulse width for this device is approximately 1.3 μ s.

The transient radiation switching threshold of particular SCR's, in most circuits, can be approximated by electrical measurements. Studies show^(38,39) that strong correlations exist between radiation-induced and electrically induced SCR switching. Strong relationships have been shown, for a limited number of SCR's, between threshold radiation-exposure rates (\dot{Y}_T) and radiation-induced threshold currents ($I_{\dot{Y}_T}$); and between $I_{\dot{Y}_T}$ and electrically induced threshold gate currents (I_{GT}). These relationships have been simplified for presentation. At this time, these simplified relationships are estimated to have general validity within a factor of four (adequate for many predictions) if the radiation predictions are performed, with respect to electrical measurements as outlined below.

The general SCR circuit applicable for radiation-threshold predictions for a particular radiation pulse width (t_{px}) is shown in Figure 2-73. Using this circuit, the following electrical parameters must be determined:

- I_{GT1} = gate threshold current at $t_p = 1 \mu$ s
- I_{GTx} = gate threshold current at pulse width of interest
($t_p = t_{px}$)
- V_{GT1} = gate threshold voltage at $t_p = 1 \mu$ s

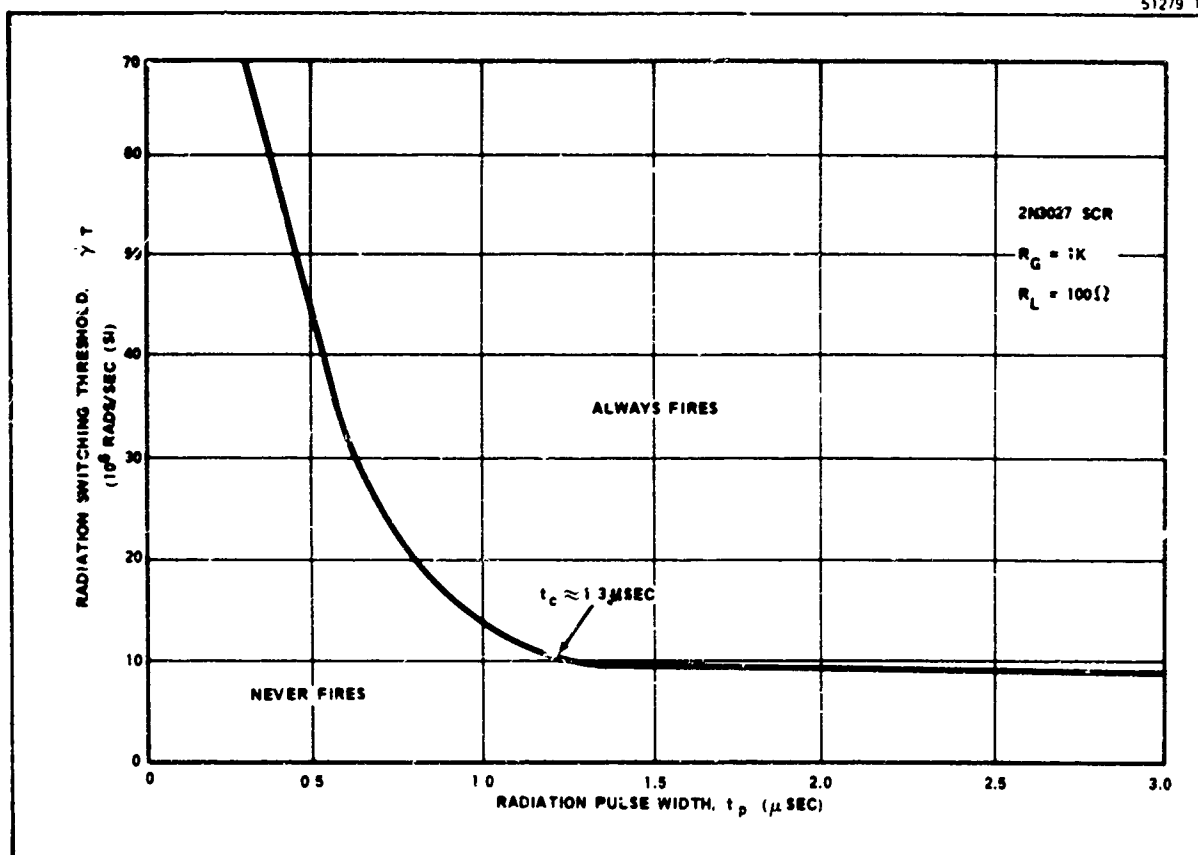


FIGURE 2-72 SCR Radiation-Induced Switching Threshold

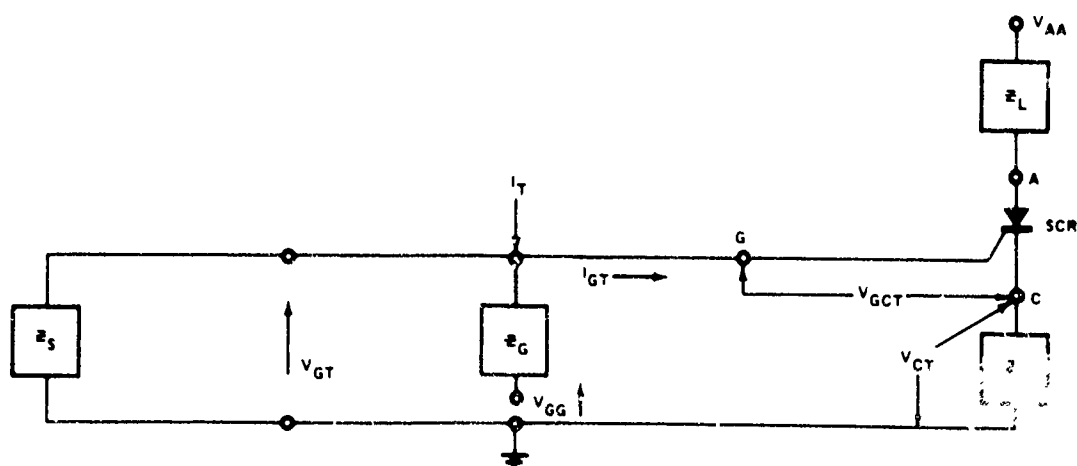


FIGURE 2-73 SCR Circuit Configuration

In addition to the above data, the switching time, t_s' , of the particular SCR must be determined. The circuit in Figure 2-74 must be used for the t_s' measurement. The empirically determined correlation between the radiation-induced ionization current, I_{Y1} , (for a 1 μ s pulse width) and the switching time t_s' is shown in Figure 2-75. Using this correlation the following formula for the threshold radiation exposure rate can be derived:

$$\dot{\gamma}_T = \frac{(10^6) I_{GTX} \left[1 + \frac{V_{GT1}}{I_{GT1} Z_S} + \frac{V_{GT1} - V_{GG}}{I_{GT1} Z_G} \right]}{t_s' \left[1.1 - 0.15/t_{px} \left(1 - e^{-t_{px}/0.15} \right) \right]} \quad (2-37)$$

where t_{px} is the radiation pulse width of interest measured in microseconds. Equation 2-37 is valid if the anode supply voltage V_{AA} is less than one-half the SCR breakover voltage and the parallel combination of the gate impedance Z_G and the source impedance (Z_S) is greater than 500 ohms. Equation 2-37 will give the mean threshold exposure rate. If worse-case prediction is required then $\dot{\gamma}_T$ should be divided by four.

Figure 2-76 illustrates some SCR parameters as a function of neutron dose. Gate turn-on voltage (V_{GT}), gate turn-on current (I_{GT}), and holding current (I_H) increase with increasing neutron dose. The holding current increase is actually an advantage in the circuit of interest because it accelerates turn-off. SCR's will be usable at doses greater than 10^{13} n/cm².

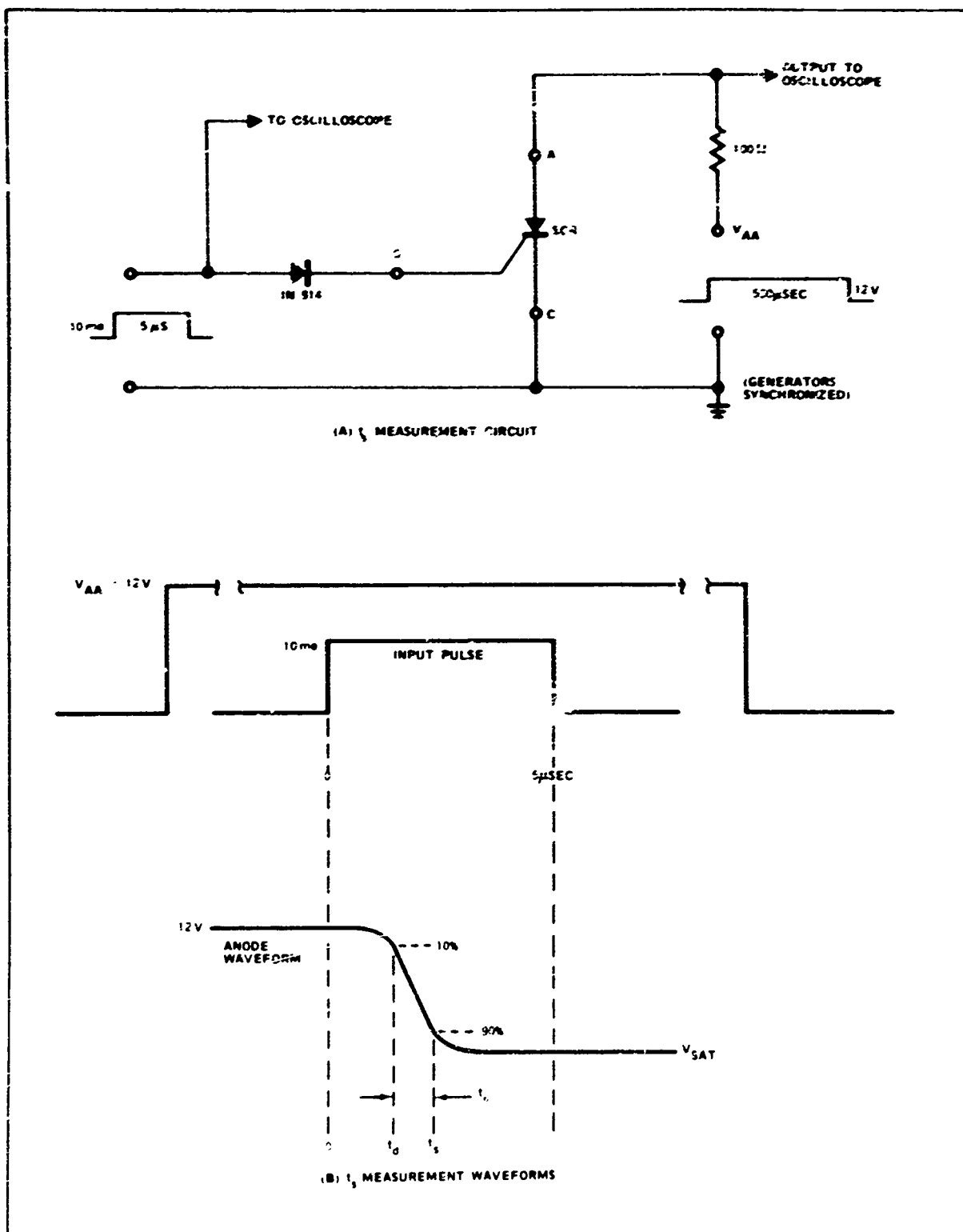


FIGURE 2-74 t_s Measurement Circuit and Waveforms

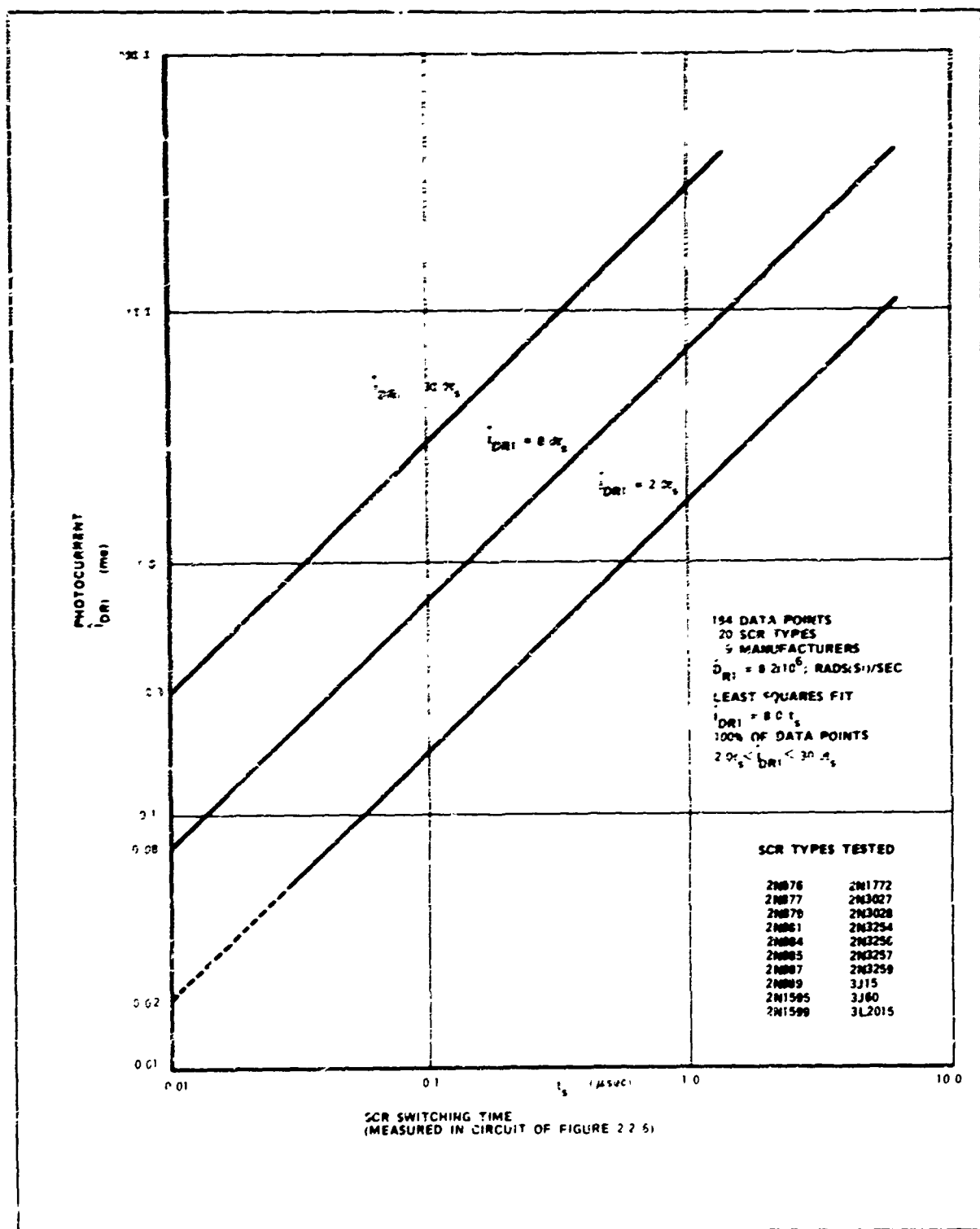


FIGURE 2-75 Photocurrent-Switching Time Correlation

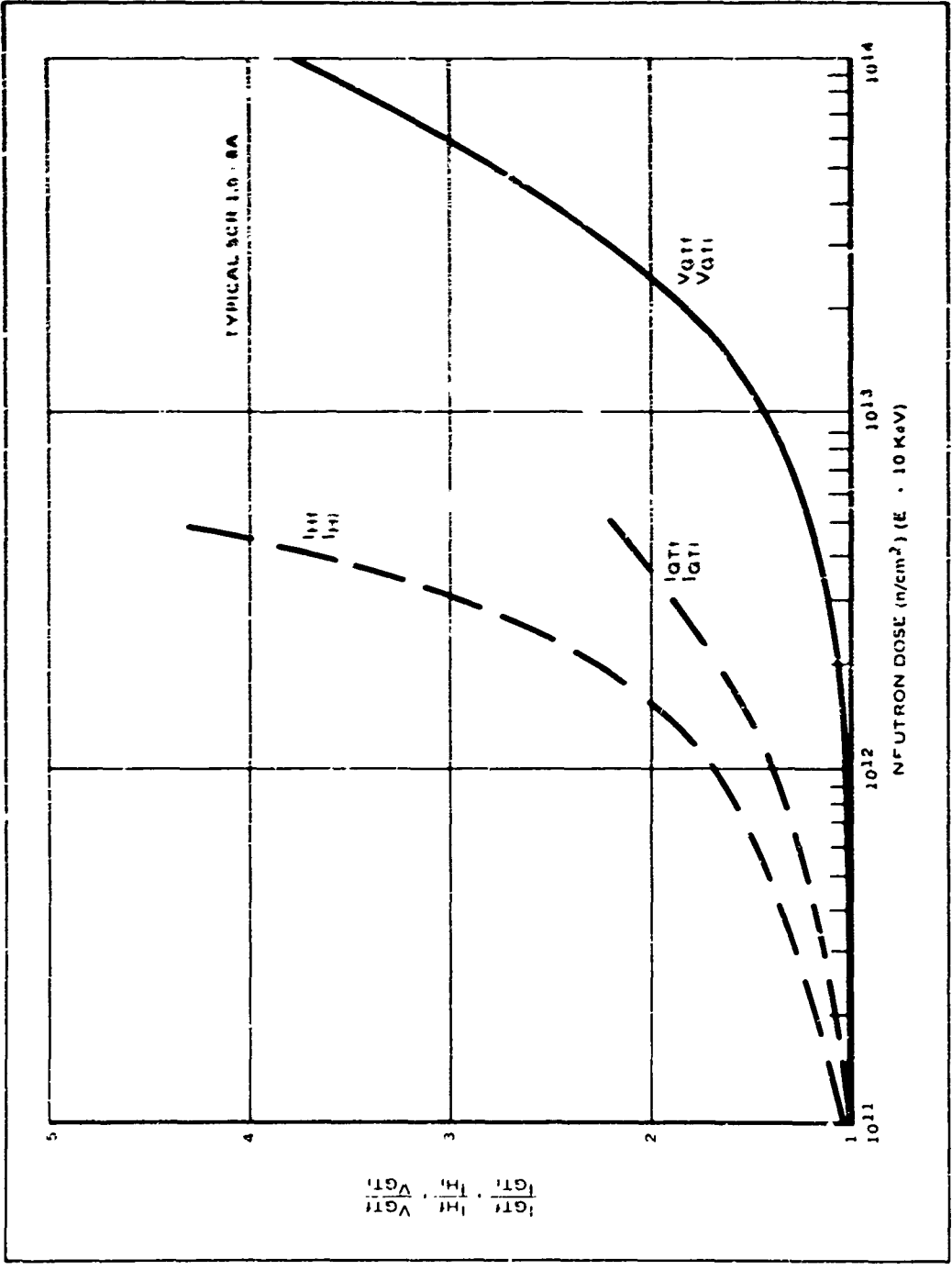


FIGURE 2-76 Neutron Dose Effects on Various SCR Parameters

If SCR circuitry is to be used in a dc system, the SCR should be used with a current limited power source. An acceptable circuit is illustrated in Figure 2-77. The capacitor (C) is charged through Q_1 , and the SCR is triggered by a short pulse. The only current source for the SCR is C, which discharges rapidly. The SCR will turn-off when the current supplied by C falls below the holding current. Under irradiation, the SCR and Q_1 will turn-on. Q_1 attempts to charge C while the SCR discharges C. The discharge time constant is much shorter than the charge time constant; therefore, the SCR will not stay on for any prolonged time due to radiation. D_1 also helps discharge C under irradiation.

2.9 Solar Cells (See Classified Supplement - Section 2.9)

2.10 Other Components

Most other electronic piece parts used in space power subsystems will not limit system survivability. Damage due to neutrons and gamma rays should be negligible when compared to minority carrier semiconductor effects. Electronic materials and parts which are considered hard are:

- . transformers
- . chokes
- . TWT's
- . cables
- . wiring
- . batteries
- . motors
- . connectors
- . strip lines
- . fuel (hydrozine)

21132-129

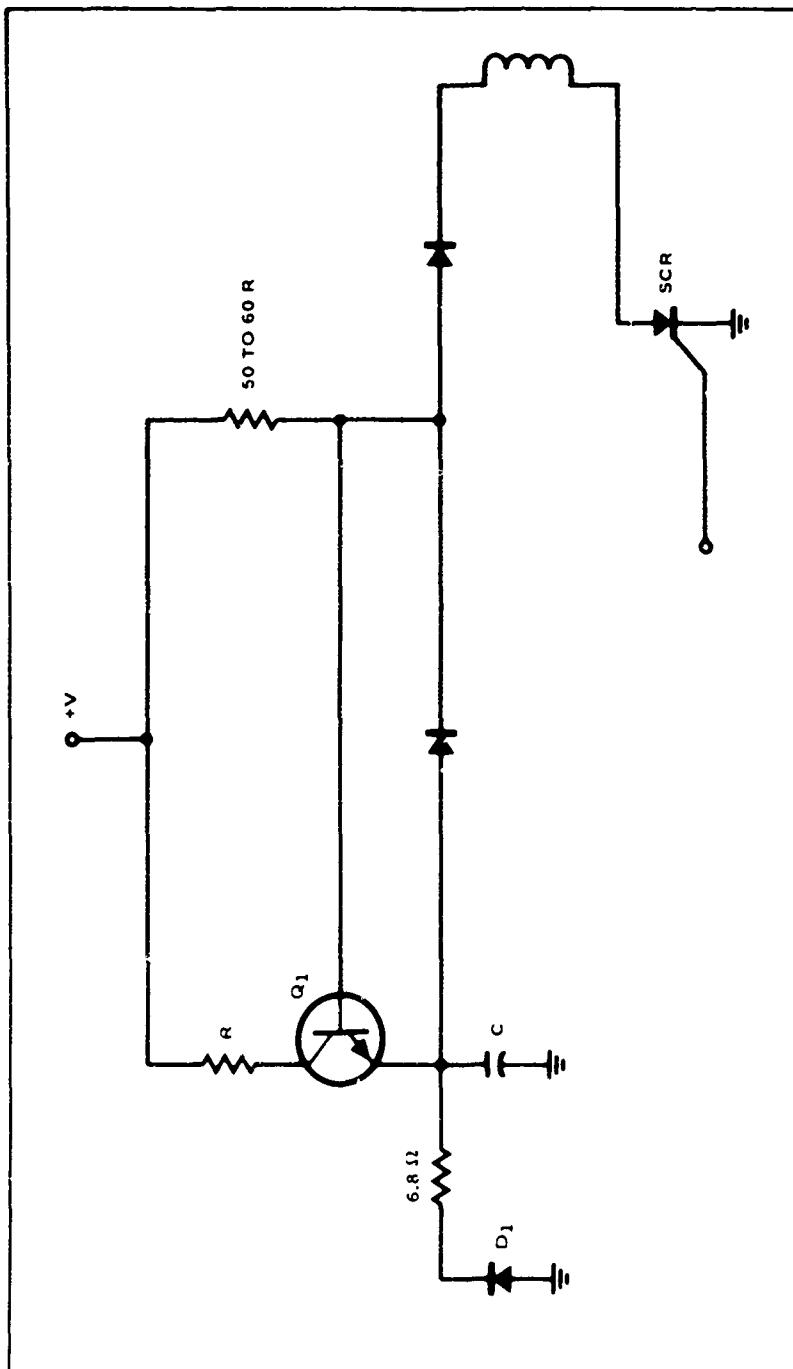


FIGURE 2-77 SCR Current Limiting Circuitry

- . passive microwave parts (mixers, hybrids, switches)
- . structural materials (metals, organics, see Section 3.0)

Quartz crystals may experience some degradation at moderate gamma dose levels. A permanent change of approximately 13 Hz is expected for a 130 MHz crystal at a dose of 5000 rad(Si). The Q decreases by a factor of 2 to 4 for a dose of 2×10^4 rad(Si), but it recovers in a few minutes after the pulse terminates.

BLANK PAGE

3.0 MATERIAL EFFECTS

3.1 Mechanisms

3.1.1 Atomic Displacements

The most characteristic effect of high energy radiation in materials is the production of displaced atoms. This effect is associated with the neutron component of the nuclear weapon environment. These atoms are formed when an incident high energy particle transfers sufficient energy to an atom of the solid to literally knock it out of its lattice position. This energetic atom, termed the primary knock-on, can in turn displace other atoms in the solid, so that a cascade of displaced atoms can result. There will occur in the material, therefore, regions in which the normal crystal structure is disordered. The sensitivity of a given material to neutrons, then is associated with the presence of these disordered regions and to the extent to which they affect a particular material or physical property.

3.1.2 Atomic Ionization

A second characteristic effect that occurs in materials exposed to high energy radiation is the excitation and ionization of atomic electrons. This can occur simultaneously with the production of atomic displacements, or it can occur as the predominant effect in a material. Generally, the effect of ionization is to be associated with the gamma or x-ray radiation component of the nuclear weapon. The extent to which ionization or displacement production dominates for the total weapon environment depends upon the material itself, that is, whether it is a non-metallic inorganic, an organic, or a metallic substance.

3.1.3 Thermomechanical Effects

A third effect that can occur in the nuclear weapon environment is associated with the x-ray component of the nuclear weapon. This effect, unlike the two effects discussed above, is best thought of as a bulk, rather than an atomic effect. It occurs when the energy deposition is such as to heat the material significantly on a time scale of the order of the radiation exposure.

3.2 Organics

The class of organic materials is a large one and includes elastomers, plastics, and organic fluids. As a general rule radiation effects in this class of material are associated with the ionizing effect of high energy radiation whether this results from gamma rays, x-rays, or indirectly from neutrons.

These materials can be divided into two commonly occurring classes. The first consisting of long chains of repeating units with a molecular weight exceeding 10^6 . These are essentially one dimensional molecules. Examples of long chain molecules are polyethylene, rubber, Teflon, and cellulose. The second is a class consisting of a three dimensional network of polymers that can be thought of as one giant molecule. Three dimensional network type materials are ureaformaldehyde, phenol-formaldehyde, and vulcanized rubber.

The sensitivity to radiation of the polymer comes from radiation induced breakage of one bond in a polymer consisting of 10^5 bonds or radiation induced cross linking. This will double or halve the molecular weight which in turn can alter the important physical properties such as viscosity, elasticity, and solubility. In addition

to these physical changes, gas evolution can also occur in some polymeric materials as a result of radiation exposure.

3.2.1 Elastomers

In the case of these polymers it should be realized that the recipes for specific types can vary in their composition and that correspondingly, the response to radiation can be somewhat different.

The elastomers generally are stable to radiation up to 10^6 rad(C) with natural rubber being among the best since it is unaffected by radiation up to about 2×10^6 rad(C). Above this there is a tendency towards decreased elasticity and increased hardness. A decrease in tensile strength is not observed until about 2×10^7 rad(C).

Polyurethane rubbers are the most radiation tolerant with a threshold at about 9×10^6 rad(C). A degradation of about 25% at an exposure of 4×10^7 rad can be expected. Vacuum irradiation has about the same effect as air irradiation. Combined radiation and temperature effects up to 260°F are the same as for radiation alone with respect to tensile strength. Cure and filler are important, however, in determining exact radiation tolerance of this class of rubber. It was found⁽¹⁾, for example, that Estane VC cured with dicumyl peroxide was the most radiation resistant compound tested. Adiprene C, reinforced with carbon-black and sulfur cured, on the other hand, showed poor resistance to radiation.

Butyl rubber is the least stable to radiation. Tensile strength and elongation are degraded 25% at about 4×10^6 rad(C)⁽²⁾.

Neoprene varies in its response to radiation, depending upon

the type of polymer, cure and additives; in general tensile strength decreases for radiation exposure in the range of 4 to 9×10^7 rad(C) and then increases again with increasing exposure. Data obtained on the effects of vacuum irradiation are in conflict. The results of Kerlin⁽³⁾ indicated that combined vacuum-gamma radiation effects were more severe than irradiation in air. At 2×10^7 rad(C), the tensile strength for vacuum-gamma irradiated samples decreased from 3134 psi to 191 psi. In another experiment⁽⁴⁾, little difference was noted between vacuum and air irradiation results at an exposure of 8×10^7 rad(C).

Silicone rubbers, in general, are less resistant than the average of other elastomers. The tensile strength increases with irradiation in air to approximately 10^7 rad(C) and then decreases rapidly. Elongation is the property most sensitive to radiation, 50% elongation being retained after exposure to 5×10^7 rad(C) at room temperature. For gamma radiation in vacuum it is found that the radiation resistance is about the same or somewhat greater than in air.

The relative behavior of elastomers under radiation is summarized in bar-graph form in Figure 3-1⁽⁵⁾.

3.2.2 Plastics

The resistance to radiation of plastics falls roughly into three classes. In the first are those showing resistant behavior to 10^7 to 10^9 rad(C). These are polystyrene, mineral-filled phenolics and polyesters, phenolic laminates, polyethylene, polyethylene terephthalate, polyvinyl chloride, epoxies and glass reinforced silicones. The 25% degradation point is in the range 10^8 to 10^9 rad(C). The second or

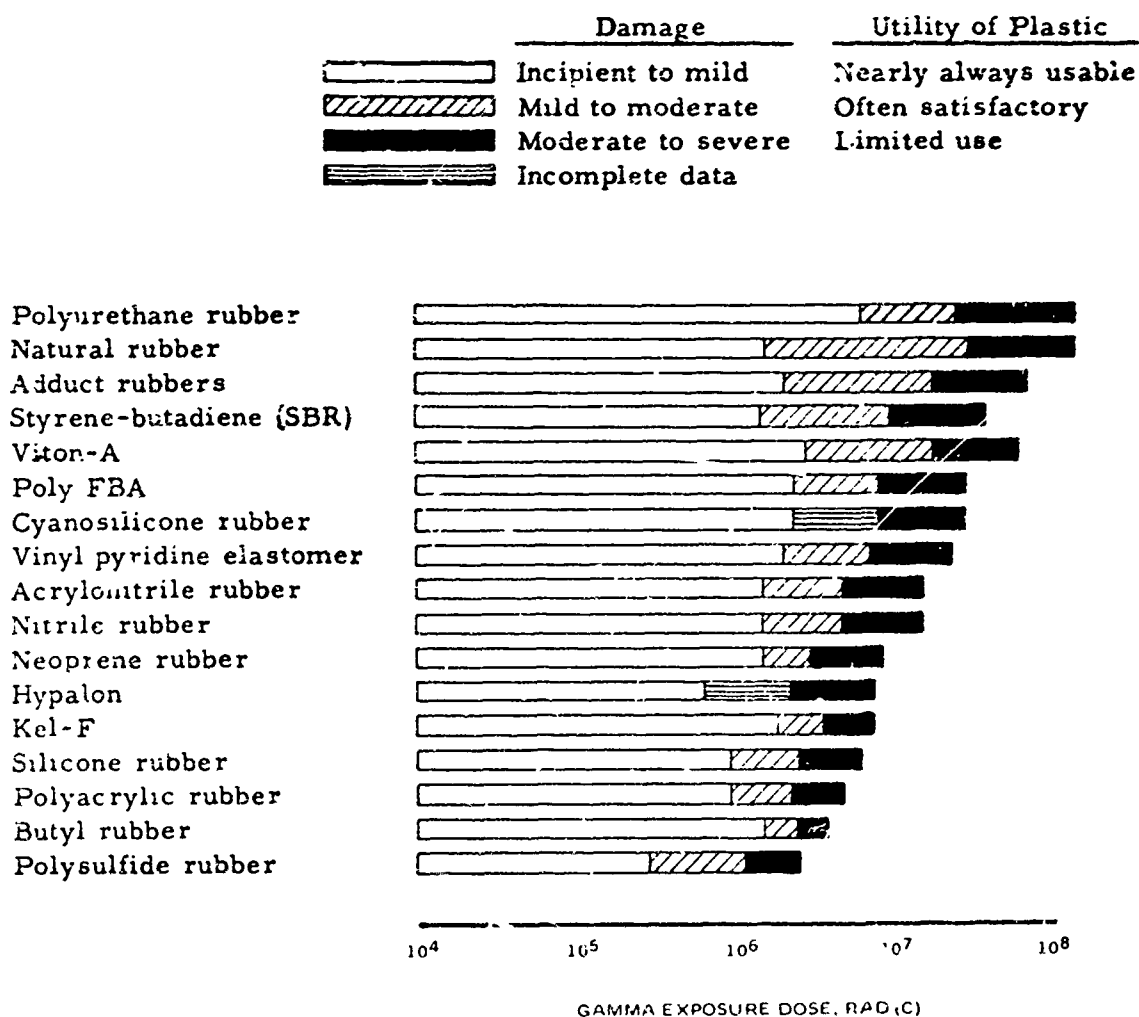


FIGURE 3-1 Relative Radiation Stability of Elastomers⁽⁵⁾

intermediate class with respect to radiation degradation include: melamine formaldehyde, unfilled phenol-formaldehyde and urea-formaldehyde. This class remains unaffected by radiation up to the range 10^6 to 10^7 rad(C) with 25% degradation at 10^7 to 10^8 rad(C). The third or poorest class is made up of the cellulose, polyamides, Teflon, and unfilled polyesters. Degradation thresholds in these plastics occur at 10^4 to 10^6 rad(C).

Because of the relative hardness of the first class of plastics above with respect to a radiation environment, further detailed discussion of it is omitted. Because of the relatively low thresholds of the last class, on the other hand, a more detailed discussion is warranted together with a somewhat less detailed discussion of the second class. The relative behavior of thermoplastics and thermosetting resins as a function of radiation dose is presented in bar-graph form in Figures 3-2 and 3-3⁽⁵⁾.

3.2.2.1 Fluorethylene Polymers

This class of polymers is perhaps unique in that its members combine exceptionally good temperature and chemical resistance together with a tendency to degrade in the presence of radiation, with the degree of radiation degradation depending critically upon the ambient. Early tests on Teflon showed a relatively poor radiation resistance in air and it was inferred that this would limit its usefulness generally. Later tests, however, indicated that its resistance to radiation exposure in vacuum is about two orders of magnitude better than its resistance when exposed in the presence of oxygen.

Of the several types of fluorocarbon polymers, FEP100 Teflon (a hexafluoropropene and tetrafluorethylene copolymer) is considerably

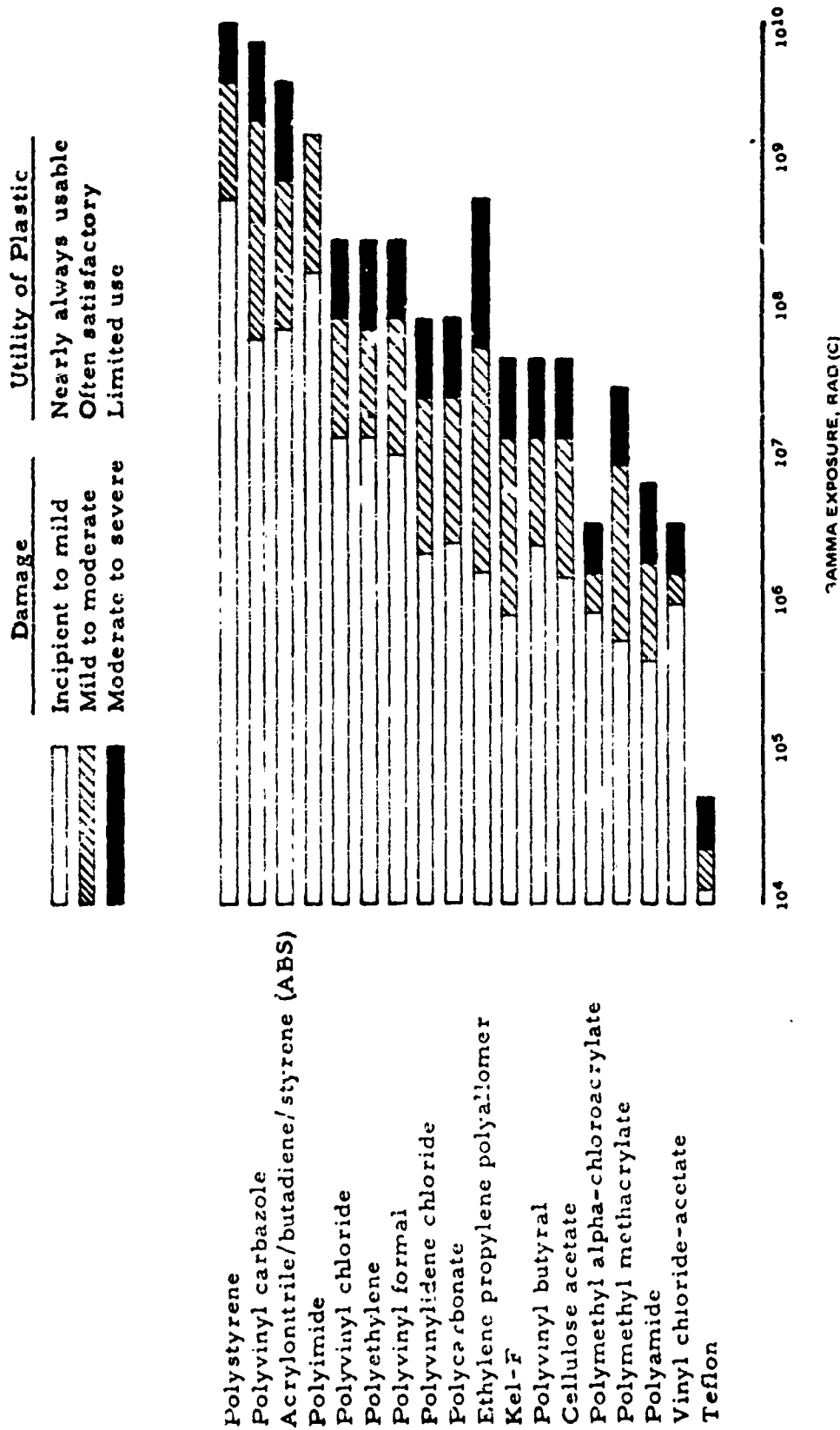


FIGURE 3-2 Relative Radiation Resistance of Thermoplastic Resins (5)

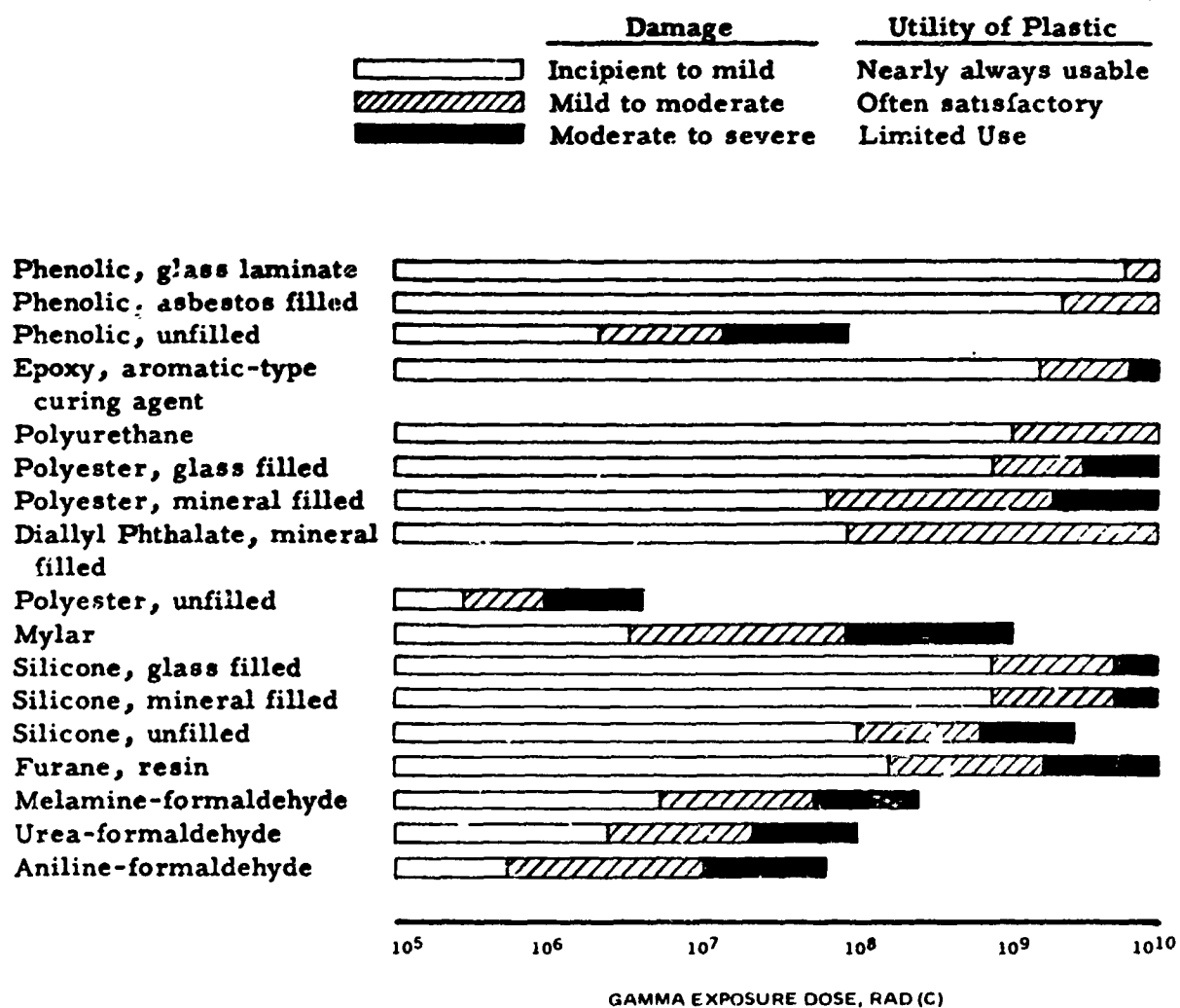


Figure 3-3 Relative Radiation Stability of Thermosetting Resins ⁽⁵⁾

more radiation resistant in air than TFE Teflon (tetrafluorethylene). The threshold damage for TFE in air is 1.7×10^4 rad(C) with a 25% degradation occurring at 3.4×10^4 rad(C). In vacuum, the tensile strength of TFE is satisfactory to 8×10^7 rad(C). FEP Teflon is also more stable under irradiation in the absence of air. A set of data comparing vacuum and air irradiation as obtained by Shaffner⁽⁶⁾ is shown in Table 3-1.

Radiation test results⁽³⁾ in Duroid 5600, a glass-fiber-reinforced Teflon show a retention of 40% of tensile strength and some flexibility at 1.2×10^8 rad(C) in air.

Tedlar⁽³⁾ (polyvinyl fluoride) in the form of a 4-mil film was radiation resistant to 10^8 rad(C) but decomposed above that level. Kynar⁽³⁾ (polyvinylidene fluoride) retained its tensile strength under irradiation in air and vacuum to a threshold of 10^7 rad(C).

In addition to the mechanical property, the dielectric behavior of the fluorocarbons is also affected by radiation. The low frequency dissipation factor of TFE Teflon is considerably affected by irradiation. The loss at high frequencies is less affected. As in the case of the mechanical property, dielectric behavior is influenced by ambient oxygen during radiation exposure and recovery. At frequencies less than 1000 Hz and at a dose of 2×10^6 rad(C) the dissipation factor of TFE-6 Teflon increases approximately 13 times its original value⁽⁷⁾. For FEP100 Teflon, in contrast, dissipation and dielectric constant are relatively unaffected by irradiation in vacuum⁽⁷⁾ at 6×10^6 rad(C).

TABLE 3-1. Comparison of Air and Vacuum Effects on FEP Teflon * (6)

	Radiation Dose (10 ⁶ rad(C))	Elongation (percent)	Tensile Strength (psi)	Dielectric Constant (± 0.05)
Atmosphere	0	165	3000	2.1
Atmosphere	0.1	152	1882	2.1
Atmosphere	0.5	37	1539	2.1
Atmosphere	1.0	21	1388	2.1
Atmosphere	5.0	-	1322	2.1
Vacuum (10 ⁻⁶ mm Hg)	1.0	92	2481	2.1
Vacuum (10 ⁻⁶ mm Hg)	5.0	73	1972	2.1
Vacuum (10 ⁻⁶ mm Hg)	51.0	38	1462	2.1
Vacuum (10 ⁻⁶ mm Hg)	150.0	16	800	2.1

* These data also apply to Teflon FEP resin. Actual experimental data even indicate a slight improvement in the above characteristics for this material. Radiation source was Co⁶⁰ isotope emitting gamma rays at 1.3 x 10⁶ rad/hour. Temperature was 25°C (77°F). Sample was 0.010-inch film of a Teflon TFE resin. Note that values for tensile strengths and elongations are known to be conservative based on current techniques of end-product fabrication.

3.2.2.2 Cellulosics

Cellulose polymers are cellulose acetate, cellulose acetate butyrate, cellulose nitrate, cellulose propionate and ethyl cellulose. They are in the class of plastics with the poorest radiation resistance. Physical properties deteriorate rapidly under gamma radiation. At 1.9×10^7 rad(C), cellulose acetate, one of the more radiation-resistant cellulosics, has deteriorated by 25%⁽³⁾.

3.2.2.3 Polyamide (Nylon)

The material is used generally for gears, bearings, valve seats, and electrical equipment. The radiation behavior of nylon depends upon its physical form. In sheet form a threshold for damage is at 8.6×10^5 rad(C). Its tensile strength increases with radiation exposure⁽⁸⁾. Nylon fiber on the other hand is reported to lose strength rapidly when irradiated in the presence of air⁽⁹⁾.

3.2.2.4 Polyesters (Unfilled)

Unfilled polyesters have poor radiation resistance. The addition of mineral fillers, however, can increase radiation stability about two orders of magnitude. Plaskan Alkyd, a mineral filled polyester, begins to deteriorate at 8.7×10^7 rad(C) while the unfilled polyester exhibited deterioration at 10^5 to 10^6 rad(C).

3.2.2.5 Amino Resins

This class of materials includes ureaformaldehyde, melamine formaldehyde, and amilene formaldehyde. They are thermosetting resins used in shock proof laminates and wiring devices, as adhesives, and in surface coating formulations.

Ureaformaldehyde is unaffected to a threshold of 7.4×10^6 rad(C), and is degraded by 25% at 1×10^8 rad(C). Urea and melamine formaldehyde when filled with cellulosic materials is observed to become brittle, blister, swell, and crumble upon exposure to gamma radiation⁽⁸⁾.

3.2.2.6 Polyimide

Fibers of this material (HT-1, DuPont Namex yarn) are unaffected to an exposure of 3×10^8 rad(C)⁽⁵⁾. Dupont "H" film considered for use as a hydrogen barrier was irradiated in liquid nitrogen. Tensile and tear strength were not affected to a significant degree at an exposure of 2×10^7 rad(C), nor did radiation effect hydrogen permeability.

3.2.3 Organic Fluids

As in the case of solid organic materials, the primary radiation effect in the fluid is the rupture of bonds leading to material degradation. For overall radiation stability, branched chain esters for example, isopropyl, are less stable than straight chain compounds⁽¹⁰⁾. Aromatic compounds are generally more stable than aliphatic structures as a result of the ability of the aromatic molecules to dissipate energy absorbed from incident radiation without bond rupture. Also the addition of aromatic compounds such as benzene to aliphatic hydrocarbons increases their radiation stability.

Because of their superior characteristics in a high temperature or combined high temperature radiation environment, the polyphenyl ethers and alkylated aromatic ethers are likely to be candidate lubricants coolants, and working fluids for space power systems. With respect to the gamma and neutron components of the nuclear weapon environment these materials possess radiation thresholds

($>10^7$ rad(C)) for degradation considerably above that likely to be encountered. Therefore no detailed discussion of their relative radiation resistance will be given. Instead bar-graph data is shown in Figure 3-3 of the relative radiation behavior of various types of lubricants. ⁽¹¹⁾

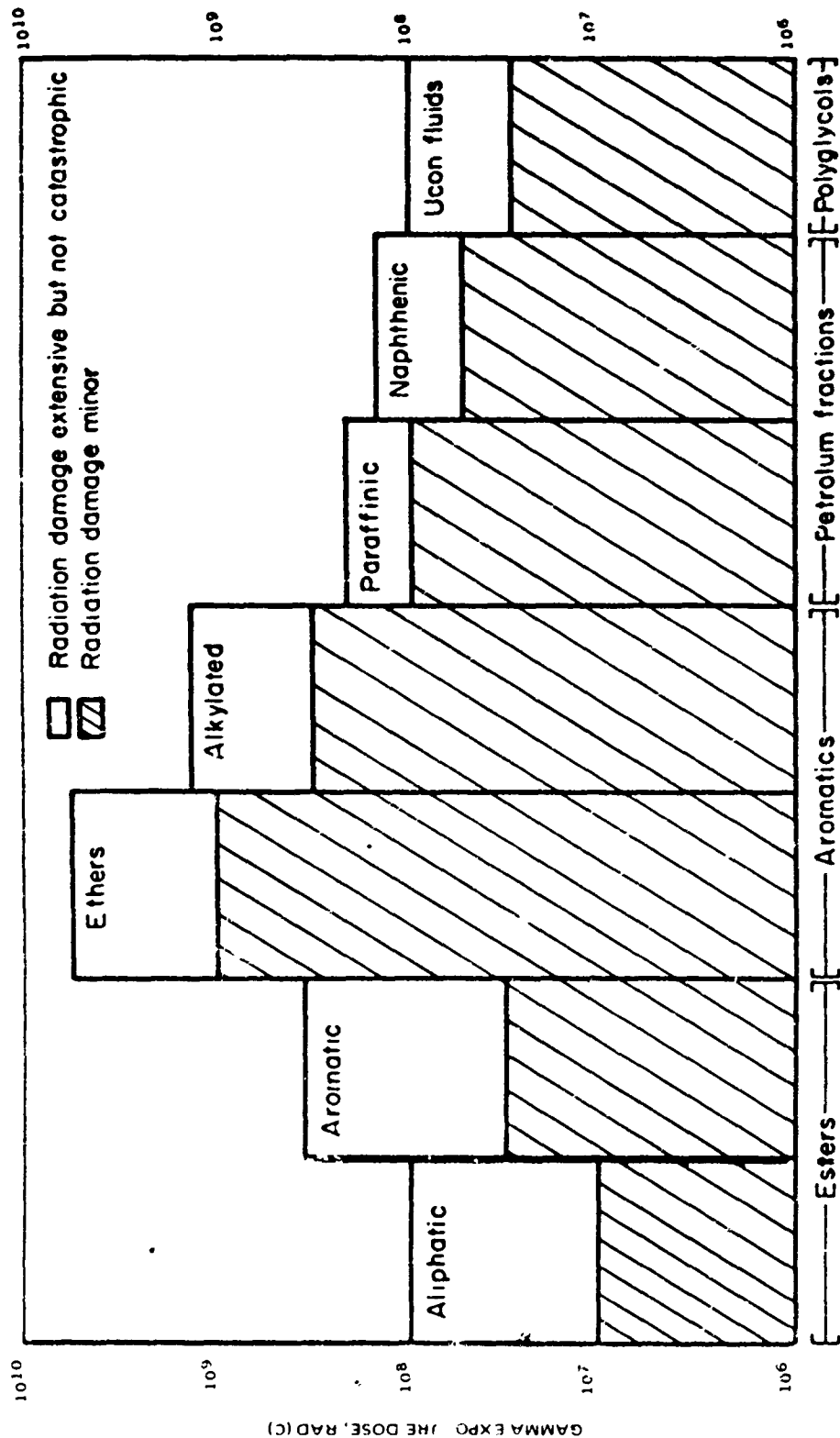


FIGURE 3-4 Approximate Tolerance of Lubricants to Gamma Radiation (11)

4.0 GENERAL SYSTEMS AND CIRCUITS CONCEPTS

4.1 Description

Effects due to the interaction of a nuclear environment with circuitry are discussed in this section. Radiation hardening guidelines and techniques which are applicable at the circuit and subsystem level are summarized.

One area of concern is the transient effects caused by high radiation dose rates. Provided a recovery to normal operation is insured, the effect of this transient radiation disturbance will be to effectively cause a system "dead time" during which the system will not function properly. This dead time may range from 50 nanoseconds to several milliseconds. Transient effects will manifest themselves at the circuit and system level as severe overloads and overdrive conditions. Component damage and burn-out, insulation failure, and the generation of spurious signals are areas of concern. A circuit, subsystem, or the complete system can be threatened by component damage or can be forced into an operating mode that is irreversible. The transient radiation interacts with the spacecraft power distribution system in such a manner as to make maximum power available for several tens of microseconds. Solar cells are excellent energy converters for ionizing radiation. At the same time the load current increases due to radiation-induced currents.

In power subsystems which use solar cell power backed up by batteries, other events may occur simultaneously with the increase in solar power capability. The battery controller switches, power supply switches (to redundant circuitry) battery charging switches and telemetry switches will be affected by the transient radiation pulse.

The radiation pulse can turn on all of these switching functions and lock them on for several tens of microseconds. Maximum energy is available to the system during this time. The solar cells can provide several times their normal current, and with the batteries connected to the primary buss, the batteries are charged with a current several times their normal rate. The system load is increased considerably, all redundant circuitry is powered, and saturation conditions exist throughout the spacecraft electronics. Large currents will flow during this time which can cause component damage if the currents are not limited to safe values. The series pass transistor in regulators may be severely overloaded during this time.

Buss limiters are sometimes incorporated into space power systems. Their function is to limit the solar array output voltage. The radiation environment will turn on the limiters but the limiters will be ineffective in shunting all of the excess current available since they themselves are current limited.

Some circuit applications (typical of satellite systems) where component damage might occur are discussed below⁽¹⁾.

Figure 4-1 illustrates an example found in a telemetry encoder. Normally only one transistor is ON at a time. Radiation can turn both transistors ON and short the power source to ground through the transistors. The power source can be current limited in this case but damage may still occur due to the low power devices generally used.

Figure 4-2 illustrates motor control (simplified) circuitry. The motor is switched to +V for acceleration and to ground for braking. Radiation can turn both transistors ON and short the power source to ground through the transistors.

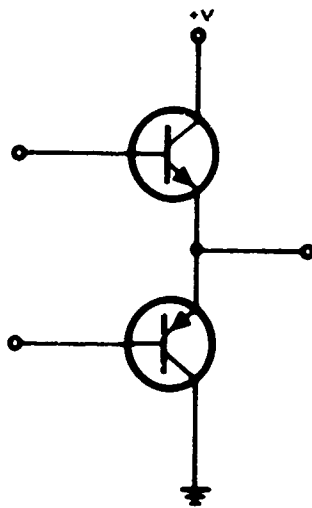


FIGURE 4-1 Telemetry Encoder Circuitry

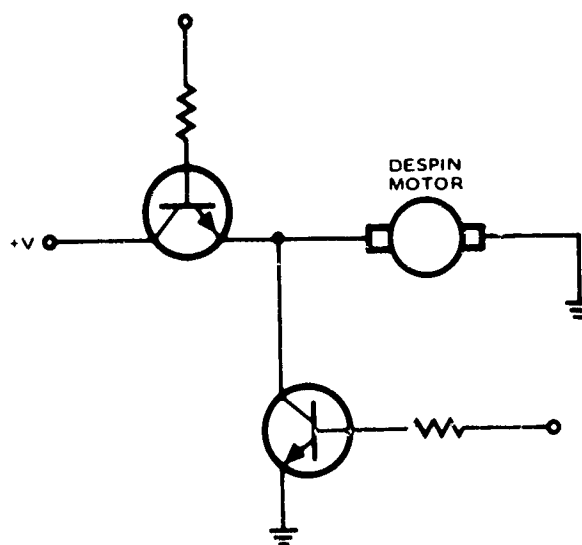


Figure 4-2 Motor Control Circuitry

Figure 4-3 illustrates a portion of a dc-dc converter where one transistor is normally ON and the other OFF. Radiation can turn both transistors ON and short the power source to ground through the transistors and the low impedance transformer winding. Each transistor is presented with a short circuit load due to the transformer action. Precautions should also be taken to insure that the oscillator in the dc-dc converter will start after the transient radiation disturbance.

Figure 4-4 illustrates a problem that might exist due to unfiltered photocurrents. The capacitor is charged prior to the radiation pulse and the diode is reverse-biased. During the transient radiation disturbance the diode conducts and presents a very low impedance to the capacitor. The high current which flows may damage the diode.

The short circuit current and time required to burn-out some specific types of transistors are shown in Table 4-1. These data are representative of the situation where a transistor is connected between an energy source and ground without adequate current limiting.

TABLE 4-1. Transistor Burn-out Current and Time

<u>Type</u>	<u>Time</u> (μ s)	<u>Current-Short Circuit</u> (A)
2N388	25	7
2N955	25	0.5
2N1308	25	100
2N1013	25	1
2N2222	25	0.34
PT2917	25	100

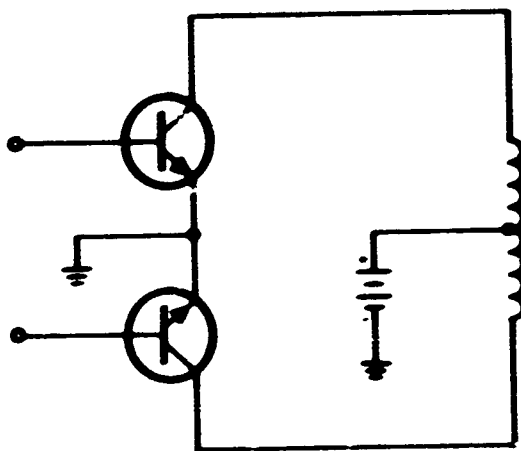


FIGURE 4-3 dc-dc Converter Circuitry

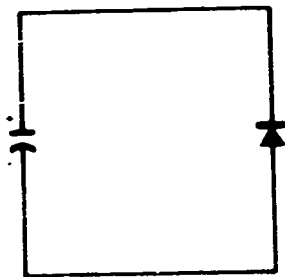


FIGURE 4-4 Diode-Capacitor Circuitry

A problem peculiar to linear circuits is that of prolonged settling time (after a transient radiation disturbance) due to the circuit time constants. Coupling and bypass capacitors, filters, and frequency shaping networks may prolong the circuit recovery time. These circuit elements should be kept to a minimum and, where possible, filters and frequency shaping networks should be located at the circuit output to eliminate the effects of circuit gain. An effort can thus be made to keep the circuit recovery time on the order of the component recovery times.

The interaction of the transient radiation disturbance with the system can be considered as the generation of a noise pulse throughout the system where each component is an effective pulse generator. The pulses generated in the components propagate through the normal signal paths, being amplified and/or cancelled in the process. The techniques for handling noise are applicable to the radiation hardening process. Filtering, cancellation, and differential techniques can be used as hardening techniques.

4.2 Linear Amplifiers

Nuclear irradiation of components causes transient and permanent disturbances within and around the individual components. A given component may have more than one parameter which is disturbed. A transistor will experience changes in base-collector leakage current, current gain, saturation voltage drop, leakage resistance, base to emitter voltage drop, etc. For a given type of transistor, however, some parameters may experience a large disturbance and other parameters may experience comparatively small disturbances. The overall effect on the circuit in which this component is used depends upon those radiation-induced variations in the parameters of the device which are

most important for the particular circuit application. For an open-loop ac amplifier, the current gain parameter is normally most important, but for a commutating switch the saturation voltage parameter is normally most important. The process of hardening requires that the circuit components be selected on the basis of a tolerable parameter change with regard to the specific circuit application which the component must fulfill.

Beta degradation due to nuclear radiation dose (primarily neutron dose) reduces the maximum gain capability of an open-loop amplifier, and consequently additional stages may be required to maintain a minimum input-output signal gain. Beta degradation may also reduce the open-loop gain capability in a closed-loop (operational) amplifier application and thus degrade the accuracy performance of the amplifier. Again, additional stages may be required in order to ensure adequate open-loop gain, after radiation exposure, to maintain a specified accuracy performance.

Successive emitter-follower stages, where NPN and PNP transistors follow each other, are of concern during transient saturation, since the collector power supplies will essentially be shorted together through the transistors. The transistors may be destroyed by the resulting excessive current flow through them.

Amplifiers which use emitter resistors to present a high input impedance, will suffer a decrease in input impedance as beta degrades, since this impedance is a function of beta times the emitter circuit resistance.

The quiescent operating point of a capacitively coupled amplifier may change if the decrease in transistor input impedance is

sufficient to load down the biasing network. If this effect is important with respect to the amplifier output, then a lower impedance bias network may be required. A permanent increase in V_{BE} due to neutron dose may also cause a change in the amplifier operating point.

The recovery time to a normal output condition of a transistor amplifier responding to a transient disturbance, is a function of the relaxation time of the transistor, the loading circuit, and the driving circuit. The relaxation time of the loading and driving circuits may greatly exceed the relaxation time of the transistor if they contain reactive (capacitive or inductive) coupling elements. These areas of significance in the radiation response of linear amplifier circuits are summarized below:

- . Changes in conductances between nodes, the creation of replacement currents, and primary photocurrents
- . Secondary photocurrents
- . Delayed component responses
- . Circuit interactions and recovery modes

Of the four causes of disturbance in linear amplifier circuits listed, the last, circuit interactions, is the fundamental cause of long recovery times or "black out" periods. The circuit designer must be acutely aware of this type of circuit disturbance.

The effects in the first item are those which closely follow the time history of the gamma radiation pulse. These effects may be

represented by the addition of simple conductance paths or current generators in an equivalent circuit. Secondary photocurrent is handled separately since it is not a simple function of device physics, but is also dependent on circuit impedances and time constants. Delayed component responses are those which persist for some time period after the ionizing radiation. One such effect is the delayed conductivity of dielectrics. The last category, circuit interactions and recovery modes, is peculiar in that it is not fundamentally a function of radiation effects on components, but rather an effect which occurs due to the electrical interaction of components in the circuit topology. This is discussed in detail in Section 4.3.

Normal methods used in minimizing overload recovery problems in conventional circuitry may be applied in solving the "black out" phase of the radiation problem. However, in conventional design, the circuit engineer need be concerned only with signals at the circuit input. Under transient radiation conditions, effective inputs are present at each component. Minimization of overload recovery after ionizing radiation is then much more difficult than for simple signal conditions.

Figure 4-5 illustrates prolongment of circuit recovery time from transient radiation.⁽²⁾ Here the signal present from a previous stage causes charge integration to occur on a coupling capacitor. This change of charge results in an undershoot at the transistor base and a subsequently long recovery time at the collector. This situation is familiar to the designers and users of nuclear pulse height analyzers, since this charge integration is nothing more than an extreme example of "base line shift". The other cause of charge changes on circuit capacitors, ionization leakage, is of course often

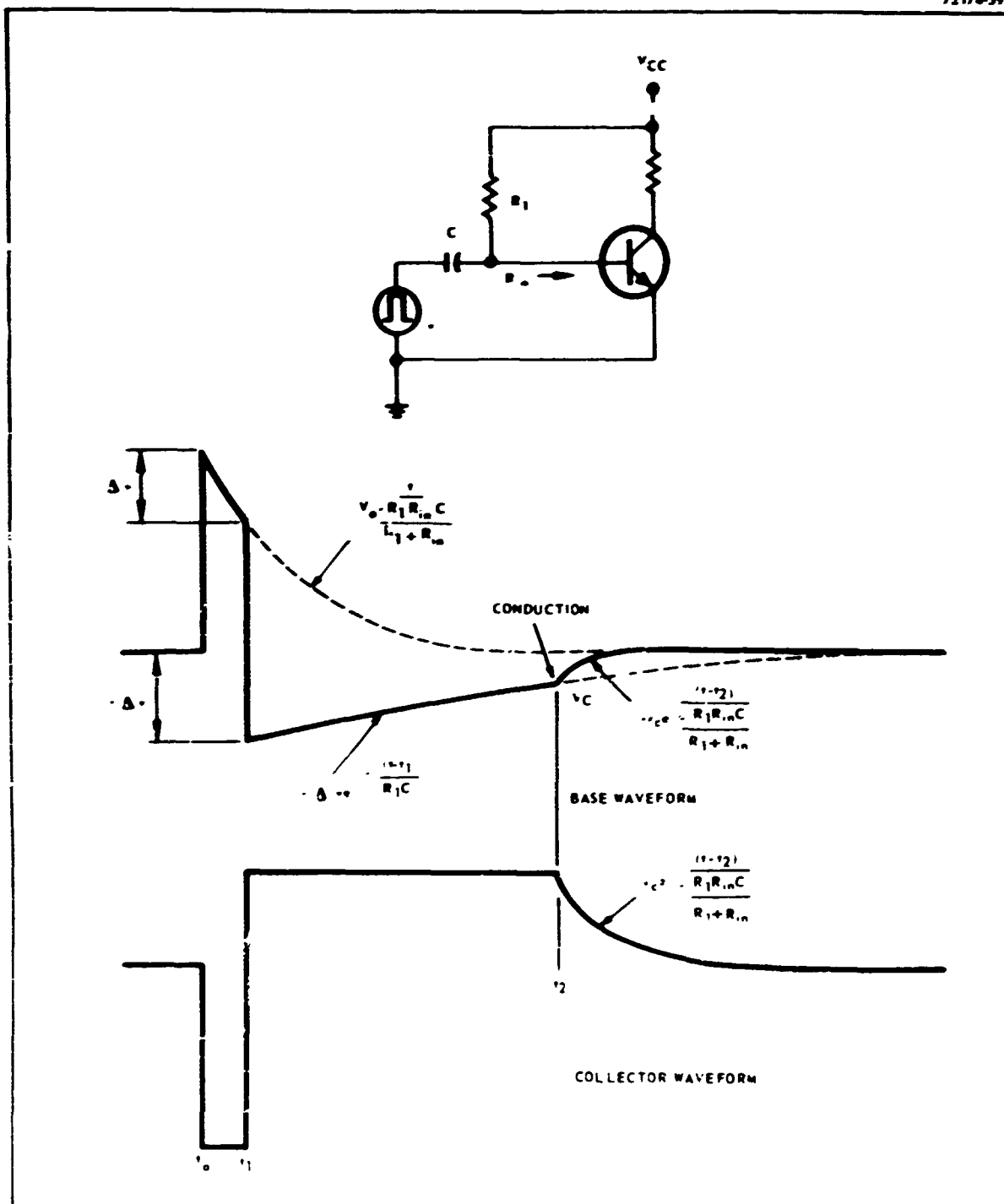


FIGURE 4-5 Prolongment of Circuit Recovery Time

significant, but must not be confused with electrical signal integration.

Direct-coupled stages normally recover as a function of the relaxation time of the transistor, and are therefore preferred, if bias stabilization criteria can be satisfied.

The other three causes of overall circuit disturbances (leakages, replacement currents, primary photocurrents and secondary photocurrents, and delayed component responses) are disturbance inputs, at the component level, which cause long recovery times. The minimization of any of these three inputs by using less radiation sensitive components will enhance overall hardness (in general) but does nothing to reduce the potential electrical recovery time if circuit topology remains unchanged. Therefore, since the circuit electrical recovery is most often the primary contributor to overall circuit malfunction and "black out", it warrants first consideration in circuit hardening.

4.3 Nonlinear Circuits

Nonlinear circuits such as flip-flops and other logic circuits will be the least vulnerable to a nuclear environment, insofar as any permanent damage that might result, although temporary inoperability may occur.

Logic circuits are nonlinear in normal operation and operate either in saturation (ON) or in cutoff (OFF) condition. The transient saturation experienced by logic circuits as a result of nuclear radiation may force them into abnormal conditions or operating sequences; e.g., upon recovery from transient saturation, a flip-flop may or may not assume the same logic condition which existed prior to radiation.

Thus, a flip-flop counter will recover to a random count after radiation-induced saturation and resume sequential operation from that point. Whether this effect is critical or not depends upon the system in which it is used and the sequential functions which it controls. If this is critical, a square loop memory core may be used to provide memory action after the cessation of ionizing radiation.

Logic driving circuits used to read digital data into and out of memory stores will also be saturated and, upon recovery, the memory locations so driven will contain random information. All of the data stored in a random access memory could be destroyed.

All commutating transistors, whose collectors are tied to a common point and whose emitters are each tied to a signal source (sensors), will be saturated simultaneously, thus shorting all driving signals together.

Digilog switches, in digital-to-analog conversion circuits, and logic switches which drive emitter followers, are vulnerable to transient radiation, since transistor saturation will short two power supplies together through the transistors. Large filter capacitors across the power-supply outputs may be undesirable since they provide the digilog switches with energy sources for large transient currents.

The decrease in beta, due to nuclear radiation, requires that the base driving current be proportionately increased (as beta decreases) to maintain a given collector-current loading. Thus, hardened switching circuits must be driven quite hard into saturation in normal operation so that they will be capable of being saturated after beta degrades. This overdrive, however, has the effect of

requiring a greater time to turn-OFF the transistor when bringing it out of the saturated state. High-speed logic switches, therefore, require special techniques to correct for this nuclear-hardening overdrive in order to maintain the switching-speed capability. Some of the hardening techniques may include low impedance circuitry, photo-current compensation, emitter loading and a balanced pair of transistors in the output stage.

The increase in I_{CO} after nuclear radiation may be important in logic switches. A reverse base-emitter voltage is required to keep the transistor cut off in the OFF state. This voltage is normally provided through resistive dividing networks in the base circuit from a reverse-bias power supply. The effect of the leakage current, I_{CO} , is to bring the transistor closer to conduction. Since I_{CO} increases due to nuclear radiation, the reverse-bias hold-off networks must be more effective, i.e., smaller resistor values and/or higher bias voltages must be used.

A small increase in V_{BE} due to nuclear radiation will tend to decrease the voltage drop across the base-drive resistor and, consequently, tend to decrease the base-drive current. This effect is compounded by a simultaneous beta degradation, as discussed previously. To maintain a given level of base-drive current after radiation, the base-drive circuit must be a lower impedance than that required for preirradiation operation.

Increased V_{SAT} due to nuclear radiation decreases the ability of the output of a saturated ON-state switch to hold a successive transistor switch in the OFF state. To compensate for this effect, the input base reverse-bias resistor network of the successive transistor

switch must be of lower impedance than normal thereby providing high "hold-OFF current" and requiring less "hold-OFF current" from the saturated state. This condition is compounded by the increase in leakage current, I_{CO} , which has the same system effect.

The nuclear radiation effects of decreased forward-current-gain characteristic (β), increased leakage current (I_{CO}), increased base-to-emitter voltage drop (V_{BE}), and increased saturation voltage (V_{SAT}) all require that logic switching circuits have "stronger" base-drive networks to ensure switching the transistor into the ON state and have "stronger" reverse-bias hold-off networks to ensure switching the transistor into the OFF state. "Stronger" networks imply lower impedances and more current thereby requiring more power and restricting fan-out.

The transient saturation experienced by both transistors in a multivibrator, used to generate clock pulses, will not force them into abnormal operating points since they normally operate in saturation or cutoff. It will, however, force them into an abnormal operating sequence since both transistors are not normally saturated simultaneously. Upon recovery from saturation, the circuit may assume a random state but should function normally provided the transistors are not damaged by transient-overload conditions. If the output side of the multivibrator is loaded with an emitter-follower, then the multivibrator emitter power supply may be shorted to the emitter-follower collector power supply through the two transistors. Correction of radiation effects on clock-pulse-generation are generally futile if the logic circuits which use this clock pulse are similarly affected. Then, for high radiation-rate and high-speed operation, all circuits must be inherently hardened.

The decrease in β after nuclear radiation requires a stronger base-drive capability to ensure good switching conditions between the two transistors. This effect can be minimized by reducing the R while proportionally increasing the C in the base RC driving network. It is assumed that the β is great enough to maintain a regenerative loop.

The increase in leakage current (I_{CO}) after nuclear radiation will tend to load down the RC discharging network on the transistor base, thus increasing the frequency of clock-pulse generation. This effect can be minimized by again reducing the base driving resistor (R) while proportionally increasing C in the RC network.

The change in V_{BE} after nuclear radiation will tend to alter the frequency of clock-pulse generation, since the base RC circuit must discharge to a different point before the OFF transistor begins to conduct. This effect can be minimized by selecting a transistor whose V_{BE} does not change appreciably as a function of nuclear radiation and by ensuring that the slope of the RC discharging waveshape is steep as it reaches the required voltage-time relationship.

The increase of the collector-to-emitter saturation voltage (V_{SAT}) will increase the frequency of clock-pulse generation. The frequency increase will be in proportion to the ratio of the increased V_{SAT} vs the voltage normally switched at the collector of the transistor.

If clock frequency is controlled by a crystal oscillator, then the output phase, frequency, and amplitude of the oscillator must be considered in the design. This consideration must include shock and temperature as well as ionization and degradation.

4.4 Photocurrent Compensation

The dominant effect of ionizing radiation upon semiconductor circuitry is the production of the primary photocurrent (i_{pp}) across semiconductor junctions. Transistors used in linear applications will amplify the primary photocurrent induced in the base by the beta gain of the device, thus resulting in large collector voltage spikes. Transistors in nonlinear applications will beta multiply the induced base photocurrent in excess of that amount required to forward bias the base junction. Thus, a normally OFF circuit may be induced to switch ON by the ionizing radiation environment. In each case the circuit will return to its normally biased condition after the ionizing radiation environment has subsided.

Neutralization of the primary photocurrent may be accomplished in several ways. Increasing the OFF bias of nonlinear circuits is one method of defeating the "turn-ON" effect of i_{pp} . This is rather inefficient, however, since more base drive current must be supplied from the source signal when the circuit is to be "turned-ON" during normal circuit operation.

A more efficient technique is that of compensation⁽³⁾ wherein a second semiconductor device is used in the circuit such that its primary photocurrent opposes and cancels the unwanted primary photocurrent. This technique is shown in Figure 4-6 where the photocurrent of diode CR-1 is of such a polarity as to oppose and cancel the primary photocurrent induced in the base of the transistor. Note that the diode CR-1 is reversed biased and does not contribute to normal operation of the total circuit. Its only functional contribution occurs during ionizing radiation. Such a technique as this can be effectively used in linear circuits as well as nonlinear circuits.

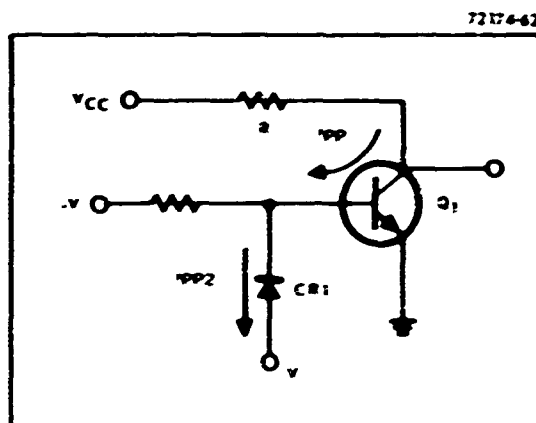


FIGURE 4-6 Circuit for Compensation of Primary Photocurrent

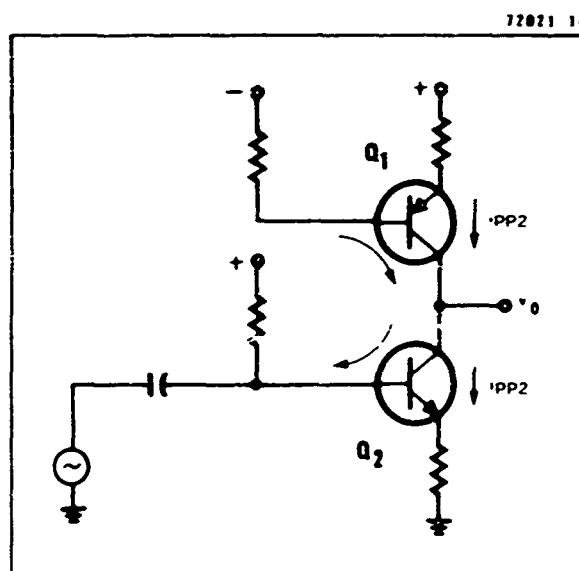


FIGURE 4-7 Circuit for Compensation of Secondary Photocurrent

Figure 4-7 illustrates another technique for compensating radiation-induced photocurrent effects. Both transistors are biased in a linear operating condition with the signal applied to the lower transistor, Q_2 . Consider the voltage at point V_0 . The effect of i_{pp1} , due to Q_1 alone, is to force point V_0 positive with respect to ground, and the effect of i_{pp2} , due to Q_2 alone, is to force point V_0 negative. Therefore, if i_{pp} effects are balanced, no effect is evident at point V_0 since the effects of Q_1 and Q_2 cancel.

A third approach is illustrated in Figure 4-8. The signal, plus radiation noise, is injected at the base of Q_1 and is added to or subtracted from the radiation-induced effect of Q_1 . The base of Q_2 would be grounded through an appropriate impedance and thus the only signal coupled through Q_2 is the radiation-induced effect in Q_2 . The signals summed at point V_0 are the signal plus noise injected (positive signal assumed) at the base of Q_1 (this signal is inverted and amplified by Q_1), the radiation-induced signal in Q_1 itself (a negative signal), and the radiation noise pulse from Q_2 that is amplified but not inverted (a positive signal). Therefore, if the positive noise signal from Q_2 is equal to the two negative noise signals summed at point V_0 , then the remaining signal at point V_0 is just the amplified signal from the base of Q_1 . Diode D, is included to help control the radiation-induced currents.

Shunting the primary photocurrent (i_{pp})⁽⁴⁾ around the collector impedance (R_1) may be accomplished as shown in Figure 4-9. When the dose rate reaches a critical value Q_1 turns ON and secondary photocurrent (i_{pp2}) begins to flow. A direct short from +V to ground would be apparent if R_2 (although small) was omitted. Therefore R_2 is required to limit current.

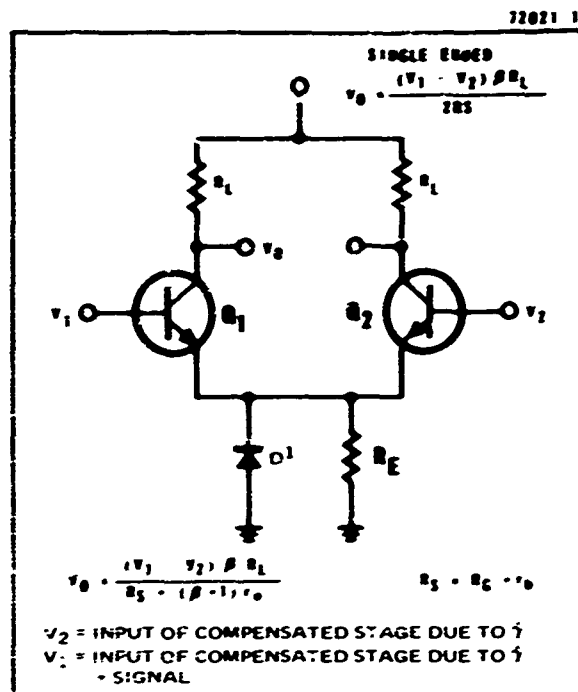


FIGURE 4-8 Circuit for Compensation of Photocurrents and Noise

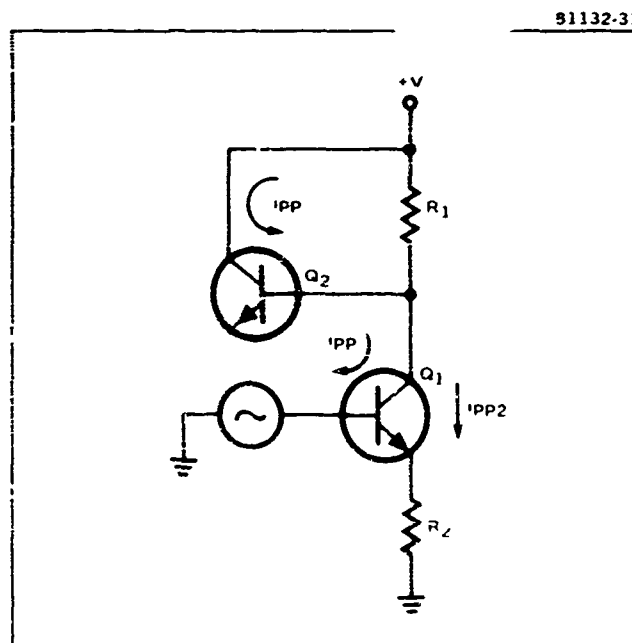


FIGURE 4-9 Circuit for Shunting Primary Photocurrent Around the Collector Impedance

(4)
Similarly, the primary photocurrent (i_{pp}) may shunt the base-emitter impedance as shown in Figure 4-10. Notice that no emitter current limiting resistor is required since R_1 limits the current through both Q_1 and Q_2 when Q_1 is turned ON.

Another technique (4) where the primary photocurrent (i_{pp}) is shunted to minimize current in the emitter load (R_L) is shown for the switch circuit in Figure 4-11. Primary photocurrent from Q_2 (i_{pp}) is shunted to ground in the normally saturated common-emitter stage Q_1 . Once again it is necessary to limit current by inserting R_3 in the collector of Q_2 .

4.5 Filtering

Relatively low-frequency circuitry can be hardened against high-frequency transients ionizing radiation by using filtering techniques in the same manner as for reducing the effects of noise.

The primary photocurrent induced by ionizing radiation may be considered as unwanted noise. The amplitude and duration of the primary photocurrent are related to the intensity and duration of the ionizing radiation. These effects may be likened to those of subjecting the circuit to a noise environment. Thus, the circuit design techniques used to defeat noise effects are also applicable to defeat ionizing radiation effects. Filtering, compensation, common mode rejection, etc., are all to some degree effective against this portion of the radiation environment.

An illustration of the power of the methods is the case of a sampled data system (5) which operated at a 10 MC clock rate through an environment of 3×10^{10} rad(Si)/s. At this level of radiation the

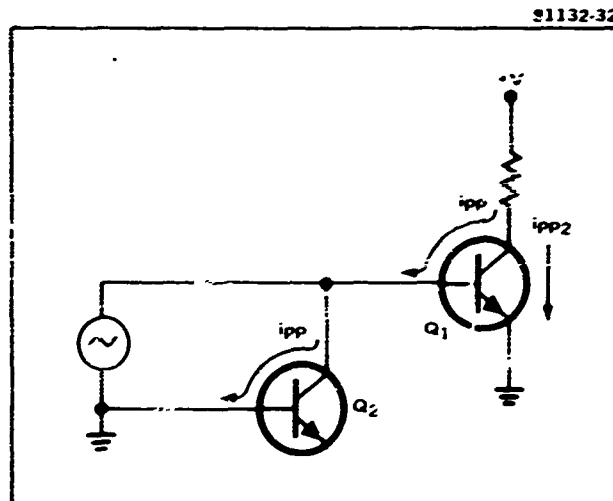


FIGURE 4-10 Circuit for Shunting Primary Photocurrent Around the Base Emitter Impedance

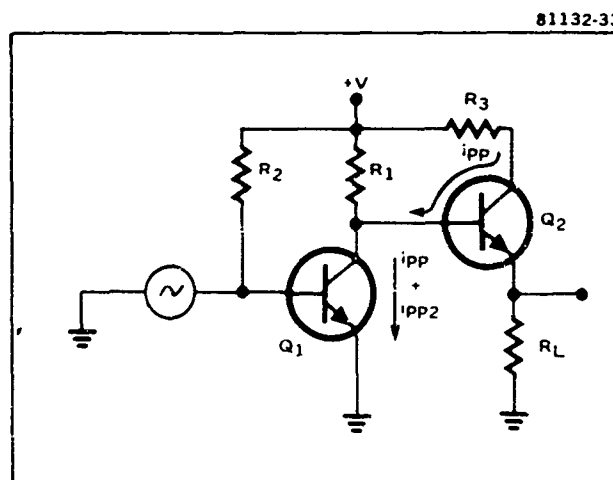


FIGURE 4-11 Circuit for Shunting Primary Photocurrent Around the Emitter Load

very best of silicon semiconductor devices will have induced primary photocurrents in the order of 50 milliamperes. Other less-resistant semiconductors will experience induced primary photocurrents of even greater magnitudes.

Figure 4-12 shows the basic sample/hold circuit designed for a sampled data system. The circuit is essentially a threshold detector filtered against the noise effects of primary photocurrent. The operating current of the tunnel diode is biased at some value less than that required to shift the operating point from the low forward-voltage state to the high forward-voltage state. An input signal of sufficient amplitude and duration will shift the operating point to the high forward-voltage state and thus be "detected". The filter capacitor prevents intense narrow pulse-widths of induced primary photocurrent from falsely switching the tunnel diode. The radiation-induced gain degradation problem in transistors is eliminated, by this sample/hold circuit technique, through use of the bistable tunnel diode configuration.

Resistor R_4 is the bias resistor selected in value to bias the tunnel diode at a quiescent operating current, below the threshold current, by a value equal to that provided by the clock input signal plus the data input signal. Capacitor C_1 and resistor R_5 provide coupling for the clock input signal.

Resistors R_1 , R_2 , and R_3 and computer diode D_1 form the input circuit which couples the data input signal to the basic filtered threshold detector. Diode D_1 acts as a nonlinear clamp that prevents an "oversignal" from triggering the threshold detector even in the absence of a clock signal input.

72174-63

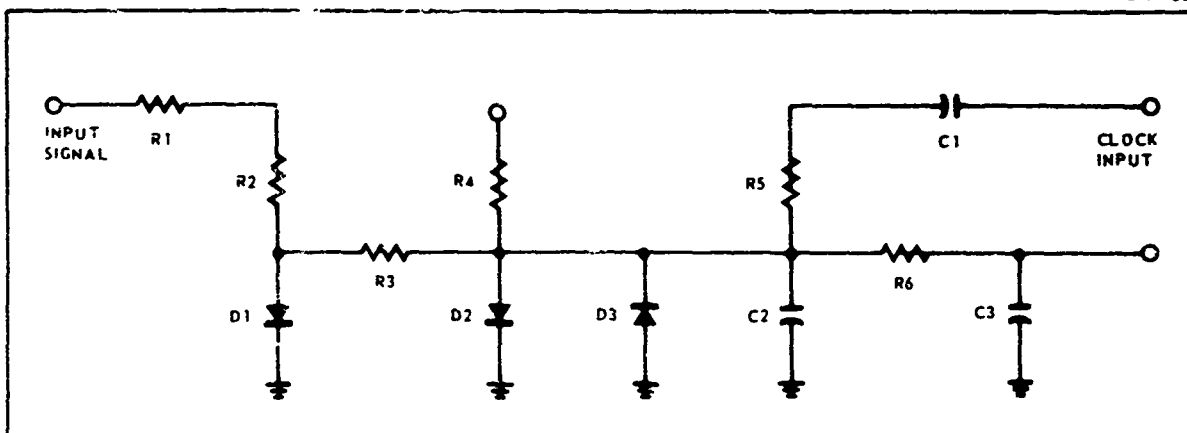


FIGURE 4-12 Sample/Hold Circuitry

Resistor R_6 provides impedance isolation between the tunnel diode and the monitoring device connected to the output of the sample/hold circuit. Capacitor C_3 is a filter capacitor on the output lead to prevent external noise from being picked up, and appearing as a false signal source to the tunnel diode.

Capacitor C_2 and diode D_3 are the radiation hardening elements in the circuit. Capacitor C_2 acts as a high frequency filter to suppress the unwanted primary photocurrent induced at the plate side of the silicon tunnel diode D_2 . The value of C_2 is chosen as large as possible without suppressing the 10 MC signal. Diode D_3 provides radiation hardness by means of the "compensation" technique. The primary photocurrent induced at the cathode of D_3 is of a polarity to oppose or cancel the primary photocurrent induced at the plate of diode D_2 . Compensating diode D_3 is selected on the basis of having an induced primary photocurrent equal in magnitude, insofar as possible, to that induced in tunnel diode D_2 .

4.6 Charge Control

A major contribution to circuit disturbance from transient radiation is caused by the change of charge on capacitors due to ionization of the capacitor dielectric.⁽⁶⁾ By reducing the energy stored in the capacitors, the response can be reduced.

Leakage occurs in capacitors both during and after irradiation. The component of leakage existing after the ionization caused by the prompt gamma spike is, in general, much less severe than that experienced during irradiation. Examination of the significance of the prompt leakage of a capacitor upon circuit transients leads to several important conclusions.

Consider the equivalent circuit for a capacitor under irradiation as shown in Figure 4-13. The injected current (I) will be considerably less than the leakage current through leakage resistance (R_1) in those cases when the capacitor (C) is relatively large ($>0.01\mu\text{f}$) and the applied voltage (V) is of a magnitude usually experienced in circuits (5 to 50 volts). The injected current (I) can, therefore, be ignored in this discussion. The leakage admittance ($1/R_1$) during radiation has been found to follow the relationship:

$$\frac{1}{R_1} = K (\dot{\gamma})^\sigma C \quad (4-1)$$

where

$\dot{\gamma}$ is the radiation dose rate (rad(Si)/s)

$K \approx 10^{-5}$ for inorganic capacitors

C is the capacitance in farads

σ has been experimentally determined to lie between 0.7 and 1.0 for most generally used capacitors.

The voltage (v) on the capacitor at any time (t) during radiation will be as shown.

$$v = V \exp^{-tK(\dot{\gamma})^\sigma} \quad (4-2)$$

The percentage change in the voltage on the capacitor during a radiation impulse of constant amplitude and 0.1 μs in duration is

given by:

$$\frac{\Delta v}{v} = \left[1 - e^{-(10^{-12}) (\dot{\gamma})^\sigma} \right] (100\%) \quad (4-3)$$

If we assume $\sigma = 1$ and solve for the dose rate at which $(\Delta v/v)\% = 10\%$, we find that:

$$\left[\ln(0.9) \right] 10^{12} = -\dot{\gamma} \quad (4-4)$$

or

$$\dot{\gamma} = 1.5 \times 10^{11} \text{ rad(Si)/s}$$

It is important to notice that the percentage discharge in the voltage across the capacitor is independent of the capacitor value (from Equation 4-2). This fact is verified experimentally by the data shown in Figure 4-14 in which a number of capacitor responses are normalized and plotted against the capacitor sizes. It should be noted that the capacitor values range over two orders of magnitude while the change in voltage on the capacitors deviates from a constant by only 20 percent. All capacitors tested used the same dielectric so that K did not change between units.

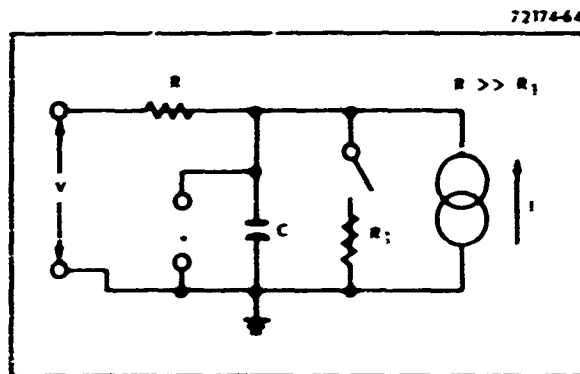


FIGURE 4-13 Equivalent Circuit of a Capacitor During Irradiation

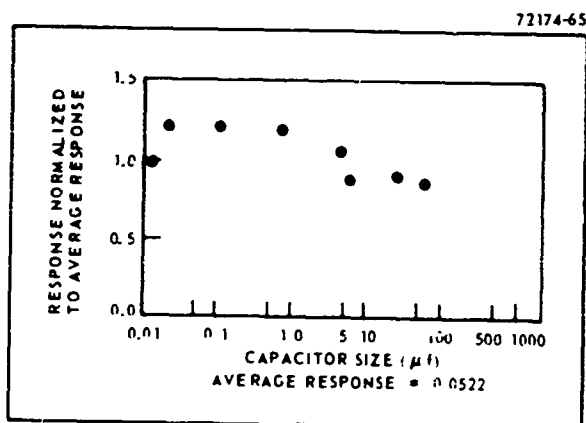


FIGURE 4-14 Capacitor Radiation Response vs Capacitor Value

From Equation 4-2 it can be seen that the transient voltage developed (v) will be zero if the quiescent voltage (V) on the capacitor is also zero. In fact, the direction and magnitude of the transient may be changed at will by changing V . A technique for reducing circuit disturbances where V is a design value is immediately obvious. That is, in any circuit where the frequency response is shaped by an RC time constant, the gamma transient response of the capacitor can be reduced significantly by reducing the quiescent voltage and, therefore the stored energy in it to zero. Figure 4-15 shows the response observed at the collector of transistor Q_1 when the coupling capacitor, C_2 , of Figure 4-16 was exposed to transient ionizing radiation and the initial voltage on the capacitor changed from +28 volts dc (bottom trace) to -12 volts dc (top trace). The circuit response is seen to vanish where the initial voltage on the capacitor is zero.

4.7 Reducing Time Constants

Three general methods may be employed to harden linear amplifiers to ionizing radiation. These methods are:

- . Reduce electrical settling time or overload time to the same order as that of the prompt gamma transient.
- . Reduce component effects by careful selection of radiation insensitive devices.
- . Keep current levels high and impedances low wherever possible.

The immediate result of the first method is to reduce the time duration of the radiation-induced circuit disturbances to the same time

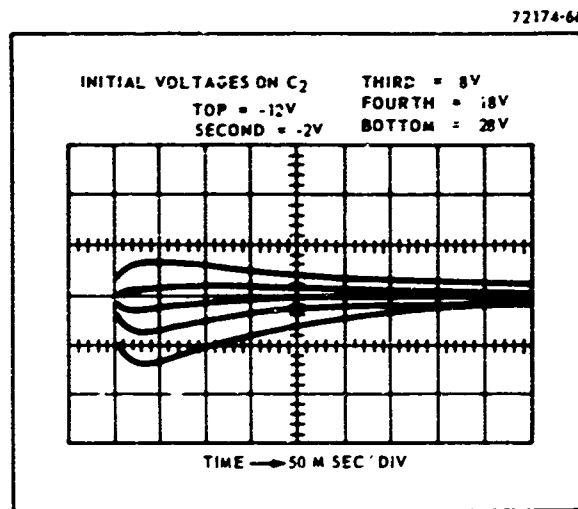


FIGURE 4-15 Transient Response vs
Capacitor Initial Conditions

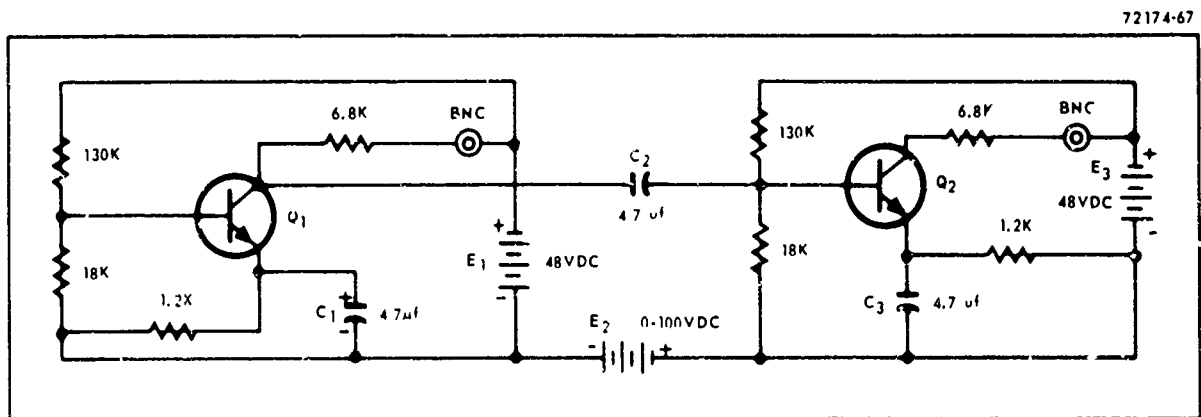


FIGURE 4-16 ac Coupled Amplifier for Testing Transient Recovery

regime as that of individual components. Some of the most commonly used circuit configurations exhibit prolonged radiation recovery. To observe the effects of the many time constants present in typical linear amplifier circuits, one need only examine the circuit transition from de-energized condition to operating condition when power is applied. While this test is rather severe, it does indicate the circuit areas which are responsible for long circuit relaxation periods.

The circuit time constants which determine the transition to operating conditions (typically coupling and bypass capacitors, transformers, etc.) are also those which determine the recovery mode from radiation disturbance. Of particular interest, are the time constants associated with the first stages of an amplifier since their effects are greatly exaggerated by circuit gains. The elimination of such time constants, as a possible hardening technique, places some restrictions on the circuit designer. However, seldom are these restrictions so severe as to preclude efficient design. It is almost always practical to directly couple stages in order to eliminate coupling capacitors and to employ differential stages to eliminate bypass capacitors. The frequency response shaping accomplished by the coupling and bypass capacitors may be performed in following stages or, preferably, at the amplifier output. If all time constants (or at least those associated with the low frequency response of the amplifier) are transferred to the circuit output, minimum settling time or overload recovery time will result. The circuit disturbance duration, in front of the frequency shaping networks, will be reduced to nearly that of the individual components.

From this point, further gains in hardness may be obtained by using the best available components and reducing the relative magnitude

of radiation responses with respect to nominal signal levels. Low circuit impedances will reduce the relative effects of ionization leakage paths. Normally high operating signal currents will tend to minimize the effects of replacement currents. Employment of linear cancellation currents or common-mode rejection techniques may afford some further hardness, but are not considered as primary hardening techniques, since results are quite erratic because of sensitivity to geometry and individual device responses.

4.8 Magnetic Devices

Since magnetic devices are very radiation resistant, they offer many advantages in radiation hardened circuit design. A few of the design techniques are listed below:

- . Inversion - The common emitter amplifier is normally used to invert ac signals. The transient response of the common emitter stage can be eliminated by using a transformer to invert the ac signal.
- . Memory - A conventional bistable flip-flop may use a square loop memory core to provide memory action after the transient radiation disturbance.
- . Differential - A differential transformer can perform the same algebraic subtraction as any differential bipolar transistor circuit with less effects from the ionizing radiation.

4.9 Summary

A summary of the potentially vulnerable situations that may

occur in circuits and other areas of concern is presented in Table 4-2. It is assumed that the basic hardening technique of component selection has already been applied based on guidelines given in the sections discussing the specific component areas.

TABLE 4-2. Possible Radiation Hardening Techniques

<u>Vulnerable Situation (Radiation Induced)</u>	<u>Possible Fixes</u>
Short circuits in complimentary pair transistors (dc-dc converters, encoders, complimentary drivers)	<ul style="list-style-type: none"> - Current limit energy source - Add current limiting resistors or magnetic circuitry
Sneak short circuit paths in integrated circuits and excessive substrate currents	<ul style="list-style-type: none"> - Current limit power supplies with resistors and/or reactors - Use dielectric isolated IC's
Energy storage elements shunted by back biased semiconductors	<ul style="list-style-type: none"> - Add current limiting resistors - Redesign capacitor input filters
Oscillator and flip-flop sticking*	<ul style="list-style-type: none"> - Insure self starting after radiation transient
Series pass transistor overload in regulators	<ul style="list-style-type: none"> - Add current limiting - Circumvent - shunt away excess current
Abnormal sequencing	<ul style="list-style-type: none"> - Circumvent - do not allow any abnormal forcing - Automatic reset
Memory disturbances	<ul style="list-style-type: none"> - Reacquisition - Circumvention - Hard memory
Integrated circuit latch-up	<ul style="list-style-type: none"> - Radiation screening - Power shut down - Use dielectric isolation
Prolonged circuit recovery	<ul style="list-style-type: none"> - Reduce time constants - Keep currents high and impedances low

*Sticking is failure to restart or reset after irradiation

APPENDIX 1

DATE OF THE CALL

11 = radiation test data available; 0 = no radiation test data available.

This tabulated the measured percentage value of beta remaining (B fml/4 original) at 1215, 1515, and 1812 m/cm².

of measured value of photocurrent (Ip) in puces/(15) cps /ET of rate of reduction of

This lists the measured value of neutron dose (n/cm^2) at which beta has degraded to 50% of original value.

q2pp1ap0pq-uzg unufjw p0ijyods e3z0n3c0jn0es b0j e0c0l e0d0.

157-0-22

OFFICE - C-100

the lists open air power ratings; * indicates the

collector-base voltage in volts

collector-emitter voltage in volts

valter base voltage la volta

2009-10-20 10:10:10

2025 03 07 10:00 AM

cost per copy

AVERAGE
This indicates the peak value of beta and the current in milliamperes where beta peaks. 200/6 indicates a beta of 200 peaking at 6 milliamperes.

This indicates a value of beta at one or two other current values in milliamperes, thus showing the beta spread characteristic.

справочна и оцетна таблица

OPERACIJA U ZASTUPNIŠTVU

[illegible]

Notes: Γ = exponential. For example $1.7 = 1 \times 10^7$ and $1.13 = 1 \times 10^{13}$.

A	Ampross
B	Bendix
C	Union Carbide
D	Cont. Dev. Corp.

3

2 3

Comments:

Transcript

1

218

25

10

1

0

101

1/6

;

A Year's Policy Study

良

...

5

1987

1771

Page 10

502

SECRET

1 20 7C	3E14	60C 1 1 1E1001	0.250	30	12 3.0 10	70 1.20 100/ 8	2.0
0		600 1 1 2N1010	0.300	15	6 4.0 7	18 1.50 75/ 10	2.0 3.0
1 7 42	7E13	60C 1 1 2N1201	0.100	40	15 6.0 8	52 3.30 100/ 10	4.0 3.5
0		60C 1 1 2N1544	0.300	25	25 3.0 4	14 7.50 50/ 10	2.5
1 15 45	2E14	500 1 1 2N1503	0.200	30	12 2.0 6	90 0.75 50/ 8	2.0
1		7E13	500 1 1 2N1917	0.200	30	15 3.0 6	18 2.50 50/ 3
0		500 1 1 2N1134	0.500	40	15 5.0 4	5 11.7 100/ 10	4.0 4.0 4P
0		500 1 1 2N1943	0.100	40	40 3.0 4	18 3.00 50/ 10	4.0
1 10 50	0.01 1E14	50C 1 1 2N1369	0.160	40	15 4.5 5	14 3.00 70/ 15	4.0
1		2E13	50C 1 1 2N1938	0.300	25	13 5.0 8	52 2.15 30/ 50
1 10 50	2E13	50C 1 1 2N1337	0.600	40	20 4.0 4	5 11.1 80/ 50	5.0 4.0
0		50C 1 1 2N1327	0.360	40	20 6.0 4	18 2.40 150/ 10	3.5
0		500 1 1 2N1309	0.400	40	20 6.0 4	46 5.40 150/ 10	4.0 4.0
1 10 56	1E14	500 1 1 2N1866	1.000	55	30 3.5 4	39 4.95 200/ 50	4.0 4.0
0		500 1 1 2N15020	0.320	40	15 4.5 6	98 0.69 80/ 10	4.0
0		450 1 1 2N1407	0.200	25	12 3.0 7	99 0.73 35/ 10	2.2
0		450 1 1 2N1303	0.600	25	12 4.0 7	5 18.0 70/300	25. 15. DRIVER
1 5 40	7E13	450 1 1 2N1649	0.400	40	15 6.0 4	46 2.70 30/100	24/10-200 8.0 4.0
1 10 50	0.01 1E14	40C 1 1 2N1368	0.360	40	15 4.5 5	14 2.31 40/ 10	4.0
0		400 1 1 2N1284	0.400	40	20 4.0 6	5 39.0 40/100	15. 10.
0		40C 1 1 2N1011	0.360	30	12 5.0 7	14 1.98 70/ 10	4.0
1 10 50 80	1E14	40C 1 1 2N1309	1.000	50	50 3.0 4	5 5.24 30/100	4.0
1 10 40	1E14	400 1 1 2N1443	0.150	12	8 5.0 4	5 14.3 80/ 5	4.0
1 17 82	2E14	40C 1 1 2N1690	0.200	40	40 4.0 6	99 1.50 30/ 4	4.0
0		360 1 1 2N1828	0.300	40	40 3.0 7	99 0.90 60/ 12	4.0
1	0.02 3E13	35C 1 1 2N1834	0.300	60	50 5.0 4	14 2.00 70/ 20	4.0
0		350 1 1 2N1834	0.300	40	30 5.0 4	99 0.70 90/ 10	4.0
1 20 75 95 0.08 3E13	35C 1 1 2N1835	0.300	25	20 3.0 4	18 1.50 70/ 20	4.0	
0		350 1 1 2N1201	0.360	40	20 6.0 4	14 4.70 100/ 10	4.0
0		350 1 1 2N1009	0.360	40	15 4.0 7	52 1.98 80/ 30	4.0
0		350 1 1 2N14	0.360	40	20 5.0 6	52 3.40 40/ 50	4.0
1 10 35 45 85 0.03 4E13	350 1 1 2N1287	0.200	40	20 3.0 4	18 7.50 35/ 10	1.1 10.16 SPREAD-SHARP UNIP	1.1 10.16 SPREAD-SHARP UNIP
0		350 1 1 2N1446	0.200	40	15 5.0 6	99 0.60 60/ 50	50/10-200 8.0 5.0
1 10 42 91	1E13	30C 1 1 2N1008	0.30	25	20 5 4	18 1.50 100/ 10	80/5-80 6
1 30	0.01 4E13	30C 1 1 2N1008	0.160	40	15 5.0 6	14 1.20 100/ 10	6.0
1 42 82	0.04 3E13	30C 1 1 2N143	0.300	20	12 5.0 7	18 4.00 50/ 40	5.0
0		300 1 1 2N1744	0.300	20	12 5.0 4	18 2.90 80/ 10	40/1-100
0	0.01	30C 1 1 2N1852	0.300	20	12 5.0 7	93 9.43 80/ 10	5.0
1 30 40	0.01 2E13	30C 1 1 2N1914	0.360	40	15 5.0 4	18 1.50 25/ 30	6.0
1	0.11 3E13	30C 1 1 2N1914	0.300	45	25 5.0 6	18 3.65 90/ 20	6.0

1	22	1E13	300	1	242841	0.100	40	15	5.0 M	14	2.0	7.0	5.0		
1	5	43	7E13	100	1	243553	1.000	65	40	4.0 M	30	4.95	40/250		
0			300	1	243684	1.000	60	40	4.0 M	94	8.60	40/ 50			
1	30	75	-17	4E13	250	1	240915	0.100	70	40	5.0 F	14	4.04	100/ 15	
0			250	1	240941	0.500	60	30	5.0 M	5	13.0	40/150	1.5		
1	13	42	2E13	250	1	241120	0.500	60	30	5.0 M	5	19.1	100/ 10	0.0 MP	
1	13	58	2E13	250	1	242219	0.500	60	30	5.0 M	5	3.15	150/150	MP	
1	10	90	2.0	1E13	250	1	242222	0.500	60	30	5.0 M	14	3.95	70/500	
0			250	1	242222A	0.500	75	40	6.0 MG	14	4.35	140/250			
0			250	1	242477	0.600	60	70	5.0 MG	5	3.30	65/ 40	10.0		
1	10	53	40	1E14	250	1	242517	0.600	60	30	5 M	5	4.95	100/150	
1	30	70	95	.05	1E13	250	1	242514	0.600	60	30	5.0 M	5	5.85	130/100
1	10	50		1E14	250	1	242540	0.500	60	30	5.0 M	14	5.45	150/150	
1	30	75	95	.12	4E13	250	1	242756	0.160	25	15	0	4.00	100/ 20	
1	35	75	.04	5E13	250	1	242845	0.160	60	30	5.0 F	14	4.00	20/ 80	
1	33		9E13	250	1	242846	0.400	60	20	5.0 F	5	4.95	40/150	0.0	
0			250	1	242854	0.600	60	70	5.0 M	5	1.45	150/150	0.0		
0			250	1	243116	0.400	60	20	5.0 M	14	2.40	150/150	0.0		
1	20	70	90	1.0	3E13	250	1	243114	1.000	100	40	4.0 M	5	5.16	100/ 40
0			250	1	243410	0.500	60	10	5.0 M	5	15.0	100/ 10	20. 0.0 LL MP		
1	25		4E13	250	1	243512	0.400	60	15	5.0 M	5	3.71	80/100	10.0	
0			250	1	243643	0.150	60	30	5.0 F	49	0.84	225/100	0.0 MG		
0			250	1	243717	1.700	60	40	4.0 M	5	20/200		10.0		
0			250	1	244953	0.160	60	30	5 G	0	0.40	400/150			
0			250	1	245028	0.120	60	30	5.0 E	44	0.69	150/150			
0	45	90	.05	1E14	200	1	242706	0.100	25	20	5 M	14	1.00	65/ 20	
0			200	1	245106	0.100	25	20	3.0 M	49	0.60	40/ 10	0.0 MP		
0			200	1	245918	0.250	60	30	5.0 M	44	28.1	80/150			
0			200	1	240785	0.500	60	30	5.0 M	5	60/150		COMP. PAIR		
0			200	1	240845	0.250	60	30	5.0 M	44	13.5	60/150	COMP. PAIR		
0			200	1	240980	0.500	40	15	5.0 M	5	50/ 10		COMP. PAIR		
0			200	1	240985	0.250	40	15	5.0 M	44	30.2	50/ 10	COMP. PAIR		
0			200	1	241122F	0.250	60	30	5.0 M	44	83.2	100/ 10	MP LI		
1	21	41	-10	1E12	200	1	241124	0.500	60	30	5.0 M	5	51.4	0	
0			200	1	241133	0.500	60	30	5.0 M	5	15.0	70/500	0.0		
0			200	1	242410	0.600	60	30	5.0 F	5	4.50	75/ 40	50. 11. SWITCH		
0			200	1	242951	0.400	60	60	5.0 M	5	4.50	80/ 10	0.0		
0			200	1	242952	0.500	60	40	5.0 M	14	4.95	80/ 10	0.0		
0			200	1	243052	0.250	35	15	5.0 F	44	27.0	75/ 10	12. 0.0 DUAL		
1	35	25	95	2E13	200	1	243252	1.000	60	30	4.0 MT	5	9.75	100/200	

1	18 62	1.2 2F13	30 1 1 2N120A	0.300 120 80 7 MT 1P 1.50 80/300	70/60-200
1			50 1 1 2N140A	0.300 60 40 4 1P 1.4 2.25 50/100	
1	10 50 45 1.0 1.15		50 1 1 2N140A	0.800 120 100 7.0 7P 1.12 80/ 40	60/1-200
1	10 50 40 0.4 1C13		50 1 1 2N140A	0.800 60 40 5 2 5 4.20 170/400	
1	14 43	2E13	50 1 1 2N140A	0.800 60 40 5.0 2 5 4.45 110/100	
1	10 55 90	1E13	50 1 1 2N140A	0.800 60 50 5 2 5 3.15 9A/100	
1	6 37	6E12	50 1 1 2N140A	0.500 100 60 3.0 MT 5 10.0 100/ 10	
1	30	1E13	50 1 1 2N140A	0.800 60 35 7 2 5 80/150	
0			50 1 1 2N140A	0.800 120 80 1.0 2 5 5.50 100/150	40/1-1000 85. 10. HIGH V 9ETA 5P450
0			40 1 1 2N114	0.800 150 150 5.0 TM 5 6.00 50/ 10	25/1-200 80. 9.0 MV
0			40 1 1 2N112	0.800 150 150 5.0 T 5 7.00 50/ 20	10/1-2-200 80. 9.0 MV
1	0.3		30 1 1 2N130	0.300 45 45 5 M 18 4.00 100/100	150/300 LL
0			30 1 1 2N130	1.000 300 300 10 M 5 12.6 100/300	
1		2E12	20 1 1 2N123	0.0 0 0 0 0 0 140/ 0	60/1-30
1	4.0		20 1 1 2N123	0.850 60 40 0 0 80/999	
1	5 55 50	1F13	16 1 1 2N1717	0.400 150 100 6.0 T 5 11.3 60/100	20/50-100/
1	20 55 88 1.6 4E1		10 1 0 2N1305	0.150 25 25 7 5 0.74 130/400	
10	30	7E11	10 1 1 2N1722	0.0 120 80 10. 1 51 40/ 99	7-5.0AMP
1		1E12	5 1 1 2N172	0.065 15 15 5.0 2 0 3.50 200/100	90/4
1		1E12	5 1 0 2N167	0.065 30 30 5.0 2 0 9.16 100/200	10/1-2-25
1		2F12	2 1 1 2N133	0.150 45 0 1.0 T 5 4.65 25/500	30/1-2-25
1		4F12	2 1 1 2N135	0.150 45 0 1.0 T 5 4.90 75/400	100/2-30
1		2E12	2 1 1 2N136	0.150 45 0 1.0 T 5 5.95 100/400	
1	40	2E11	2 1 1 2N137A	0.400 100 100 8 TV 5 5.00 60/200	10/1-2-25
1		3F12	1 1 1 2N132	0.150 45 0 1.0 T 5 4.65 75/400	17/5-60
1		2E12	1 1 1 2N139	0.200 55 55 1 7 11 8.12 17/120	15/5-60
1		2E12	1 1 1 2N141	0.200 125 45 1 7 11 14.0 15/150	
1		2F12	1 1 0 2N146	0.200 0 0 0 0 0 0	
1	20 80	0.9 3E13	1 1 0 2N145	0.120 25 15 20 R 5 0.99 90/500	

1	75	4E13	100 0 1 2M195	0.160	20	15	4 PM 1A	100/200	
1		.06	100 0 0 2M199	0.025	20	15	0	9 1.40	20/100
1		.06	100 0 0 2M190	0.060	15	12	0	9 6.95	20/100
1	48 90	9E13	100 0 0 2M204	0.150	20	15	0	9 1.80	100/100
0			100 0 0 2M210	0.125	60	60	25	7 1.85	100/10
1		.13	2E13	100 0 1 2M265	0.360	25	25	4.0 MT	4A 12.4
1		.13	2E13	100 0 1 2M267	0.400	25	25	4.0 FT	4A 12.4
0			100 0 1 2M368	0.300	25	25	4.0 0	99	AC/ 50
0			100 0 1 2M370	0.300	50	30	9.0 T	94 0.49	10/ 50
0			100 0 1 2M379	0.360	60	60	5.0 M	5 6.75	500/ 1
1	8 53	1E13	100 0 1 2M381	0.400	60	60	5.0 M	5 21.8	600/ 1
1	50	.17	1E13	100 0 1 2M383	0.200	60	60	5.0 M	94 30.0
1	30 75	2.1	4E12	60 0 1 2M722	0.400	50	35	5.0 MT	1A 5.60
1	25 68	0.5	3E12	60 0 1 2M132	0.400	50	35	5 5TY	5 5.60
0			60 0 1 2M135	0.300	60	45	6.0 TG	5 4.0	200/ 1
1	5 60	95	1.13	40 0 1 2M1259	0.120	40	40	0.5 R	44
0			40 0 1 2M484	0.300	150	150	6.0 F	94	150/ 10
1	30 70	0.5	2E13	100 0 0 2M1307	0.150	30	25	7	5 0.66
1	30 70	6E12	60 0 1 2M461	0.150	25	25		1A 4.00	37/500
1	5 53	93	1E13	70 0 1 2M2187	0.150	30	30	0	0
1	14 31	48	.11	7E11	60 0 1 3493	0.300	50	10	MG 72 34.5
1	00 45	7.1	2E12	50 0 0 2M1144	1.000	45	20	20 A	8 2.48
1		.04	50 0 0 2M11848	1.000	45	20	20 M	8 4.13	70/500
1	48 75	0.7	4E13	40 0 0 2M404	0.150	25	24	12 18Y	5 0.42
1	20 70	0.1	10 0 1 2M329A	0.385	50	30	1	5 9.00	0
1	20 60	99	1.6	1E13	0.200	45	30	30 M	4 1.65

12.

LL

MP LL

LL MC MP

OTHER MANUF. FC. WUGUES

0.0 6.0 MG LL MP

MANUF BY MAC

MANE BY PHILCO

INCH

BETA SAT. AT 750 MA

BETA SAT. AT 750 MA

WETA CONSTRUCTION

POWER & PLANT

[illegible]

0			150	1	1	241543	40.000	65	40	4.0	XL	3	40/200	
1	10 50	1F13	140	1	1	241287	25.000	100	40	4.0	M	94	40.0	40/250
0			100	1	1	241294	25.000	40	40	2.0	M	1	20.3	40/400
0			100	1	1	241297	25.000	60	40	3.0	M	3	52.0	20/000
0			100	1	1	241400	17.500	60	40	4.0	M	94	45.0	n
0			100	1	1	241507	70.000	65	40	4.0	E	94	33.0	n
1000	55	1F13	50	1	1	241189	125.000	140	100	5.0	P	94	40.0	40/000
0			40	1	1	241000	15.000	140	100	5.0	P	94	15/000	
0			40	1	1	241901	125.000	140	100	5.0	P	94	999	
1	23 72	2E12	14	1	1	241934	4.000	125	40	4.0	T	94	47.0	40/000
0			10	1	1	241015	2.000	999	999	5.0	S	5	50/ 14	
1		3F12	10	1	1	241408	4.000	100	100	5.0	T	5	n	30/50-2000
1	5 40	4F11	10	1	1	241724	3.000	120	40	10.0	T	94	n	
1	10 26 43 -16	3F11	5	1	1	241394	1.500	40	45	2.0	C	5	27.5	7.0 4.0 50
1	16 44 76 2.9	7F12	2	1	1	40341	70.000	90	0	0	R	40	13.0	
1	15 45 76 2.9	7F12	2	1	1	40341	70.000	70	70	35	R	40	13.0	
1		4F11	1	1	1	401015	150.000	30	30	25	M	94	15.0	
1	200	5F11	1	1	1	241016	150.000	100	100	25	M	94	19.1	100/100
1	25	3F11	1	1	1	241016C	150.000	150	150	25	M	94	32.0	n
1	25	2F11	1	1	1	241016	150.000	200	200	25	M	94	50.0	n
1	30 220	F11	1	1	1	241016E	150.000	240	250	25	M	94	40.1	45/100
1	50	4F11	1	1	1	241406	25.000	100	55	12	R	0	6.70	45/400
1	10 40	4F11	1	0	0	241453	100.000	120	120	0	0	26	45/000	35/100
1	600		1	0	0	24174	150.000	40	70	R	R	34	3.40	15/000
1	200		1	1	1	241400	75.000	100	100	40	40	3	8.25	50/000

BLANK PAGE

REFERENCES

SECTION 2

1. Thatcher, Richard K., "Transient Radiation Effects on Electronics Handbook," DASA 1420, August 1967, Battelle Memorial Institute. (Unclassified)
2. Bell, J. E., et. al., "Transistor Quality Statistics in a Pulsed Ionizing Radiation Environment - t_{BR}," USNRDL-TRC-13, September 1966, Contract N228(62479) 69539, Hughes Aircraft Company. (Unclassified)
3. Carr, E. A., et. al., "Simplified Techniques for Predicting TREE Response," AFWL-TR-65-65, September 1965, Contract AF 29(601)-6404, Hughes Aircraft Company. (Unclassified)
4. Walker, K. R., et. al., "Simplified Engineering Techniques for Predicting Diode and Transistor Photocurrent," HDL-017-1, March 1968, Contract DAAG39-67-C-0017, Hughes Aircraft Company. (Unclassified)
5. Ashar, K.C., "Transit Time in High-Speed Switching Transistors," Solid State Design, February 1964, p. 24. (Unclassified)
6. Butcher, D. T., Private Communication, April 1968, Hughes Aircraft Company. (Unclassified)
7. Russell, R. L., "Techniques of Estimating Radiation Responses," April 1968, Hughes Aircraft Internal IDC. (Unclassified)
8. Peck, D.S., et.al., Bell System Technical Journal, 42, 1963, p 95. (Unclassified)
9. IBM Journal, September 1964 and IEEE Transactions on Electron Devices, March 1965. (Unclassified)
10. Atalla, W., Proceedings of the IEEE, 7 B, Supl No. 17, 106, p 1130, 1959. (Unclassified)
11. Brown, W. L., Physics Review, 91, p 518, 1953. (Unclassified)
12. Mitchell, J. P. and Wilson, D.K., Bell Systems Technical Journal, 66, p 1, 1967 (Unclassified)

13. Blair, R. R., *IEEE Transactions on Nuclear Science*, NS-10, November 1963. (Unclassified)
14. Cocca, U., and W. B. Koepp-Baker, "Radiation Effects in Electronics," *ASTM*, STP 384, 1965. (Unclassified)
15. Hughes, H., *IEEE Transactions on Nuclear Science*, NS-12, p 53, 1964.
16. Binder, D. et al., "Analytical and Experimental Prediction of Fusion Neutron Radiation Effects - Volume I Theoretical and Experimental Studies," *AFWL-66-41*, July 1966, Contract AF29(601)-6721, Hughes Aircraft Company. (Unclassified)
17. Binder, D. and D. T. Butcher, "Rapid Annealing in Silicon Transistors," *AFWL-TR-66-145*, February 1967, Contract AF 29(601)-7198, Hughes Aircraft Company. (Unclassified)
18. Perkins, C. W. et. al., "Radiation Effects on (Monolithic) Microelectronic Circuits," *ECOM-01313-F*, November 1966, Contract DA28-043 AMC-01313(E), Hughes Aircraft Company. (Unclassified)
19. Bowman, W.C., et. al., "Microcircuit Radiation Response Mechanisms" *RADC-TR-67-455*, Final Report, October 1967, The Boeing Company (Unclassified)
20. Kinoshita, G. et. al., "Radiation Induced Regeneration Through PN Junction Isolation in Monolithic Integrated Circuits," *IEEE Transactions on Nuclear Science*, NS-12, October 1965. (Unclassified)
21. Leavy, J. F. and R. A. Poll, "A Study of Transient-Radiation-Induced Latch-Up," Final Report, May 5, 1967, Contract N00014-66-C-0347, General Atomic. (Unclassified)
22. Smith, V. R., "Study of the Latch-Up Effect of Transient Radiation on a Demodulator Chopper Integrated Circuit," Paper presented at the *IEEE Conference on Nuclear and Space Radiation Effects*, Columbus, Ohio, 13 July 1967. (Unclassified)
23. Bownan, W. C., et. al., "Mechanism for Radiation-Induced Latch-Up in a Microcircuit," Paper presented at the *NEREM Meeting*, Boston, Mass., November 1968. (Unclassified)
24. Bell, J. E. and R. D. Loveland, "Radiation Effects on Guided Missile Electronic Equipment-III," *FR 64-10-267*, 15 July 1964, Contract N0w64-0406-d, Hughes Aircraft Company. (Unclassified)

25. Perkins, C. W., et. al., "Radiation Effects on (Monolithic) Micro-electronic Circuits," ECOM-01313-4, August 1966, Contract DA28-043 AMC-01313(E), Hughes Aircraft Company. (Unclassified)
26. Marshall, R. W., Hughes Aircraft Company, Internal IDC, 19 Sept 1967. (Unclassified)
27. Unpublished data, Hughes Aircraft Company, Radiation Effects Research Department, 1968. (Unclassified)
28. Kear, G. H., "Thermomechanical Radiation Damage to Electronics Components," Contract N00014-67-C-0495, Lockheed Missiles and Space Company (Secret RD)
29. Wicklein, H. W., et. al., "Advanced Guidance System Radiation Studies (U)," BSD-TR-66-38, December 1966, Contract AF04(694)-838, The Boeing Company. Secret RD
30. Lindquist, P. E., "Transient Radiation Effects in Low Power Integrated Circuits," Hughes Aircraft Company, Internal IDC 2951.10/118, March 1968. (Unclassified)
31. Russell, R. L. and K. R. Walker, "Measured Radiation Response of the 911 Read Amplifier," Task Report, March 1968, Contract FOA8EV-440383, Hughes Aircraft Company. (Unclassified)
32. Private Communication, Hughes Aircraft Company - Semiconductor Division.
33. Wunsch, D. C. and R. R. Bell, "Determination of Threshold Failure Levels of Semiconductor Diodes and Transistors to Pulse Voltages," Paper presented at the IEEE Conference on Nuclear and Space Radiation Effects, Missoula, Montana, August 1968, Braddock, Dunn and McDonald. (Unclassified)
34. Davies, R. L. and F. E. Gentry, "Control of Electric Field at the Surface of PN Junctions," IEEE Transactions on Electron Devices, ED-11, July 1964. (Unclassified)
35. 1968 IR&D Program, First Quarterly Report, FR 68-10-338, 4 April 1968, Hughes Aircraft Company. (Unclassified)
36. Orndorff, R. M. and D. B. Smith, "Estimates of Thresholds for Permanent Degradation of Electronic Circuits from a Nuclear Detonation," ESD-TR-68-197, 13 June 1968, Contract AF19(628)-5167, Hughes Aircraft Company. (Unclassified)

37. Walker, K. R., et. al., "Predicting Transistor Photocurrent Using Avalanche Thoery," USNRDL-TRC-68-3, February 1968, Contract N00228-67-C-0835, Hughes Aircraft Company. (Unclassified)
38. Bell, J. E. and R. D. Loveland, "Radiation Effects on Guided Missile Electronic Equipment VI (U)," FR 66-17-66, 15 March 1966, Contract N0w 65-0221-d, Hughes Aircraft Company. (Confidential)
39. Bell, J. E. and R. D. Loveland, "Radiation Effects on Guided Missile Electronic Equipment V (U)," FR 65-10-169, 15 July 1965, Contract N0w 65-0221-d, Hughes Aircraft Company. (Confidential)

REFERENCES

SECTION 3

1. Born, J. W. "Nuclear Radiation Resistant Polymers and Polymeric Compounds," WADC-TR-55-5; 8, Part VII, March 1962, Tech Doc Rept, April 1, 1960 - May 31, 1961, AF 33(616)-7491, B. F. Goodrich Co. (Unclassified)
2. "The Effect of Nuclear Radiation on Elastomeric and Plastic Materials," REIC Rept No. 3, May 31, 1958, Battelle Memorial Institute. (Unclassified)
3. Kerlin, E. E., "Investigation of Combined Effects of Radiation and Vacuum and of Radiation and Cryotemperatures on Engineering Materials, Vol. I., Radiation-Vacuum Tests," FZK-161-1, January 5, 1963, NAS 8-2450, General Dynamics. (Unclassified)
4. Bonanni, A. P. and C. A. Cassalo, "The Effects of Gamma Radiation and High Vacuum on Polymeric Materials," NAEC-AML-1712, August 20, 1963, Naval Air Engineering Center. (Unclassified)
5. "The Effect of Nuclear Radiation on Elastomeric and Plastic Components and Materials," REIC Rept No. 21, August 31, 1964, Battelle Memorial Institute. (Unclassified)
6. Snaffner, J. P., "Effects of Radiation on Teflon Resins in Space," J. of Teflon 2 (1), January 1961. (Unclassified)
7. Jolley, G. E. and J. C. Reed, "The Effects of Space Environments on Insulation of Teflon, TFE and FEP Resins," Eleventh Annual Signal Corps Wire and Cable Symposium, Asbury Park, New Jersey, November 28-30, 1962. (Unclassified)
8. Sisman, O., C. D. Bopp, "Physical Properties of Irradiated Plastics," ORNL-928, June 29, 1951. (Unclassified)
9. Little, K., "Effect of Irradiation on Nylon and Polyethylene Terephthalate," Nature, 173, 680, April 1954. (Unclassified)
10. Wagner, R. M. and L. H. Towle, "Effects of High Energy, High-Intensity Electromagnetic Radiation on Organic Liquids," Contract AF33(616)-3738, Semiannual Report No. 1, November 12, 1957. (Unclassified)
11. "The Effect of Nuclear Radiation on Lubricants and Hydraulic Fluids," REIC Rept No. 4, April 30, 1958, Battelle Memorial Institute. (Unclassified)

REFERENCES

SECTION 4

1. "Survivability Analysis of Proposed System," 20 March 1968, Hughes Aircraft Company. (Unclassified)
2. Bell, J. E. and R. D. Loveland, "Radiation Effects on Guided Missile Electronic Equipment-IV (U)," FR 65-10-45, 15 January 1965, Contract NOW 64-0406-d, Hughes Aircraft Company. (Confidential)
3. Bell, J. E. and R. D. Loveland, "Radiation Effects on Guided Missile Electronic Equipment V (U)," FR 65-10-169, 15 July 1965, Contract NOW 65-0221-d, Hughes Aircraft Company. (Confidential)
4. "Improvements in Transistor Models and Circuit Hardening for TREE Applications," AFWL-TR-67-71, December 1967, Contract AF22(601)-7063, The Boeing Company. (Unclassified)
5. Orndorff, R. M., "Research and Design Studies of a Radiation Hardened Sampled Data System," AFWL-TR-66-49, June 1966, Contract 29(601)-6756, Hughes Aircraft Company. (Unclassified)
6. Bell, J. E. and R. D. Loveland, "Radiation Effects on Guided Missile Electronic Equipment-III (U)," FR 64-10-267, 15 July 1964, Contract NOW 64-0406-d, Hughes Aircraft Company. (Confidential)

BIBLIOGRAPHY

1. E. R. Leach, et al, "The Space Radiation Environment and Its Interaction with Matter," Battelle Memorial Institute, REIC Report No. 37, July 15, 1965. Contract No. AF 33(615)-1124
2. "Improvements in Transistor Models and Circuit Hardening for TREE Applications," The Boeing Company, Report No. AFML-TR-67-71, December 1967. Contract No. AF29(601)-7683.
3. M. W. Walkden, "The Effect of Temperature on the Performance of New and Irradiated Silicon Solar Cells," Ministry of Technology, Farnborough, Hants. Royal Aircraft Establishment, Technical Report No. 67091, April 1967.
4. A. J. Moses, "Study of the Effects of Space Radiation on Solar Panel Covering Materials," Hughes Aircraft Co. Engineering Report, Eng. Record No. 293, 21 December 1967.
5. R. R. Brown, et al., "Space Radiation Equivalence for Effects on Transistors," The Boeing Company, NASA CR-814, July 1967. Contract No. NAS' 9573.
6. "ATS Power Subsystem Radiation Effects Study," Hughes Aircraft Co. Engineering Record No. 296, December 1967. Contract NAS 5-3823
7. "Development of Solar Panel System for Thermally Annealing Radiation Damaged Solar Cells," The Boeing Company, First Quarterly Report. 1 July 1967 - 1 October 1967. Contract No. NAS 5-10445.
8. "Development and Fabrication of Radiation Resistant High Efficiency Solar Cells." Heliotek, P. Payne, et al., First Periodic Report 24 August 1966 - 24 February 1967. Contract No. NAS 5-10272.
9. M. Kangilaski, "The Effects of Neutron Radiation on Structural Materials," Battelle Memorial Institute, REIC Report No. 45, June 30, 1967. Contract No. NASW-1568.
10. First Quarterly Report 1968 IR&D Program. Hughes Aircraft Co., Ground Systems Group, 4 April 1968, FR 68-10-338.
11. Second Quarterly Report 1968 IR&D Program. Hughes Aircraft Co., Ground Systems Group, 27 June 1968, FR 68-10-615.

12. "Handbook of Space Environmental Effects on Solar Cell Power Systems," Exotech Inc., W. C. Cooley, et al., January 1968, Report No. TR-025, Contract No. NASr-1345.
13. J. J. Wysocki, et al., "Recovery from Radiation Damage in Solar Cells Doped with Lithium," Radio Corporation of America, Annual Report 21 June 1966 - 20 June 1967. Contract NAS 5-10239.
14. Richard R. Brown, Conference Paper, "Equivalence of Radiation Particles for Permanent Damage in Semiconductor Devices," The Boeing Company, June 1963, Paper No. CP 63-1109.
15. "Analysis of Radiation Induced Coupling Effects Between Integrated Circuit Elements," International Business Machines Corp, October 1967, Report No 1, Contract No. F 19628-67-0306.
16. Max Frank, et al., "Development of a nondestructive Radiation Effects Prediction Technique," Bendix Aviation Corp. Report No. AFML-TR-67-109, January 1968, Contract No. AF29(501)-7110.
17. M. W. Cobb, et al, "The Feasibility of a Programmed Heat Shield for Solar Cell Performance Control," Philco Corp., October 1965, WDL-TR2623, Contract NAS 2-2564.
18. E. J. Stofel, "Solar Cell Power Systems for Air Force Satellites," Aerospace Corporation, May 1967, Report No. TR-1001(2250-2)-7, Contract No. AF 04(695)-1101.
19. "Space Materials Handbook," Second Edition, Lockheed, January 1965, Report No. ML-TDR-64-40, Contract No. AF 33(657)-10107.
20. E. H. Snow, et al., "Radiation Study on MOS Structures," Fairchild Camera and Instrument Corp, January 1968, Report No. 4, Contract No. AF199628)-5747.
21. D. W. Ritchie, et al, "An Evaluation of Photovoltaic Devices for Future Spacecraft Power Demands," California Institute of Technology, Report No. 32-1268, May 1968, Contract No. NAS 7-100.
22. E. J. Evans, "A Feasibility Study of the Application of Amorphous Semiconductors to Radiation Hardening of Electronic Systems," Picatinny Arsenal, Report No. 3695, June 1968.
23. J. W. Harrity, et al, "Radiation Effects in Dielectric Materials," Gulf General Atomic Corp, May 1968, Report No. EQDM-02446-5, Contract No. DA28-043 AMC-02446(E).

24. Paul Berman, "Effects of Solar Proton Flares on the Power Output of Solar Cells Having Various Configurations," California Institute of Technology, Report No. 32-1251, February 1968, Contract No. NAS 7-100.
25. "Development of Solar-Panel System for Thermally Annealing Radiation Damaged Solar Cells," The Boeing Co., First Quarterly Report, 1 July 67-1 October 67, Contract No. NAS5-10445.
26. W. C. Cooley, et al, "Handbook on Space Radiation Effects to Solar Cell Power Systems," Exotech Inc., July 22, 1963, Contract No. NASw-598.
27. K. R. Walker, et al, "Predicting Transistor Photocurrent Using Avalanche Theory," Hughes Aircraft Company, February 1968, Report No. FR-67-10-624, Contract No. N00228-67-C-0835.
28. J. E. Bell, et al, "Simplified Techniques for Predicting TREE Responses," Hughes Aircraft Company, September 1965, Report No. AFWL-TR-65-65, Contract No. AF 29(601)-6404.
29. J. E. Drenan, et al., "Space Radiation Damage to Electronic Components and Materials," Battelle Memorial Institute, January 1966, REIC Report No. 39, Contract No. AF 33(615)-1124.
30. C. W. Perkins, et al, "Radiation Effects on (Monolithic) Micro-electronic Circuits," Hughes Aircraft Co., Report No. 5, November 1966, Contract No. DA 28-043 AMC-01313(E).
31. Frank A. Frankovsky, "Study of Effect of High-Intensity Pulsed Nuclear Radiation on Electronic Parts and Materials (Scorre)," International Business Machines Corp, July 1966, Report No. 5, Contract No. DA28-043-AMC-00212(E).
32. R. A. Poll, et al., "Study of Transient-Radiation-Induced Latch-up," General Dynamics, May 1967, Final Report GA-7969, Contract No. N00014-66-C0347.
33. Pat H. McIngvale, "Experimental Determination of Permanent Nuclear Radiation Effects on Army Missile Control System Electronics," U. S. Army Missile Command, May 1967, Report No. RG-TR-67-13, Project No. DASA 16.029.
34. K. R. Walker, et al., "Simplified Engineering Techniques for Predicting Diode and Transistor Photocurrent," Hughes Aircraft Company, March 1968, Report No. FR-67-10-559, Contract No. DAAG 39-67-C-0017.

35. Appendix, "Semiconductor Device Neutron Damage Characteristics," taken from "Radiation Effects on Guided Missile Electronic Equipment," Hughes Aircraft Company, March 1966, Report No. FR-66-17-66, Contract No. NOW65-0221-d.
36. D. C. Wunsch, et al., "Determination of Threshold Failure Levels of Semiconductor Diodes and Transistors Due To Pulse Voltages," Braddock, Dunn and McDonal, Inc., Conference Paper 1968, IEEE Annual Conference on Nuclear and Space Radiation Effects.
37. Charles F. Palandati, "Electron Radiation Effects on Silver-Zinc Cells," Goddard Space Flight Center, April 1968, Document No. X-716-68-136.
38. E. A. Carr, "Transient Radiation Effects in Semiconductor Devices, Experimental Correlation," Conference Paper, Hughes Aircraft Company, Contract No. AF29(601)-6404.
39. J. E. Bell, "Detailed Example of Engineering Hand Analysis," Conference Paper, Hughes Aircraft Company, September 1964.
40. B. Reinicke, K. Zander, "Anderung der Elektrischen Eigenschaften von Si-Solarzellen durch Neutronen-Bestrahlung," Hahn-Meitner-Institut Fur Kernforschung; Berlin, July 1967.
41. J. Bernard, Introduction A L'Etude De L'Irradiation Des Cellules Solaires En Couches Minces," Centre D'Etudes Et De Recherches En Technologie Spatiale; Toulouse, November 1967, Note Technique NT-02-2.
42. "Solar Cell Space Manual Outline," (Rough Draft) Centralab.
43. "TOS Radiation Program Report," Analysis and Evaluation of Test Results, Radio Corporation of America, September 1965.
44. Ramond C. Waddel, "Early Results from the Solar Cell Radiation Damage Experiment on ATS-1," Goddard Space Flight Center, April 1967, Document No. X-711-67-176.
45. C. A. Carosella, "Shielding of Solar Cells Against Van Allen Belt Protons," Naval Research Laboratory.
46. Bruce J. Faraday, et al, "Thermal Annealing of Proton-Irradiated Silicon Solar Cells," Conference Paper IEEE 6th Photovoltaic Specialists Conference March 1967, Naval Research Laboratory.

47. Joseph J. Wysocki, "Role of Lithium in Damage and Recovery of Irradiated Silicon Solar Cells," IEEE Transactions on Nuclear Science, Vol NS-14, No. 6, December 1967, Page 103.
48. J. R. Carter, Jr., "Radiation Damage in Lithium Doped Silicon," IEEE Transactions on Nuclear Science, Vol. NS-14, No. 6, December 1967, Page 110.
49. Charles L. Mack, "The Internal Radiation Environment of Cylindrical Spacecraft," IEEE Transactions on Nuclear Science, Vol. NS-14, No. 6, December 1967, Page 204.
50. R. H. Dickhaut, et al, "Radiation-Resistant Power Circuits," IEEE Transactions on Nuclear Science, Vol. NS-14, No. 6, December 1967, Page 228.
51. R. R. Brown, "Surface Effects in Silicon Solar Cells," IEEE Transactions on Nuclear Science, Vol. NS-14, No 6, December 1967, Page 260.
52. E. C. Smith, et al., "Theoretical and Experimental Determinations of Neutron Energy Deposition in Silicon," IEEE Transactions on Nuclear Science, Vol. NS-13, No 6, December 1966, Page 11.
53. H. H. Sander, et al., "Transient Annealing in Semiconductor Devices Following Pulsed Neutron Irradiation," IEEE Transactions On Nuclear Science, Vol. NS-13, No. 6, December 1966, Page 53.
54. R. B. Oswald, Jr., "Fracture of Silicon and Germanium Induced by Pulsed Electron Irradiation," IEEE Transactions on Nuclear Science, Vol. NS-13, No. 6, December 1966, Page 63.
55. D. H. Habing, et al, "Anomalous Photocurrent Generation in Transistor Structures," IEEE Transactions on Nuclear Science, Vol. NS-13, No. 6, December 1966, Page 86.
56. George C. Messenger, "Radiation Effects on Microcircuits," IEEE Transactions on Nuclear Science, Vol. NS-13, No. 6, December 1966, Page 141.
57. Donal J. Hamman, "Space-Radiation Effects in Integrated Circuits," IEEE Transactions on Nuclear Science, Vol. NS-13, No. 6, December 1966, Page 160.

58. J. J. Wysocki, "Lithium-Doped Radiation-Resistant Silicon Solar Cells," *IEEE Transactions on Nuclear Science*, Vol. NS-13, No. 6, December 1966, Page 168.
59. L. W. Aukerman, et al., "Effects of Radiation Damage on the Behavior of GaAs p-n Junctions," *IEEE Transactions on Nuclear Science*, Vol. NS-13, No. 6, December 1966, Page 174.

UNCLASSIFIED

Security Classification

DOCUMENT CONTROL DATA - R & D		
Security Classification of title, body of abstract and indexing annotation to be entered when the overall report is classified.		
1. ORIGINATING ACTIVITY (Corporate author) Hughes Aircraft Company Fullerton, California 92634		2a. REPORT SECURITY CLASSIFICATION UNCLASSIFIED
		2b. GROUP
3. REPORT TITLE Radiation Effects on Space Power Subsystems (Handbook) - Volume II Part 1		
4. DESCRIPTOR NOTES (Type of report and inclusive dates) Final Report 27 December 67 - 15 November 68		
5. AUTHOR(S) (First name, middle initial, last name) R. H. Kingsland R. L. Russell V. R. Hornold R. L. Skavland R. D. Loveland		
6. REPORT DATE November 1968	7a. TOTAL NO. OF PAGES 243	7b. NO. OF REFS 39
8a. CONTRACT OR GRANT NO. F04701-68-C-0145	9a. ORIGINATOR'S REPORT NUMBER(S) FR 69-10-69	
8b. PROJECT NO. 682J	9b. OTHER REPORT NUMBER(S) (Any other numbers that may be assigned this report) SAMSO-TR-69-7 Volume II Part 1	
10. DISTRIBUTION STATEMENT This document is subject to special export controls and each transmittal to foreign governments or foreign nationals may be made only with prior approval of: Hq SAMSO (SMTS), Air Force Unit Post Office, Los Angeles, California 90045.		
11. SUPPLEMENTARY NOTES The distribution of this report is limited because it contains technology restricted by Mutual Security Acts		12. SPONSORING MILITARY ACTIVITY Space and Missile Systems Organization Air Force Systems Command Los Angeles, California 90045
13. ABSTRACT This report provides data and guide lines which will enable circuit designers to assess and design for the effects of radiation on space power subsystems. Radiation effects on resistors, capacitors, bipolar transistors, diodes, integrated circuits, MOSFET's, SCR's and other electronic components are included. In addition, a section on catastrophic failure in semiconductors dealing with latch-up and burn-out is presented. Radiation effects on plastic and elastomeric materials commonly used in space systems are given. Various system and circuit hardening concepts for the electronic circuit designer are presented. Part II, a classified supplement not included in this volume, contains information on the radiation environment, shielding techniques, radiation effects on metals and alloys and solar cells, and thermo-mechanical effects.		

DD FORM 1473

UNCLASSIFIED

Security Classification

UNCLASSIFIED

Security Classification

14 KEY WORDS	LINK A		LINK B		LINK C	
	ROLE	WT	ROLE	WT	ROLE	WT
Radiation Effects on Resistors						
Radiation Effects on Capacitors						
Radiation Effects on Bipolar Transistors						
Radiation Effects on Diodes						
Radiation Effects on Integrated Circuits						
Radiation Effects on MOSFET's						
Radiation Effects on SCR's						
Radiation Effects on Plastics						
Radiation Effects on Elastomers						
Radiation-Induced Latch-Up						
Radiation-Induced Burn-Out						
System Hardening Concepts						
Circuit Hardening Concepts						

UNCLASSIFIED

Security Classification